University of Reading

Reconstruction of monsoon dynamics during the late Quaternary using speleothem data and model simulations

Doctor of Philosophy

School of Archaeology, Geography and Environmental Science

Sarah E. Parker

March 2022

Declaration

I confirm that this is my own work and the use of all material from other sources has been properly and fully acknowledged.

Signed

Sarah E. Parker

Abstract

Monsoon climates have varied on multiple timescales through the late Quaternary; Monsoons expanded and contracted in response to orbital forcing, interannual-interdecadal variability responded to the changing importance of climate modes, and abrupt events were triggered by rapid shifts in oceanic circulation. Individual speleothem oxygen isotope ($\delta^{18}O_{spel}$) records have documented this variability, often with high temporal resolutions and good age control. However, few comprehensive regional and global-scale analyses of these speleothem records exist. In this thesis, the Speleothem Isotopes Synthesis and AnaLysis database is used to reconstruct past monsoon climate at a range of timescales, including multi-millennial to interannual-interdecadal timescales, and across centennial-scale abrupt events. The use of a large-scale database enabled novel statistical techniques to be used on these records, including: regression modelling, to determine the climate processes that drive Holocene $\delta^{18}O_{spel}$ evolution; compositing, to construct regional signals and assess uncertainty; ordination techniques, to determine the relationship between record similarity and geographic location; new techniques to reconstruct interannual-interdecadal variability; and breakpoint analysis and significance testing to identify abrupt events. Reconstructions were compared to climate models, to provide insight into the processes driving the observed changes.

Comparison of regional Holocene $\delta^{18}O_{spel}$ composites with isotope-enabled climate models suggests that monsoon $\delta^{18}O_{spel}$ is primarily driven by changes in regional precipitation and atmospheric circulation. Holocene trends emphasise the importance of orbital forcing, with modification by internal feedbacks. Reconstructions and climate-model simulations of regional monsoon interannual-interdecadal variability through the Holocene suggest a non-linear relationship with orbital forcing, likely because of the complex interplay between insolation and climate modes. Finally, speleothem records show the 8.2 ka event is the most significant abrupt event in the Holocene. This thesis provides the most extensive global 8.2 ka synthesis yet, showing a globally coherent monsoon response and rapid global transmission.

Acknowledgements

First and foremost, I would like to thank my primary supervisor Sandy Harrison for her sustained support and patience through my PhD. Thank you for helping me develop into an independent researcher, but still always being there to support me when I needed it. I also thank Laia Comas-Bru, for always being supportive, approachable and patient to my many questions about speleothems.

I would also like to thank our research team, for their continued support and feedback, especially the team's programmers/data managers, A and Roberto, who's general support with processing data, R, SQL and Fortran has been invaluable. Also, a special thanks to Mark Turner, who would regularly check in to see how I was doing and provided encouragement.

I acknowledge funding from the European Research Council grant 'Global Change 2.0: Unlocking the past for a clearer future'.

Thank you to the SISAL working group members. Without their work and efforts to build the SISAL database, this PhD would not have been possible.

Thank you to my family, who have always supported and always encouraged me, from an 11-year old aspiring scientist to now.

I would also like to thank my partner Nat. Thank you for supporting me over these last 3.5 years, and always being there to obnoxiously critique the "form" of my data visualisations. I really appreciate you being there to keep me grounded, especially when working from home through the pandemic.

Contents

List of Figures

List of Tables

List of Abbreviations

$\delta^{18}O$ = oxygen isotopic composition

$\delta^{18}O_{precip}$ = oxygen isotopic composition of precipitation$\delta^{18}O_{spel}$ = speleothem oxygen isotopic composition AMO = Atlantic Multidecadal Oscillation

BP = Before Present (1950)

CAM = Central American monsoon

COHMAP = Cooperative Holocene Mapping project

EAM = East Asian monsoon

EH = early Holocene

ENSO = El Niño Southern Oscillation

IADV = interannual-interdecadal variability

IAM = Indonesian-Australian monsoon

IOD = Indian Ocean Dipole

ISM = Indian (summer) monsoon

ITCZ = Intertropical Convergence Zone

ka = kilo annum, 10^3 years

LGM = Last Glacial Maximum

LH = late Holocene

LIG = Last Interglacial

MAP = mean annual precipitation

MAT = mean annual temperature

MH = mid-Holocene

MJJAS = May to September

MLR = multiple linear regression

NDJFM = November to March

NH = northern hemisphere

OIPC = Online Isotopes in Precipitation Calculator

PCoA = Principal Coordinate Analysis

PDO = Pacific Decadal Oscillation

PMIP = Palaeoclimate Modelling Intercomparison Project

RDA = Redundancy Analysis

SAfM = Southern African monsoon

SAM = South American monsoon

s.d. = standard deviation

SH = southern hemisphere

SISAL = Speleothem Isotopes Synthesis and AnaLysis

SST = sea-surface temperature

V-PDB = Vienna Pee-Dee Belemnite

V-SMOW = Vienna Standard Mean Ocean Water

WAfM = West African monsoon

1. Introduction

1.1 Overview

More than two thirds of the global population live in regions under the influence of monsoon climate (Wang *et al.*, 2021). Monsoon precipitation exerts significant influence upon water resources, crop production and the health and wellbeing of billions of people. Understanding of these climate systems, and the predictability of the rainy season, is therefore important. Monsoon climates are studied extensively using instrumental records. However, this research is limited to the last ~70 years and therefore provides a limited understanding of climate on longer timescales (interdecadal and beyond). The focus on the recent period also cannot provide insight into monsoon climates under significantly different conditions from today. The study of past climate (palaeoclimate) using geological, biological and geochemical archives have provided a valuable perspective for monsoon climate research.

Speleothem oxygen isotope ($\delta^{18}O$) records have proven to be a useful tool in reconstructing past monsoon variability (Kaushal *et al.*, 2018; Deininger *et al.*, 2019; Zhang *et al.*, 2019) throughout the Quaternary period (the palaeomonsoon). Hundreds of speleothem $\delta^{18}O$ records have been published in recent decades (Comas-Bru and Harrison, 2019), and many of these records have recently been compiled into the SISAL (Speleothem Isotopes Synthesis and AnaLysis) database (Atsawawaranunt *et al.*, 2018; Comas-Bru *et al.*, 2020). The database provides an opportunity to reconstruct monsoon variability, at the regional and global scale that is necessary to understand climate. Furthermore, access to more than 350,000 oxygen isotope measurements from hundreds of globally distributed sites has provided the opportunity to employ novel statistical approaches. This speleothem data can also be compared to climate models to provide a fuller picture of monsoon climate.

In this thesis, the SISAL database is used, together with palaeoclimate model simulations and statistical approaches to develop our understanding of the regional monsoons during the Late Quaternary. This introductory chapter summarises monsoon climates from a global and regional perspective, in the present

(section 1.2) and the late Quaternary (section 1.3). Section 1.4 summarises how speleothem $\delta^{18}O$ records can be used to reconstruct past monsoon variability, and the complexities involved in the interpretation of these records. Section 1.5 introduces the SISAL database. Section 1.6 introduces the use of data-model comparisons, and the unique perspective it brings to palaeomonsoon research. The final section outlines the thesis aims and structure.

1.2 Monsoon climate

Monsoon climates are broadly defined by their rainy summers and drier winters, often accompanied by a seasonal reversal in winds. Wang and Ding (2008) delineated the monsoon regions based on the following criteria:

- The annual precipitation range (defined as mean summer precipitation minus mean winter precipitation) exceeds 300 mm. Summer is defined as May to September (MJJAS) in the northern hemisphere and as November to March (NDJFM) in the southern hemisphere
- This annual precipitation range also exceeds 50 % of annual mean precipitation

Based on this definition, monsoon climates are found across most of the tropics (Fig. 1.1).

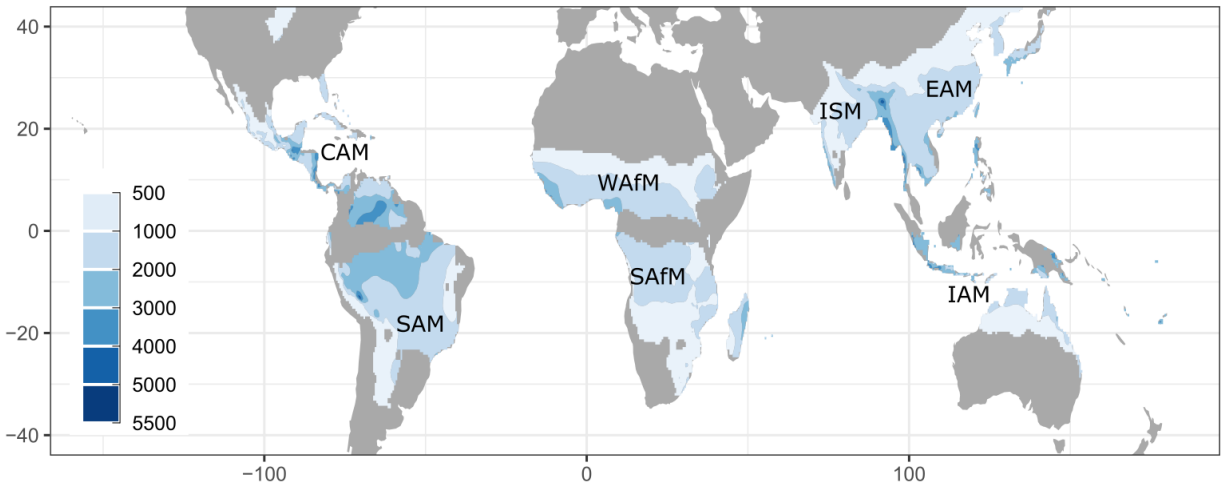

Figure 1.1 Global monsoon domain (coloured regions) amended from Mohtadi et al. (2016), calculated using the monsoon climate criteria from Wang and Ding (2008). The colour scale indicates total annual precipitation (mm), which was derived from monthly, gridded precipitation data for 1901 to 2020 from the Climate Research Unit TS 4.05 dataset (Harris et al., 2020). The monsoon regions are: Central American monsoon (CAM), South American monsoon (SAM), West African monsoon (WAfM), Southern African monsoon (SAfM), Indian monsoon (ISM), East Asian monsoon (EAM) and Indonesian-Australian monsoon (IAM).

Monsoon climates can be understood within the context of planetary-scale circulation (Biasutti *et al.*, 2018; Geen *et al.*, 2020). Summer monsoon circulation systems and the intertropical convergence zone (ITCZ) represent a zone of moist air convergence, spanning the tropics. During the boreal summer, the northern hemisphere tropics receive more energy from the sun. Here, moist air ascends and transports the excess energy away from the surface and across the equator to the southern hemisphere (Fig. 1.2). Ascending moist air cools adiabatically, resulting in a band of high precipitation across the tropics (Biasutti *et al.*, 2018). During the southern hemisphere summer, there is an opposite configuration: summer monsoon convection and the ITCZ is centred over the southern hemisphere tropics and excess energy is transported from the southern to the northern hemisphere. Although the monsoons and the ITCZ are both driven by meridional energy gradients and are therefore intrinsically linked, they have distinct features. Monsoons have additional shallow meridional circulation and rotational circulation (associated with low-level cyclones) (Fig. 1.2). Furthermore, more intense convection and higher re-evaporation of rain occurs over the summer monsoon regions (Biasutti *et al.*, 2018).

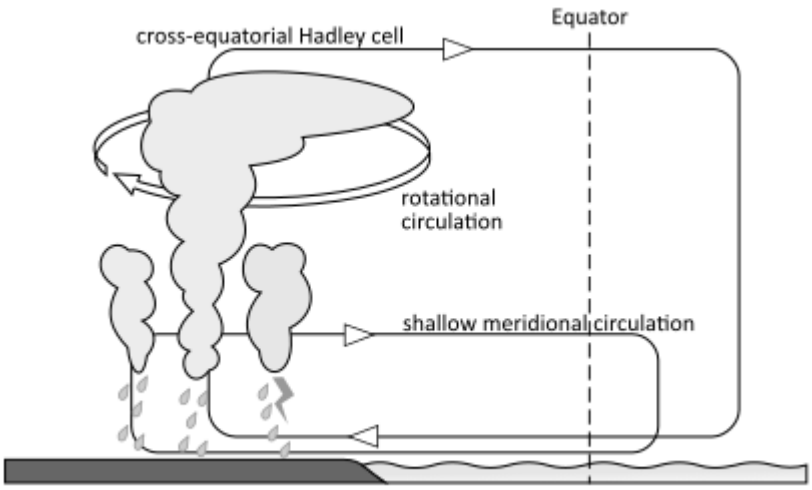

Figure 1.2 Schematic view of monsoon climate, adapted from Seth et al. (2019) and Biasutti et al. (2018). Within the energy budget framework, monsoons are interpreted as cross-equatorial circulations, closely linked to the ITCZ and Hadley circulation. Features of typical summer monsoons are shown, including rotational circulation (associated with low-level cyclones), shallow meridional circulation, intense convection (represented by anvil-shaped cloud) and lightening.

The response of monsoon climates to meridional energy gradients is explained by this framework of large-scale energy budgets. This framework also explains the globally coherent behaviour of monsoon climates, termed the “global monsoon” (Trenberth, Stepaniak and Caron, 2000). In this global context, the northern and southern hemisphere monsoon systems act coherently, with an antiphase response between the

northern and southern hemisphere. This is observed in the annual cycle, where the northern hemisphere systems expand northwards and rain intensifies during the northern hemisphere summer, then wane as the summer season ends. As the northern hemisphere monsoons are waning, the southern hemisphere summer monsoons begin as the seasonal cycle enters the southern hemisphere summer. Some global-scale coherency is also observed on intraseasonal to interdecadal timescales, because of the interaction between ENSO (El Niño Southern Oscillation) and monsoon rainfall (Wang *et al.*, 2012; Yim *et al.*, 2014), with most land summer monsoon rainfall decreasing during El Niño events.

Although the global monsoon concept is key to understanding monsoon dynamics over a broad range of timescales, individual monsoon regions exhibit their own distinct features due to differences in land-sea configuration, topography and interaction with climate modes (Wang *et al.*, 2014). Six distinct monsoon regions have been recognised: the Central American monsoon (CAM), South American monsoon (SAM), West African monsoon (WAfM), Southern African monsoon (SAfM), Asian monsoon and Indonesian-Australian monsoon (IAM) (Zhang and Wang, 2008). The Asian monsoon can be divided into sub-regions, including the Indian monsoon (ISM) and East Asian monsoon (EAM). Each region has its own unique evolution of the rainy season, as described below.

Central American monsoon

The summer monsoon season begins in June to July (Adams and Comrie, 1997; Barlow, Nigam and Berbery, 1998) and occurs as a northward moving band of precipitation (Zhang and Wang, 2008). Easterly trade winds deliver moisture from the Atlantic Ocean into the region. Easterly winds split into two branches (Fig. 1.3a), with one moving north to deliver moisture to the Gulf of Mexico. The other branch continues westwards, delivering moisture to the central American isthmus (Mestas-Nuñez, Enfield and Zhang, 2007; Amador, 2008). The rainy season ends in September to October with the rainy band withdrawing southwards (Adams and Comrie, 1997; Barlow, Nigam and Berbery, 1998).

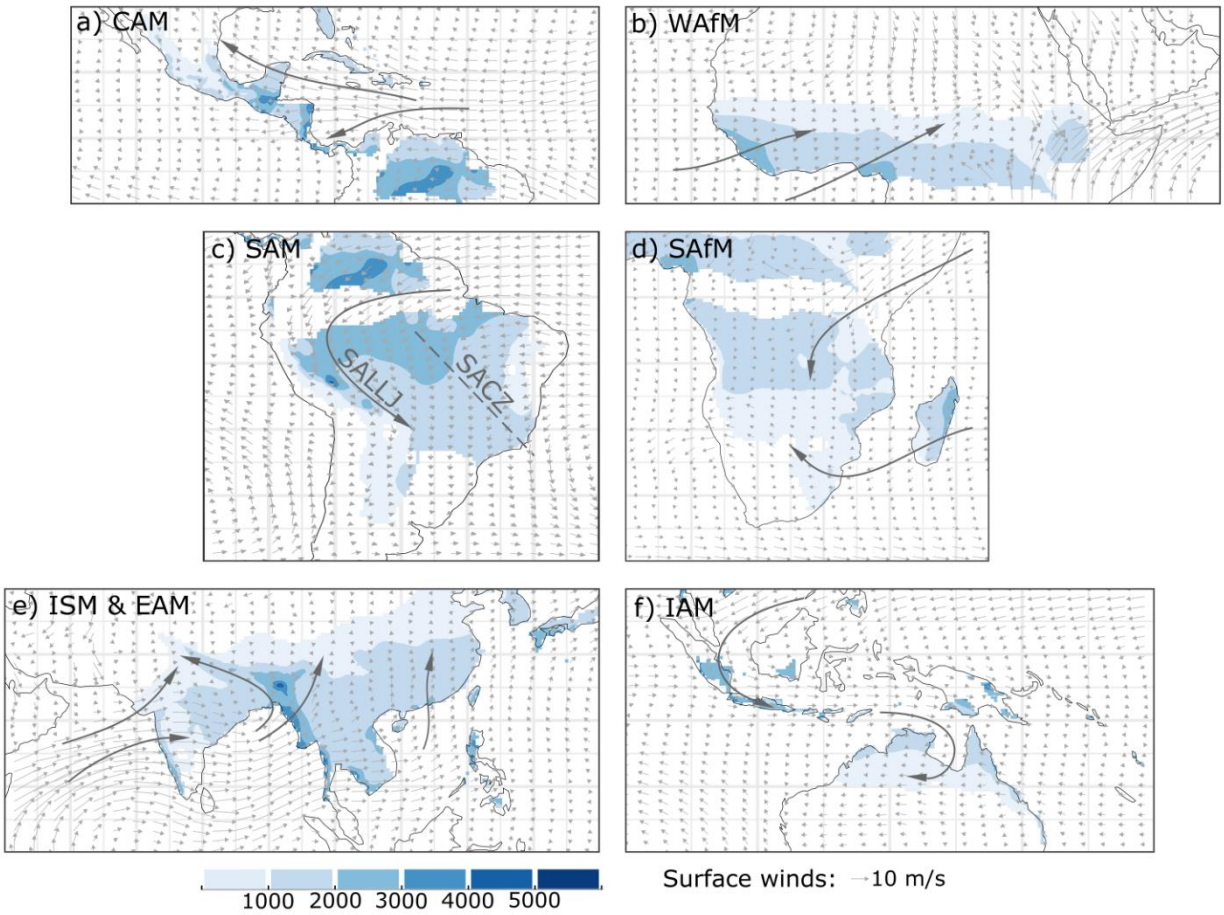

Figure 1.3 Maps showing the seven monsoon regions: a) Central American monsoon (CAM), b) West African monsoon (WAfM), c) South American monsoon (SAM) with the South American Low-Level Jet (SALLJ) and South American Convergence Zone (SACZ) shown, d) South African monsoon (SAfM), e) Indian monsoon (ISM) and East Asian monsoon (EAM), and f) Indonesian-Australian monsoon (IAM). Colours show the modern extent of the summer monsoons, using the definition of monsoon climate from Wang and Ding (2008) and precipitation data for 1901 to 2020 from the Climate Research Unit 4.05 dataset (Harris et al., 2020). The colour gradient denotes total annual precipitation (mm). Also illustrated is the summer 850 hPa winds, from the ERA5 dataset (Hersbach et al., 2020). The main flow-paths of the low-level monsoon circulation are shown as arrows.

South American monsoon

The rainy season begins over South America in October, with an abrupt shift of convection southwards over the Amazon Basin (Marengo *et al.*, 2012). The intense convection contributes to the formation of an upper-level high pressure zone over Bolivia (the Bolivian High) and a low-level low pressure zone in the Chaco region (Vera *et al.*, 2006). This configuration reinforces the South American low-level jet (Fig. 1.3c), which transports moisture away from the core region to the La Plata basin (Berbery and Barros, 2002; Marengo *et al.*, 2012). The easterly winds of the South Atlantic low-level jet are deflected by the

orographic barrier of the Andes (Marengo *et al.*, 2012). The monsoon is at its greatest extent from December to February. A defining feature of this phase is the South American convergence zone, a southeast-northwest oriented zone of convection that extends from the core monsoon region to the southwest Atlantic (Kodama, 1992; Marengo *et al.*, 2012). Upper-level convergence develops over north-eastern South America as a consequence of the Bolivian High (Fig. 1.3c), causing air subsidence and arid conditions in this region. There is therefore a southwest-northeast antiphase precipitation pattern over South America during the summer monsoon season (Berbery and Barros, 2002).

West African monsoon

The West African summer monsoon begins over the Guinean coast (near the equator) in late April or early May. Here, rainfall is supported by moist air transported by low-level winds from the Gulf of Guinea (Cook and Vizy, 2019). This band of rainfall remains here and intensifies until late June or early July, because the African easterly jet (located just north of the gulf) places a strong meridional wind gradient over the region, preserving an inertially stable environment over the Gulf of Guinea. When the African easterly jet moves northwards, the wind gradient weakens and reverses, causing inertial instability over the Guinean coast. The rain band then rapidly jumps northwards to the southern Sahel region (~10°N), sometimes within the span of a few days (Sultan and Janicot, 2003; Hagos and Cook, 2007). Sahel rainfall intensifies, reaching a maximum in mid-August (Cook and Vizy, 2019). The summer monsoon rain is fed by moisture from the eastern Atlantic (Fig. 1.3b), fed by the low-level West African westerly jet (Pu and Cook, 2012; Liu, Cook and Vizy, 2020). Summer monsoon precipitation accounts for 75 to 90 % of the total annual rainfall in the Sahel region (Lebel, Diedhiou and Laurent, 2003). From August to September, rainfall decreases as the rain band migrates smoothly back towards the equator (Geen *et al.*, 2020). There are no jumps during monsoon retreat because the high Coriolos parameter in the higher latitude Sahel region means that inertial instability does not occur regularly here.

Southern African monsoon

The SAfM begins in November, close to the equator (over Angola and southern Democratic Republic of Congo) and expands east and south, reaching Madagascar by December and north-eastern South Africa by January (Zhang and Wang, 2008). The summer monsoon is fed by northeasterlies that transport moisture from the western tropical Indian Ocean, and easterlies, bringing moist air from north of Madagascar (Hart, Reason and Fauchereau, 2010). The rainy season retreats northwards and westwards from February to April (Geen *et al.*, 2020).

Indian monsoon

The onset of the ISM is marked by a low-level wind reversal from winter easterlies to summer westerlies (Wang and LinHo, 2002). The onset is in May to June over the southern Bay of Bengal and the southern Indian peninsula, with the summer monsoon rain band spreading northwards from these locations (Mao and Wu, 2007; Wang, Ding and Joseph, 2009; Walker and Bordoni, 2016). The summer monsoon low-level winds have two main branches: one branch delivers moisture from the Arabian Sea eastwards over the Indian peninsula and up to the Himalayas. The second branch delivers moisture from the Bay of Bengal to northern India, with one part of this branch deflected to the northwest by the Himalayas and another part delivering moisture to the Tibetan Plateau (Kaushal *et al.*, 2018). The Indian monsoon region receives 78% of the annual rainfall during the summer season (Parthasarathy, Munot and Kothawale, 1994). The rain band retreats southwards in late September (Wang and LinHo, 2002).

East Asian monsoon

The EAM region is characterised by a seasonal reversal of low-level winds, with winter northerlies reversing to southerlies in the summer (Wang and LinHo, 2002). The EAM is unique amongst the regional monsoons because it extends from the tropics into the extratropics (Chiang *et al.*, 2015) . The summer monsoon has a complex evolution; the summer monsoon rain belt moves northwards in two abrupt meridional shifts, tied to meridional shifts in the westerly jet, controlled by the presence of the Tibetan Plateau (Ding and Chan, 2005; Chiang *et al.*, 2015). In early May, in the so-called “pre-Meiyu” phase, the

rain belt is located over southern China. The rain belt shifts northwards abruptly in mid-June, bringing rainfall to the Yangtze River Basin and Japan. This stage is termed the "Meiyu" (or "Baiu" in Japan). The second abrupt shift occurs in mid-July, bringing rainfall to northern China and the Korean peninsula, whilst central and south China become drier. The rain belt retreats southwards rapidly from the end of August to early September (Ding and Chan, 2005).

Indonesian-Australian monsoon

The IAM is intrinsically linked to the Asian monsoon. During the southern hemisphere summer, northerlies over Asia cross the equator, transporting moisture from the South China Sea and Indian Ocean to the region and "feeding" the rainy season (Wheeler and McBride, 2012). The summer monsoon season begins over Java, in October to November and extends southwards to north Australia by late December (Zhang and Wang, 2008). Withdrawal occurs through March (Zhang and Wang, 2008). During the dry winter monsoon, low-level winds are reversed, with cross-equatorial flow delivering moisture to the Asian monsoon (where the summer monsoon season is occurring).

These patterns of summer monsoon rainfall advance and retreat are affected on intraseasonal to interdecadal timescales by the influence of internal climate modes. ENSO is an influential mode for global interannual monsoon rainfall variability, arising from ocean-atmosphere interactions in the tropical Pacific (McPhaden, Zebiak and Glantz, 2006). However, its influence on different monsoon regions varies. During El Niño years, easterlies in the tropical Pacific are weakened, causing reduced upwelling of cool subsurface waters and therefore cooler sea-surface temperatures (SSTs) in the central and eastern Pacific. This drives drought conditions over the Indian peninsula (Kumar, Rajagopalan and Cane, 1999; Seetha *et al.*, 2020), the maritime continent (Hendon, 2003), northern Australia (Chung and Power, 2017), the Amazon basin and north-east South America, whilst flooding is often observed across south-eastern South America (Cai *et al.*, 2020). Wetter conditions are observed over the Yangtze River Basin (Zhang *et al.*, 2016) and the CAM region (Higgins, Chen and Douglas, 1999) during El Niño events. Drier conditions are generally

observed over southern Africa (Ratnam *et al.*, 2014) and the WAfM region (Rodríguez-Fonseca *et al.*, 2011; Pomposi *et al.*, 2016). During La Niña years, easterlies are enhanced and SSTs over the central and eastern Pacific are anomalously cold. This has roughly opposite climate impacts to El Niño events, including wetter conditions over parts of the Indian peninsula (Seetha *et al.*, 2020), the IAM region (Hendon, 2003; Chung and Power, 2017) and drier conditions over south-east South America (Cai *et al.*, 2020) and the CAM region (Higgins, Chen and Douglas, 1999)

Monsoon climates are also influenced by the Pacific Decadal Oscillation (PDO) (Mantua *et al.*, 1997), where SSTs in the Pacific Ocean fluctuate on decadal timescales; when PDO is negative, anomalously cool SSTs occur along west coast of North America and anomalously warm SSTs in the central-north Pacific, and vice-versa for positive PDO phases. Positive PDO phases have been associated with drier conditions over eastern Australia and much of central America, whilst wet anomalies have been observed over Mexico, south-east and central South America (Mantua and Hare, 2002). The PDO also modulates the ENSO-rainfall relationships over Australia (Power *et al.*, 1999; Chung and Power, 2017), the Indian sub-continent (Krishnamurthy and Goswami, 2000; Yoon and Yeh, 2010), central America (Gershunov and Barnett, 1998) and South America (Andreoli and Kayano, 2005).

The Indian Ocean Dipole (IOD) is characterised by interannual fluctuations between anomalously cool (negative IOD) and anomalously warm (positive IOD) SSTs in the western Indian Ocean relative to the east Indian Ocean (Abram *et al.*, 2015). When IOD is positive, ISM (Ashok, Guan and Yamagata, 2001), SAfM (Marchant *et al.*, 2007) and central China rainfall (Yuan *et al.*, 2008) is higher, whilst drier conditions occur over the IAM region (Marchant *et al.*, 2007) and south China (Yuan *et al.*, 2008).

The multi-decadal-scale oscillation between warmer and cooler SSTs in the Atlantic Ocean (Atlantic Multidecadal Oscillation, AMO) also exerts an influence on precipitation in monsoon regions. During the warm phases of AMO (positive AMO), wetter conditions are observed across the CAM (Sutton and Hodson, 2005), WAfM (Martin and Thorncroft, 2014), EAM and ISM regions (Goswami *et al.*, 2006; Lu, Dong and Ding, 2006; Zhang and Delworth, 2006). However, a positive AMO has been linked to droughts in the Amazon basin (Aragão *et al.*, 2018; Barichivich *et al.*, 2018).

Overall, there are numerous processes that can influence monsoon climate; changes in meridional energy gradients drive a global monsoon response, while local processes and the interaction of monsoon precipitation with climate modes can produce a more complicated response at the regional level. The relationship between monsoon climates and these modes has been studied extensively using the instrumental record. However, the relatively short length of this record limits confidence in the climate impacts of the multidecadal modes (i.e. PDO, AMO). Furthermore, modern-day observations do not provide any insight into how these modes varied (and interacted with one another) under conditions significantly different to today. Palaeoclimate records (including speleothems) can therefore provide important insights into monsoon evolution.

1.3 Current knowledge of the palaeomonsoons

1.3.1 Orbital forcing of the palaeomonsoon

Palaeoclimate records provide information about monsoon variability at a range of timescales, from interannual to multi-millennial timescales. They can also be used to examine the spatial patterns of monsoon variability at these timescales, including the presence of globally coherent responses and regional distinctions. Palaeoclimate research can therefore expand our knowledge of monsoon climates beyond what is known from the instrumental record.

The basic cause of past monsoon variability on multi-millennial timescales is orbitally induced changes in incoming solar radiation (insolation). There are three orbital cycles (on less than one-million-year timescales): precession (on a 19,000 and 23,000 year cycle), obliquity (on a 41,000 year cycle) and eccentricity (on a 100,000 and 400,000 year cycles) (Fig. 1.4). Precession results from changes in Earth's rotational axis with respect to perihelion (Earth's closest position to the Sun) and aphelion (the furthest position). At precession minima, perihelion occurs during the northern hemisphere summer solstice, whilst aphelion occurs during the southern hemisphere summer. This drives higher northern hemisphere summer insolation and an enhanced northern hemisphere seasonal cycle, whilst the southern hemisphere seasonal cycle is reduced. During precession maxima, the opposite occurs, with an enhanced southern hemisphere seasonal cycle of insolation. Obliquity refers to changes in the tilt of Earth's axis.

When Earth's axial tilt is greater, both hemispheres tilt more strongly towards the sun during the summer. Therefore, summer insolation is higher (and the seasonal cycle is enhanced) in both hemispheres, with the strongest insolation changes seen in the higher latitudes. Eccentricity results from changes in the shape of the Earth's orbit, from nearly circular to slightly elliptical. When Earth's orbit is more elliptical, the difference in distance between perihelion and aphelion is greater than when the orbit is nearly circular. Therefore, eccentricity has the effect of either enhancing or dampening the effect of precession.

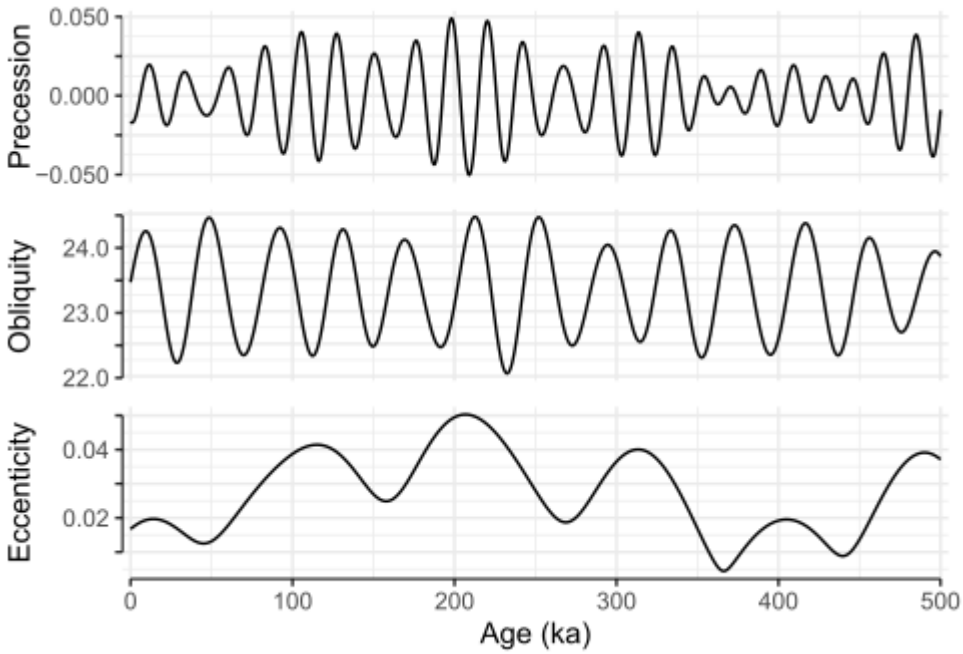

Figure 1.4 Changes in climatic precession, obliquity (degrees) and eccentricity over the last 500 ka, using the Berger (1978) algorithm and the palinsol package in R (Crucifix, 2016).

Together, these orbital cycles affect the latitudinal and seasonal energy gradients of insolation and can therefore be expected to influence the global monsoon. There is an increasing amount of evidence that there is indeed a close relationship between orbital forcing and monsoon climate. For example, long speleothem records from the EAM and SAM regions show speleothem $\delta^{18}O$ variability that is in phase with local summer insolation and antiphased between the hemispheres (Wang *et al.*, 2006, 2007; Cheng, Edwards, *et al.*, 2009) (Fig. 1.5). The early to mid-Holocene period (9,000 to 6,000 years BP) is a widely studied period, when precession caused increased (reduced) northern (southern) hemisphere summer insolation compared to today (Fig. 1.6). These insolation differences are expected to drive an enhancement of the northern hemisphere monsoons and a weakening of the southern hemisphere

monsoons, and an increasing amount of palaeoclimate evidence supports this overall picture; A large intensification and northwards expansion of the WAfM is observed at this time, with shrubland and permanent lakes extending into areas that are currently desert (Street and Grove, 1979; Street-Perrott and Perrott, 1993; Lézine *et al.*, 2011). Wetter conditions at the mid-Holocene are inferred in the CAM region from lake (Metcalfe, Barron and Davies, 2015) and marine sedimentary records (Haug *et al.*, 2001). Across the ISM and EAM, lake levels are higher at these times (Goldsmith *et al.*, 2017a; Misra, Tandon and Sinha, 2019), suggesting a wetter monsoon season than present. Pollen-based reconstructions from China also show higher moisture (Zhao *et al.*, 2009), and ISM and EAM speleothem records show more depleted oxygen isotope compositions during the early and mid-Holocene (Dykoski *et al.*, 2005; Fleitmann *et al.*, 2007; Cosford *et al.*, 2008; Cai *et al.*, 2021), interpreted as a stronger summer monsoon. Meanwhile in the southern hemisphere, a weakened SAM and drier conditions across much of the South American continent during the early and mid-Holocene have been inferred from pollen and lake records (Prado *et al.*, 2013; Smith and Mayle, 2018). Less depleted oxygen isotope compositions are observed across South American speleothem records at the same time (Bernal *et al.*, 2016; Bustamante *et al.*, 2016), supporting the view of a weakened summer monsoon. In the SAfM region, drier conditions are inferred at the early and mid-Holocene from lake and pollen records (Singarayer and Burrough, 2015; Chevalier, Brewer and Chase, 2017). The early to mid-Holocene monsoon precipitation response is less clear in the IAM region; drier conditions have been inferred from pollen records from northwest Australia (McGowan et al., 2012) and from marine sediment records from the Maritime continent (Mohtadi et al., 2011). This is the expected signal from reduced southern hemisphere summer insolation, however other records show wetter conditions. For example, increased rainfall is inferred from lake records in central Australia (Johnson *et al.*, 1999; Magee *et al.*, 2004) and pollen records suggest an expansion of rainforest in Australia at this time (Rowe, 2007).

At the Last Interglacial (127 ka), high precession and eccentricity together caused an even more enhanced (reduced) seasonal cycle of insolation in the northern (southern) hemisphere (Fig. 1.6). Palaeoclimate evidence is more limited during this time period, but generally supports a picture of stronger northern hemisphere monsoons and weaker southern hemisphere monsoons. A global compilation by Scussolini

et al. (2019) of numerous palaeoclimate archives (lake, pollen, speleothem records etc.) show drier conditions across the CAM, WAfM, ISM and EAM. In the SH, signals are more mixed, although most records from the core of the SAM and SAfM regions show drier conditions at the Last Interglacial than present, whilst the IAM gives a somewhat mixed picture of both wetter and drier anomalies. A close relationship between orbitally-induced insolation changes and monsoon variability is supported by numerous climate model simulations (Kutzbach and Guetter, 1986; Braconnot *et al.*, 2004; Marzin and Braconnot, 2009; Brierley *et al.*, 2020).

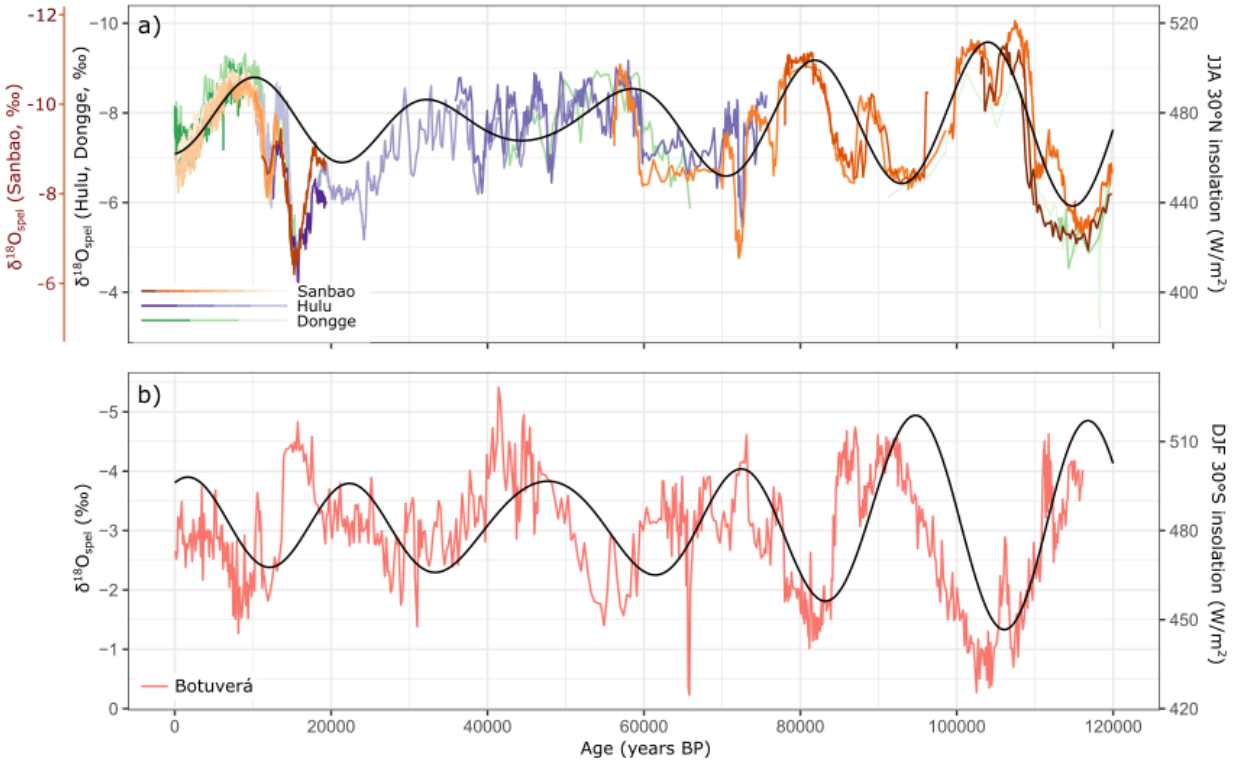

Figure 1.5 Speleothem $\delta^{18}O$ records of the last 120,000 years from a) the East Asian Monsoon region, using records from Sanbao (Wang et al., 2008; Dong et al., 2010), Hulu (Wang et al., 2001) and Dongge (Yuan et al., 2004; Wang et al., 2005) caves, and b) the South American Monsoon region, using a record from Botuverá cave (Cruz et al., 2005). The speleothem records are compared with 30°N and 30°S summer insolation (Berger, 1978), shown in black.

Whilst there is generally a globally coherent monsoon evolution (with interhemispheric antiphasing) amongst monsoon regions in response to orbital forcing, regional differences do occur via internal feedbacks and because of local differences. This is clear from evidence of past IAM variability; The lack of a clear drying signal across the region suggests that there is not a direct, linear relationship with insolation during the Holocene. Ocean-atmosphere climate model simulations have emphasised the importance of

ocean feedbacks on IAM rainfall at the mid-Holocene (Zhao and Harrison, 2012), suggesting that the complex response in this region could be related to oceanic influence. Over the WAfM region, the magnitude of mid-Holocene intensification and northwards expansion cannot be fully captured by climate models although they do show a general amplification (Brierley et al., 2020). Part of this disagreement between the data and models may relate to the low-quality of palaeoclimate archives in the region (low resolutions, poor age controls) and the inability of climate models to accurately simulate the magnitude and extent of observed climate change. However, the agreement with observations is better when changes in vegetation, lakes and wetlands are accurately incorporated (Rachmayani, Prange and Schulz, 2015; Chen *et al.*, 2020), suggesting that land-surface feedbacks are influential in modulating the WAfM's response to orbital forcing.

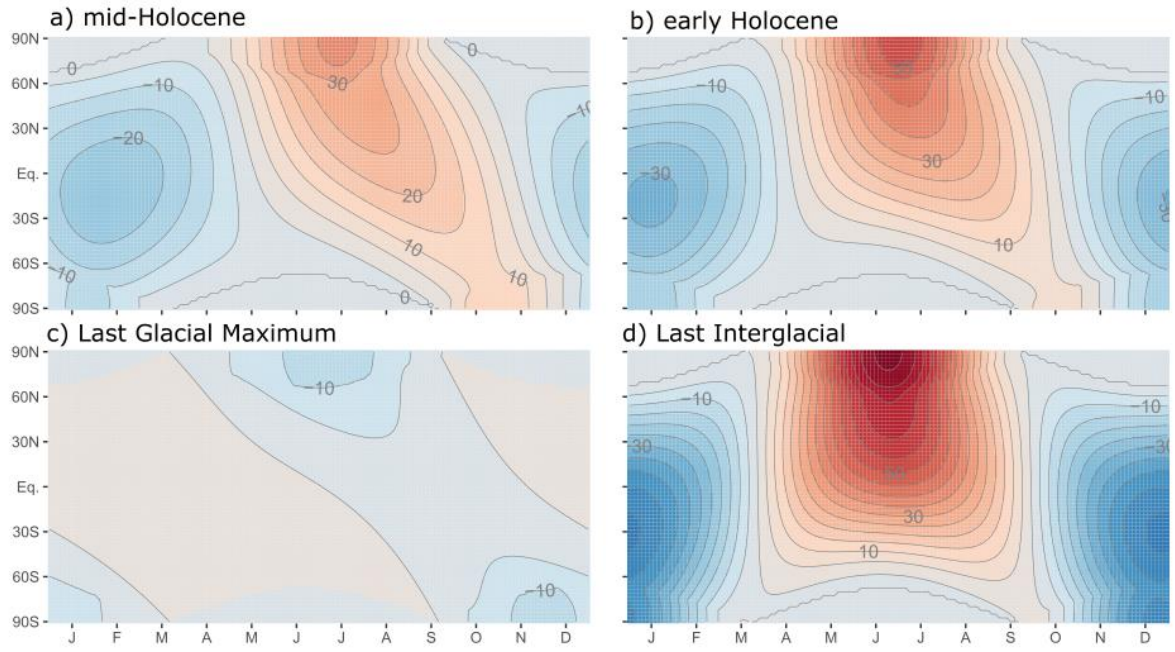

Figure 1.6 Monthly and latitudinal differences in insolation (relative to present day) that arise from orbital changes (Berger, 1978) at the a) mid-Holocene (6 ka), b) early Holocene (9 ka), Last Glacial Maximum (21 ka), and d) Last Interglacial (127 ka).

Another complexity in understanding the response of monsoon climates to orbital forcing comes from the influence of internal modes of climate variability, such as ENSO and AMO. Palaeoclimate records show that these modes varied in response to orbital forcing, and this likely influenced monsoon precipitation in the past. Coral and mollusc records from the tropical Pacific show that ENSO variability was dampened at the mid-Holocene, a feature that is also simulated by climate models (Carré *et al.*, 2021). The PDO also

changed through the Holocene (Ivanochko *et al.*, 2008; Kirby *et al.*, 2010; Chen, Zhao and Zhang, 2021). A lake-record from California (Kirby *et al.*, 2010), reconstructed east-west Pacific SST gradients and PDO-related precipitation anomalies from east Asia (Chen, Zhao and Zhang, 2021) all show an extended positive PDO phase at the early Holocene and at ~3.5 to 3 ka. Chen et al. (2021) also inferred a negative PDO phase from 3 ka onwards. A comparison of their reconstructions with climate models supports a relationship between orbital forcing and the PDO through the Holocene. Reconstructed AMO variability suggests that there was a stronger centennial AMO-like climate pattern during the late Holocene compared to the early Holocene (Feng, Hu and Oglesby, 2011), whilst Knudsen et al. (2011) suggested that the timing of the largest AMO signal varied depending on latitude, in response to large-scale circulation changes with orbital forcing. Coral and precipitation pattern based IOD reconstructions show stronger and more persistent positive IOD events at the mid-Holocene, with a shift to increased negative phases from the mid to late Holocene (Abram *et al.*, 2007; Niedermeyer *et al.*, 2014). Climate models simulate changes in the amplitude of interannual to interdecadal monsoon precipitation variability (IADV) through the Holocene in response to orbital forcing. For example, simulated ISM IADV amplitude increases from the mid-Holocene to present in response to insolation-driven changes in ENSO amplitude (Braconnot, Crétat, *et al.*, 2019; Crétat *et al.*, 2020). At the same time, simulated IADV in the WAfM decreased, reflecting changes in Atlantic SSTs (Braconnot, Crétat, *et al.*, 2019). These modelled changes in monsoon precipitation IADV in response to orbitally induced insolation changes need to be tested using terrestrial palaeoclimate records of IADV amplitude.

1.3.2 Abrupt events

The orbitally-induced changes in past monsoon climate have been punctuated by numerous short-lived (decadal to centennial scale) excursions (Gupta, Anderson and Overpeck, 2003; Stríkis *et al.*, 2011; Cai *et al.*, 2015). Many of these abrupt events have been linked to large influxes of meltwater into the North Atlantic at times when the northern hemisphere ice sheets were retreating. During the last glacial period, pronounced cold, ice-rafting events (termed Heinrich events) have been inferred as triggering dry, arid conditions in the northern hemisphere tropics (Wang *et al.*, 2001; Deplazes *et al.*, 2014; Han *et al.*, 2015) and wetter conditions in the southern hemisphere tropics (Cruz *et al.*, 2006a; Cruz *et al.*, 2006b; Wang *et*

al., 2006). During the early Holocene period, abrupt events identified in Greenland ice cores at 11.4, 9.3 and 8.2 ka (Vinther *et al.*, 2006) have also been linked to meltwater pulses (Barber *et al.*, 1999; Fisher, Smith and Andrews, 2002; Yu *et al.*, 2010). Observations suggest that these events are global in extent. The 8.2 ka event was recently used by the International Commission on Stratigraphy to divide the early Holocene from the mid-Holocene (Walker *et al.*, 2018) because the event has been detected in numerous records cross the globe. The event is one of the clearest features in the Greenland ice core records (Vinther *et al.*, 2006), where it is expressed as an abrupt ~165 year-long cooling event (Thomas *et al.*, 2007). The 8.2 ka event has also been identified in numerous palaeomonsoon records (Wu *et al.*, 2012; Liu and Hu, 2016; Tan *et al.*, 2020; Chawchai *et al.*, 2021) and a global synthesis of palaeoenvironmental records showing this event has been made by Morrill *et al.* (2013). These records show a general trend of drier conditions across the northern hemisphere monsoons and wetter conditions across the SH monsoons. However, questions remain regarding the timing, duration and magnitude of the palaeomonsoon response to the 8.2 ka North Atlantic freshening.

Another well-studied Holocene event is the 4.2 ka event, used to divide the mid-Holocene from the late Holocene (Walker *et al.*, 2018). This event is registered by numerous palaeo-records across the Middle East and Mediterranean (Kaniewski *et al.*, 2018; Bini *et al.*, 2019) where it is characterised by generally cool and dry conditions (Wayewski et al., 2004). The drought conditions at this time have been linked to the collapse of several ancient civilisations (Weiss, 2016). The 4.2 ka event has also been reported in tropical regions, with drier conditions inferred from palaeo-records from the ISM (Dixit et al., 2013; Kathayat et al., 2018; Giesche et al., 2018) and the EAM region (Xiao *et al.*, 2018; Ran and Chen, 2019). Wetter conditions have been inferred from two isotope palaeo-records from the SAfM region (Railsback *et al.*, 2018) and an Andean ice core (Thompson, Mosley-Thompson and Henderson, 2000) suggests that the 4.2 ka event was registered on the west coast of the SAM region. However, 4.2 ka signals can often show local and regional variation (Bini *et al.*, 2019; Scuderi *et al.*, 2019), with (often substantial) differences in the timing, duration and evolution of 4.2 ka excursions. Therefore, uncertainties remain as to the nature of the event, including whether the event was truly globally extensive and synchronous.

Furthermore, the trigger of the event remains unclear, with several mechanisms such as freshwater forcing, volcanicity and internal variability all proposed.

Other abrupt events in the Holocene have been identified, often linked to cold events in the North Atlantic (termed Bond events) (Bond *et al.*, 1997). Positive $\delta^{18}O$ excursions observed in speleothem records from Asia show a similar timing to the Bond events, and have been interpreted as a weakened summer monsoon in response to these cold events (Wang *et al.*, 2005; Tan *et al.*, 2020). This view is corroborated by a marine record from the Arabian Sea (Gupta, Anderson and Overpeck, 2003), where abrupt periods of weakened ISM (inferred from foraminifera abundance) also coincide with Bond events. Speleothem and lake records from South America (Baker *et al.*, 2005; Stríkis *et al.*, 2011) have been interpreted as showing wetter conditions during Bond events. This evidence points towards an antiphase interhemispheric response, with drier conditions in the northern hemisphere monsoons and wetter conditions in the southern hemisphere monsoons. However, these events are not consistently recorded in the majority of palaeo-records, and some records only register a few of the Bond events, so it remains unclear whether they were truly a significant feature of the global monsoon climate.

While there is a need to identify the presence and timing of abrupt events in monsoon palaeoclimate records and map these signals to reconstruct to climate responses, there are several factors that make it difficult to identify abrupt events in palaeo-records unambiguously. These events are short-lived (i.e. only a few hundred years long, or less) and therefore palaeo-records need to register climate changes with a minimal amount of lag or smoothing. Sampling resolution also needs to be sufficiently high to register these events. Secondly, age uncertainties need to be sufficiently low, to identify an excursion in a record as a specific abrupt event with confidence. Finally, the signal needs to be of larger magnitude than the noise of the record. Noise can arise from measurement uncertainties, interannual to interdecadal climate variability and from non-climate influences on the paleoclimate archive. For example, speleothem oxygen isotope records can be influenced by changes in the soil, karst and cave system (see section 1.4). These complications emphasise the need to identify and reconstruct abrupt climate events using (a) statistical approaches, to ensure signals are significant above the noise of the records, and (b) a careful examination

of the age uncertainties, to ensure unrelated events are not mistakenly identified as the same event. In this thesis, a statistical approach is taken with a global dataset of speleothem records to identify whether previously identified abrupt events are global in extent. Such analyses can provide insight into how monsoons respond to abrupt changes outside the tropics and whether the responses were consistent across monsoon regions.

1.4 Speleothem oxygen isotope record

1.4.1 Speleothem records

Speleothems are secondary calcium carbonate deposits that form on the roof, walls and floor of caves (Moore, 1952). They form when rainwater reacts with CO_2 to form a weak carbonic acid, which interacts with and dissolves the calcium carbonate bedrock above the cave. When this calcium carbonate solution enters the lower pCO_2 environment in the cave, CO_2 degassing results in supersaturation of the calcium carbonate solution, driving the precipitation of speleothems (Fig. 1.7a) (Kaufmann, 2003). Speleothems therefore contain signals from rainfall and conditions/processes within the soil, the karst above the cave (epikarst) and cave.

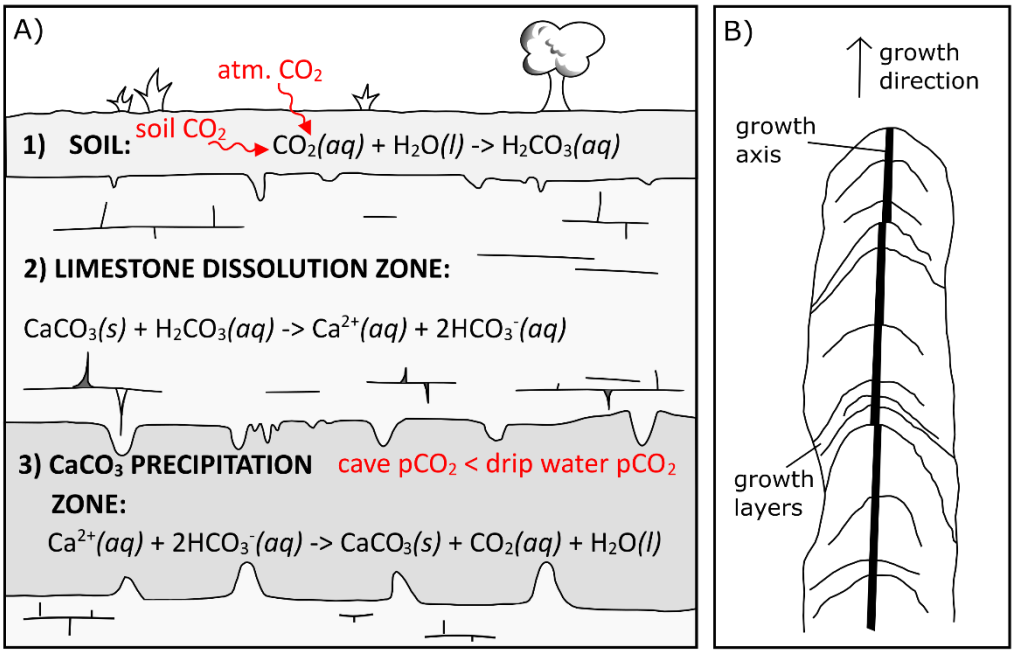

Figure 1.7 A) Processes of calcium carbonate ($CaCO_3$) dissolution and precipitation, resulting in speleothem growth, b) an example of the internal structure of a stalagmite.

Speleothems come in many shapes and forms (Hill and Forti, 1995), however most palaeoclimate research uses stalagmites because sampling along their growth axis (Fig. 1.7b) represents a time series. Flowstone (Hellstrom, McCulloch and Stone, 1998) and stalactites (Bar-Matthews *et al.*, 2003; Braun *et al.*, 2019) are used less frequently due to their more complex internal structures.

The calcium carbonate composition of speleothems, generally in the form of calcite or aragonite, can be dated precisely using Uranium-Thorium (U-Th) dating (Richards, 2003; Scholz and Hoffmann, 2008). The approach relies on the incorporation of soluble U into speleothems, but negligible amounts of insoluble Th, creating disequilibrium in the ^{238}U-^{234}U-^{230}Th system. This system returns to secular equilibrium at a rate determined by the half-lives of ^{234}U and ^{230}Th, of 245,620 and 75,584 years respectively (Cheng, Lawrence Edwards, *et al.*, 2013). U-Th ages can therefore be calculated using these values and measurements of $^{234}U/^{238}U$ and $^{230}Th/^{238}U$, dating materials up to 600,000 years (Scholz and Hoffmann, 2008). The method relies on the assumptions that no Th was incorporated into the speleothem initially, and the system remained closed after deposition. If either of these assumptions are violated, calculated ages may be inaccurate. Larger age uncertainties can arise in the U-Th dating of speleothems when samples span a range of ages, either because samples need to be large (to incorporate a suitable amount of U and Th for analysis) or because the speleothem grew slowly. The accuracy and precision of U-Th ages therefore varies between speleothems. However, many speleothems have age controls of <50 years which makes them an ideal tool for examining the timings of past climate variability. When speleothems are older than 600,000 years, U-Pb dating can be used (Richards *et al.*, 1998; Woodhead *et al.*, 2006), while lamina counting can provide very precise chronologies in younger (and actively growing) speleothems (Baker *et al.*, 2008). Speleothems can therefore provide a record of past climate, spanning very short to very long timescales.

A further advantage of speleothem records is their (often) high sampling resolution, obtained via laser ablation or micromilling techniques. This can provide annual or even seasonal resolution when speleothems have high growth rates (Frappier *et al.*, 2007; Chen *et al.*, 2016). When signals are

transmitted rapidly through the epikarst, speleothems can record past climate with a high degree of detail.

1.4.2 Oxygen isotope processes in the hydrological cycle

Several physical, geochemical and isotopic characteristics of speleothems have been used to infer past climates and environments, but the most frequently measured variable is the oxygen isotopic composition. The oxygen isotopic composition refers to the ratio of lighter ^{16}O isotopes to the heavier ^{18}O isotopes, relative to a universal standard. It is given in delta notation:

$$\delta\,^{18}O\ (‰) = \frac{^{16}O/\,^{18}O_{sample} - \,^{16}O/\,^{18}O_{standard}}{^{16}O/\,^{18}O_{standard}}\ x\ 1000 \qquad 1.1$$

Where the standard is Vienna Pee Dee Belemnite (V-PDB) for calcium carbonate and Vienna Standard Mean Ocean Water (V-SMOW) for water (Sharp, 2017). ‰ is parts per million, or per mille.

Changes in the oxygen isotopic composition of a substance occurs with phase changes and reactions due to the mass difference between ^{16}O and ^{18}O (Sharp, 2017). The heavier ^{18}O forms stronger, more stable bonds than ^{16}O, hence it is preferentially incorporated into phases with higher bond energies. For example, when water evaporates, ^{18}O will preferentially remain in the water phase whilst ^{16}O will be preferentially incorporated into the vapour. When oxygen isotope fractionation occurs under equilibrium, the degree of fractionation is temperature dependent (Clark and Fritz, 1997; Sharp, 2017). If a system has not reached equilibrium (i.e. the rate of exchange between two phases/reservoirs is not balanced, or is unidirectional), termed kinetic fractionation, less isotope exchange occurs, impacting the degree of fractionation.

The use of speleothem $\delta^{18}O$ as a palaeoclimate archive relies on the assumption that the $\delta^{18}O$ of speleothems ($\delta^{18}O_{spel}$) reflects the $\delta^{18}O$ of rainfall ($\delta^{18}O_{precip}$) above the cave. $\delta^{18}O_{precip}$ reflects the degree of oxygen isotope fractionation that occurs throughout the hydrological cycle. However, there are numerous climate processes that impact $\delta^{18}O_{precip}$ (Fig. 1.8). The initial $\delta^{18}O$ of water vapour depends on the oceanic surface water $\delta^{18}O$ at the moisture source. Seawater $\delta^{18}O$ values vary spatially (Fig. 1.9) and

temporally, depending on the balance between precipitation and evaporation, ocean circulation, freshwater runoff and global ice volume (Delaygue, Jouzel and Dutay, 2000; LeGrande and Schmidt, 2006; Munksgaard *et al.*, 2012). The initial $\delta^{18}O$ of water vapour that evaporates from seawater also depends on local temperature, since equilibrium fractionation is temperature dependent. Equilibrium fractionation during evaporation is defined by Clark and Fritz (1997):

$$1000\, ln\, \propto_{liquid-vapour} = 1.137\,(10^6/T_k^2) - 0.4156\,(10^3/T_k) - 2.0667 \qquad 1.2$$

Where T_K is temperature in kelvin. Kinetic isotope fractionation (where water vapour is rapidly removed from the ocean surface) also influences the $\delta^{18}O$ of initial water vapour. The degree of kinetic fractionation depends largely on the relative humidity and wind speed over the ocean surface (Lachniet, 2009).

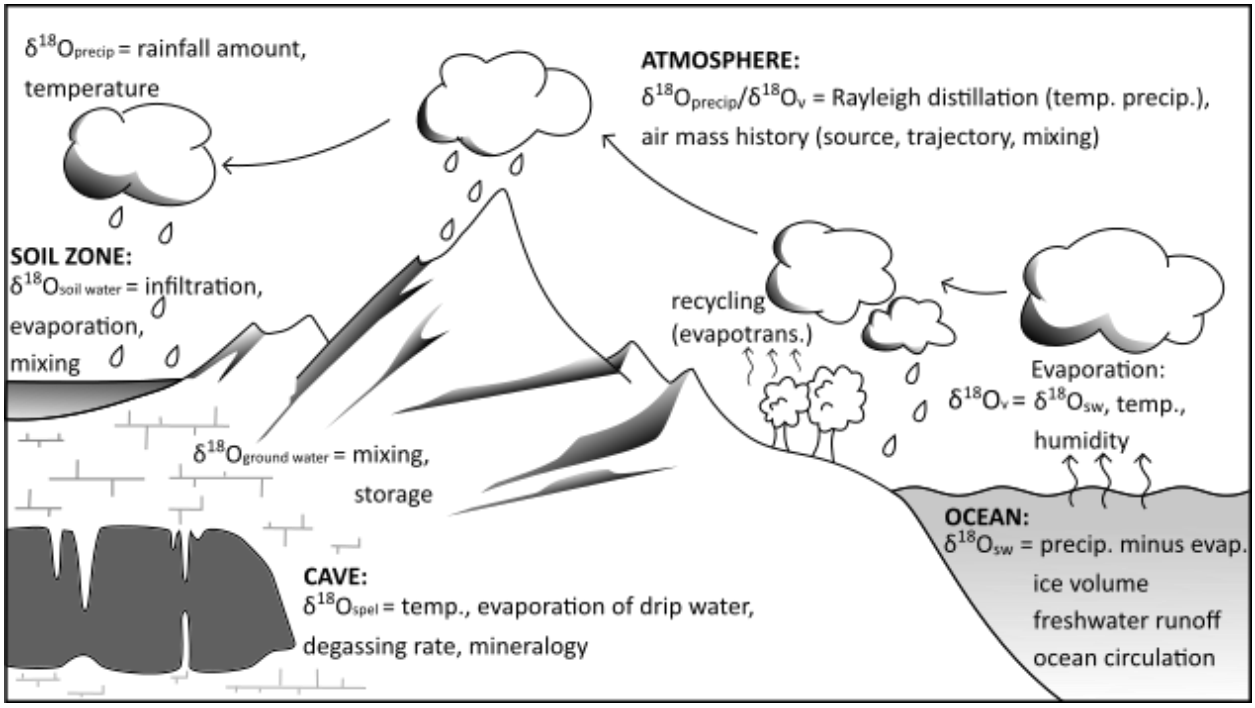

Figure 1.8 Summary of the processes influencing speleothem $\delta^{18}O$, modified from Lachniet (2009). Processes span evaporation from the initial oceanic moisture source, transport and mixing in the atmosphere, precipitation at the cave site and modification through the soil, epikarst and cave, before the $\delta^{18}O$ signal is incorporated into the speleothem. The main controlling processes at each step are summarised.

Following evaporation, water vapour is transported by atmospheric circulation and undergoes isotope fractionation with phase changes along a moisture pathway. During condensation, ^{18}O is preferentially incorporated into the water droplets rather than the vapour. This leaves the remaining vapour depleted

in ^{18}O (lower $\delta^{18}O$), so that any subsequent precipitation is also more depleted. Consequently, with progressive rainout along a moisture transport pathway, the $\delta^{18}O$ of vapour become gradually more depleted, and the precipitation that condenses from this vapour also becomes gradually more depleted. This process is termed "Rayleigh distillation" (Dansgaard, 1964; Clark and Fritz, 1997).

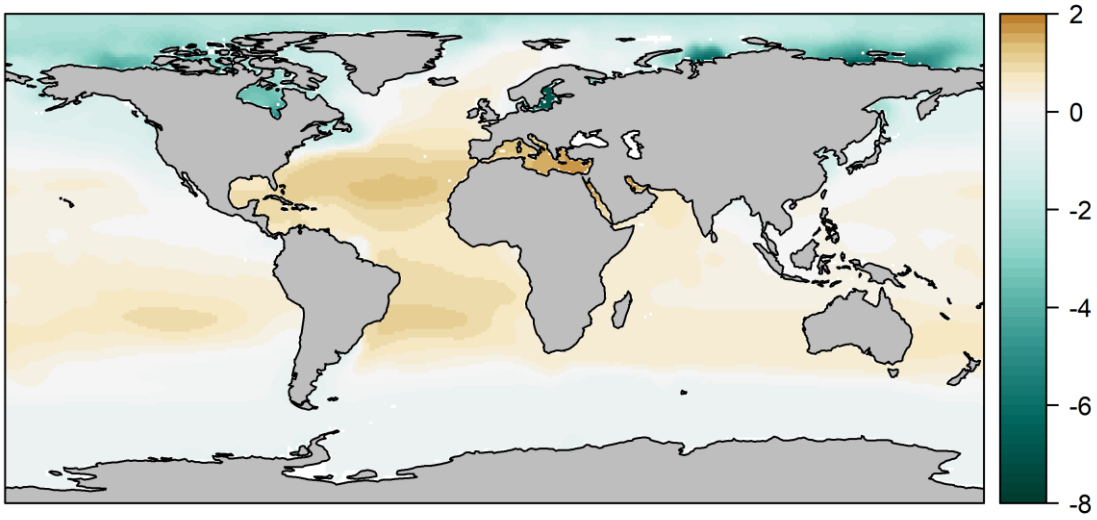

Figure 1.9 Map of surface oceanic $\delta^{18}O$ (SMOW) values, using the dataset from LeGrande and Schmidt (2006). Data is derived using oceanic $\delta^{18}O$ measurements from the last 50 years, interpolated to a smoothed global gridded dataset using regional $\delta^{18}O$/salinity relationships. $\delta^{18}O$ values vary between ocean basins, and latitudinally.

A greater degree of rainout along a moisture pathway (enhanced Rayleigh distillation) drives lower $\delta^{18}O_{precip}$ values (Yuan *et al.*, 2004). $\delta^{18}O_{precip}$ values also depend on the air temperatures along the moisture pathway. This is partly because cooling is required for condensation and rainout, and partly because of the temperature-dependence of isotope fractionation (Lachniet, 2009). This results in a positive relationship between temperature and $\delta^{18}O_{precip}$, referred to as the "temperature effect", and is observed at mid to high latitudes (Dansgaard, 1964; Rozanski, Araguás-Araguás and Gonfiantini, 1993).

Rayleigh distillation drives a gradual decrease in $\delta^{18}O_{precip}$ across continents as air masses move inland (the continental effect: Dansgaard, 1964; Rozanski, Araguás-Araguás and Gonfiantini, 1993; Clark and Fritz, 1997) and in depleted $\delta^{18}O_{precip}$ values over high elevation regions, where orographic lifting and adiabatic cooling results in increased rainout (the altitude effect: Clark and Fritz, 1997). Atmospheric circulation typically advects moisture towards the poles, and therefore progressive Rayleigh distillation, together with lower air temperatures and less cloud condensation, results in lower $\delta^{18}O_{precip}$ values at higher

latitudes. Overall, Rayleigh distillation results in spatially heterogeneous $\delta^{18}O_{precip}$ values across the globe, ranging from -30 to 5 ‰ (Fig. 1.10: (Bowen and Revenaugh, 2003).

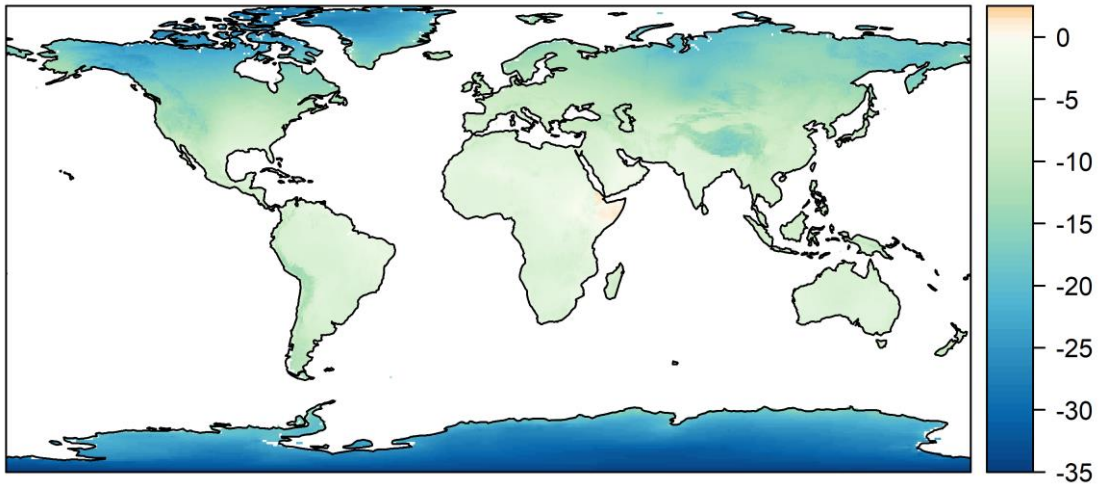

Figure 1.10 Annual amount-weighted $\delta^{18}O$ of precipitation ($\delta^{18}O_{precip}$) from the Online Isotopes in Precipitation Calculator (OIPC: Bowen and Revenaugh, 2003). Data is based on spatial interpolation of $\delta^{18}O$ measurements from 348 stations. Spatial patterns in $\delta^{18}O$ exhibit strong latitudinal gradients, with more depleted $\delta^{18}O_{precip}$ values at higher latitudes. Lower $\delta^{18}O_{precip}$ values occur in high elevation regions, such as the Tibetan Plateau and the Andes, reflecting the altitude effect.

The $\delta^{18}O_{precip}$ is also affected by the return of moisture to the atmosphere via evapotranspiration, termed precipitation recycling (Salati *et al.*, 1979; Gat, 1996). No overall oxygen isotope fractionation occurs during transpiration (Zimmerman, Ehhalt and Münnich, 1969), so the moisture returned has the same $\delta^{18}O$ values as the precipitation over the locality. This counteracts the effect of rainout and therefore reduces the rate of isotopic depletion along a moisture pathway, minimising the continental effect (Salati *et al.*, 1979). Evaporation from bare soil or surface water bodies produces vapour that is more depleted in ^{18}O. However, this fractionation will have a similar magnitude to the fractionation that occurs with precipitation (unless temperatures are radically different), so the overall impact on Rayleigh distillation should be smaller than transpiration. The impact of recycling on $\delta^{18}O$ therefore depends on the proportion of transpiration to evaporation (depending on plant cover) although it is typically assumed that transpiration dominates continental recycling (Koster, de Valpine and Jouzel, 1993).

Changes in the length and/or configuration of the moisture pathway influence the degree of Rayleigh distillation and therefore, $\delta^{18}O_{precip}$ can be influenced by changes in atmospheric circulation. For example,

stronger monsoon circulation can transport moist air from more distal regions with longer transport pathways, allowing for enhanced Rayleigh distillation (Araguás-Araguás, Froehlich and Rozanski, 1998; Wang *et al.*, 2001). Thus, the $\delta^{18}O$ delivered to the region during an enhanced monsoon will be more depleted (Yuan *et al.*, 2004; Cruz, Burns, *et al.*, 2005; Breitenbach *et al.*, 2010; Cheng *et al.*, 2019). Moisture delivered to a region via different pathways will generally have distinctive $\delta^{8}O_{precip}$ values (Araguás-Araguás, Froehlich and Rozanski, 1998), due to differences in moisture source and degree of rainout along the pathway. Changes in $\delta^{18}O$ can therefore be driven by changes in the dominant moisture pathways to a region. Different air parcels, with their distinct $\delta^{18}O$ values can also mix, further influencing the $\delta^{18}O$ at a site (Araguás-Araguás, Froehlich and Rozanski, 1998; Aggarwal *et al.*, 2004; Sengupta and Sarkar, 2006). This means that $\delta^{18}O_{precip}$ reflects air mass history, driven by atmospheric circulation changes.

In the monsoon regions, ^{18}O depleted moisture from distant ocean sources is delivered in summer, contrasting with the relatively less depleted moisture that is delivered to the region during the winter dry season (Araguás-Araguás, Froehlich and Rozanski, 1998; Wang *et al.*, 2001). In winter, moisture is sourced from a more local ocean source, or from continental air masses. Changes in $\delta^{18}O_{precip}$ values can hence be driven by changes in the ratio of summer to winter precipitation (seasonality), which closely correlates with summer precipitation amount and is analogous to summer monsoon intensity (Wang *et al.*, 2001).

The amount and intensity of precipitation at a site may further influence $\delta^{18}O_{precip}$ values, with higher precipitation amounts driving more depleted $\delta^{18}O_{precip}$ values. This "amount effect" can be explained by the processes of rainfall re-evaporation and diffusive exchange, and recycling of sub-cloud layer vapour by depleted vapour from convective downdrafts (Lee and Fung, 2008; Risi, Bony and Vimeux, 2008).

Since all these processes influence the oxygen isotopic composition of rainfall at a cave site, changes in the $\delta^{18}O$ of precipitation can reflect changes in a) $\delta^{18}O$ of moisture source, b) location of moisture source, c) temperature, humidity and wind speed at the moisture source, d) degree of rainout along a moisture pathway, e) configuration of moisture pathway, f) length of moisture pathway, g) air temperatures along pathway, h) precipitation recycling, i) seasonality and j) precipitation intensity at the locality.

1.4.3 Oxygen isotope processes in the soil, epikarst and cave

Part of the precipitation above a cave site infiltrates into the soil, whilst the remaining fraction is lost to evapotranspiration and runoff. Soil $\delta^{18}O$ therefore represents the amount-weighted mean $\delta^{18}O$ of infiltrating precipitation (Baker *et al.*, 2019). Infiltration often only occurs when the precipitation rate exceeds a threshold (Jones and Banner, 2003; Pape *et al.*, 2010). For sites located in monsoon regions, soil water $\delta^{18}O$ signals will be biased towards the rainy summer seasons. Evaporation from the uppermost part of the soil will enrich the $\delta^{18}O$ values (Gat, 1996; Tang and Feng, 2001). Soil moisture of different ages may mix, further modifying $\delta^{18}O$ values (Comas-Bru and McDermott, 2015).

Soil water percolates down into the epikarst, feeding groundwater. Epikarst water of different origins and ages (with differing $\delta^{18}O$ signals) are stored and mixed (Yonge *et al.*, 1985; Perrin, Jeannin and Zwahlen, 2003). The degree of mixing that occurs depends on the residence time of ground water in the epikarst, which in turn depends on climate factors such as infiltration rates, and physical factors such as the thickness of bedrock overlying the cave and the type of moisture flow through the bedrock (Fairchild and Baker, 2012). Cave monitoring studies suggest that residence times are highly variable amongst drip water sites and between caves, varying from less than a year at sites in e.g. tropical regions where precipitation and infiltration rates are high (Cruz, Karmann, *et al.*, 2005; Cobb *et al.*, 2007), to several decades when cave drip water is fed by slow groundwater seepage (Even *et al.*, 1986). Overall, $\delta^{18}O$ signals of climate variability become attenuated due to mixing in the epikarst, although the degree of attenuation depends on the residence time of water in this zone.

Within the cave, further modification of $\delta^{18}O$ signals occur at the drip water site and during the precipitation of calcium carbonate and the growth of the speleothem (Mickler, Stern and Banner, 2006). Evaporation of drip water may occur when humidity is less than 85 % and the residence time of the drips are sufficiently long (Dreybrodt and Deininger, 2014), resulting in an enrichment of $\delta^{18}O$ values. If speleothem growth occurs under equilibrium conditions, $\delta^{18}O_{spel}$ is controlled by the $\delta^{18}O$ of drip water, mineralogy (i.e. calcite or aragonite; Kim and O'Neil, 1997) and temperature. Cave temperature is generally very stable away from the entrance and corresponds to the mean annual surface air

temperature (MAT) above the cave (Yonge *et al.*, 1985). Although MAT can change through time, the effect on $\delta^{18}O_{spel}$ is very small: approximately -0.2 ‰/°C (Kim and O'Neil, 1997), defined by:

$$1000 \ln \alpha_{(calcite\text{-}water)} = 18.03 (10^3 T^{-1}) - 32.42 \quad 1.3$$

Where 1000 ln $\alpha_{(calcite\text{-}water)}$ is the equilibrium fractionation between drip water and calcite and T is the temperature in kelvin. The effect of changing cave temperature on $\delta^{18}O_{spel}$ is therefore likely to be much smaller than changes in the $\delta^{18}O$ of drip water.

Equilibrium conditions occur when there is sufficient time for isotope exchange to occur. However, if calcium carbonate precipitation is rapid because of rapid CO_2 degassing, equilibrium is not reached. The speed at which CO_2 degassing occurs is dependent on the pCO_2 gradient between the drip water and the cave. The pCO_2 of drip water and the cave are controlled predominantly by soil pCO_2 and cave ventilation (Baldini *et al.*, 2008), respectively. Since this kinetic fractionation modifies the $\delta^{18}O$ signal, it is necessary to determine whether the speleothem grew at (or close to) equilibrium or not. The "Hendy test" is widely used to investigate this by sampling $\delta^{18}O$ and $\delta^{13}C$ (carbon isotopes) along a growth layer (Hendy, 1971): if kinetic isotope fractionation has occurred, $\delta^{18}O$ will increase moving away from the central growth axis, and $\delta^{18}O$ and $\delta^{13}C$ will also covary. However, whilst this test considers whether kinetic isotope fractionation occurred along the whole growth layer, it is possible that calcium carbonate precipitated at equilibrium at the tip of the stalagmite (i.e. at the growth axis) and then underwent rapid degassing and kinetic isotope fractionation away from the growth axis. Furthermore, $\delta^{18}O$ and $\delta^{13}C$ can covary due to climate processes. A speleothem record may therefore fail the Hendy test and yet still have equilibrium growth along its axis.

A different approach to determine whether speleothem records grew at isotopic equilibrium is the replication test (Dorale and Liu, 2009). Speleothems located in different parts of the same cave site are fed by different drip pathways, with distinct drip rates and rates of CO_2 degassing and calcium carbonate precipitation (Dorale and Liu, 2009). These differences between exact speleothem locations can drive differences in $\delta^{18}O_{spel}$ through kinetic fractionation and epikarst processes. If coeval speleothems from

the same cave show the same $\delta^{18}O_{spel}$ values and trends, this suggests that the signals are related to climate.

1.4.4 Interpretation of monsoon speleothem records

Interpretation of speleothem $\delta^{18}O$ records often use modern-day correlations between climate data and $\delta^{18}O_{precip}$ values to determine which climate processes are the most influential drivers of $\delta^{18}O$ variability. The spatial variability of $\delta^{18}O_{precip}$ in the tropics today is strongly correlated to precipitation amount (Dansgaard, 1964; Rozanski, Araguás-Araguás and Gonfiantini, 1993), so tropical speleothem $\delta^{18}O$ records have often been interpreted as a signal of changes in precipitation amount. Speleothem $\delta^{18}O$ records across the ISM (Burns *et al.*, 1998; Yadava, Ramesh and Pant, 2004; Sinha *et al.*, 2005, 2011), EAM (Cai *et al.*, 2010), IAM (Partin *et al.*, 2007; Griffiths *et al.*, 2009a; Carolin *et al.*, 2016; Krause *et al.*, 2019), SAfM (Scroxton et al., 2017), CAM (Lachniet *et al.*, 2004; Bernal *et al.*, 2011; Winter *et al.*, 2020) and SAM (Stríkis *et al.*, 2011; Novello *et al.*, 2017) have all been interpreted as an amount effect signal. Other studies have emphasised the importance of upstream precipitation (i.e. Rayleigh distillation) for monsoon $\delta^{18}O_{spel}$ values, rather than precipitation at the site itself. This interpretation has been put forward for several monsoon regions, including the EAM (Yuan *et al.*, 2004; Hu *et al.*, 2008), SAM (Kanner *et al.*, 2013; Bustamante *et al.*, 2016) and the ISM (Kathayat *et al.*, 2016). Other studies have interpreted speleothem $\delta^{18}O$ changes as a seasonality signal, with more negative $\delta^{18}O_{spel}$ values relating to a higher contribution of summer monsoon rainfall (observed as having characteristically low $\delta^{18}O_{precip}$) to the annual total (Wang *et al.*, 2001, 2005; Dykoski *et al.*, 2005; Cheng, Edwards, *et al.*, 2009). Changes in the dominant moisture pathway, or changes in the length and/or configuration of a moisture pathway (driven by atmospheric circulation changes) have also been suggested as a leading cause of observed monsoon $\delta^{18}O_{spel}$ variability. Changes in moisture pathway have been invoked as influential for $\delta^{18}O_{spel}$ in the ISM (Breitenbach *et al.*, 2010; Myers *et al.*, 2015), EAM (Cheng *et al.*, 2012; Tan, 2014; Zhao *et al.*, 2019) and IAM (Griffiths *et al.*, 2009b; Wurtzel *et al.*, 2018), supported by back-trajectory analyses. A stronger summer monsoon can drive more negative $\delta^{18}O_{spel}$ values through a combination of all these processes, including increased precipitation amounts (both local, regional and upstream), enhanced seasonality and a longer moisture

pathway (with stronger summer monsoon circulation) so these various interpretations are not necessarily contradictory.

However, understanding which processes contribute to observed $\delta^{18}O_{spel}$ changes is important to contextualise the records within the overall picture of past monsoon climate change. Furthermore, accurate and precise interpretation of the speleothem records allows them to be effectively compared to other palaeoclimate archives that record the same processes. For example, if $\delta^{18}O_{spel}$ records are significantly influenced by atmospheric circulation changes, they could be compared to wind-based palaeoclimate archives such as marine records of upwelling or dust records. If records reflect precipitation changes, they would be best compared to lake-level records, tree ring width and pollen-based precipitation reconstructions. Furthermore, these different processes can become decoupled at different times in the past. The amount of precipitation in eastern China, for example, is not coupled to EAM intensity (Cheng *et al.*, 2012), due to the complex summer EAM rainfall advance, suggesting that EAM speleothems may reflect atmospheric circulation changes rather than precipitation. One aspect of this thesis is to explore whether it is possible to determine which processes are important in explaining changes in $\delta^{18}O_{spel}$ in different regions using data-model comparisons and statistical approaches.

1.5 The SISAL database

The SISAL (Speleothem Isotopes Synthesis and AnaLysis) database contains oxygen and carbon isotope records worldwide (Atsawawaranunt *et al.*, 2018; Comas-Bru *et al.*, 2020). Version 2 (SISALv2) of the database (Comas-Bru *et al.*, 2020) contains 353,969 $\delta^{18}O$ measurements from 676 individual speleothem records and 15 composites (both referred to as entities). These records are distributed globally across 293 sites (Fig. 1.11). The database contains approximately 72 % of published records identified by the SISAL working group, considerably more than any other repository.

The database includes key metadata (Fig. 1.12), facilitating quality control. For example, cave site elevation data allows users to identify (and exclude or correct for) high elevation sites where $\delta^{18}O$ values have high magnitudes (relative to other records) due to the altitude effect. The mineralogy of speleothem samples is also given (calcite, aragonite, mixed), allowing users to account for the different isotope fractionation of these mineralogies.

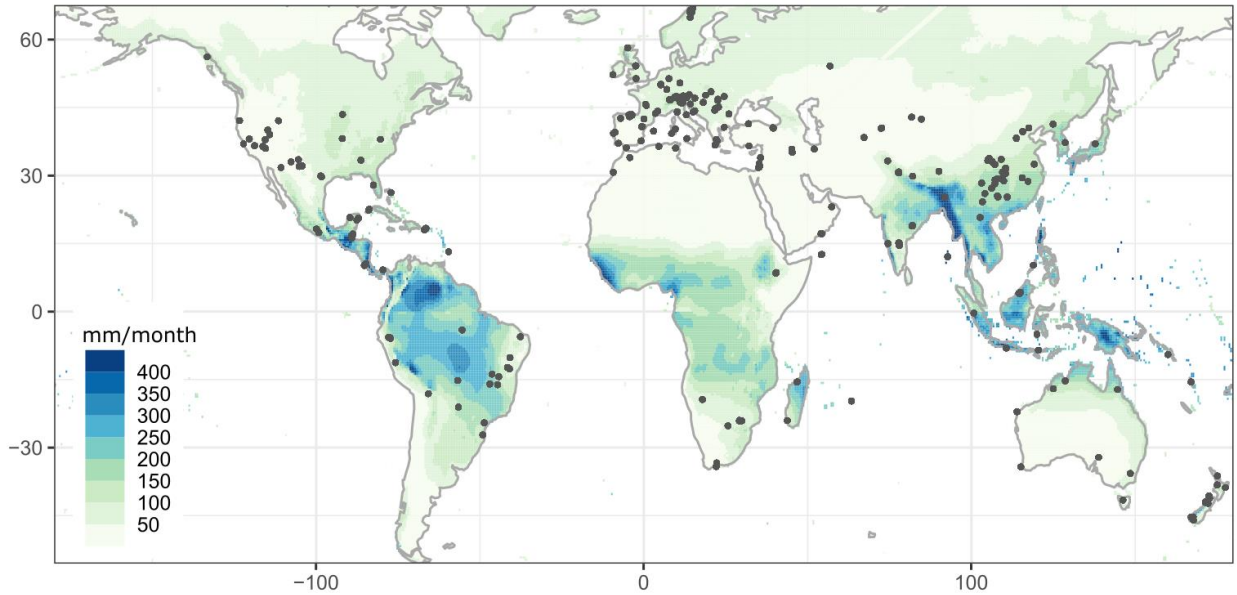

Figure 1.11 Spatial distribution of speleothem records in the SISAL version 2 database, shown with summer precipitation rate (mm/month), where summer is May to September in the northern hemisphere and November to March in the southern hemisphere.

SISALv2 also includes new chronologies, from seven different age-depth modelling approaches: linear interpolation, linear regression, Bchron, Bacon, OxCal, COPRA and StalAge. These SISAL chronologies include age uncertainties, obtained using the 95 % confidence intervals from the age-depth models. This is a significant advantage of the database because the majority of speleothem records in the database (79 %) had no age uncertainty data provided in the original publications. Comparison across the different SISALv2 age modelling approaches give a fuller picture of age uncertainty, which is crucial for assessing the timing and synchronicity of past climate change, especially on timescales smaller than the typical age uncertainties of speleothem records.

The spatial distribution of SISAL $\delta^{18}O$ records is generally good for the monsoon regions (Fig. 1.11), with the exception of the core of the WAfM. The temporal distribution of data (Fig. 1.13) is good for the Holocene epoch (11,700 years BP to present), although data availability beyond this period deteriorates.

There are only 40 records from the tropics (30°S to 30°N) spanning the Last Glacial Maximum period from 20.5 to 21.5 ka, for example, and 8 records spanning the Last Interglacial period from 126.5 to 127.5 ka.

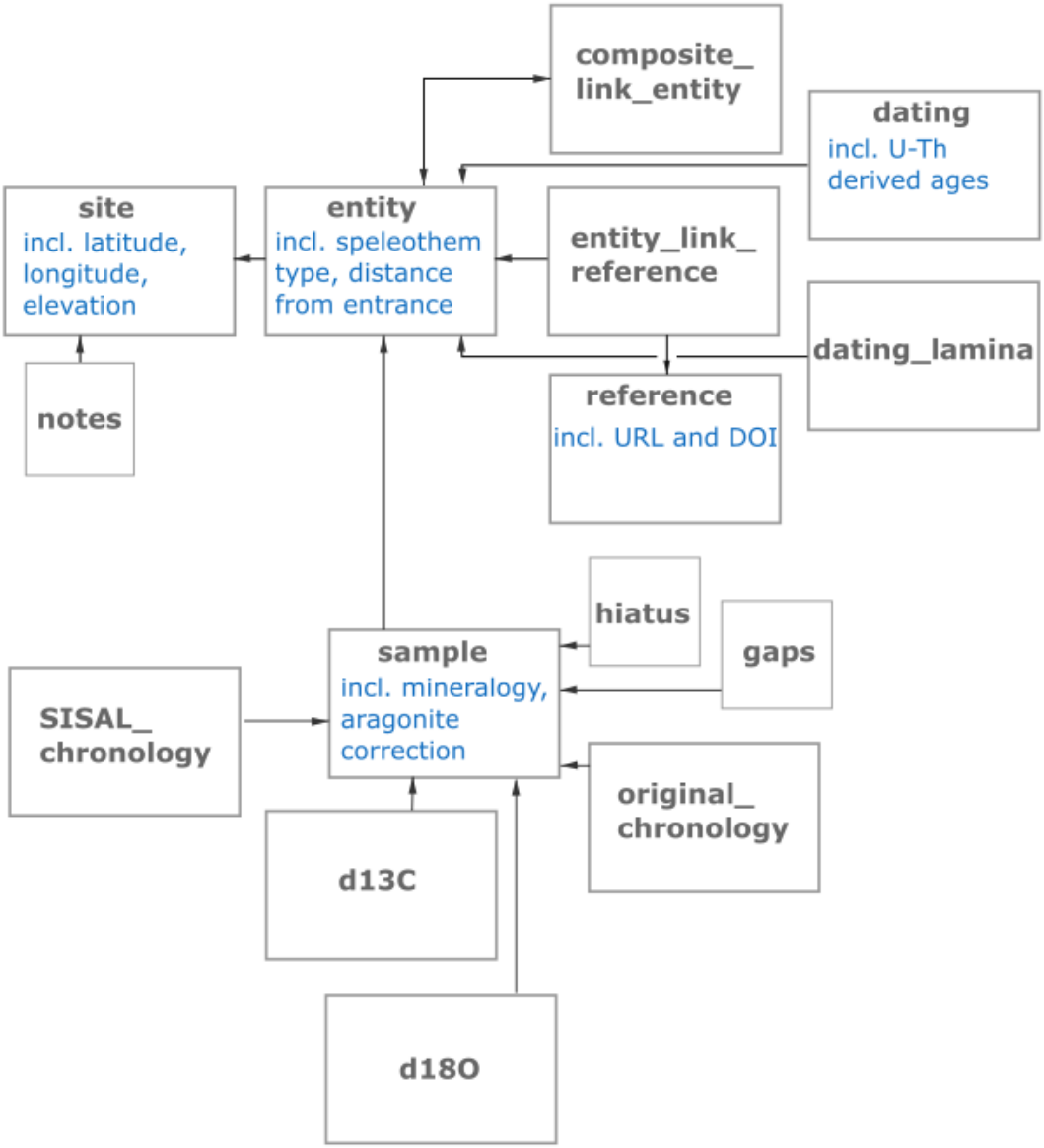

Figure 1.12 The structure and contents of the SISAL version 2 database, including the table names and some of the key variables included. For more detail, see Comas-Bru et al. (2020).

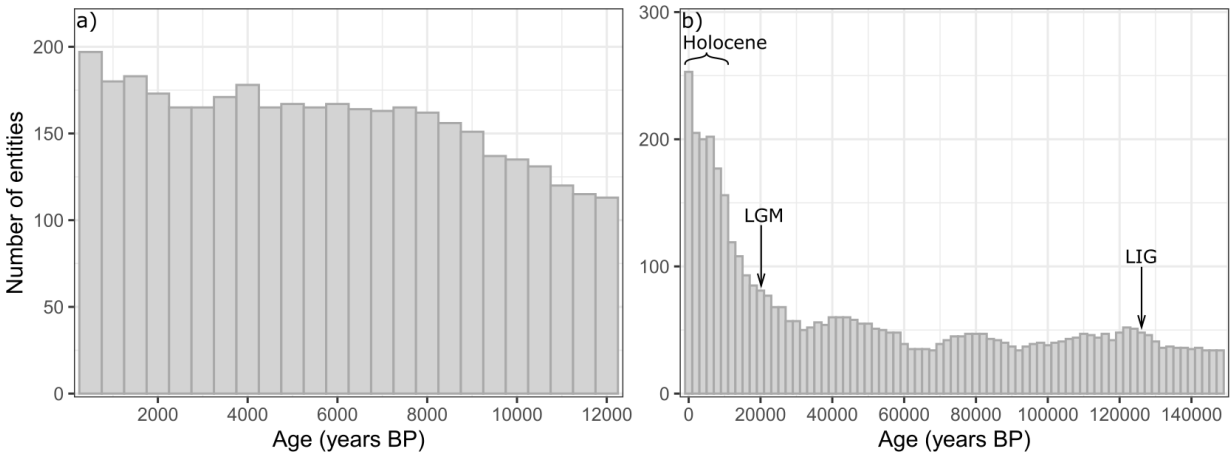

Figure 1.13 Temporal distribution of speleothem $\delta^{18}O$ data in the SISAL version 2 database, spanning a) the Holocene, using 200-year bins and b) the last 135,000 years, using 2,000 years bins. Key time periods examined in this thesis are indicated.

1.6 Data-model comparisons

1.6.1 Climate models

Global climate models represent the physical processes of the climate system in a numerical way, where the planet is represented using horizontal grids and vertical levels (McGuffie *et al.*, 2014). The model dynamics include equations expressing the conservation of momentum, energy and mass. Processes that occur on a smaller scale than a model grid box are dealt with using parameterisations, whereby sub-grid quantities are transformed to grid-scale quantities. For example, convective cloud systems, which develop over an area of a few kilometres, are parametrised to represent the mean precipitation and energy release over the entire grid. The earliest climate models only simulated the atmosphere and other components of the climate system were prescribed. Later versions of these models include representation of the oceans and ocean circulation, the cryosphere, and the land surface including vegetation growth and dynamics. These components can be combined to dynamically interact with one another in Earth System Models.

Numerous palaeoclimate simulations have been run using climate models. Most simulations are run as equilibrium experiments, whereby boundary conditions (orbital configuration, trace gases, ice sheets etc.) are prescribed, then the simulation is run for sufficiently long to reach an equilibrium state under these conditions. These provide “snapshot” pictures of past climate conditions. The Palaeoclimate Modelling

Intercomparison Project (PMIP) has coordinated experiments for key time periods with standardised experimental protocols that can be run by multiple modelling groups (Joussaume and Taylor, 1995; Joussaume *et al.*, 1999; Braconnot *et al.*, 2007a; Braconnot *et al.*, 2007b; Kageyama *et al.*, 2018), including the mid and early Holocene (Braconnot *et al.*, 2004; Marzin and Braconnot, 2009; Brierley *et al.*, 2020), the Last Glacial Maximum (Kageyama, Harrison and Abe-Ouchi, 2005; Kageyama *et al.*, 2021), Last Interglacial (Otto-Bliesner *et al.*, 2021) and the mid-Pliocene warm period (Haywood *et al.*, 2011). Transient experiments provide a picture of the evolution of climate through time by prescribing changing boundary conditions at regular intervals (i.e., every decade or annually). There are far fewer transient palaeoclimate simulations than there are equilibrium experiments because they are computationally expensive to run. However, transient palaeoclimate experiments provide a unique perspective on climate changes that is not possible with snapshot experiments, including information about the linkage between modes of climate variability and the slow evolution of the climate system in response to external forcing. PMIP includes transient simulations of the last millennium (Jungclaus *et al.*, 2017), where changing orbital, solar, volcanic and land-use/cover boundary conditions are prescribed. This experiment provides insight into the contributions of internal variability versus external forcing under conditions that are similar to today. On longer timescales, the Trace-21ka transient experiments have simulated climate evolution spanning the Last Glacial Maximum, the deglaciation and the Holocene (Liu *et al.*, 2009). An ensemble of mid-Holocene to present transient simulations have been run by the PACMEDY (PAlaeo-Constraints on Monsoon Evolution and Dynamics) project (Braconnot, Zhu, *et al.*, 2019; Bader *et al.*, 2020; Shi *et al.*, 2021) to investigate monsoon dynamics. Working groups within PMIP are currently running transient simulations of the deglaciation (21 to 9 ka) (Ivanovic *et al.*, 2016) and the penultimate deglaciation (140 to 127 ka) (Menviel *et al.*, 2019). These simulations will provide insights into the climate response to the large changes in boundary conditions that occur through these deglaciations, including orbital configuration, greenhouse gases, ice sheet geometry and meltwater fluxes. Transient simulations for the glacial period (Menviel *et al.*, 2014; Menviel, Spence and England, 2015; Bagniewski, Meissner and Menviel, 2017) have been used to investigate Dansgaard-Oeschger cycles and Heinrich events.

1.6.2 Isotope-enabled simulations

Speleothem $\delta^{18}O$ records can be compared with simulated changes in monsoon climate variables (e.g. regional precipitation) (Flohr *et al.*, 2017; Voarintsoa *et al.*, 2019; Zhang *et al.*, 2021), although these comparisons are not direct. However, some climate models now include stable water isotope tracers, enabling direct data-model comparisons with isotope records (Comas-Bru *et al.*, 2019; Hu *et al.*, 2019; Bühler *et al.*, 2021). In an isotope-enabled model, isotope tracers are incorporated into all aspects of the climate model that include water (Sturm, Zhang and Noone, 2010). Processes of equilibrium and kinetic isotope fractionation, Rayleigh distillation and mixing lines are included. Isotope processes are generally well-understood and are therefore a minimal source of uncertainty in model outputs. Inaccuracies in isotope-enabled simulations usually relate to the misrepresentation of physical processes (Caley and Roche, 2013; Risi et al., 2010). For example, inaccurately simulated precipitation over a region will translate into inaccurate $\delta^{18}O_{precip}$ values.

Isotope-enabled climate models have been widely used to simulate $\delta^{18}O$ under present conditions (Lee *et al.*, 2007; Caley and Roche, 2013) but only a few simulations have been made for past climates. Equilibrium experiments have been made with isotope-enabled models of the mid-Holocene, Last Glacial Maximum, Last Interglacial and idealised Heinrich events (Risi *et al.*, 2010; Pausata *et al.*, 2011; Wackerbarth *et al.*, 2012; Holloway *et al.*, 2016; Werner *et al.*, 2016, 2018; Gierz, Werner and Lohmann, 2017; Cauquoin, Werner and Lohmann, 2019).

1.6.3 What can be learnt from data-model comparisons?

Palaeoclimate simulations have provided valuable insight into climate under significantly different conditions from today. They provide detailed and quantitative climate values, enabling investigation of the processes and mechanisms of climate change. However, despite ongoing improvements, climate models do not fully and accurately represent all climate processes and are known to underestimate regional climate changes in the past (Braconnot *et al.*, 2012; Harrison *et al.*, 2014; Harrison *et al.*, 2015). Palaeoclimate archives (including speleothems) document what actually happened in the past but it may be difficult to explain the observed changes because they can influenced by multiple climate factors and

non-climate processes. Models and palaeoclimate data have therefore often been used together to gain a better understanding of past climate change.

Observations have often been used to evaluate the accuracy of palaeoclimate simulations. Accurate climate features in a simulation suggest that the model can provide a physically plausible underlying conceptual explanation. Some of the earliest work that employed this data-model comparison approach was carried out by the Cooperative Holocene Mapping Project (COHMAP) (COHMAP Members, 1988). COHMAP created large-scale syntheses of palaeoclimate (pollen and lake-status) data to reconstruct global climate at 3,000 year intervals over the last 18,000 years (Kutzbach and Street-Perrott, 1985). Model experiments in COHMAP showed that the orbitally induced increase in summer insolation over the northern hemisphere caused enhanced summer monsoon rainfall, including the northwards expansion of lakes in north Africa. Since COHMAP, palaeo-data syntheses have become larger and more numerous. Palaeoclimate simulations have become more complex, with higher resolutions, allowing data-model comparison research to develop further. Later studies have continued to confirm to close relationship between orbitally induced insolation changes and the monsoons (Marzin and Braconnot, 2009; Dallmeyer *et al.*, 2015; Brierley *et al.*, 2020). Data-model comparisons have also been used to demonstrate the importance of internal feedbacks. For example, climate model simulations of the mid-Holocene WAfM expansion show better agreement with palaeo-records when both orbital changes and realistic changes in vegetation and soil are incorporated, compared to orbital forcing only simulations (Kutzbach *et al.*, 1996; Claussen and Gayler, 1997). These data-model comparison studies demonstrate the significant influence of land-surface feedbacks on the Holocene evolution of the WAfM, something that could not have been inferred from palaeo-records alone. Numerous data-model comparison studies have shown the importance of land-surface, ocean and ice-sheet feedbacks in producing observed past changes in monsoon climates (Texier *et al.*, 1997; Ganopolski *et al.*, 1998; Peyron *et al.*, 2006; Zhao and Harrison, 2012; Chandan and Peltier, 2020). This data-model comparison approach has not been much used in speleothem research, in large part because no globally comprehensive and coordinated synthesis of speleothem data existed until SISAL version 1 was published in 2018 (Atsawawaranunt *et al.*, 2018). The increasing number of isotope-enabled model simulations allows for a direct comparison with speleothem

$\delta^{18}O$ records (Comas-Bru *et al.*, 2019). Speleothem system models (modelling $\delta^{18}O$ changes in the soil, epikarst and cave) have also provided a means of more directly comparing models (simulated $\delta^{18}O_{precip}$) with $\delta^{18}O_{spel}$ observations (Wackerbarth *et al.*, 2012). Several studies have compared isotope-enabled simulations with speleothem records to evaluate the accuracy of climate models (Wackerbarth *et al.*, 2012; Gierz, Werner and Lohmann, 2017; Comas-Bru *et al.*, 2019), however speleothem data-model comparison research can also provide valuable insight into $\delta^{18}O_{precip}$-climate relationships under past conditions and therefore aid the interpretation of $\delta^{18}O_{spel}$ records. Many speleothem studies use present-day relationships between climate and $\delta^{18}O$ (observed in spatial patterns and on intraseasonal to interannual timescales) to interpret speleothem $\delta^{18}O$ records, however these relationships may have been different in the past, when moisture sources and pathways were different. A few studies have carried out data-model comparisons to provide a better understanding of the processes and drivers of past $\delta^{18}O_{spel}$ variability (e.g. LeGrande and Schmidt, 2009; Lewis *et al.*, 2010; Tabor *et al.*, 2018; Hu *et al.*, 2019), but these studies generally use a limited number of speleothem records and often only focus on one monsoon region. In this thesis, a large number of speleothem records (facilitated by the SISAL database) are compared with climate model simulations across several monsoon regions to develop explanations for the past changes in monsoon climate.

1.7 Thesis aims and structure

This thesis exploits the SISAL database, together with climate model simulations, to reconstruct and investigate past monsoon variability. It addresses several of the gaps outlined in the previous sections, including the investigation of what drove $\delta^{18}O_{spel}$ in the past, investigating the influence of orbital forcing versus internal feedbacks, and the identification and examination of abrupt events.

This thesis is presented as three stand-alone papers, formatted in the style of the journals to which they were submitted.

Chapter 2 consists of the following paper:

Parker, S.E., Harrison, S.P., Comas-Bru, L., Kaushal, N., LeGrande, A.N. & Werner, M., 2021. A data–model approach to interpreting speleothem oxygen isotope records from monsoon regions. *Climate of the Past,* 17(3), 1119-1138, https://doi.org/10.5194/cp-17-1119-2021.

This paper explores the regional and global monsoon variability through the Holocene epoch and between the mid-Holocene, Last Glacial Maximum and Last Interglacial, to investigate the influence of orbitally induced insolation changes. Regional speleothem trends were compared to isotope-enabled climate models, to investigate the climate drivers of $\delta^{18}O_{spel}$ trends. The specific objectives were:

- To investigate the coherency of monsoon $\delta^{18}O_{spel}$ records at the regional and global-scale, and the coherency between regional trends and summer insolation. Comparisons separate out the importance of orbitally driven insolation changes driving a global monsoon response versus the internal feedbacks causing regional differences.
- To identify the plausible drivers of past $\delta^{18}O_{spel}$ variability, by comparing regional $\delta^{18}O_{spel}$ with simulated changes in regional $\delta^{18}O_{precip}$ and key climate variables including precipitation, air temperature, recycling, and atmospheric circulation.

Chapter 3 consists of the following paper:

Parker, S.E., Harrison, S.P. and Braconnot, P., 2021. Speleothem records of monsoon interannual-interdecadal variability through the Holocene. *Environmental Research Communications,* 3(12), 121002, https://doi.org/10.1088/2515-7620/ac3eaa.

This paper provides regional composites of changes in the amplitude of interannual-interdecadal variability as recorded by speleothems through the Holocene epoch. This is the first time that speleothem records have been used to document changes in interannual-interdecadal variability at a composite regional level. These reconstructions were compared to an ensemble of transient Holocene climate model simulations. This chapter addresses two specific objectives:

- To investigate if site-specific confounding factors influence regional composite interannual-interdecadal reconstructions.
- To investigate the relationship between orbitally induced insolation changes through the Holocene and monsoon interannual-interdecadal variability.

Chapter 4 consists of the following paper:

Parker, S.E. and Harrison, S.P. 2022. The timing, duration and magnitude of the 8.2 ka event in global speleothem records. *Scientific Reports,* 12(10542), https://doi.org/10.1038/s41598-022-14684-y.

The study investigates the presence and significance of abrupt events in the Holocene. It provides a global synthesis of $\delta^{18}O_{spel}$ anomalies associated with the 8.2 ka abrupt cold event. The following objectives were addressed:

- To identify the globally significant events of the Holocene epoch
- To investigate the palaeomonsoon response to abrupt events: is there a global monsoon pattern or do regional distinctions exist?
- To assess the rapidity at which abrupt event signals are transmitted globally and therefore elucidate the responsible teleconnections

1.8 References

Abram, N. J. *et al.* (2007) 'Seasonal characteristics of the Indian Ocean Dipole during the Holocene epoch', *Nature*, 445(7125), pp. 299–302. doi: 10.1038/nature05477.

Abram, N. J. *et al.* (2015) 'Optimized coral reconstructions of the Indian Ocean Dipole: An assessment of location and length considerations', *Paleoceanography*, 30(10), pp. 1391–1405. doi: 10.1002/2015PA002810.

Adams, D. K. and Comrie, A. C. (1997) 'The North American Monsoon', *Bulletin of the American*

Meteorological Society, 78(10), pp. 2197–2213. doi: 10.1175/1520-0477(1997)078<2197:TNAM>2.0.CO;2.

Affolter, S. *et al.* (2019) 'Central Europe temperature constrained by speleothem fluid inclusion water isotopes over the past 14,000 years', *Science advances*, 5(6), p. eaav3809.

Aggarwal, P. K. *et al.* (2004) 'Stable isotope evidence for moisture sources in the asian summer monsoon under present and past climate regimes', *Geophysical Research Letters*, 31(8), pp. 2–5. doi: 10.1029/2004GL019911.

Aggarwal, P. K. *et al.* (2012) 'Stable isotopes in global precipitation: A unified interpretation based on atmospheric moisture residence time', *Geophysical Research Letters*, 39(11). doi: 10.1029/2012GL051937.

Aguiar, W. *et al.* (2021) 'Magnitude of the 8.2 ka event freshwater forcing based on stable isotope modelling and comparison to future Greenland melting', *Scientific Reports*, 11(1), p. 5473. doi: 10.1038/s41598-021-84709-5.

Allan, M. *et al.* (2018) 'High-resolution reconstruction of 8.2-ka BP event documented in Père Noël cave, southern Belgium', *Journal of Quaternary Science*, 33(7), pp. 840–852. doi: 10.1002/jqs.3064.

Alley, R. B. *et al.* (1997) 'Holocene climatic instability: A prominent, widespread event 8200 yr ago', *Geology*, 25(6), pp. 483–486. doi: 10.1130/0091-7613(1997)025<0483:HCIAPW>2.3.CO;2.

Amador, J. A. (2008) 'The Intra-Americas Sea low-level jet: Overview and future research', *Annals of the New York Academy of Sciences*, 1146, pp. 153–188. doi: 10.1196/annals.1446.012.

Andreoli, R. V. and Kayano, M. T. (2005) 'ENSO-related rainfall anomalies in South America and associated circulation features during warm and cold Pacific decadal oscillation regimes', *International Journal of Climatology*, 25(15), pp. 2017–2030. doi: 10.1002/joc.1222.

Aragão, L. E. O. C. *et al.* (2018) '21st Century drought-related fires counteract the decline of Amazon

deforestation carbon emissions', *Nature Communications*, 9(1), p. 536. doi: 10.1038/s41467-017-02771-y.

Araguás-Araguás, L., Froehlich, K. and Rozanski, K. (1998) 'Stable isotope composition of precipitation over southeast Asia', *Journal of Geophysical Research Atmospheres*, 103(D22), pp. 28721–28742. doi: 10.1029/98JD02582.

Ashok, K., Guan, Z. and Yamagata, T. (2001) 'Impact of the Indian Ocean dipole on the relationship between the Indian monsoon rainfall and ENSO', *Geophysical Research Letters*, 28(23), pp. 4499–4502. doi: 10.1029/2001GL013294.

Asmerom, Y. *et al.* (2007) 'Solar forcing of Holocene climate: New insights from a speleothem record, southwestern United States', *Geology*, 35(1), p. 1. doi: 10.1130/G22865A.1.

Atsawawaranunt, K. *et al.* (2018) 'The SISAL database: A global resource to document oxygen and carbon isotope records from speleothems', *Earth System Science Data*, 10, pp. 1687–1713. doi: 10.5194/essd-10-1687-2018.

Ayliffe, L. K. *et al.* (2013) 'Rapid interhemispheric climate links via the Australasian monsoon during the last deglaciation', *Nature Communications*, 4(1), pp. 1–6. doi: 10.1038/ncomms3908.

Bader, J. *et al.* (2020) 'Global temperature modes shed light on the Holocene temperature conundrum', *Nature Communications*, 11(1), p. 4726. doi: 10.1038/s41467-020-18478-6.

Bagniewski, W., Meissner, K. J. and Menviel, L. (2017) 'Exploring the oxygen isotope fingerprint of Dansgaard-Oeschger variability and Heinrich events', *Quaternary Science Reviews*, 159, pp. 1–14. doi: 10.1016/j.quascirev.2017.01.007.

Bailey, A., Posmentier, E. and Feng, X. (2018) 'Patterns of evaporation and precipitation drive global isotopic changes in atmospheric moisture', *Geophysical Research Letters*, 45(14). doi: 10.1029/2018GL078254.

Baker, A. *et al.* (2008) 'Annually laminated speleothems: a review', *International Journal of Speleology*, 37(3), pp. 193–206. doi: 10.5038/1827-806X.37.3.4.

Baker, A. *et al.* (2019) 'Global analysis reveals climatic controls on the oxygen isotope composition of cave drip water', *Nature Communications*, 10(2984). doi: 10.1038/s41467-019-11027-w.

Baker, P. A. *et al.* (2005) 'Holocene hydrologic variation at Lake Titicaca, Bolivia/Peru, and its relationship to North Atlantic climate variation', *Journal of Quaternary Science*, 20(7–8), pp. 655–662. doi: 10.1002/jqs.987.

Baldini, J. U. L. *et al.* (2008) 'Very high-frequency and seasonal cave atmosphere P_{CO2} variability: Implications for stalagmite growth and oxygen isotope-based paleoclimate records', *Earth and Planetary Science Letters*, 272(1–2), pp. 118–129. doi: 10.1016/j.epsl.2008.04.031.

Bar-Matthews, M. *et al.* (2003) 'Sea–land oxygen isotopic relationships from planktonic foraminifera and speleothems in the Eastern Mediterranean region and their implication for paleorainfall during interglacial intervals', *Geochimica et Cosmochimica Acta*, 67(17), pp. 3181–3199. doi: 10.1016/S0016-7037(02)01031-1.

Bar-Matthews, M., Ayalon, A. and Kaufman, A. (1997) 'Late Quaternary paleoclimate in the eastern Mediterranean region from stable isotope analysis of speleothems at Soreq Cave, Israel', *Quaternary Research*, 47(2), pp. 155–168. doi: 10.1006/qres.1997.1883.

Barber, D. C. *et al.* (1999) 'Forcing of the cold event of 8,200 years ago by catastrophic drainage of Laurentide lakes', *Nature*, 400(6742), pp. 344–348. doi: 10.1038/22504.

Barichivich, J. *et al.* (2018) 'Recent intensification of Amazon flooding extremes driven by strengthened Walker circulation', *Science Advances*, 4(9). doi: 10.1126/sciadv.aat8785.

Barlow, M., Nigam, S. and Berbery, E. H. (1998) 'Evolution of the North American monsoon system', *Journal of Climate*, 11(9), pp. 2238–2257. doi: 10.1175/1520-0442(1998)011<2238:EOTNAM>2.0.CO;2.

Bartlein, P. J., Harrison, S. P. and Izumi, K. (2017) 'Underlying causes of Eurasian midcontinental aridity in simulations of mid-Holocene climate', *Geophysical Research Letters*, 44(17), pp. 9020–9028. doi: 10.1002/2017GL074476.

Battisti, D. S., Ding, Q. and Roe, G. H. (2014) 'Coherent pan-Asian climatic and isotopic response to orbital forcing of tropical insolation', *Journal of Geophysical Research: Atmospheres*, 119(21), pp. 11,997-12,020. doi: 10.1002/2014JD021960.

Benson, A. *et al.* (2021) 'A speleothem record from Portugal reveals phases of increased winter precipitation in western Iberia during the Holocene', *Holocene*, 31(8), pp. 1339–1350. doi: 10.1177/09596836211011666.

Berbery, E. H. and Barros, V. R. (2002) 'The hydrologic cycle of the La Plata basin in South America', *Journal of Hydrometeorology*, 3(6), pp. 630–645. doi: 10.1175/1525-7541(2002)003<0630:THCOTL>2.0.CO;2.

Berkelhammer, M. *et al.* (2010) 'Persistent multidecadal power of the Indian Summer Monsoon', *Earth and Planetary Science Letters*, 290(1–2), pp. 166–172. doi: 10.1016/j.epsl.2009.12.017.

Bernal, J. P. *et al.* (2011) 'A speleothem record of Holocene climate variability from southwestern Mexico', *Quaternary Research*, 75(1), pp. 104–113. doi: 10.1016/j.yqres.2010.09.002.

Bernal, J. P. *et al.* (2016) 'High-resolution Holocene South American monsoon history recorded by a speleothem from Botuverá Cave, Brazil', *Earth and Planetary Science Letters*, 450, pp. 186–196.

Biasutti, M. *et al.* (2018) 'Global energetics and local physics as drivers of past, present and future monsoons', *Nature Geoscience*, 11(6), pp. 392–400. doi: 10.1038/s41561-018-0137-1.

Bini, M. *et al.* (2019) 'The 4.2 ka BP Event in the Mediterranean region: an overview', *Climate of the Past*, 15(2), pp. 555–577. doi: 10.5194/cp-15-555-2019.

Boch, R., Spötl, C. and Kramers, J. (2009) 'High-resolution isotope records of early Holocene rapid

climate change from two coeval stalagmites of Katerloch Cave, Austria', *Quaternary Science Reviews*, 28(23–24), pp. 2527–2538. doi: 10.1016/j.quascirev.2009.05.015.

Bond, G. *et al.* (1997) 'A pervasive millennial-scale cycle in North Atlantic Holocene and glacial climates', *Science*, 278(5341), pp. 1257–1266. doi: 10.1126/science.278.5341.1257.

Bond, G. *et al.* (2001) 'Persistent Solar Influence on North Atlantic Climate During the Holocene', *Science*, 294(5549), pp. 2130–2136. doi: 10.1126/science.1065680.

Bowen, G. J. and Revenaugh, J. (2003) 'Interpolating the isotopic composition of modern meteoric precipitation', *Water Resources Research*, 39(10). doi: 10.1029/2003WR002086.

Boyd, M. (2015) *Speleothems from warm climates: holocene records from the Caribbean and Mediterranean regions*. Stockholm University.

Braconnot, P. *et al.* (2004) 'Evaluation of PMIP coupled ocean-atmosphere simulations of the Mid-Holocene', in Battarbee, R. W., Gasse, F., and Stickley, C. E. (eds) *Past Climate Variability through Europe and Africa. Developments in Paleoenvironmental Research*. Dordrecht: Springer, pp. 515–533. doi: 10.1007/978-1-4020-2121-3_24.

Braconnot, P., Crétat, J., *et al.* (2019) 'Impact of multiscale variability on last 6000 years Indian and West African monsoon rain', *Geophysical Research Letters*, 46(23), pp. 14021–14029. doi: 10.1029/2019GL084797.

Braconnot, P., Zhu, D., *et al.* (2019) 'Strengths and challenges for transient Mid- to Late Holocene simulations with dynamical vegetation', *Climate of the Past*, 15(3), pp. 997–1024. doi: 10.5194/cp-15-997-2019.

Bradley, C. *et al.* (2010) 'Hydrological uncertainties in the modelling of cave drip-water $\delta^{18}O$ and the implications for stalagmite palaeoclimate reconstructions', *Quaternary Science Reviews*, 29(17–18), pp. 2201–2214. doi: 10.1016/j.quascirev.2010.05.017.

Braun, K. *et al.* (2019) 'Late Pleistocene records of speleothem stable isotopic compositions from Pinnacle Point on the South African south coast', *Quaternary Research (United States)*, 91(1), pp. 265–288. doi: 10.1017/qua.2018.61.

Breitenbach, S. F. M. *et al.* (2010) 'Strong influence of water vapor source dynamics on stable isotopes in precipitation observed in Southern Meghalaya, NE India', *Earth and Planetary Science Letters*, 292(1–2), pp. 212–220. doi: 10.1016/j.epsl.2010.01.038.

Brierley, C. M. *et al.* (2020) 'Large-scale features and evaluation of the PMIP4-CMIP6 *midHolocene* simulations', *Climate of the Past*, 16(5), pp. 1847–1872. doi: 10.5194/cp-16-1847-2020.

Brücher, T. *et al.* (2014) 'Comparing modelled fire dynamics with charcoal records for the Holocene', *Climate of the Past*, 10(2), pp. 811–824. doi: 10.5194/cp-10-811-2014.

Bühler, J. C. *et al.* (2021) 'Comparison of the oxygen isotope signatures in speleothem records and iHadCM3 model simulations for the last millennium', *Climate of the Past*, 17(3), pp. 985–1004. doi: 10.5194/cp-17-985-2021.

Burns, S. J. *et al.* (1998) 'Speleothem-based paleoclimate record from northern Oman', *Geology*, 26(6), p. 499. doi: 10.1130/0091-7613(1998)026<0499:SBPRFN>2.3.CO;2.

Bustamante, M. G. *et al.* (2016) 'Holocene changes in monsoon precipitation in the Andes of NE Peru based on $\delta^{18}O$ speleothem records', *Quaternary Science Reviews*, 146, pp. 274–287. doi: 10.1016/J.QUASCIREV.2016.05.023.

Cai, W. *et al.* (2020) 'Climate impacts of the El Niño–Southern Oscillation on South America', *Nature Reviews Earth & Environment*, 1(4), pp. 215–231. doi: 10.1038/s43017-020-0040-3.

Cai, Y. *et al.* (2010) 'The variation of summer monsoon precipitation in central China since the last deglaciation', *Earth and Planetary Science Letters*, 291(1–4), pp. 21–31. doi: 10.1016/j.epsl.2009.12.039.

Cai, Y. *et al.* (2015) 'Variability of stalagmite-inferred Indian monsoon precipitation over the past

252,000 y', *Proceedings of the National Academy of Sciences of the United States of America*, 112(10), pp. 2954–2959. doi: 10.1073/pnas.1424035112.

Cai, Y. *et al.* (2021) 'Holocene variability of East Asian summer monsoon as viewed from the speleothem $\delta^{18}O$ records in central China', *Earth and Planetary Science Letters*, 558. doi: 10.1016/j.epsl.2021.116758.

Caley, T. and Roche, D. M. (2013) 'δ18O water isotope in the LOVECLIM model (version 1.0)-Part 3: A palaeo-perspective based on present-day data-model comparison for oxygen stable isotopes in carbonates', *Geoscientific Model Development*, 6, pp. 1505–1516. doi: 10.5194/gmd-6-1505-2013.

Carolin, S. A. *et al.* (2016) 'Northern Borneo stalagmite records reveal West Pacific hydroclimate across MIS 5 and 6', *Earth and Planetary Science Letters*, 439, pp. 182–193. doi: 10.1016/j.epsl.2016.01.028.

Carré, M. *et al.* (2021) 'High-resolution marine data and transient simulations support orbital forcing of ENSO amplitude since the mid-Holocene', *Quaternary Science Reviews*, 268, p. 107125. doi: 10.1016/j.quascirev.2021.107125.

Cauquoin, A., Werner, M. and Lohmann, G. (2019) 'Water isotopes-climate relationships for the mid-Holocene and preindustrial period simulated with an isotope-enabled version of MPI-ESM', *Climate of the Past*, 15(6), pp. 1913–1937. doi: 10.5194/cp-2019-72.

Chandan, D. and Peltier, W. R. (2020) 'African Humid Period Precipitation Sustained by Robust Vegetation, Soil, and Lake Feedbacks', *Geophysical Research Letters*, 47(21). doi: 10.1029/2020GL088728.

Chawchai, S. *et al.* (2021) 'Hydroclimate variability of central Indo-Pacific region during the Holocene', *Quaternary Science Reviews*, 253. doi: 10.1016/j.quascirev.2020.106779.

Chen, C., Zhao, W. and Zhang, X. (2021) 'Pacific Decadal Oscillation-like variability at a millennial timescale during the Holocene', *Global and Planetary Change*, 103448. doi: 10.1016/j.gloplacha.2021.103448.

Chen, S. *et al.* (2016) 'A high-resolution speleothem record of western equatorial Pacific rainfall: Implications for Holocene ENSO evolution', *Earth and Planetary Science Letters*, 442, pp. 61–71. doi: 10.1016/j.epsl.2016.02.050.

Chen, W. *et al.* (2020) 'Feedbacks of soil properties on vegetation during the Green Sahara period', *Quaternary Science Reviews*, 240, p. 106389. doi: 10.1016/j.quascirev.2020.106389.

Cheng, H. *et al.* (2006) 'A penultimate glacial monsoon record from Hulu Cave and two-phase glacial terminations', *Geology*, 34(3), pp. 217–220. doi: 10.1130/G22289.1.

Cheng, H., Edwards, R. L., *et al.* (2009) 'Ice age terminations', *Science*, 326(5950), pp. 248–252. doi: 10.1126/science.1177840.

Cheng, H., Fleitmann, D., Edwards, R. L., Wang, X., Cruz, F. W., Auler, A. S., Mangini, A., Wang, Y., Kong, X., Burns, S. J., *et al.* (2009) 'Timing and structure of the 8.2 kyr B.P. event inferred from $\delta^{18}O$ records of stalagmites from China, Oman, and Brazil', *Geology*, 37(11), pp. 1007–1010. doi: 10.1130/G30126A.1.

Cheng, H., Fleitmann, D., Edwards, R. L., Wang, X., Cruz, F. W., Auler, A. S., Mangini, A., Wang, Y., Kong, X. and Burns, S. J. (2009) 'Timing and structure of the 8.2 kyr BP event inferred from δ18O records of stalagmites from China, Oman, and Brazil', *Geology*, 37(11), pp. 1007–1010.

Cheng, H. *et al.* (2012) 'The Global Paleomonsoon as seen through speleothem records from Asia and the Americas', *Climate Dynamics*, 39(5), pp. 1045–1062. doi: 10.1007/s00382-012-1363-7.

Cheng, H., Sinha, A., *et al.* (2013) 'Climate change patterns in Amazonia and biodiversity', *Nature Communications*, 4(1), pp. 1–6. doi: 10.1038/ncomms2415.

Cheng, H., Lawrence Edwards, R., *et al.* (2013) 'Improvements in 230Th dating, ^{230}Th and ^{234}U half-life values, and U–Th isotopic measurements by multi-collector inductively coupled plasma mass spectrometry', *Earth and Planetary Science Letters*, 371–372, pp. 82–91. doi: 10.1016/j.epsl.2013.04.006.

Cheng, H. *et al.* (2016) 'The Asian monsoon over the past 640,000 years and ice age terminations', *Nature*. doi: 10.1038/nature18591.

Cheng, H. *et al.* (2019) 'Chinese stalagmite paleoclimate researches: A review and perspective', *Science China Earth Sciences*, 62(10), pp. 1489–1513. doi: 10.1007/s11430-019-9478-3.

Chevalier, M., Brewer, S. and Chase, B. M. (2017) 'Qualitative assessment of PMIP3 rainfall simulations across the eastern African monsoon domains during the mid-Holocene and the Last Glacial Maximum', *Quaternary Science Reviews*, 156, pp. 107–120. doi: 10.1016/j.quascirev.2016.11.028.

Chiang, J. C. H. *et al.* (2015) 'Role of seasonal transitions and westerly jets in East Asian paleoclimate', *Quaternary Science Reviews*. doi: 10.1016/j.quascirev.2014.11.009.

Chung, C. T. Y. and Power, S. B. (2017) 'The non-linear impact of El Niño, La Niña and the Southern Oscillation on seasonal and regional Australian precipitation', *Journal of Southern Hemisphere Earth Systems Science*, 67(1), p. 25. doi: 10.1071/ES17004.

Clark, I. and Fritz, P. (1997) *Environmental Isotopes in Hydrology*. New York: Lewis Publishers.

Claussen, M. and Gayler, V. (1997) 'The Greening of the Sahara during the Mid-Holocene: Results of an Interactive Atmosphere-Biome Model', *Global Ecology and Biogeography Letters*, 6(5), pp. 369–377. doi: 2997337.

Cobb, K. M. *et al.* (2007) 'Regional-scale climate influences on temporal variations of rainwater and cave dripwater oxygen isotopes in northern Borneo', *Earth and Planetary Science Letters*, 263(3–4), pp. 207–220. doi: 10.1016/j.epsl.2007.08.024.

COHMAP Members (1988) 'Climatic Changes of the Last 18,000 Years: Observations and Model Simulations', *Science*, 241(4869), pp. 1043–1052. doi: 10.1126/science.241.4869.1043.

Cole, J. E. *et al.* (1999) 'Climatic controls on interannual variability of precipitation $\delta^{18}O$: Simulated influence of temperature, precipitation amount, and vapor source region', *Journal of Geophysical*

Research Atmospheres, 104(D12), pp. 14223–14235. doi: 10.1029/1999JD900182.

Comas-Bru, L., Harrison, Sandy P;, *et al.* (2019) 'Evaluating model outputs using integrated global speleothem records of climate change since the last glacial', *Climate of the Past*, 15(4), pp. 1557–1579. doi: 10.5194/cp-15-1557-2019.

Comas-Bru, L., Harrison, Sandy P., *et al.* (2019) 'Evaluating model outputs using integrated global speleothem records of climate change since the last glacial', *Climate of the Past Discussions*. doi: 10.5194/cp-2019-25.

Comas-Bru, L. *et al.* (2020) 'SISALv2: a comprehensive speleothem isotope database with multiple age–depth models', *Earth System Science Data*, 12(4), pp. 2579–2606. doi: 10.5194/essd-12-2579-2020.

Comas-Bru, L. and Harrison, S. P. (2019) 'SISAL: Bringing Added Value to Speleothem Research', *Quaternary*, 2(1), p. 7. doi: 10.3390/quat2010007.

Comas-Bru, L. and McDermott, F. (2015) 'Data-model comparison of soil–water $\delta^{18}O$ at a temperate site in N. Spain with implications for interpreting speleothem $\delta^{18}O$', *Journal of Hydrology*, 530, pp. 216–224. doi: 10.1016/j.jhydrol.2015.09.053.

Conroy, J. L. *et al.* (2008) 'Holocene changes in eastern tropical Pacific climate inferred from a Galápagos lake sediment record', *Quaternary Science Reviews*, 27(11–12), pp. 1166–1180. doi: 10.1016/j.quascirev.2008.02.015.

Cook, K. H. and Vizy, E. K. (2019) 'Contemporary Climate Change of the African Monsoon Systems', *Current Climate Change Reports*, 5(3), pp. 145–159. doi: 10.1007/s40641-019-00130-1.

Cosford, J. *et al.* (2008) 'Millennial-scale variability in the Asian monsoon: Evidence from oxygen isotope records from stalagmites in southeastern China', *Palaeogeography, Palaeoclimatology, Palaeoecology*, 266(1–2), pp. 3–12. doi: 10.1016/J.PALAEO.2008.03.029.

Craig, H. and Gordon, L. I. (1965) 'Deuterium and oxygen 18 variations in the ocean and the marine

atmosphere', in Tongiorgi, E. (ed.) *Stable isotopes in Oceanographic Studies and Paleotemperatures*. Pisa: Consiglio Nazionake delle Ricerche Laboratoria di Geologia Nucleare, pp. 9–130.

Crétat, J. *et al.* (2020) 'Mid-Holocene to present-day evolution of the Indian monsoon in transient global simulations', *Climate Dynamics*, 55(9–10), pp. 2761–2784. doi: 10.1007/s00382-020-05418-9.

Cruz, F. W., Burns, S. J., *et al.* (2005) 'Insolation-driven changes in atmospheric circulation over the past 116,000 years in subtropical Brazil', *Nature*, 434(7029), pp. 63–66. doi: 10.1038/nature03365.

Cruz, F. W., Karmann, I., *et al.* (2005) 'Stable isotope study of cave percolation waters in subtropical Brazil: Implications for paleoclimate inferences from speleothems', *Chemical Geology*, 220(3–4), pp. 245–262. doi: 10.1016/j.chemgeo.2005.04.001.

Cruz, Francisco W. *et al.* (2006) 'A stalagmite record of changes in atmospheric circulation and soil processes in the Brazilian subtropics during the Late Pleistocene', *Quaternary Science Reviews*, 25(21–22), pp. 2749–2761. doi: 10.1016/j.quascirev.2006.02.019.

Cruz, F.W. *et al.* (2006) 'Reconstruction of regional atmospheric circulation features during the late Pleistocene in subtropical Brazil from oxygen isotope composition of speleothems', *Earth and Planetary Science Letters*, 248(1–2), pp. 495–507. doi: 10.1016/j.epsl.2006.06.019.

Cruz, F. W. *et al.* (2009) 'Orbitally driven east-west antiphasing of South American precipitation', *Nature Geoscience*, 2(3), pp. 210–214. doi: 10.1038/ngeo444.

Daley, T. J. *et al.* (2011) 'The 8200yr BP cold event in stable isotope records from the North Atlantic region', *Global and Planetary Change*, 79(3–4), pp. 288–302. doi: 10.1016/j.gloplacha.2011.03.006.

Dallmeyer, A. *et al.* (2015) 'The evolution of sub-monsoon systems in the Afro-Asian monsoon region during the Holocene - Comparison of different transient climate model simulations', *Climate of the Past*, 11(2), pp. 305–326. doi: 10.5194/cp-11-305-2015.

Daniau, A. -L. *et al.* (2012) 'Predictability of biomass burning in response to climate changes', *Global*

Biogeochemical Cycles, 26(4), p. 2011GB004249. doi: 10.1029/2011GB004249.

Dansgaard, W. (1964) 'Stable isotopes in precipitation', *Tellus*, 16(4), pp. 436–468. doi: 10.3402/tellusa.v16i4.8993.

Dee, S. *et al.* (2015) 'PRYSM: An open-source framework for PRoxY System Modeling, with applications to oxygen-isotope systems', *Journal of Advances in Modeling Earth Systems*, 7(3), pp. 1220–1247. doi: 10.1002/2015MS000447.

Deininger, M. *et al.* (2019) 'Late Quaternary variations in the South American monsoon system as inferred by speleothems—New perspectives using the SISAL database', *Quaternary*, 2(1), p. 6. doi: 10.3390/quat2010006.

Delaygue, G., Jouzel, J. and Dutay, J. C. (2000) 'Oxygen 18-salinity relationship simulated by an oceanic general circulation model', *Earth and Planetary Science Letters*, 178(1–2), pp. 113–123. doi: 10.1016/S0012-821X(00)00073-X.

Deplazes, G. *et al.* (2014) 'Weakening and strengthening of the Indian monsoon during Heinrich events and Dansgaard-Oeschger oscillations', *Paleoceanography*, 29(2), pp. 99–114. doi: 10.1002/2013PA002509.

Ding, Y. and Chan, J. C. L. (2005) 'The East Asian summer monsoon: an overview', *Meteorology and Atmospheric Physics*, 89(1–4), pp. 117–142. doi: 10.1007/s00703-005-0125-z.

Dominguez-Villar, D. *et al.* (2009) 'Oxygen isotope precipitation anomaly in the North Atlantic region during the 8.2 ka event', *Geology*, 37(12), pp. 1095–1098. doi: 10.1130/G30393A.1.

Domínguez-Villar, D. *et al.* (2017) 'The control of the tropical North Atlantic on Holocene millennial climate oscillations', *Geology*, 45(4), pp. 303–306. doi: 10.1130/G38573.1.

Dong, J. *et al.* (2010) 'A high-resolution stalagmite record of the Holocene East Asian monsoon from Mt Shennongjia, central China', *Holocene*, 20(2), pp. 257–264. doi: 10.1177/0959683609350393.

Dorale, J. A. and Liu, Z. (2009) 'Limitations of hendy test criteria in judging the paleoclimatic suitability of speleothems and the need for replication', *Journal of Cave and Karst Studies*, 71(1), pp. 73–80.

Drăguşin, V. *et al.* (2014) 'Constraining Holocene hydrological changes in the Carpathian-Balkan region using speleothem δ18O and pollen-based temperature reconstructions', *Climate of the Past*, 10(4), pp. 1363–1380. doi: 10.5194/cp-10-1363-2014.

Dreybrodt, W. and Deininger, M. (2014) 'The impact of evaporation to the isotope composition of DIC in calcite precipitating water films in equilibrium and kinetic fractionation models', *Geochimica et Cosmochimica Acta*, 125, pp. 433–439. doi: 10.1016/j.gca.2013.10.004.

Duan, P. *et al.* (2021) 'The timing and structure of the 8.2 ka event revealed through high-resolution speleothem records from northwestern Madagascar', *Quaternary Science Reviews*, 268, p. 107104.

Dykoski, C. A. *et al.* (2005) 'A high-resolution, absolute-dated Holocene and deglacial Asian monsoon record from Dongge Cave, China', *Earth and Planetary Science Letters*, 233(1–2), pp. 71–86. doi: 10.1016/J.EPSL.2005.01.036.

Emile-Geay, J. *et al.* (2016) 'Links between tropical Pacific seasonal, interannual and orbital variability during the Holocene', *Nature Geoscience*, 9, pp. 168–173. doi: 10.1038/ngeo2608.

Even, H. *et al.* (1986) 'Timing the transport of water through the upper vadose zone in a Karstic system above a cave in Israel', *Earth Surface Processes and Landforms*, 11(2), pp. 181–191. doi: 10.1002/esp.3290110208.

Fairchild, I. J. and Baker, A. (2012) *Speleothem Science: From Process to Past Environments*. 1st edn. Chichester: Wiley-Blackwell.

Feng, S., Hu, Q. and Oglesby, R. J. (2011) 'Influence of Atlantic sea surface temperatures on persistent drought in North America', *Climate Dynamics*, 37(3–4), pp. 569–586. doi: 10.1007/s00382-010-0835-x.

Fisher, T. G., Smith, D. G. and Andrews, J. T. (2002) 'Preboreal oscillation caused by a glacial Lake Agassiz

flood', *Quaternary Science Reviews*, 21(8–9), pp. 873–878.

Fleitmann, D. *et al.* (2003) 'Holocene forcing of the Indian Monsoon recorded in a stalagmite from southern Oman', *Science*, 300(5626), pp. 1737–1739. doi: 10.1126/science.1083130.

Fleitmann, D. *et al.* (2004) 'Palaeoclimatic interpretation of high-resolution oxygen isotope profiles derived from annually laminated speleothems from Southern Oman', *Quaternary Science Reviews*, 23(7–8), pp. 935–945. doi: 10.1016/j.quascirev.2003.06.019.

Fleitmann, D. *et al.* (2007) 'Holocene ITCZ and Indian monsoon dynamics recorded in stalagmites from Oman and Yemen (Socotra)', *Quaternary Science Reviews*, 26(1–2), pp. 170–188. doi: 10.1016/j.quascirev.2006.04.012.

Flohr, P. *et al.* (2017) 'Late Holocene droughts in the Fertile Crescent recorded in a speleothem from northern Iraq', *Geophysical Research Letters*, 44(3), pp. 1528–1536. doi: 10.1002/2016GL071786.

Frappier, A. B. *et al.* (2007) 'Stalagmite stable isotope record of recent tropic cyclone events', *Geology*, 35(2), pp. 111–114. doi: 10.1130/G23145A.1.

Friedman, I. *et al.* (2002) 'Stable isotope composition of waters in the Great Basin, United States 1. Air-mass trajectories', *Journal of Geophysical Research Atmospheres*. doi: 10.1029/2001JD000565.

Ganopolski, A. *et al.* (1998) 'The Influence of Vegetation-Atmosphere-Ocean Interaction on Climate During the Mid-Holocene', *Science*, 280(5371), pp. 1916–1919. doi: 10.1126/science.280.5371.1916.

Gat, J. R. (1996) 'Oxygen and hydrogen isotopes in the hydrological cycle', *Annual Review of Earth and Planetary Sciences*, 24(1), pp. 225–262. doi: 10.1146/annurev.earth.24.1.225.

Geen, R. *et al.* (2020) 'Monsoons, ITCZs, and the Concept of the Global Monsoon', *Reviews of Geophysics*, 58(4), pp. 1–45. doi: 10.1029/2020RG000700.

Gershunov, A. and Barnett, T. P. (1998) 'Interdecadal Modulation of ENSO Teleconnections', *Bulletin of the American Meteorological Society*, 79(12), pp. 2715–2725. doi: 10.1175/1520-

0477(1998)079<2715:IMOET>2.0.CO;2.

Giannini, A., Kushnir, Y. and Cane, M. A. (2000) 'Interannual Variability of Caribbean Rainfall, ENSO, and the Atlantic Ocean', *Journal of Climate*, 13(2), pp. 297–311. doi: 10.1175/1520-0442(2000)013<0297:IVOCRE>2.0.CO;2.

Gierz, P., Werner, M. and Lohmann, G. (2017) 'Simulating climate and stable water isotopes during the Last Interglacial using a coupled climate-isotope model', *Journal of Advances in Modeling Earth Systems*, 9(5), pp. 2027–2045. doi: 10.1002/2017MS001056.

Goldsmith, Y. *et al.* (2017a) 'Northward extent of East Asian monsoon covaries with intensity on orbital and millennial timescales', *Proceedings of the National Academy of Sciences*, 114(8), pp. 1817–1821. doi: 10.1073/pnas.1616708114.

Goldsmith, Y. *et al.* (2017b) 'Northward extent of East Asian monsoon covaries with intensity on orbital and millennial timescales', *Proceedings of the National Academy of Sciences*, 114(8), pp. 1817–1821. doi: 10.1073/pnas.1616708114.

Goswami, B. N. *et al.* (2006) 'A physical mechanism for North Atlantic SST influence on the Indian summer monsoon', *Geophysical Research Letters*, 33(2), p. L02706. doi: 10.1029/2005GL024803.

Gregoire, L. J., Payne, A. J. and Valdes, P. J. (2012) 'Deglacial rapid sea level rises caused by ice-sheet saddle collapses', *Nature*, 487(7406), pp. 219–222. doi: 10.1038/nature11257.

Griffiths, M. L. *et al.* (2009a) 'Increasing Australian-Indonesian monsoon rainfall linked to early Holocene sea-level rise', *Nature Geoscience*, 2(9), pp. 636–639. doi: 10.1038/ngeo605.

Griffiths, M. L. *et al.* (2009b) 'Increasing Australian-Indonesian monsoon rainfall linked to early Holocene sea-level rise', *Nature Geoscience*, 2(9), pp. 636–639. doi: 10.1038/ngeo605.

Gupta, A. K., Anderson, D. M. and Overpeck, J. T. (2003) 'Abrupt changes in the Asian southwest monsoon during the holocene and their links to the North Alantic Ocean', *Nature*, 421(6921), pp. 354–

357. doi: 10.1038/nature01340.

Gupta, A. K., Das, M. and Anderson, D. M. (2005) 'Solar influence on the Indian summer monsoon during the Holocene', *Geophysical Research Letters*, 32(17). doi: 10.1029/2005GL022685.

Hagos, S. M. and Cook, K. H. (2007) 'Dynamics of the West African monsoon jump', *Journal of Climate*, 20(21), pp. 5264–5284. doi: 10.1175/2007JCLI1533.1.

Han, Z. *et al.* (2015) 'Extreme monsoon aridity episodes recorded in South China during Heinrich Events', *Palaeogeography, Palaeoclimatology, Palaeoecology*, 440, pp. 467–474. doi: 10.1016/j.palaeo.2015.09.037.

Harrison, S. P. *et al.* (2003) 'Mid-Holocene climates of the Americas: a dynamical response to changed seasonality', *Climate Dynamics*, 20(7–8), pp. 663–688. doi: 10.1007/s00382-002-0300-6.

Harrison, S. P. and Prentice, C. I. (2003) 'Climate and CO_2 controls on global vegetation distribution at the last glacial maximum: analysis based on palaeovegetation data, biome modelling and palaeoclimate simulations', *Global Change Biology*, 9(7), pp. 983–1004. doi: 10.1046/j.1365-2486.2003.00640.x.

Hart, N. C. G., Reason, C. J. C. and Fauchereau, N. (2010) 'Tropical-extratropical interactions over southern Africa: Three cases of heavy summer season rainfall', *Monthly Weather Review*, 138(7), pp. 2608–2623. doi: 10.1175/2010MWR3070.1.

Haug, G. H. *et al.* (2001) 'Southward migration of the intertropical convergence zone through the holocene', *Science*, 293(5533), pp. 1304–1308. doi: 10.1126/science.1059725.

Haywood, A. M. *et al.* (2011) 'Pliocene Model Intercomparison Project (PlioMIP): experimental design and boundary conditions (Experiment 2)', *Geoscientific Model Development*, 4(3), pp. 571–577. doi: 10.5194/gmd-4-571-2011.

He, Chengfei *et al.* (2021) 'Abrupt Heinrich Stadial 1 cooling missing in Greenland oxygen isotopes', *Science Advances*, 7(25). doi: 10.1126/sciadv.abh1007.

He, C. *et al.* (2021) 'Hydroclimate footprint of pan-Asian monsoon water isotope during the last deglaciation', *Science Advances*, 7(4). doi: 10.1126/sciadv.abe2611.

Hellstrom, J., McCulloch, M. and Stone, J. (1998) 'A detailed 31,000-year record of climate and vegetation change, from the isotope geochemistry of two New Zealand speleothems', *Quaternary Research*, 50(2), pp. 167–178. doi: 10.1006/qres.1998.1991.

Hendon, H. H. (2003) 'Indonesian Rainfall Variability: Impacts of ENSO and Local Air–Sea Interaction', *Journal of Climate*, 16(11), pp. 1775–1790. doi: 10.1175/1520-0442(2003)016<1775:IRVIOE>2.0.CO;2.

Hendy, C. H. (1971) 'The isotopic geochemistry of speleothems-I. The calculation of the effects of different modes of formation on the isotopic composition of speleothems and their applicability as palaeoclimatic indicators', *Geochimica et Cosmochimica Acta*, 35(8), pp. 801–824. doi: 10.1016/0016-7037(71)90127-X.

Higgins, R. W., Chen, Y. and Douglas, A. V. (1999) 'Interannual Variability of the North American Warm Season Precipitation Regime', *Journal of Climate*, 12(3), pp. 653–680. doi: 10.1175/1520-0442(1999)012<0653:IVOTNA>2.0.CO;2.

Hill, C. A. and Forti, P. (1995) 'The classification of cave minerals and speleothems', *International Journal of Speleology*, 24(1), pp. 77–82. doi: 10.5038/1827-806X.24.1.5.

Hoffman, J. S. *et al.* (2012) 'Linking the 8.2 ka event and its freshwater forcing in the Labrador Sea', *Geophysical Research Letters*, 39(18). doi: 10.1029/2012GL053047.

Holloway, M. D. *et al.* (2016) 'Reconstructing paleosalinity from δ18O: Coupled model simulations of the Last Glacial Maximum, Last Interglacial and Late Holocene', *Quaternary Science Reviews*, 131(Part B), pp. 350–364. doi: 10.1016/j.quascirev.2015.07.007.

Hu, C. *et al.* (2008) 'Quantification of Holocene Asian monsoon rainfall from spatially separated cave records', *Earth and Planetary Science Letters*, 266(3–4), pp. 221–232. doi: 10.1016/j.epsl.2007.10.015.

Hu, Jun *et al.* (2019) 'Deciphering oxygen isotope records from Chinese speleothems with an isotope-enabled climate model', *Paleoceanography and Paleoclimatology*, 34(12), pp. 2098–2112. doi: 10.1029/2019PA003741.

Hu, J. *et al.* (2019) 'Deciphering Oxygen Isotope Records From Chinese Speleothems With an Isotope-Enabled Climate Model', *Palaeogeography, Palaeoclimatology, Palaeoecology*, 43, pp. 2098–2112.

Ivanochko, T. S. *et al.* (2008) 'Geochemical reconstruction of Pacific decadal variability from the eastern North Pacific during the Holocene', *Canadian Journal of Earth Sciences*, 45(11), pp. 1317–1329. doi: 10.1139/E08-037.

Ivanovic, R. F. *et al.* (2016) 'Transient climate simulations of the deglaciation 21–9 thousand years before present (version 1) – PMIP4 Core experiment design and boundary conditions', *Geoscientific Model Development*, 9(7), pp. 2563–2587. doi: 10.5194/gmd-9-2563-2016.

Johnson, B. J. *et al.* (1999) '65,000 Years of Vegetation Change in Central Australia and the Australian Summer Monsoon', *Science*, 284(5417), pp. 1150–1152. doi: 10.1126/science.284.5417.1150.

Jolly, D. *et al.* (1998) 'Simulated climate and biomes of Africa during the late quaternary', *Quaternary Science Reviews*, 17(6–7), pp. 629–657. doi: 10.1016/S0277-3791(98)00015-8.

Jones, I. C. and Banner, J. L. (2003) 'Estimating recharge thresholds in tropical karst island aquifers: Barbados, Puerto Rico and Guam', *Journal of Hydrology*, 278(1–4), pp. 131–143. doi: 10.1016/S0022-1694(03)00138-0.

Jungclaus, J. H. *et al.* (2017) 'The PMIP4 contribution to CMIP6 – Part 3: The last millennium, scientific objective, and experimental design for the PMIP4 *past1000* simulations', *Geoscientific Model Development*, 10(11), pp. 4005–4033. doi: 10.5194/gmd-10-4005-2017.

Kageyama, M. *et al.* (2021) 'The PMIP4 Last Glacial Maximum experiments: preliminary results and comparison with the PMIP3 simulations', *Climate of the Past*, 17(3), pp. 1065–1089. doi: 10.5194/cp-17-1065-2021.

Kaniewski, D. *et al.* (2018) 'The 4.2 ka BP event in the Levant', *Climate of the Past*, 14(10), pp. 1529–1542. doi: 10.5194/cp-14-1529-2018.

Kanner, L. C. *et al.* (2013) 'High-resolution variability of the South American summer monsoon over the last seven millennia: Insights from a speleothem record from the central Peruvian Andes', *Quaternary Science Reviews*, 75, pp. 1–10. doi: 10.1016/j.quascirev.2013.05.008.

Kathayat, G. *et al.* (2016) 'Indian monsoon variability on millennial-orbital timescales', *Scientific Reports*, 6, p. 24374. doi: 10.1038/srep24374.

Kathayat, G. *et al.* (2021) 'Interannual oxygen isotope variability in Indian summer monsoon precipitation reflects changes in moisture sources', *Communications Earth & Environment*, 2(1), p. 96. doi: 10.1038/s43247-021-00165-z.

Kaufmann, G. (2003) 'Stalagmite growth and palaeo-climate: The numerical perspective', *Earth and Planetary Science Letters*, 214(1–2), pp. 251–266. doi: 10.1016/S0012-821X(03)00369-8.

Kaushal, N. *et al.* (2018) 'The Indian Summer Monsoon from a Speleothem $\delta^{18}O$ Perspective—A Review', *Quaternary*, 1(3), p. 29. doi: 10.3390/quat1030029.

Kim, S.-T. and O'Neil, J. R. (1997) 'Equilibrium and nonequilibrium oxygen isotope effects in synthetic carbonates', *Geochimica et Cosmochimica Acta*, 61(16), pp. 3461–3475. doi: 10.1016/S0016-7037(97)00169-5.

Kirby, M. E. *et al.* (2010) 'A Holocene record of Pacific Decadal Oscillation (PDO)-related hydrologic variability in Southern California (Lake Elsinore, CA)', *Journal of Paleolimnology*, 44(3), pp. 819–839. doi: 10.1007/s10933-010-9454-0.

Kleiven, H. (Kikki) F. *et al.* (2008) 'Reduced North Atlantic Deep Water Coeval with the Glacial Lake Agassiz Freshwater Outburst', *Science*, 319(5859), pp. 60–64. doi: 10.1126/science.1148924.

Knudsen, M. F. *et al.* (2011) 'Tracking the Atlantic Multidecadal Oscillation through the last 8,000 years',

Nature Communications, 2(1), p. 178. doi: 10.1038/ncomms1186.

Kobashi, T. *et al.* (2017) 'Volcanic influence on centennial to millennial Holocene Greenland temperature change', *Scientific reports*, 7(1), pp. 1–10.

Kodama, Y. (1992) 'Large-scale common features of subtropical precipitation zones (the Baiu frontal zone, the SPCZ, and the SACZ) part I: Characteristics of subtropical frontal zones', *Journal of the Meteorological Society of Japan*, 70(4), pp. 813–836. doi: 10.2151/jmsj1965.70.4_813.

Koster, R. D., de Valpine, D. P. and Jouzel, J. (1993) 'Continental water recycling and $H_2{}^{18}O$ concentrations', *Geophysical Research Letters*, 20(20), pp. 2215–2218. doi: 10.1029/93GL01781.

Krause, C. E. *et al.* (2019) 'Spatio-temporal evolution of Australasian monsoon hydroclimate over the last 40,000 years', *Earth and Planetary Science Letters*, 513, pp. 103–112. doi: 10.1016/j.epsl.2019.01.045.

Krishnamurthy, V. and Goswami, B. N. (2000) 'Indian Monsoon–ENSO Relationship on Interdecadal Timescale', *Journal of Climate*, 13(3), pp. 579–595. doi: 10.1175/1520-0442(2000)013<0579:IMEROI>2.0.CO;2.

Kumar, K. K., Rajagopalan, B. and Cane, M. A. (1999) 'On the Weakening Relationship Between the Indian Monsoon and ENSO', *Science*, 284(5423), pp. 2156–2159. doi: 10.1126/science.284.5423.2156.

Kutzbach, J. *et al.* (1996) 'Vegetation and soil feedbacks on the response of the African monsoon to orbital forcing in the early to middle Holocene', *Nature*, 384(6610), pp. 623–626. doi: 10.1038/384623a0.

Kutzbach, J. E. and Guetter, P. J. (1986) 'The Influence of Changing Orbital Parameters and Surface Boundary Conditions on Climate Simulations for the Past 18 000 Years', *Journal of the Atmospheric Sciences*, 43(16), pp. 1726–1759. doi: 10.1175/1520-0469(1986)043<1726:TIOCOP>2.0.CO;2.

Kutzbach, J. E. and Street-Perrott, F. A. (1985) 'Milankovitch forcing of fluctuations in the level of tropical lakes from 18 to 0 kyr BP', *Nature*, 317(6033), pp. 130–134. doi: 10.1038/317130a0.

Lachniet, M. S. *et al.* (2004) 'Tropical response to the 8200 yr B.P. cold event? Speleothem isotopes indicate a weakened early Holocene monsoon in Costa Rica', *Geology*, 32(11), p. 957. doi: 10.1130/G20797.1.

Lachniet, M. S. (2009) 'Climatic and environmental controls on speleothem oxygen-isotope values', *Quaternary Science Reviews*, 28(5–6), pp. 412–432. doi: 10.1016/j.quascirev.2008.10.021.

Lebel, T., Diedhiou, A. and Laurent, H. (2003) 'Seasonal cycle and interannual variability of the Sahelian rainfall at hydrological scales', *Journal of Geophysical Research: Atmospheres*, 108(8), pp. 1–11. doi: 10.1029/2001jd001580.

Lechleitner, F. A. *et al.* (2018) 'The Potential of Speleothems from Western Europe as Recorders of Regional Climate: A Critical Assessment of the SISAL Database', *Quaternary*, 1(3), p. 30. doi: 10.3390/quat1030030.

Lee, J. E. *et al.* (2007) 'Analysis of the global distribution of water isotopes using the NCAR atmospheric general circulation model', *Journal of Geophysical Research Atmospheres*, 112(D16). doi: 10.1029/2006JD007657.

Lee, J. E. and Fung, I. (2008) '"Amount effect" of water isotopes and quantitative analysis of post-condensation processes', *Hydrological Processes*, 22(1), pp. 1–8. doi: 10.1002/hyp.6637.

LeGrande, A. N. and Schmidt, G. A. (2006) 'Global gridded data set of the oxygen isotopic composition in seawater', *Geophysical Research Letters*, 33(12). doi: 10.1029/2006GL026011.

LeGrande, A. N. and Schmidt, G. A. (2008) 'Ensemble, water isotope-enabled, coupled general circulation modeling insights into the 8.2 ka event', *Paleoceanography*, 23(PA3207). doi: 10.1029/2008PA001610.

LeGrande, A. N. and Schmidt, G. A. (2009) 'Sources of Holocene variability of oxygen isotopes in paleoclimate archives', *Climate of the Past*, 5(3), pp. 441–455. doi: 10.5194/cp-5-441-2009.

Lewis, S. C. *et al.* (2010) 'Water vapour source impacts on oxygen isotope variability in tropical precipitation during Heinrich events', *Climate of the Past*, 6(3), pp. 325–343. doi: 10.5194/cp-6-325-2010.

Lézine, A.-M. *et al.* (2011) 'Sahara and Sahel vulnerability to climate changes, lessons from Holocene hydrological data', *Quaternary Science Reviews*, 30(21–22), pp. 3001–3012. doi: 10.1016/j.quascirev.2011.07.006.

Li, Y. *et al.* (2014) 'Synchronous or asynchronous Holocene Indian and East Asian summer monsoon evolution: A synthesis on Holocene Asian summer monsoon simulations, records and modern monsoon indices', *Global and Planetary Change*, 116, pp. 30–40. doi: 10.1016/j.gloplacha.2014.02.005.

Liu, W., Cook, K. H. and Vizy, E. K. (2020) 'Role of the West African westerly jet in the seasonal and diurnal cycles of precipitation over West Africa', *Climate Dynamics*, 54(1–2), pp. 843–861. doi: 10.1007/s00382-019-05035-1.

Liu, Y. H. *et al.* (2013) 'Links between the East Asian monsoon and North Atlantic climate during the 8,200 year event', *Nature Geoscience*, 6(2), pp. 117–120.

Liu, Y. and Hu, C. (2016) 'Quantification of southwest China rainfall during the 8.2 ka BP event with response to North Atlantic cooling', *Climate of the Past*, 12(7), pp. 1583–1590. doi: 10.5194/cp-12-1583-2016.

Liu, Z. *et al.* (2009) 'Transient Simulation of Last Deglaciation with a New Mechanism for Bølling-Allerød Warming', *Science*, 325(5938), pp. 310–314. doi: 10.1126/science.1171041.

Liu, Z. *et al.* (2014) 'Chinese cave records and the East Asia Summer Monsoon', *Quaternary Science Reviews*, 83, pp. 115–128. doi: 10.1016/j.quascirev.2013.10.021.

LoDico, J. M., Flower, B. P. and Quinn, T. M. (2006) 'Subcentennial-scale climatic and hydrologic variability in the Gulf of Mexico during the early Holocene', *Paleoceanography*, 21(3). doi: 10.1029/2005PA001243.

Lu, R., Dong, B. and Ding, H. (2006) 'Impact of the Atlantic Multidecadal Oscillation on the Asian summer monsoon', *Geophysical Research Letters*, 33(24), p. L24701. doi: 10.1029/2006GL027655.

Magee, J. W. *et al.* (2004) 'Continuous 150 k.y. monsoon record from Lake Eyre, Australia: Insolation-forcing implications and unexpected Holocene failure', *Geology*, 32(10), pp. 885–888. doi: 10.1130/G20672.1.

Maher, B. A. (2008) 'Holocene variability of the East Asian summer monsoon from Chinese cave records: A re-assessment', *Holocene*, 18(6), pp. 861–866. doi: 10.1177/0959683608095569.

Maher, B. A. and Thompson, R. (2012) 'Oxygen isotopes from Chinese caves: records not of monsoon rainfall but of circulation regime', *Journal of Quaternary Science*, 27(6), pp. 615–624. doi: 10.1002/jqs.2553.

Mantua, N. J. *et al.* (1997) 'A Pacific Interdecadal Climate Oscillation with Impacts on Salmon Production', *Bulletin of the American Meteorological Society*, 78(6), pp. 1069–1079. doi: 10.1175/1520-0477(1997)078<1069:APICOW>2.0.CO;2.

Mantua, N. J. and Hare, S. R. (2002) 'The Pacific Decadal Oscillation', *Journal of Oceanology*, 58, pp. 35–44. doi: 10.1023/A:1015820616384.

Mao, J. and Wu, G. (2007) 'Interannual variability in the onset of the summer monsoon over the Eastern Bay of Bengal', *Theoretical and Applied Climatology*, 89(3–4), pp. 155–170. doi: 10.1007/s00704-006-0265-1.

Marchant, R. *et al.* (2007) 'The Indian Ocean dipole – the unsung driver of climatic variability in East Africa', *African Journal of Ecology*, 45(1), pp. 4–16. doi: 10.1111/j.1365-2028.2006.00707.x.

Marengo, J. A. *et al.* (2012) 'Recent developments on the South American monsoon system', *International Journal of Climatology*, 32(1), pp. 1–21. doi: 10.1002/joc.2254.

Martin Calvo, M., Prentice, I. C. and Harrison, S. P. (2014) 'Climate versus carbon dioxide controls on

biomass burning: a model analysis of the glacial–interglacial contrast', *Biogeosciences*, 11(21), pp. 6017–6027. doi: 10.5194/bg-11-6017-2014.

Martin, E. R. and Thorncroft, C. D. (2014) 'The impact of the AMO on the West African monsoon annual cycle', *Quarterly Journal of the Royal Meteorological Society*, 140(678), pp. 31–46. doi: 10.1002/qj.2107.

Marzin, C. and Braconnot, P. (2009) 'Variations of Indian and African monsoons induced by insolation changes at 6 and 9.5 kyr BP', *Climate Dynamics*, 33(2–3), pp. 215–231. doi: 10.1007/s00382-009-0538-3.

Matero, I. S. O. *et al.* (2017) 'The 8.2 ka cooling event caused by Laurentide ice saddle collapse', *Earth and Planetary Science Letters*, 473, pp. 205–214. doi: 10.1016/j.epsl.2017.06.011.

McDermott, F. (2004) 'Palaeo-climate reconstruction from stable isotope variations in speleothems: A review', *Quaternary Science Reviews*, 23(7–8), pp. 901–918. doi: 10.1016/j.quascirev.2003.06.021.

McPhaden, M. J., Zebiak, S. E. and Glantz, M. H. (2006) 'ENSO as an integrating concept in earth science', *Science*, 314(5806), pp. 1740–1745. doi: 10.1126/science.1132588.

Menviel, L. *et al.* (2014) 'Hindcasting the continuum of Dansgaard–Oeschger variability: mechanisms, patterns and timing', *Climate of the Past*, 10(1), pp. 63–77. doi: 10.5194/cp-10-63-2014.

Menviel, L. *et al.* (2019) 'The penultimate deglaciation: protocol for Paleoclimate Modelling Intercomparison Project (PMIP) phase 4 transient numerical simulations between 140 and 127 ka, version 1.0', *Geoscientific Model Development*, 12(8), pp. 3649–3685. doi: 10.5194/gmd-12-3649-2019.

Menviel, L., Spence, P. and England, M. H. (2015) 'Contribution of enhanced Antarctic Bottom Water formation to Antarctic warm events and millennial-scale atmospheric CO2 increase', *Earth and Planetary Science Letters*, 413, pp. 37–50. doi: 10.1016/j.epsl.2014.12.050.

Mestas-Nuñez, A. M., Enfield, D. B. and Zhang, C. (2007) 'Water vapor fluxes over the Intra-Americas Sea: Seasonal and interannual variability and associations with rainfall', *Journal of Climate*, 20(9), pp. 1910–1922. doi: 10.1175/JCLI4096.1.

Metcalfe, S. E., Barron, J. A. and Davies, S. J. (2015) 'The Holocene history of the North American Monsoon: "known knowns" and "known unknowns" in understanding its spatial and temporal complexity', *Quaternary Science Reviews*, pp. 1–27. doi: 10.1016/j.quascirev.2015.04.004.

Mickler, P. J., Stern, L. A. and Banner, J. L. (2006) 'Large kinetic isotope effects in modern speleothems', *Geological Society of America Bulletin*, 118(1–2), pp. 65–81. doi: 10.1130/B25698.1.

Misra, P., Tandon, S. K. and Sinha, R. (2019) 'Holocene climate records from lake sediments in India: Assessment of coherence across climate zones', *Earth-Science Reviews*, 190, pp. 370–397. doi: 10.1016/j.earscirev.2018.12.017.

Moerman, J. W. *et al.* (2013) 'Diurnal to interannual rainfall δ18O variations in northern Borneo driven by regional hydrology', *Earth and Planetary Science Letters*. doi: 10.1016/j.epsl.2013.03.014.

Moore, G. W. (1952) 'Speleothem - A new cave term', *National Speleological Society News*, 10(6), p. 2.

Morrill, C. *et al.* (2013) 'Proxy benchmarks for intercomparison of 8.2 ka simulations', *Climate of the Past*, 9(1), pp. 423–432. doi: 10.5194/cp-9-423-2013.

Morrill, C. *et al.* (2014) 'Large sensitivity to freshwater forcing location in 8.2 ka simulations', *Paleoceanography*, 29(10), pp. 930–945. doi: 10.1002/2014PA002669.

Munksgaard, N. C. *et al.* (2012) 'First continuous shipboard $\delta^{18}O$ and δD measurements in sea water by diffusion sampling—cavity ring-down spectrometry', *Environmental Chemistry Letters*, 10(3), pp. 301–307. doi: 10.1007/s10311-012-0371-5.

Myers, C. G. *et al.* (2015) 'Northeast Indian stalagmite records Pacific decadal climate change: Implications for moisture transport and drought in India', *Geophysical Research Letters*, 42(10), pp. 4124–4132. doi: 10.1002/2015GL063826.

Niedermeyer, E. M. *et al.* (2014) 'Hydroclimate of the western Indo-Pacific Warm Pool during the past 24,000 years', *Proceedings of the National Academy of Sciences of the United States of America*, 111(26),

pp. 9402–9406. doi: 10.1073/pnas.1323585111.

Novello, V. F. *et al.* (2017) 'A high-resolution history of the South American Monsoon from Last Glacial Maximum to the Holocene', *Scientific Reports*, 7(1), p. 44267. doi: 10.1038/srep44267.

Ön, Z. B. *et al.* (2021) 'A Bayesian test for the 4.2 ka BP abrupt climatic change event in southeast Europe and southwest Asia using structural time series analysis of paleoclimate data', *Climatic Change*, 165(1–2). doi: 10.1007/s10584-021-03010-6.

Otto-Bliesner, B. L. *et al.* (2021) 'Large-scale features of Last Interglacial climate: results from evaluating the *lig127k* simulations for the Coupled Model Intercomparison Project (CMIP6)–Paleoclimate Modeling Intercomparison Project (PMIP4)', *Climate of the Past*, 17(1), pp. 63–94. doi: 10.5194/cp-17-63-2021.

Owen, R. A. *et al.* (2016) 'Calcium isotopes in caves as a proxy for aridity: Modern calibration and application to the 8.2 kyr event', *Earth and Planetary Science Letters*, 443, pp. 129–138.

Pape, J. R. *et al.* (2010) 'Controls on oxygen isotope variability in precipitation and cave drip waters, central Texas, USA', *Journal of Hydrology*, 385(1–4), pp. 203–215. doi: 10.1016/j.jhydrol.2010.02.021.

Parthasarathy, B., Munot, A. A. and Kothawale, D. R. (1994) 'All-India monthly and seasonal rainfall series: 1871-1993', *Theoretical and Applied Climatology*, 49(4), pp. 217–224. doi: 10.1007/BF00867461.

Partin, J. W. *et al.* (2007) 'Millennial-scale trends in west Pacific warm pool hydrology since the Last Glacial Maximum', *Nature*, 449(7161), pp. 452–455. doi: 10.1038/nature06164.

Pausata, F. S. R. *et al.* (2011) 'Chinese stalagmite $\delta^{18}O$ controlled by changes in the Indian monsoon during a simulated Heinrich event', *Nature Geoscience*, 4(7), pp. 474–480. doi: 10.1038/ngeo1169.

Peckover, E. N. *et al.* (2019) 'Coupled stalagmite–Alluvial fan response to the 8.2 ka event and early Holocene palaeoclimate change in Greece', *Palaeogeography, Palaeoclimatology, Palaeoecology*, 532, p. 109252.

Perrin, J., Jeannin, P.-Y. and Zwahlen, F. (2003) 'Epikarst storage in a karst aquifer: a conceptual model

based on isotopic data, Milandre test site, Switzerland', *Journal of Hydrology*, 279(1–4), pp. 106–124. doi: 10.1016/S0022-1694(03)00171-9.

Peyron, O. *et al.* (2006) 'Quantitative reconstructions of annual rainfall in Africa 6000 years ago: Model-data comparison', *Journal of Geophysical Research*, 111(D24), p. D24110. doi: 10.1029/2006JD007396.

Pomposi, C. *et al.* (2016) 'Understanding Pacific Ocean influence on interannual precipitation variability in the Sahel', *Geophysical Research Letters*, 43(17), pp. 9234–9242. doi: 10.1002/2016GL069980.

Power, M. J. *et al.* (2008) 'Changes in fire regimes since the Last Glacial Maximum: An assessment based on a global synthesis and analysis of charcoal data', *Climate Dynamics*, 30, pp. 887–907. doi: 10.1007/s00382-007-0334-x.

Power, S. *et al.* (1999) 'Inter-decadal modulation of the impact of ENSO on Australia', *Climate Dynamics*, 15(5), pp. 319–324. doi: 10.1007/s003820050284.

Prado, L. F. *et al.* (2013) 'A mid-Holocene climate reconstruction for eastern South America', *Climate of the Past*, 9(5), pp. 2117–2133. doi: 10.5194/cp-9-2117-2013.

Pu, B. and Cook, K. H. (2012) 'Role of the west African westerly jet in sahel rainfall variations', *Journal of Climate*, 25(8), pp. 2880–2896. doi: 10.1175/JCLI-D-11-00394.1.

Rachmayani, R., Prange, M. and Schulz, M. (2015) 'North African vegetation-precipitation feedback in early and mid-Holocene climate simulations with CCSM3-DGVM', *Climate of the Past*, 11(2). doi: 10.5194/cp-11-175-2015.

Railsback, L. B. *et al.* (2018) 'The timing, two-pulsed nature, and variable climatic expression of the 4.2 ka event: A review and new high-resolution stalagmite data from Namibia', *Quaternary Science Reviews*, 186, pp. 78–90. doi: 10.1016/j.quascirev.2018.02.015.

Ran, M. and Chen, L. (2019) 'The 4.2 ka BP climatic event and its cultural responses', *Quaternary International*, 521, pp. 158–167. doi: 10.1016/j.quaint.2019.05.030.

Ratnam, J. V. *et al.* (2014) 'Remote Effects of El Niño and Modoki Events on the Austral Summer Precipitation of Southern Africa', *Journal of Climate*, 27(10), pp. 3802–3815. doi: 10.1175/JCLI-D-13-00431.1.

Richards, D. A. *et al.* (1998) 'U-Pb dating of a speleothem of Quaternary age', *Geochimica et Cosmochimica Acta*, 62(23–24), pp. 3683–3688. doi: 10.1016/S0016-7037(98)00256-7.

Richards, D. A. (2003) 'Uranium-series Chronology and Environmental Applications of Speleothems', *Reviews in Mineralogy and Geochemistry*, 52(1), pp. 407–460. doi: 10.2113/0520407.

Risi, C. *et al.* (2010) 'Water-stable isotopes in the LMDZ4 general circulation model: Model evaluation for present-day and past climates and applications to climatic interpretations of tropical isotopic records', *Journal of Geophysical Research Atmospheres*, 115(D12). doi: 10.1029/2009JD013255.

Risi, C., Bony, S. and Vimeux, F. (2008) 'Influence of convective processes on the isotopic composition ($\delta^{18}O$ and δD) of precipitation and water vapor in the tropics: 2. Physical interpretation of the amount effect', *Journal of Geophysical Research Atmospheres*, 113(D19). doi: 10.1029/2008JD009943.

Rodríguez-Fonseca, B. *et al.* (2011) 'Interannual and decadal SST-forced responses of the West African monsoon', *Atmospheric Science Letters*, 12(1), pp. 67–74. doi: 10.1002/asl.308.

Rohling, E. J. and Pälike, H. (2005) 'Centennial-scale climate cooling with a sudden cold event around 8,200 years ago', *Nature*, 434(7036), pp. 975–979. doi: 10.1038/nature03421.

Rowe, C. (2007) 'A palynological investigation of Holocene vegetation change in Torres Strait, seasonal tropics of northern Australia', *Palaeogeography, Palaeoclimatology, Palaeoecology*, 251(1), pp. 83–103. doi: 10.1016/j.palaeo.2007.02.019.

Rozanski, K., Araguás-Araguás, L. and Gonfiantini, R. (1993) 'Isotopic patterns in modern global precipitation', *Geophysical Monograph*, 75, pp. 1–36. doi: 10.1029/GM078p0001.

Salati, E. *et al.* (1979) 'Recycling of water in the Amazon Basin: An isotopic study', *Water Resources*

Research, 15(5), pp. 1250–1258. doi: 10.1029/WR015i005p01250.

Schmidt, M. W. *et al.* (2012) 'Solar forcing of Florida Straits surface salinity during the early Holocene', *Paleoceanography*, 27(3). doi: 10.1029/2012PA002284.

Scholz, D. and Hoffmann, D. (2008) '^{230}Th/U-dating of fossil corals and speleothems', *E&G Quaternary Science Journal*, 57(1/2), pp. 52–76. doi: 10.3285/eg.57.1-2.3.

Scuderi, L. A. *et al.* (2019) 'The 4.2 ka BP Event in northeastern China: a geospatial perspective', *Climate of the Past*, 15(1), pp. 367–375. doi: 10.5194/cp-15-367-2019.

Scussolini, P. *et al.* (2019) 'Agreement between reconstructed and modeled boreal precipitation of the last interglacial', *Science Advances*, 5(11), pp. 1–12. doi: 10.1126/sciadv.aax7047.

Seetha, C. J. *et al.* (2020) 'Significant changes in the ENSO-monsoon relationship and associated circulation features on multidecadal timescale', *Climate Dynamics*, 54(3–4), pp. 1491–1506. doi: 10.1007/s00382-019-05071-x.

Sengupta, S. and Sarkar, A. (2006) 'Stable isotope evidence of dual (Arabian Sea and Bay of Bengal) vapour sources in monsoonal precipitation over north India', *Earth and Planetary Science Letters*, 250(3–4), pp. 511–521. doi: 10.1016/j.epsl.2006.08.011.

Shao, X. *et al.* (2006) 'Long-term trend and abrupt events of the Holocene Asian monsoon inferred from a stalagmite δ^{18}O record from Shennongjia in Central China', *Chinese Science Bulletin*, 51(2), pp. 221–228. doi: 10.1007/s11434-005-0882-6.

Sharp, Z. (2017) *Principles of Stable Isotope Geochemistry*. 2nd Editio. Pearson. doi: https://doi.org/10.25844/h9q1-0p82.

Shi, X. *et al.* (2021) 'Calendar effects on surface air temperature and precipitation based on model-ensemble equilibrium and transient simulations from PMIP4 and PACMEDY', *Climate of the Past Discussions*. doi: 10.5194/cp-2021-163.

Singarayer, J. S. and Burrough, S. L. (2015) 'Interhemispheric dynamics of the African rainbelt during the late Quaternary', *Quaternary Science Reviews*, pp. 48–67. doi: 10.1016/j.quascirev.2015.06.021.

Sinha, A. *et al.* (2005) 'Variability of Southwest Indian summer monsoon precipitation during the Bølling-Ållerød', *Geology*, 33(10), p. 813. doi: 10.1130/G21498.1.

Sinha, A. *et al.* (2011) 'The leading mode of Indian Summer Monsoon precipitation variability during the last millennium', *Geophysical Research Letters*, 38(15). doi: 10.1029/2011GL047713.

Sinha, A. *et al.* (2015) 'Trends and oscillations in the Indian summer monsoon rainfall over the last two millennia', *Nature Communications*, 6(1), p. 6309. doi: 10.1038/ncomms7309.

Sjolte, J. and Hoffmann, G. (2014) 'Modelling stable water isotopes in monsoon precipitation during the previous interglacial', *Quaternary Science Reviews*, 85, pp. 119–135. doi: 10.1016/j.quascirev.2013.12.006.

Smith, R. J. and Mayle, F. E. (2018) 'Impact of mid- to late Holocene precipitation changes on vegetation across lowland tropical South America: a paleo-data synthesis', *Quaternary Research*, 89(1), pp. 134–155. doi: 10.1017/qua.2017.89.

Street-Perrott, F. A. and Perrott, R. A. (1993) 'Holocene vegetation, lake levels and climate of Africa', in Wright, H. E. et al. (eds) *Global climates since the last glacial maximum*. Minneapolis: University of Minnesota Press, pp. 318–356.

Street, F. A. and Grove, A. T. (1979) 'Global maps of lake-level fluctuations since 30,000 yr B.P.', *Quaternary Research*. doi: 10.1016/0033-5894(79)90092-9.

Stríkis, N. M. *et al.* (2011) 'Abrupt variations in South American monsoon rainfall during the Holocene based on a speleothem record from central-eastern Brazil', *Geology*, 39(11), pp. 1075–1078. doi: 10.1130/G32098.1.

Sturm, C., Zhang, Q. and Noone, D. (2010) 'An introduction to stable water isotopes in climate models:

Benefits of forward proxy modelling for paleoclimatology', *Climate of the Past*, 6(1), pp. 115–129. doi: 10.5194/cp-6-115-2010.

Sultan, B. and Janicot, S. (2003) 'The West African monsoon dynamics. Part II: The "preonset" and "onset" of the summer monsoon', *Journal of Climate*, 16(21), pp. 3407–3427. doi: 10.1175/1520-0442(2003)016<3407:TWAMDP>2.0.CO;2.

Sutton, R. T. and Hodson, D. L. R. (2005) 'Atlantic Ocean Forcing of North American and European Summer Climate', *Science*, 309(5731), pp. 115–118. doi: 10.1126/science.1109496.

Tabor, C., Otto-Bliesner, B. and Liu, Z. (2020) 'Speleothems of South American and Asian Monsoons Influenced by a Green Sahara', *Geophysical Research Letters*, 47(22), pp. 1–11. doi: 10.1029/2020GL089695.

Tabor, C. R. *et al.* (2018) 'Interpreting Precession-Driven $\delta^{18}O$ Variability in the South Asian Monsoon Region', *Journal of Geophysical Research: Atmospheres*, 123(11), pp. 5927–5946. doi: 10.1029/2018JD028424.

Tan, L. *et al.* (2020) 'Holocene Monsoon Change and Abrupt Events on the Western Chinese Loess Plateau as Revealed by Accurately Dated Stalagmites', *Geophysical Research Letters*, 47(21), p. e2020GL090273. doi: 10.1029/2020GL090273.

Tan, M. (2014) 'Circulation effect: Response of precipitation $\delta^{18}O$ to the ENSO cycle in monsoon regions of China', *Climate Dynamics*, 42(3–4), pp. 1067–1077. doi: 10.1007/s00382-013-1732-x.

Tang, K. and Feng, X. (2001) 'The effect of soil hydrology on the oxygen and hydrogen isotopic compositions of plants' source water', *Earth and Planetary Science Letters*, 185(3–4), pp. 355–367. doi: 10.1016/S0012-821X(00)00385-X.

Texier, D. *et al.* (1997) 'Quantifying the role of biosphere-atmosphere feedbacks in climate change: coupled model simulations for 6000 years BP and comparison with palaeodata for northern Eurasia and northern Africa', *Climate Dynamics*, 13(12), pp. 865–881. doi: 10.1007/s003820050202.

Thomas, E. R. *et al.* (2007) 'The 8.2ka event from Greenland ice cores', *Quaternary Science Reviews*, 26(1–2), pp. 70–81. doi: 10.1016/j.quascirev.2006.07.017.

Thompson, L. G., Mosley-Thompson, E. and Henderson, K. A. (2000) 'Ice-core palaeoclimate records in tropical South America since the Last Glacial Maximum', *Journal of Quaternary Science*, 15(4), pp. 377–394. doi: 10.1002/1099-1417(200005)15:4<377::AID-JQS542>3.0.CO;2-L.

Tindall, J. C. and Valdes, P. J. (2011) 'Modeling the 8.2ka event using a coupled atmosphere-ocean GCM', *Global and Planetary Change*, 79(3–4), pp. 312–321. doi: 10.1016/j.gloplacha.2011.02.004.

Trenberth, K. E., Stepaniak, D. P. and Caron, J. M. (2000) 'The global monsoon as seen through the divergent atmospheric circulation', *Journal of Climate*, 13(22), pp. 3969–3993. doi: 10.1175/1520-0442(2000)013<3969:TGMAST>2.0.CO;2.

Truebe, S. A., Ault, T. R. and Cole, J. E. (2010) 'A forward model of cave dripwater $\delta^{18}O$ and application to speleothem records', *IOP Conference Series: Earth and Environmental Science*, 9, p. 012022. doi: 10.1088/1755-1315/9/1/012022.

Vera, C. *et al.* (2006) 'Toward a unified view of the American monsoon systems', *Journal of Climate*, 19(20), pp. 4977–5000. doi: 10.1175/JCLI3896.1.

Vinther, B. M. *et al.* (2006) 'A synchronized dating of three Greenland ice cores throughout the Holocene', *Journal of Geophysical Research: Atmospheres*, 111(D13). doi: 10.1029/2005JD006921.

Voarintsoa, N. R. G. *et al.* (2019) 'Investigating the 8.2 ka event in northwestern Madagascar: Insight from data–model comparisons', *Quaternary Science Reviews*, 204, pp. 172–186. doi: 10.1016/j.quascirev.2018.11.030.

Wackerbarth, A. *et al.* (2012) 'Simulated oxygen isotopes in cave drip water and speleothem calcite in European caves', *Climate of the Past*, 8(6), pp. 1781–1799. doi: 10.5194/cp-8-1781-2012.

Waelbroeck, C. *et al.* (2002) 'Sea-level and deep water temperature changes derived from benthic

foraminifera isotopic records', *Quaternary Science Reviews*, 21(1–3), pp. 295–305. doi: 10.1016/S0277-3791(01)00101-9.

Wagner, A. J. *et al.* (2013) 'Model support for forcing of the 8.2 ka event by meltwater from the Hudson Bay ice dome', *Climate Dynamics*, 41(11–12), pp. 2855–2873. doi: 10.1007/s00382-013-1706-z.

Walker, J. M. and Bordoni, S. (2016) 'Onset and withdrawal of the large-scale South Asian monsoon: A dynamical definition using change point detection', *Geophysical Research Letters*, 43(22), pp. 11,815-11,822. doi: 10.1002/2016GL071026.

Walker, M. *et al.* (2018) 'Formal ratification of the subdivision of the Holocene Series/Epoch (Quaternary System/Period): two new Global Boundary Stratotype Sections and Points (GSSPs) and three new stages/subseries', *Episodes*, 41(4), pp. 213–223. doi: 10.18814/epiiugs/2018/018016.

Waltgenbach, S. *et al.* (2020) 'Climate and structure of the 8.2 ka event reconstructed from three speleothems from Germany', *Global and Planetary Change*, 193, p. 103266.

Wang, B. *et al.* (2012) 'Recent change of the global monsoon precipitation (1979-2008)', *Climate Dynamics*, 39(5), pp. 1123–1135. doi: 10.1007/s00382-011-1266-z.

Wang, B. *et al.* (2021) 'Monsoons climate change assessment', *Bulletin of the American Meteorological Society*, 102(1), pp. E1–E19. doi: 10.1175/BAMS-D-19-0335.1.

Wang, B. and Ding, Q. (2008) 'Global monsoon: Dominant mode of annual variation in the tropics', *Dynamics of Atmospheres and Oceans*, 44(3–4), pp. 165–183. doi: 10.1016/j.dynatmoce.2007.05.002.

Wang, B., Ding, Q. and Joseph, P. V. (2009) 'Objective definition of the Indian summer monsoon onset', *Journal of Climate*, 22(12), pp. 3303–3316. doi: 10.1175/2008JCLI2675.1.

Wang, B. and LinHo (2002) 'Rainy season of the Asian-Pacific summer monsoon', *Journal of Climate*, 15(4), pp. 386–398. doi: 10.1175/1520-0442(2002)015<0386:RSOTAP>2.0.CO;2.

Wang, P. X. *et al.* (2014) 'The global monsoon across timescales: Coherent variability of regional

monsoons', *Climate of the Past*, pp. 2007–2052. doi: 10.5194/cp-10-2007-2014.

Wang, X. *et al.* (2006) 'Interhemispheric anti-phasing of rainfall during the last glacial period', *Quaternary Science Reviews*, 25(23–24), pp. 3391–3403. doi: 10.1016/j.quascirev.2006.02.009.

Wang, X. *et al.* (2007) 'Millennial-scale precipitation changes in southern Brazil over the past 90,000 years', *Geophysical Research Letters*, 34(23). doi: 10.1029/2007GL031149.

Wang, Y. *et al.* (2005) 'The Holocene Asian monsoon: Links to solar changes and North Atlantic climate', *Science*, 308(5723), pp. 854–857. doi: 10.1126/science.1106296.

Wang, Y. *et al.* (2008) 'Millennial- and orbital-scale changes in the East Asian monsoon over the past 224,000 years', *Nature*, 451(7182), pp. 1090–1093. doi: 10.1038/nature06692.

Wang, Y. J. *et al.* (2001) 'A high-resolution absolute-dated late Pleistocene monsoon record from Hulu Cave, China', *Science*, 294(5550), pp. 2345–2348. doi: 10.1126/science.1064618.

Werner, M. *et al.* (2016) 'Glacial-interglacial changes in $H_2{}^{18}O$, HDO and deuterium excess-results from the fully coupled ECHAM5/MPI-OM Earth system model', *Geoscientific Model Development*, 9(2), pp. 647–670. doi: 10.5194/gmd-9-647-2016.

Werner, M. *et al.* (2018) 'Reconciling glacial Antarctic water stable isotopes with ice sheet topography and the isotopic paleothermometer', *Nature Communications*, 9(1), pp. 1–10. doi: 10.1038/s41467-018-05430-y.

Wheeler, M. C. and McBride, J. L. (2012) 'Australasian monsoon', in Lau, W. K. (ed.) *Intraseasonal Variability in the Atmosphere-Ocean Climate System*. Berlin, Heidelberg: Springer Berlin Heidelberg, pp. 147–197. doi: 10.1007/978-3-642-13914-7_5.

Winter, A. *et al.* (2020) 'Initiation of a stable convective hydroclimatic regime in Central America circa 9000 years BP', *Nature Communications 2020 11:1*, 11(1), pp. 1–8. doi: 10.1038/s41467-020-14490-y.

Wohlfahrt, J., Harrison, S. P. and Braconnot, P. (2004) 'Synergistic feedbacks between ocean and

vegetation on mid- and high-latitude climates during the mid-Holocene', *Climate Dynamics*, 22(2–3), pp. 223–238. doi: 10.1007/s00382-003-0379-4.

Woodhead, J. *et al.* (2006) 'U-Pb geochronology of speleothems by MC-ICPMS', *Quaternary Geochronology*. doi: 10.1016/j.quageo.2006.08.002.

Wu, J. Y. *et al.* (2012) 'Stable isotope and trace element investigation of two contemporaneous annually-laminated stalagmites from northeastern China surrounding the 8.2 ka event', *Climate of the Past*, 8(5), pp. 1497–1507. doi: 10.5194/cp-8-1497-2012.

Wurtzel, J. B. *et al.* (2018) 'Tropical Indo-Pacific hydroclimate response to North Atlantic forcing during the last deglaciation as recorded by a speleothem from Sumatra, Indonesia', *Earth and Planetary Science Letters*, 492, pp. 264–278. doi: 10.1016/J.EPSL.2018.04.001.

Xiao, J. *et al.* (2018) 'The 4.2 ka BP event: multi-proxy records from a closed lake in the northern margin of the East Asian summer monsoon', *Climate of the Past*, 14(10), pp. 1417–1425. doi: 10.5194/cp-14-1417-2018.

Yadava, M. G., Ramesh, R. and Pant, G. B. (2004) 'Past monsoon rainfall variations in peninsular India recorded in a 331-year-old speleothem', *Holocene*, 14(4), pp. 517–524. doi: 10.1191/0959683604hl728rp.

Yim, S. Y. *et al.* (2014) 'A comparison of regional monsoon variability using monsoon indices', *Climate Dynamics*, 43(5–6), pp. 1423–1437. doi: 10.1007/s00382-013-1956-9.

Yonge, C. J. *et al.* (1985) 'Stable isotope studies of cave seepage water', *Chemical Geology: Isotope Geoscience Section*, 58(1–2), pp. 97–105. doi: 10.1016/0168-9622(85)90030-2.

Yoon, J. and Yeh, S.-W. (2010) 'Influence of the Pacific Decadal Oscillation on the Relationship between El Niño and the Northeast Asian Summer Monsoon', *Journal of Climate*, 23(17), pp. 4525–4537. doi: 10.1175/2010JCLI3352.1.

Yu, G. *et al.* (2003) 'LGM lake records from China and an analysis of climate dynamics using a modelling approach', *Global and Planetary Change*, 38(3–4), pp. 223–256. doi: 10.1016/S0921-8181(02)00257-6.

Yu, S.-Y. *et al.* (2010) 'Freshwater Outburst from Lake Superior as a Trigger for the Cold Event 9300 Years Ago', *Science*, 328(5983), pp. 1262–1266. doi: 10.1126/science.1187860.

Yuan, D. *et al.* (2004) 'Timing, duration, and transitions of the Last Interglacial Asian monsoon', *Science*, 304(5670), pp. 575–578. doi: 10.1126/science.1091220.

Yuan, Y. *et al.* (2008) 'Influences of the Indian Ocean dipole on the Asian summer monsoon in the following year', *International Journal of Climatology*, 28(14), pp. 1849–1859. doi: 10.1002/joc.1678.

Zhang *et al.* (2019) 'The Asian Summer monsoon: Teleconnections and forcing Mechanisms—A review from Chinese speleothem $\delta^{18}O$ records', *Quaternary*, 2(3), p. 26. doi: 10.3390/quat2030026.

Zhang, H. *et al.* (2021) 'A data-model comparison pinpoints Holocene spatiotemporal pattern of East Asian summer monsoon', *Quaternary Science Reviews*, 261, p. 106911. doi: 10.1016/j.quascirev.2021.106911.

Zhang, R. and Delworth, T. L. (2006) 'Impact of Atlantic multidecadal oscillations on India/Sahel rainfall and Atlantic hurricanes', *Geophysical Research Letters*, 33(17), p. L17712. doi: 10.1029/2006GL026267.

Zhang, S. and Wang, B. (2008) 'Global summer monsoon rainy seasons', *International Journal of Climatology*, 28, pp. 1563–1578. doi: 10.1002/joc.

Zhang, W. *et al.* (2016) 'Unraveling El Niño's impact on the East Asian Monsoon and Yangtze River summer flooding', *Geophysical Research Letters*, 43(21). doi: 10.1002/2016GL071190.

Zhao, J. *et al.* (2019) 'Reconstructing the western boundary variability of the Western Pacific Subtropical High over the past 200 years via Chinese cave oxygen isotope records', *Climate Dynamics*, 52(5–6), pp. 3741–3757. doi: 10.1007/s00382-018-4456-0.

Zhao, Y. *et al.* (2009) 'Vegetation response to Holocene climate change in monsoon-influenced region of

China', *Earth-Science Reviews*, 97(1–4), pp. 242–256. doi: 10.1016/j.earscirev.2009.10.007.

Zhao, Y. and Harrison, S. P. (2012) 'Mid-Holocene monsoons: A multi-model analysis of the inter-hemispheric differences in the responses to orbital forcing and ocean feedbacks', *Climate Dynamics*, 39(6), pp. 1457–1487. doi: 10.1007/s00382-011-1193-z.

Zimmerman, U., Ehhalt, D. and Münnich, K. O. (1969) 'Soil water movement and evapotranspiration: changes in the isotopic composition of the water', in *Isotopes in Hydrology*. Vienna: International Atomic Energy Agency, pp. 567–584.

2 A data–model approach to interpreting speleothem oxygen isotope records from monsoon regions

2.1 Preface

The following chapter is a paper published in Climate of the Past and is available to read online at https://doi.org/10.5194/cp-17-1119-2021. It has been written and referenced in the style guidelines of this journal. The authors were Sarah E. Parker, Sandy P. Harrison, Laia Comas-Bru, Nikita Kaushal, Allegra N. LeGrande and Martin Werner. The study was designed by SEP, SPH, LCB and NK. MW and ANLG provided climate model outputs. SEP ran the analyses. The first draft of the paper was written by SEP, SPH and LCB, and all authors contributed to the final article. Estimated contributions are SEP: 50 %; SPH: 10 %; LCB: 10 %; NK: 10 %; ANLG: 10 % and MW: 10%

The study explores regional and global-scale monsoon evolution through the Holocene and between the mid-Holocene, Last Glacial Maximum and Last Interglacial. Oxygen isotope data-model comparisons are used to elucidate the climate processes that are driving speleothem oxygen isotope observations. This paper demonstrates the global-scale coherency of monsoon speleothem records, although with some regional distinctions, emphasising the importance of orbital forcing and internal feedbacks. The data-model comparisons demonstrate the importance of regional precipitation and atmospheric circulation changes for regional speleothem $\delta^{18}O$ evolution.

2.2 Abstract

Reconstruction of past changes in monsoon climate from speleothem oxygen isotope ($\delta^{18}O$) records is complex because $\delta^{18}O$ signals can be influenced by multiple factors including changes in precipitation, precipitation recycling over land, temperature at the moisture source, and changes in the moisture source region and transport pathway. Here, we analyse > 150 speleothem records of the Speleothem Isotopes Synthesis and AnaLysis (SISAL) database to produce composite regional trends in $\delta^{18}O$ in monsoon

regions; compositing minimises the influence of site-specific karst and cave processes that can influence individual site records. We compare speleothem $\delta^{18}O$ observations with isotope-enabled climate model simulations to investigate the specific climatic factors causing these regional trends. We focus on differences in $\delta^{18}O$ signals between the mid-Holocene, the peak of the Last Interglacial (Marine Isotope Stage 5e) and the Last Glacial Maximum as well as on $\delta^{18}O$ evolution through the Holocene. Differences in speleothem $\delta^{18}O$ between the mid-Holocene and the Last Interglacial in the East Asian and Indian monsoons are small, despite the larger summer insolation values during the Last Interglacial. Last Glacial Maximum $\delta^{18}O$ values are significantly less negative than interglacial values. Comparison with simulated glacial–interglacial $\delta^{18}O$ shows that changes are principally driven by global shifts in temperature and regional precipitation. Holocene speleothem $\delta^{18}O$ records show distinct and coherent regional trends. Trends are similar to summer insolation in India, China and southwestern South America, but they are different in the Indonesian–Australian region. Redundancy analysis shows that 37 % of Holocene variability can be accounted for by latitude and longitude, supporting the differentiation of records into individual monsoon regions. Regression analysis of simulated precipitation $\delta^{18}O$ and climate variables show significant relationships between global Holocene monsoon $\delta^{18}O$ trends and changes in precipitation, atmospheric circulation and (to a lesser extent) source area temperature, whereas precipitation recycling is non-significant. However, there are differences in regional-scale mechanisms: there are clear relationships between changes in precipitation and $\delta^{18}O$ for India, southwestern South America and the Indonesian–Australian regions but not for the East Asian monsoon. Changes in atmospheric circulation contribute to $\delta^{18}O$ trends in the East Asian, Indian and Indonesian–Australian monsoons, and a weak source area temperature effect is observed over southern and central America and Asia. Precipitation recycling is influential in southwestern South America and southern Africa. Overall, our analyses show that it is possible to differentiate the impacts of specific climatic mechanisms influencing precipitation $\delta^{18}O$ and use this analysis to interpret changes in speleothem $\delta^{18}O$.

2.3 Introduction

The oxygen isotopic ($\delta^{18}O$; the $^{18}O/\ ^{16}O$ ratio relative to a standard, in per mille, ‰) composition of speleothems is widely used to infer past regional climates (Bar-Matthews, Ayalon and Kaufman, 1997; McDermott, 2004; Wang *et al.*, 2008). Speleothem oxygen isotope ($\delta^{18}O_{spel}$) signals are inherited from $\delta^{18}O$ in precipitation ($\delta^{18}O_{precip}$) above the cave, which in turn is determined by the initial $\delta^{18}O$ of water vapour as it evaporates at the oceanic moisture source region, the degree of rainout and evaporation from source to cave site, and air temperature changes encountered throughout the moisture transport pathway (Lachniet, 2009; Fairchild and Baker, 2012). Understanding the effects and contribution of each of these climate processes to $\delta^{18}O_{precip}$ (and therefore $\delta^{18}O_{spel}$) is essential to inferring palaeoclimate from speleothem $\delta^{18}O$ records.

Initial $\delta^{18}O$ is determined by oceanic $\delta^{18}O$ at the evaporative moisture source region (Craig and Gordon, 1965), which varies spatially (LeGrande and Schmidt, 2006) and through time (e.g. Waelbroeck *et al.*, 2002). During evaporation from the moisture source, ^{16}O is preferentially incorporated into the vapour, whilst subsequent fractionation during atmospheric transport occurs by Rayleigh distillation; as air masses cool and moisture condenses, heavier ^{18}O is enriched in the liquid phase and removed by precipitation. With progressive rainout along a moisture pathway, precipitation becomes gradually more depleted (Dansgaard, 1964). Within this framework, $\delta^{18}O_{precip}$ is controlled by two variables: temperature and the amount of precipitation along a moisture pathway. The temperature effect stems from the cooling required for progressive rainout during Rayleigh distillation (Dansgaard, 1964; Rozanski, Araguás-Araguás and Gonfiantini, 1993). The temperature $\delta^{18}O$ impact is dominant at mid to high latitudes, whilst observations suggest that changes in upstream and local precipitation dominate changes in the $\delta^{18}O_{precip}$ signal at tropical latitudes. The negative relationship between local precipitation and $\delta^{18}O_{precip}$, often referred to as the "amount effect" (Dansgaard, 1964; Bailey, Posmentier and Feng, 2018), results from the re-evaporation and diffusive exchange between precipitation and water vapour during deep convective precipitation (Risi, Bony and Vimeux, 2008). However, Rayleigh distillation is complicated by changes in atmospheric circulation and moisture recycling. Changes in the area from which the moisture

is sourced will modify $\delta^{18}O_{precip}$ because the initial $\delta^{18}O$ values differ between sources (Cole *et al.*, 1999; Friedman *et al.*, 2002), whilst changes in the moisture transport pathway and/or distance between the source and cave site can result in differing degrees of fractionation associated with condensation and evaporation (Aggarwal *et al.*, 2012; Bailey, Posmentier and Feng, 2018). The isotopic composition of atmospheric water vapour may also be modified by precipitation recycling over land, as evapotranspiration returns moisture from precipitation back to the atmosphere, thereby minimising the $\delta^{18}O$precip/distance gradient along an advection path that occurs with Rayleigh distillation (Salati *et al.*, 1979; Gat, 1996).

Speleothem $\delta^{18}O$ records from monsoon regions show multi-millennial variability that has been interpreted as documenting the waxing and waning of the monsoons in response to changes in summer insolation, often interpreted predominantly as a change in the absolute amount of precipitation (Fleitmann *et al.*, 2003; Cheng, Sinha, *et al.*, 2013) or a change in the ratio of more negative $\delta^{18}O$ summer precipitation to less negative $\delta^{18}O$ winter precipitation (Wang *et al.*, 2001; Dong *et al.*, 2010). However, the multiplicity of processes that influence $\delta^{18}O$ before its incorporation in the speleothem makes it difficult to attribute the climatic causes of changes in individual speleothem records unambiguously. In the East Asian monsoon, for example, speleothem $\delta^{18}O$ records have been interpreted as a summer monsoon signal, manifested as a change in the amount of water vapour removed along the moisture trajectory (Yuan *et al.*, 2004), and/or as a change in the contribution of summer precipitation to annual totals (Wang *et al.*, 2001; Cheng *et al.*, 2006, 2016; Cheng, Fleitmann, Edwards, Wang, Cruz, Auler, Mangini, Wang, Kong, Burns, *et al.*, 2009) based on the relationship between modern $\delta\ ^{18}O_{precip}$ and climate. Other interpretations of Chinese monsoon $\delta^{18}O_{spel}$ have included rainfall source changes (Tan, 2009, 2011, 2014) or local rainfall changes (Tan et al., 2015). Maher (2008) interpreted $\delta^{18}O_{spel}$ as reflecting changes in moisture source area, based on differences between $\delta^{18}O_{spel}$ and loess/palaeosol records of rainfall and the strong correlation between East Asian and Indian monsoon speleothems. Maher and Thompson (2012) used a mass balance approach to show that the changes in precipitation (either local or upstream) or rainfall seasonality required to reproduce $\delta^{18}O_{spel}$ trends would be unreasonably large. Thus, they argued that changes in moisture source were required to explain shifts in

$\delta^{18}O$ both on glacial–interglacial timescales and during interglacials. Overall, there are several plausible climate mechanisms that could contribute to $\delta^{18}O_{spel}$ on multi-millennial timescales. East Asian monsoon speleothem records are often interpreted as a combination of several of these processes (Dykoski *et al.*, 2005; Cheng *et al.*, 2016) which generally represent monsoon intensity (Cheng *et al.*, 2019). There are also multiple interpretations of the causes of $\delta^{18}O_{spel}$ variability in other monsoon regions. In the Indian monsoon region, speleothem $\delta^{18}O$ records are interpreted primarily as an amount effect signal (Fleitmann *et al.*, 2004; Berkelhammer *et al.*, 2010), supported by modern $\delta^{18}O_{precip}$ and climate observations (e.g. Battacharya et al., 2003). However, other studies have suggested that $\delta^{18}O_{precip}$ changes in this region are driven primarily by large-scale changes in monsoon circulation; hence, Indian monsoon $\delta^{18}O_{spel}$ should be interpreted as a moisture source and/or trajectory signal (Breitenbach *et al.*, 2010; Sinha *et al.*, 2015). In the Indonesian–Australian monsoon region, $\delta^{18}O_{spel}$ variability has been interpreted as a precipitation amount signal (Carolin *et al.*, 2016; Krause *et al.*, 2019) or a precipitation seasonality signal (Griffiths *et al.*, 2009a; Ayliffe *et al.*, 2013), based on modern $\delta^{18}O_{precip}$ and climate observations (Cobb *et al.*, 2007; Moerman *et al.*, 2013), and/or as a moisture source and/or trajectory signal (Griffiths *et al.*, 2009a; Wurtzel *et al.*, 2018). South American speleothem records have been interpreted as records of monsoon intensity, due to changes in the amount of precipitation over the region (Cruz, Burns, *et al.*, 2005; Wang *et al.*, 2006; Cheng, Sinha, *et al.*, 2013), changes in the degree of upstream precipitation and evapotranspiration (Cheng, Sinha, *et al.*, 2013), or changes in the ratio of precipitation sourced from the low-level jet versus the Atlantic (F.W. Cruz *et al.*, 2006; Wang *et al.*, 2006).

These interpretations generally rely on modern $\delta^{18}O_{precip}$ and climate observations, which may not have remained constant through time. The sources of $\delta^{18}O$ variability can also be explored using isotope-enabled climate models (e.g. Hu *et al.*, 2019), which incorporate known isotope effects and, therefore, provide plausible explanations for $\delta^{18}O_{spel}$ trends. Modelling studies suggest that changes in East Asian monsoon $\delta^{18}O_{precip}$, during Heinrich events (Lewis *et al.*, 2010; Pausata *et al.*, 2011) and on an orbital timescale (LeGrande and Schmidt, 2009; Battisti, Ding and Roe, 2014), do not reflect local rainfall variability but instead reflect changes in the $\delta^{18}O$ of vapour delivered to the region. Variability in the $\delta^{18}O$ of vapour delivered to East Asia on orbital timescales has been diagnosed as being due to changes in

precipitation upstream of the region (Battisti, Ding and Roe, 2014), changes in moisture source location (Tabor *et al.*, 2018; Jun Hu *et al.*, 2019) or changes in the strength of monsoon winds (LeGrande and Schmidt, 2009; Liu *et al.*, 2014). $\delta^{18}O_{precip}$ variability in the East Asian monsoon during Heinrich events has also been attributed to non-local isotope fractionation (Lewis *et al.*, 2010; Pausata *et al.*, 2011). Modelling results suggest that changes in precipitation amount are the predominant source of $\delta^{18}O$ variability in the Indian monsoon during the Holocene (LeGrande and Schmidt, 2009) and in the glacial (Lewis *et al.*, 2010) as well as in the South American and Indonesian–Australian regions during Heinrich events (Lewis *et al.*, 2010) and the Last Interglacial (Sjolte and Hoffmann, 2014).

In this study, we combine speleothem $\delta^{18}O$ records of the Speleothem Isotopes Synthesis and AnaLysis (SISAL) database with isotope-enabled palaeoclimate simulations from two climate models to investigate the plausible mechanisms driving changes in $\delta^{18}O$ in monsoon regions through the Holocene (last 11 700 years) and between the mid-Holocene, the peak of the Last Interglacial and the Last Glacial Maximum. We compare $\delta^{18}O_{spel}$ signals across geographically separated cave sites to extract a regional signal, thereby minimising the influence of karst and in-cave processes, such as the mixing of groundwaters from different precipitation events or changes in cave ventilation, that can be important for the $\delta^{18}O_{spel}$ of individual records. We use principal coordinate analysis (PCoA) to identify regions with geographically coherent $\delta^{18}O_{spel}$ records and then examine how these regions behave on glacial–interglacial timescales and through the Holocene. We use isotope-enabled model simulations to investigate the potential causes of $\delta^{18}O_{spel}$ variability in regions where the models reproduce the largescale $\delta^{18}O$ changes shown by observations. We exploit the fact that models produce internally physically consistent changes to explore potential and plausible causes of the trends observed in speleothem records across specific monsoon regions, using multiple regression analysis.

2.4 Methods

2.4.1 Speleothem oxygen isotope data

Speleothem $\delta^{18}O$ records were obtained from the SISAL (Speleothem Isotopes Synthesis and AnaLysis) database (Atsawawaranunt et al., 2018; Comas-Bru et al., 2020a, b). Records were selected based on the following criteria:

- they are located in monsoon regions, between 35° S and 40° N;
- the mineralogy is known and does not vary (i.e. between calcite and aragonite) through time, because oxygen isotope fractionation during speleothem precipitation is different for calcite and aragonite;
- for the analysis of mid-Holocene (MH), Last Glacial Maximum (LGM) and Marine Isotope Stage 5e during the Last Interglacial (LIG) $\delta^{18}O$ signals, the records contain samples within at least one of these time periods, defined as 6000 ± 500 years BP for the MH, 21 000 ± 1000 years BP for the LGM and 125 000 ± 1000 years BP for the LIG, where BP (before present) is 1950 CE;
- for the PCoA, the records have a temporal coverage of at least 4000 years in the Holocene;
- for Holocene trend analyses, speleothems have a record of the period from 7000 to 3000 years BP;
- they are the most recent update of the record from a site available in version 2 of the SISAL database.

This resulted in the selection of 125 records from 44 sites for the PCoA analysis, 64 records from 38 sites for the analysis of MH, LGM and LIG signals, and 79 records from 40 sites for the Holocene trend analysis (Fig. 2.1). Although the SISALv2 database contains multiple age models for some sites, we use the published age models given by the original authors for all records.

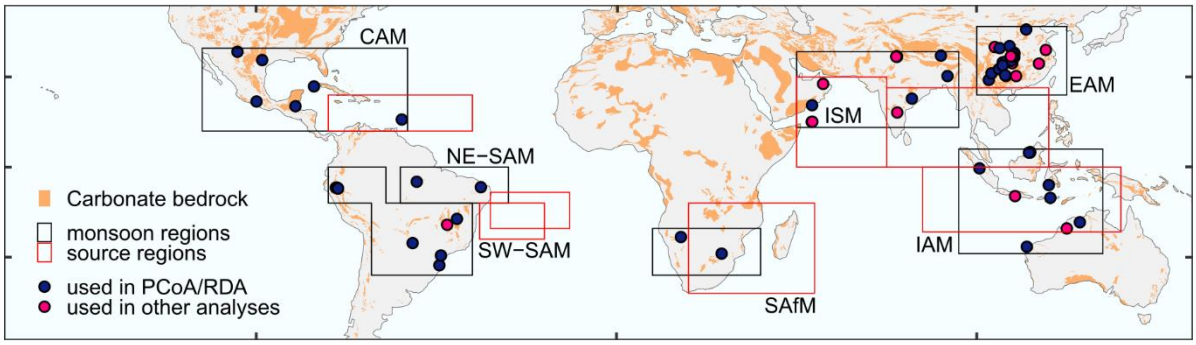

Figure 2.1. Spatial distribution of speleothem records used is this study. Colours indicate the sites used in principal coordinates analysis (PCoA) and redundancy analysis (RDA) to separate monsoon regions, and sites not used in PCoA and RDA but used in subsequent analyses. The individual regional monsoons are shown by boxes: CAM denotes the Central American monsoon (latitude from 10 to 33° , longitude from −115 to −58°), SW-SAM denotes the southwestern South American monsoon (latitude from −10 to 0° , longitude from −80 to −64° ; latitude from −30 to −10° , longitude −68 to −40°), NE-SAM denotes the northeastern South American monsoon (latitude from −10 to 0° , longitude: −60 to −30°), SAfM denotes the southern African monsoon (latitude from −30 to −17° , longitude from 10 to 40°), ISM denotes the Indian summer monsoon (latitude from 11 to 32° , longitude from 50 to 95°), EAM denotes the East Asian monsoon (latitude from 20 to 39° , longitude from 100 to 125°) and IAM denotes the Indonesian–Australian monsoon (latitude from −24 to 5°, longitude from 95 to 135°). Source region limits used in the multiple linear regression analysis are also shown. The background carbonate lithology is from the WOrld Karst Aquifer Mapping (WOKAM) project (Goldschneider et al., 2020).

2.4.2 Climate model simulations

There are relatively few palaeoclimate simulations made with models that incorporate oxygen isotope tracers, and the available simulations do not necessarily focus on the same periods or use the same modelling protocols. Here, we use simulations of opportunity from two isotope-enabled climate models: ECHAM5 (version 5 of the European Centre for medium-range weather forecasting model in HAMburg) and GISS ModelE-R (Goddard Institute for Space Studies Model version E-R). The ECHAM5 simulations provide an opportunity to examine large-scale changes between glacial and interglacial states, using simulations of the MH, LGM and LIG. The GISS ModelE-R ocean–atmosphere coupled general circulation model was used to investigate the evolution of $\delta^{18}O$ evolution during the Holocene, using eight time slice (9, 6, 5, 4, 3, 2, 1 and 0 ka) experiments. Although simulations of the MH 6 ka time slice are available with both models, there are differences in the protocol used for the two experiments which preclude direct comparison of the simulations.

The ECHAM5-wiso MH experiment (Wackerbarth et al., 2012; Werner, 2019) was forced by orbital parameters (based on Berger and Loutre, 1991) and greenhouse gas (GHG) concentrations (CO_2 = 280 ppm, CH_4 = 650 ppb, N_2O = 270 ppb) appropriate to 6 ka. Changes in sea surface temperature (SST) and

sea ice were derived from a transient Holocene simulation (Varma et al., 2012). The control simulation for the MH experiment was an ECHAM-wiso simulation of the period from 1956 to 1999 (Langebroek et al., 2011), using observed SSTs and sea ice cover. This control experiment was forced by SSTs and sea ice only, with atmospheric circulation free to evolve. The ECHAM5-wiso LGM experiment (Werner, 2019; Werner et al., 2018) was forced by orbital parameters (Berger and Loutre, 1991), GHG concentrations (CO_2 = 185 ppm, CH_4 = 350 ppb, N_2O = 200 ppb), land–sea distribution and ice sheet height and extent appropriate to 21 ka; SST and sea ice cover were prescribed from the GLAMAP dataset (Schäfer-Neth and Paul, 2003). Sea surface water and sea ice $\delta^{18}O$ were uniformly enriched by 1‰ at the start of the experiment. The control simulation for the LGM experiment used present-day conditions, including orbital parameters and GHG concentrations set to modern values, and SSTs and sea ice cover from the last 20 years (1979–1999). Both the MH and LGM simulations were run at T106 horizontal grid resolution, approximately 1.1° × 1.1° at the Equator. Comparison of the MH and LGM simulations with speleothem data globally (Figs. S1 and S2 in the Supplement; Comas-Bru et al., 2019) show that the ECHAM model reproduces the broadscale spatial gradients and the sign of isotopic changes at the majority of cave sites (MH: 72 %; LGM: 76 %). However, the changes compared with present are generally more muted in the simulations than shown by the speleothem records.

The LIG experiment (Gierz et al., 2017b, a) was run using the ECHAM5/MPI-OM Earth system model, with stable water isotope diagnostics included in the ECHAM5 atmosphere model (Werner et al., 2011), the dynamic vegetation model JSBACH (Haese et al., 2012) and the MPIOM ocean–sea-ice module (Xu et al., 2012). This simulation was run at a T31L19 horizontal grid resolution, approximately 3.75° × 3.75°. The LIG simulation was forced by orbital parameters derived from Berger and Loutre (1991) and GHG concentrations (CO_2 = 276 ppm, CH_4 = 640 ppb, N_2O = 263 ppb) appropriate to 125 ka, but it was assumed that the ice sheet configuration and land–sea geography remain unchanged from modern; therefore no change was made to the isotopic composition of sea water. The LIG simulation is compared to a pre-industrial (PI) control with appropriate insolation, GHG and ice sheet forcing for 1850 CE. The sign of simulated isotopic changes in the LIG is in good agreement with ice core records from Antarctica and Greenland and speleothem records from Europe, the Middle East and China (Gierz et al., 2017b),

although, as with the MH and LGM, the observed changes tend to be larger than the simulated changes (Fig. S3).

There are GISS ModelE-R (LeGrande and Schmidt, 2009) simulations for eight time slices during the Holocene (9, 6, 5, 4, 3, 2, 1 and 0 ka). The 0 ka experiment is considered as the pre-industrial control (ca. 1880 CE). Orbital parameters were based on Berger and Loutre (1991), and GHG concentrations were adjusted based on ice core reconstructions (Brook et al., 2000; Indermühle et al., 1999; Sowers, 2003) for each time slice. A remnant Laurentide ice sheet was included in the 9 ka simulation, following Licciardi et al. (1998), and the corresponding adjustment was made to mean ocean salinity and ocean water $\delta^{18}O$ to account for this (Carlson et al., 2008). The ice sheet in all the other experiments was specified to be the same as modern; therefore, no adjustment was necessary. The simulations were run using the M20 version of GISS ModelE-R, which has a horizontal resolution of 4° × 5°. Each experiment was run for 500 years, and we use the last 100 simulated years for the analyses. Comparison of the simulated trends in $\delta^{18}O$ show good agreement with Greenland ice core records, marine records from the tropical Pacific and Chinese speleothem records (LeGrande and Schmidt, 2009). However, as is the case with the ECHAM simulations, the model tends to produce changes that are less extreme than those shown by the observations (Figs. S4, S5, S6).

2.4.3 Principal coordinate analysis and redundancy analysis

We used PCoA to identify regionally coherent patterns in the speleothem $\delta^{18}O$ records for the Holocene. PCoA is a multivariate ordination technique that uses a distance matrix to represent inter-object (dis)similarity in reduced space (Gower, 1966; Legendre and Legendre, 1998). Speleothem records from individual sites are often discontinuous; missing data are problematic for many ordination techniques. PCoA is more robust to missing data than other methods (Kärkkäinen and Saarela, 2015; Rohlf, 1972). We used a correlation matrix of speleothem records as the (dis)similarity measure. The temporal resolution of speleothem records was first standardised by calculating a running average mean with non-overlapping 500-year windows. This procedure produces a single composite record when there are several records for a given site. PCoA results were displayed as a biplot, where sites ordinated close to one another (i.e., with

similar PCoA scores) show similar Holocene trends, and sites ordinated far apart have dissimilar trends. We used the "broken stick" model (Bennett, 1996) to identify which PCoA axes were significant. We used redundancy analysis (RDA: Legendre and Legendre, 1998; Rao, 1964) with latitude and longitude as predictor variables to identify if PCoA (dis)similarities were related to geographical location, and principal components analysis (PCA) to identify the main patterns of variation. As these explanatory variables are not dimensionally homogeneous, they were centred on their means and standardised to allow direct comparison of the gradients. PCoA and RDA analyses were carried out using the "vegan" package in R (Oksanen et al., 2019).

2.4.4 Glacial-interglacial changes in $\delta^{18}O$

We examined shifts in $\delta^{18}O_{spel}$ observations and in annual precipitation-weighted mean $\delta^{18}O_{precip}$ from ECHAM-wiso in regions influenced by the monsoon, between the MH, LGM and LIG. Values are given as anomalies with respect to the present day for speleothems or the control simulation experiment for model outputs. Comas-Bru et al. (2019) have shown that differences in speleothem $\delta^{18}O$ data between the 20th century and the pre-industrial period (i.e., 1850±15 CE) are within the temporal and measurement uncertainties of the data; thus, the use of different reference periods (i.e., PI for the ECHAM LIG experiment, 20th century for ECHAM MH, LGM experiments) should have little effect on our analyses. We used mean site $\delta^{18}O_{spel}$ values for each period for the regions identified in the PCoA analysis. Where there are multiple speleothem $\delta^{18}O$ records for a site in a time period, they were averaged to calculate mean $\delta^{18}O_{spel}$. Three sites above 3500 m were excluded from the calculation of the means because high-elevation sites have more negative $\delta^{18}O$ values than their low-elevation counterparts, and their inclusion would distort the regional estimates.

There are relatively few speleothems covering both the present day and the period of interest (i.e., MH, LGM or LIG), precluding the calculation of $\delta^{18}O_{spel}$ anomalies from the speleothem data. Therefore, we calculated anomalies with respect to the modern period (1960–2017 CE) using the Online Isotopes in Precipitation Calculator (OIPC: Bowen, 2018; Bowen and Revenaugh, 2003), a global gridded dataset of interpolated mean annual precipitation-weighted $\delta^{18}O_{precip}$ data, as reference. This dataset combines data

from 348 stations from the Global Network of Isotopes in Precipitation (IAEA/WMO, 2018), covering part or all of the 1960– 2014 period, and other records available at the Waterisotopes Database (Waterisotopes Database, 2017).

OIPC $\delta^{18}O_{precip}$ was converted to its speleothem equivalent assuming that (i) precipitation-weighted mean annual $\delta^{18}O_{precip}$ is equivalent to mean annual drip-water $\delta^{18}O$ (Yonge et al., 1985) and that (ii) precipitation of calcite is consistent with the empirical speleothem-based kinetic fractionation factor of Tremaine et al. (2011) and precipitation of aragonite follows the fractionation factor from Grossman and Ku (1986), as formulated by Lachniet (2015):

$$\delta^{18}O_{calcite\_SMOW} = w\delta^{18}O_{precip\_SMOW} + \left(\left(\frac{16.1 \cdot 1000}{T}\right) - 24.6\right) \ (T \ in \ K) \quad 2.1$$

$$\delta^{18}O_{aragonite\_SMOW} = w\delta^{18}O_{precip\_SMOW} + \left(\left(\frac{18.34 \cdot 1000}{T}\right) - 31.954\right) \ (T \ in \ K) \quad 2.2$$

where $\delta^{18}O_{calcite\_SMOW}$ and $\delta^{18}O_{aragonite\_SMOW}$ are the respective speleothem isotopic composition for calcite and aragonite speleothems with reference to the VSMOW (Vienna Standard Mean Ocean Water) standard (in per mille), $w\delta^{18}O_{precip}$ is the OIPC precipitation-weighted annual mean isotopic composition of precipitation with respect to the VSMOW standard and T is the mean annual cave temperature (in kelvin). We used the long-term (1960–2016) mean annual surface air temperature from the CRU-TS4.01 database (Harris and Jones, 2017; Harris et al., 2020) at each site as a surrogate for mean annual cave air temperature. The resolution of the gridded data means that $w\delta^{18}O_{precip\_SMOW}$ and T may be the same for nearby sites.

We use the VSMOW to VPDB (Vienna Pee Dee Belemnite) conversion from Coplen et al. (1983), which is independent of speleothem mineralogy:

$$\delta^{18}O_{PDB} = 0.97001 \cdot \delta^{18}O_{SMOW} - 29.29 \quad 2.3$$

where $\delta^{18}O_{PDB}$ is relative to the VPDB standard, and $\delta^{18}O_{SMOW}$ is relative to VSMOW standard.

Average uncertainties in the speleothem age–depth models are ~ 50 years during the Holocene. This interval is smaller than the time windows used in this analysis; therefore, the age uncertainty is expected to have a negligible impact on the results. We investigated the influence of age uncertainties on the LGM and LIG $\delta^{18}O_{spel}$ anomalies by examining the impact of using different window widths (±500, ±700, ±1000, ±2000 years) on the regional mean $\delta^{18}O_{spel}$ anomalies.

We used anomalies of $w\delta^{18}O_{precip}$, mean annual surface air temperature (MAT) and mean annual precipitation (MAP) from the ECHAM5-wiso simulations to investigate the changes in $\delta^{18}O_{spel}$ between the MH, LGM and LIG as well as their association with changes in climate. Values were calculated from land grid cells (> 50 % land) ±3° around each speleothem site. This distance was chosen with reference to the coarsest-resolution simulation (LIG, ca. 3.75° × 3.75°). Gridded values of MAT and MAP were weighted by the proportion of each grid cell that lies within ±3° of the site, and linear distance-weighted means were calculated for each site and time slice. We only considered regions with at least one speleothem record for each of the three time periods, although these were not required to be the same sites, and where the observed shifts in $\delta^{18}O_{spel}$ were in the same direction and of a similar magnitude to the simulated $w\delta^{18}O_{precip}$.

2.4.5 Holocene and Last Interglacial regional trends

Regional speleothem $\delta^{18}O$ changes through the Holocene were examined by creating composite time series for each region identified in the PCoA analysis with at least four Holocene records (> 5000 years long). Regional composites were constructed using a four-step procedure, modified from Marlon et al. (2008):

1. The $\delta^{18}O$ data for individual speleothems were transformed to z scores, so all records have a standardised mean and variance:

$$z\ score_i = \left(\delta^{18}O_i - \overline{\delta^{18}O_{(base\ period)}}\right) / s\delta^{18}O_{(base\ period)} \quad 2.4$$

Where $\overline{\delta^{18}O}$ is the mean, and sδ^{18}O is the standard deviation of δ^{18}O for a common base period. A base period of 7000 to 3000 years BP was chosen to maximise the number of records included in each composite.

2. The standardised data for a site were resampled by applying a 100-year non-overlapping running mean with the first bin centred at 50 years BP, in order to create a single site time series while ensuring that highly resolved records do not dominate the regional composite.
3. Each regional composite was constructed using locally weighted regression (Cleveland and Devlin, 1988) with a window width of 3000 years and fixed target points in time.
4. Confidence intervals (5th and 95th percentiles) for each composite were generated by bootstrap resampling by site over 1000 iterations.

There are too few sites to construct regional composites for the peak of the LIG (Marine Isotope Stage 5e); thus, the trends in $\delta^{18}O_{spel}$ were examined using records from individual sites covering the period from 130 to 116 ka BP.

We calculated Holocene regional composites from annual precipitation-weighted mean $\delta^{18}O_{precip}$ anomalies simulated by the GISS model. Simulated $\delta^{18}O_{precip}$ trends were calculated using linear distance-weighted mean $\delta^{18}O_{precip}$ values from land grid cells (> 50 % land) within ±4° around each site. This distance was determined by the grid resolution of the model. Regional composites were then produced using bootstrap resampling in the same way as for the speleothem data. The simulated anomalies are relative to the control run rather than the specified base period used for the speleothem-based composites, so absolute values of simulated and observed Holocene trends are expected to differ. Preliminary analyses showed that neither the mean values nor trends in $\delta^{18}O_{precip}$ were substantially different if the sampled area was reduced to match the sampling used for the ECHAM-based box plot analysis, or was increased to encompass the larger regions shown in Fig. 2.1 and used in the multiple regression analysis.

2.4.6 Multiple regression analysis

We investigate the underlying relationships between regional $\delta^{18}O_{precip}$ (and by extension $\delta^{18}O_{spel}$ and monsoon climate through the Holocene using multiple linear regression (MLR). We use annual

precipitation-weighted mean $\delta^{18}O_{precip}$ anomalies and climate variables from GISS ModelE-R. Climate variables were chosen to represent the four potential large-scale drivers of regional changes in the speleothem $\delta^{18}O$ records. Specifically, we use changes in mean precipitation and precipitation recycling over the monsoon regions, and changes in mean surface air temperature and surface wind direction over the moisture source regions. Whereas the influence of changes in precipitation, recycling and temperature are relatively direct measures, the change in surface wind direction over the moisture source region is used as an index of potential changes in the moisture source region and transport pathway. The boundaries of each monsoon region (Fig. 2.1) were defined to include all the speleothem sites used to construct the Holocene $\delta^{18}O_{spel}$ composites. Moisture source area limits (Fig. 2.1) were defined based on moisture tracking studies (Bin et al., 2013; Breitenbach et al., 2010; D'Abreton and Tyson, 1996; Drumond et al., 2008, 2010; Durán-Quesada et al., 2010; Kennett et al., 2012; Nivet et al., 2018; Wurtzel et al., 2018) and GISS simulated summer surface winds. All climate variables were extracted for the summer months, defined as May to September (MJJAS) for Northern Hemisphere regions and November to March (NDJFM) for Southern Hemisphere regions (Wang and Ding, 2008) on the basis that these regions are dominated by summer season precipitation (Fig. S7). Only grid cells with > 50 % land were used to extract variables over monsoon regions, and only grid cells with < 50 % land were used to extract variables over moisture source regions. The inputs to the MLR for each time interval were calculated as anomalies from the control run.

Precipitation recycling was calculated as the ratio of locally sourced precipitation versus total precipitation. Although the GISS ModelE-R mid-Holocene experiment explicitly estimates recycling using vapour source distribution tracers (Lewis et al., 2014), this was not done for all the Holocene time slice simulations. Therefore, we calculate a precipitation recycling index (RI), following Brubaker et al. (1993):

$$RI = \frac{P_R}{P} = \frac{E}{2Q_H + E'} \qquad 2.5$$

where locally sourced (recycled) precipitation (P_R) is estimated using total evaporation over a region (E), and total precipitation (P) is estimated as the sum of total evaporation and net incoming moisture flux

integrated across the boundaries of the region (Q_H). Therefore, RI expresses the change in the contribution of local, recycled precipitation independently of any overall change in precipitation amount.

We incorporate mean meteorological variables and $\delta^{18}O_{precip}$ for all Holocene time slices (1 to 9 ka) and all monsoon regions into the MLR model. Thus, the relationships constrained by the overall (global) MLR model represent the combined response across all monsoon regions. We use the pseudo-R^2 to determine the goodness of fit for the global MLR model and t values (the regression coefficient divided by its standard error) to determine the strength of each relationship. Partial residual plots were used to show the relationship between each predictor variable and $\delta^{18}O_{precip}$ when the effects of the other variables are held constant.

All statistical analyses were performed in R (R Core Team, 2019), and plots were generated using ggplot (Wickham, 2016).

2.5 Results

2.5.1 Principal coordinate analysis and redundancy analysis

PCoA shows the (dis)similarity of Holocene $\delta^{18}O_{spel}$ evolution across individual records and, thus, allows an objective regionalisation of these records. The first two PCoA axes are significant, according to the broken stick test, and account for 65 % and 20 % of $\delta^{18}O_{spel}$ variability respectively (Table 2.1). The PCoA scores differentiate records geographically (Fig. 2.2a): Southern Hemisphere monsoon regions such as the southwestern South American monsoon (SW-SAM) and South African monsoon (SAfM) are characterised by low PCoA1 scores, whereas Northern Hemisphere monsoons such as the Indian summer monsoon (ISM) and the East Asian monsoon (EAM) are characterised by higher PCoA1 scores. This indicates that regions can be differentiated based on their temporal evolution as captured by the first PCoA axis. Most Southern Hemisphere regions also have lower PCoA2 scores, although this is not consistent over time.

	PCoA1	PCoA2	PCoA3	PCoA4	PCoA5
Eigenvalue	**269.06**	**85.22**	16.81	10.25	5.55
Explained (%)	**64.87**	**20.55**	4.054	2.47	1.34
Cumulative (%)	**64.87**	**85.42**	89.47	91.94	93.28

Table 2.1 Results of the principal coordinates analysis (PCoA). Significant axes, as determined by the broken stick method (Bennett, 1996), are shown in bold.

	RDA1	RDA2
Latitude	**0.88**	-0.47
Longitude	**0.75**	0.67
Eigenvalue	0.73	0.04
Explained (%)	36.7	2.2

Table 2.2 Results of the redundancy analysis (RDA). Variables that are significantly correlated (P <0.01) with RDA axes are shown in bold.

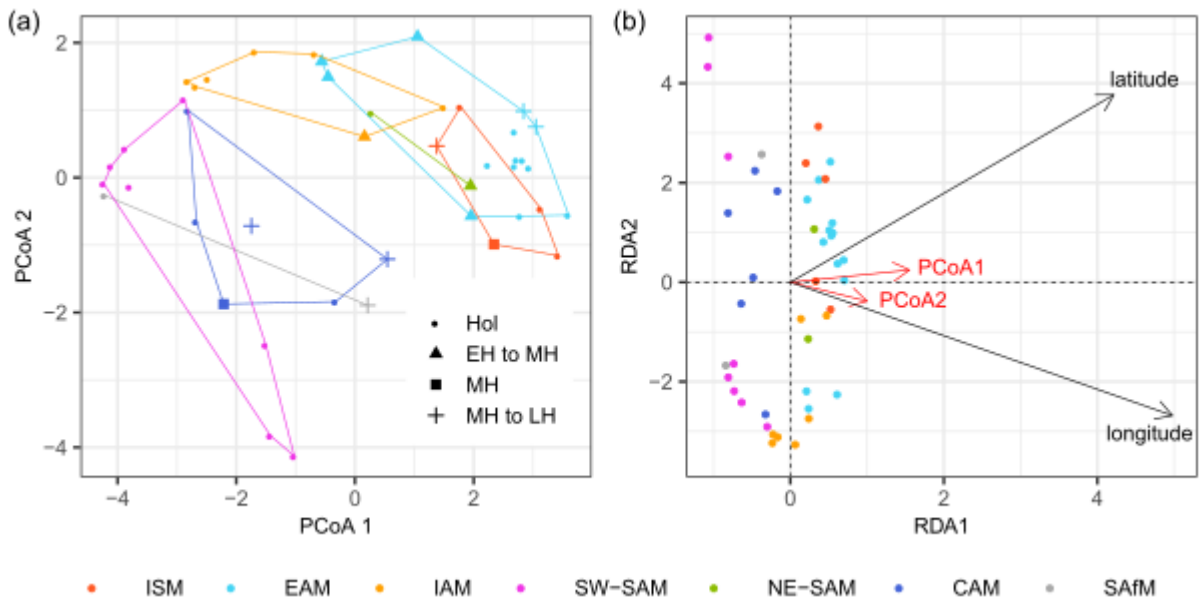

Figure 2.2 Results of the principal coordinate analysis (PCoA) and redundancy analysis (RDA). (a) PCoA biplot showing the loadings of each site on the first two axes, which represent 85 % of the total variance. Shapes indicate the Holocene coverage of each site, where sites with a coverage ≥ 8000 years represent most or all of the Holocene (Hol). Sites with a temporal coverage of < 8000 years are coded to show whether they represent the early Holocene to mid-Holocene (EH to MH; record midpoint > 8000 years BP), the mid-Holocene (MH; record midpoint between 8000 and 5000 years BP) or the mid-Holocene to late Holocene (LH to MH; midpoint < 5000 years BP). (b) RDA triplot, where the response variables are the PCoa1 and PCoA2 axes explained by latitude and longitude. The direction of the PCoA axes have been fixed so that they align with the explanatory variables.

Speleothem records from the Central American monsoon (CAM) and the Indonesian–Australian monsoon (IAM) have PCoA scores that are an intermediate between the Northern Hemisphere and Southern Hemisphere regions. PCoA clearly separates the South American records into a northeastern region (NE-SAM), with scores similar to other Northern Hemisphere monsoon regions, and a southwestern region (SW-SAM), with scores similar to other Southern Hemisphere regions. The RDA supports a geographical control on the (dis)similarity of speleothem $\delta^{18}O$ records over the Holocene (Fig. 2.2b). RDA1 explains 37 % of the variability and is significantly correlated with both latitude and longitude (Table 2.2).

2.5.2 Regional interglacial-glacial differences

To investigate the causes of shifts in $\delta^{18}O$ between the MH, LGM and LIG, we compare simulated and observed regional $\delta^{18}O$ signals during these periods with shifts in climate variables (precipitation and temperature). Only the ISM, EAM and IAM regions have sufficient speleothem data (i.e. at least one record from every time period) to allow comparisons across the MH, LGM and LIG (Fig. 2.3) and have similar shifts in observed $\delta^{18}O_{spel}$ and simulated $\delta^{18}O_{precip}$. The regional mean $\delta^{18}O_{spel}$ anomalies calculated for different time windows (±500, ±700, ±1000, ±2000 years) vary by less than 0.35 ‰ for the LGM (ISM: < 0.16 ‰; EAM: < 0.35 ‰; IAM: < 0.22 ‰) and 0.48‰ for the LIG (ISM: < 0.16 ‰; EAM: < 0.48 ‰; IAM: < 0.11 ‰), indicating that age uncertainties have a minimal impact on these mean values. The most positive $\delta^{18}O_{spel}$ anomalies in all three regions occur at the LGM, with more negative anomalies for the MH and LIG. The simulated $\delta^{18}O_{precip}$ anomalies show a similar pattern, with more positive anomalies during the LGM than during the MH or the LIG. The amplitude of this pattern is also similar between $\delta^{18}O_{precip}$ and $\delta^{18}O_{spel}$, when the observations are converted to their drip water equivalent (Fig. S8). The differences in regional $\delta^{18}O_{spel}$ anomalies between MH and LIG differ across the three regions. In both the ISM and the EAM, differences in δ^{18}Ospel values between the MH and LIG are small (Fig. 2.3a, b), although ISM LIG $\delta^{18}O_{spel}$ values are slightly more negative than MH values. In the IAM, MH values are less negative than the LIG (Fig. 2.3c). However, there are only a limited number of speleothem records from the ISM and IAM during the LIG, so the apparent differences between the two intervals in these regions may not be meaningful. Glacial–interglacial shifts are also seen in simulated temperature and precipitation, with

warmer and wetter conditions during interglacials and cooler and drier conditions during the LGM in all three regions. Differences in simulated precipitation between the MH and the LIG could help explain the differences between $\delta^{18}O_{spel}$ in the ISM and IAM, as the LIG is wetter than the MH in the ISM and drier than the MH in the IAM. However, the LIG is also drier than the MH in the EAM, a feature that appears inconsistent with the lack of differentiation between the $\delta^{18}O$ signals in this region.

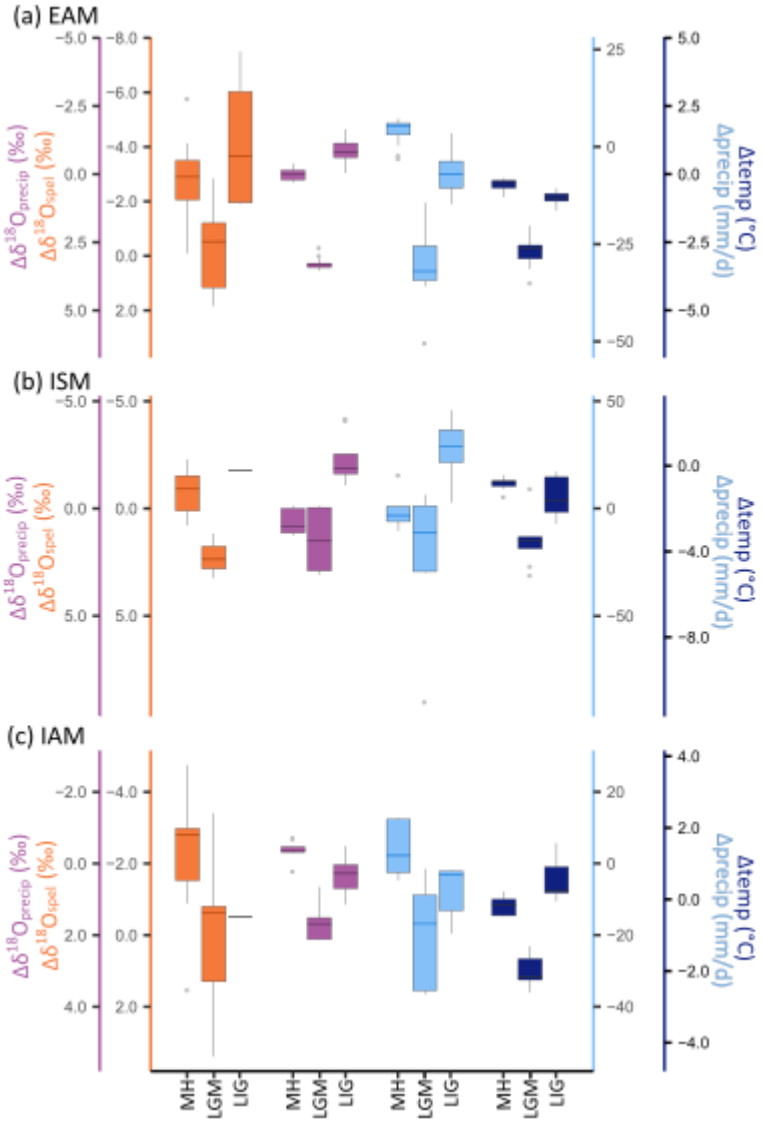

Figure 2.3 Speleothem $\delta^{18}O$ anomalies compared to anomalies of $\delta^{18}O_{precip}$, precipitation and temperature from the ECHAM simulations for the (a) East Asian (EAM), (b) Indian (ISM) and (c) Indonesian–Australian (IAM) monsoons. The boxes show the median value (line) and the interquartile range, and the whiskers show the minimum and maximum values, with outliers represented by grey dots. Note that the isotope axes are reversed, so that the most negative anomalies are at the top of the plot, to be consistent with the assumed relationship with the direction of change in precipitation and temperature.

2.5.3 Regional-scale interglacial $\delta^{18}O$ evolution

There are four monsoon regions with sufficient data to examine regional Holocene $\delta^{18}O$ trends: EAM, ISM, SW-SAM and IAM (Fig. 2.4). The IAM region has the fewest records (n = 7), whereas the EAM has the largest number of records (n = 14). The regional composites are expressed as z scores, i.e. changes with respect to the mean and variance of $\delta^{18}O$ for the base period (3000–7000 years BP). The confidence intervals on the regional composites are small for all regions, except SW-SAM in the early Holocene.

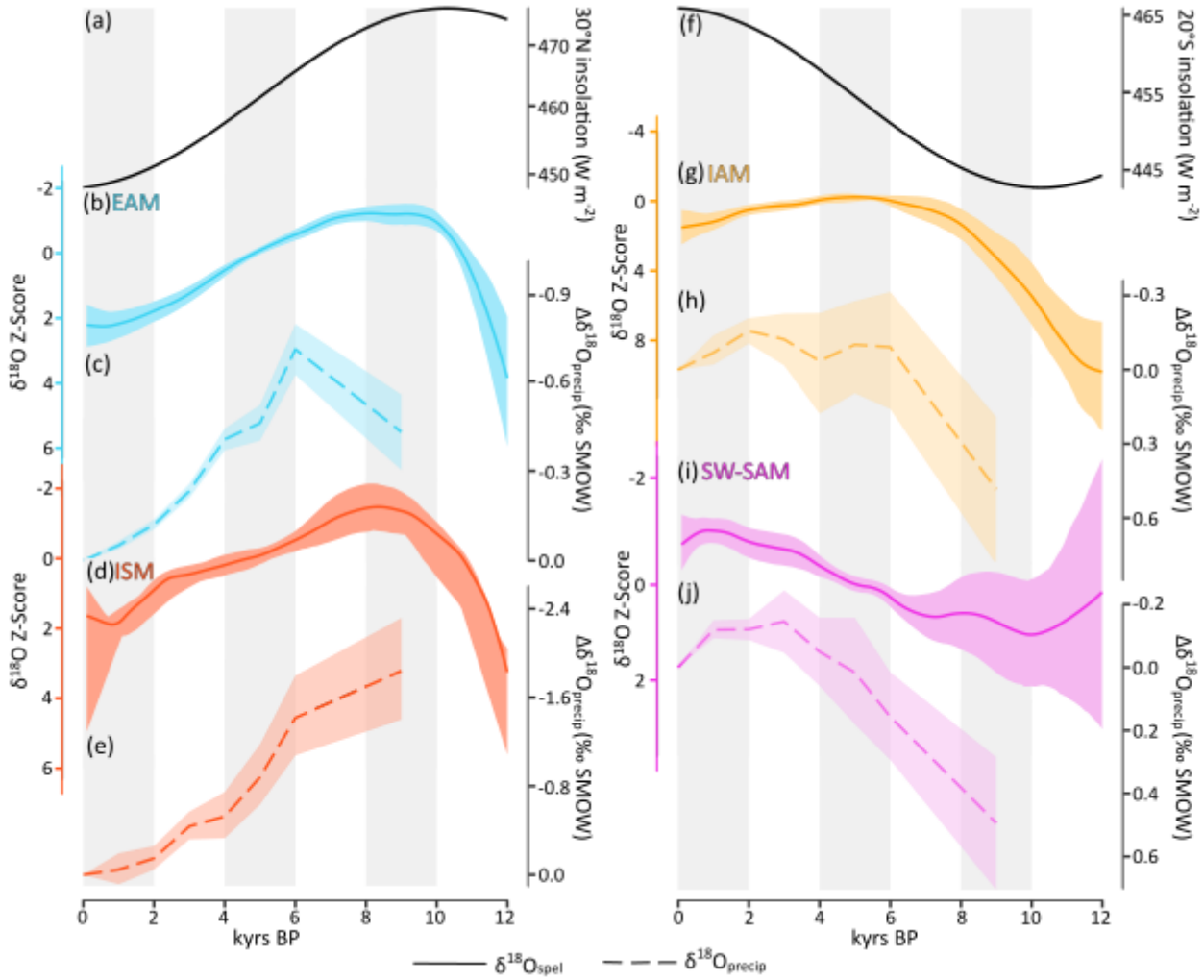

Figure 2.4 Evolution of regional speleothem $\delta^{18}O$ signals through the Holocene compared to $\delta^{18}O_{precip}$ simulated by the GISS model. Panels (a–e) show Northern Hemisphere monsoons (EAM denotes the East Asian monsoon; ISM denotes the Indian summer monsoon) and summer (May through September) insolation at 30°N (Berger, 1978). Panels (f–j) show Southern Hemisphere monsoons (SW-SAM denotes the southwestern South American monsoon; IAM denotes the Indonesian–Australian monsoon) and summer (November through March) insolation for 20° S (Berger, 1978). The speleothem δ 18O changes are expressed as z scores, with a smoothed loess fit (3000-year window), and confidence intervals obtained by bootstrapping by site. $\delta^{18}O_{precip}$ values are expressed as anomalies from the pre-industrial control simulation. Note that the isotope axes are reversed, so that the most negative anomalies are at the top of the plot, to be consistent with the assumed relationship with the changes in insolation.

The EAM and ISM regions (Fig. 2.4a–e) show the most positive $\delta^{18}O_{spel}$ z scores around 12 ka followed by a rapid decrease towards their most negative values at ~ 9.5 and ~ 9 ka respectively. The $\delta^{18}O_{spel}$ z scores in the EAM are relatively constant from 9.5 to ~ 7 ka, whereas this plateau is present but less marked in the ISM. There is a gradual trend towards more positive $\delta^{18}O_{spel}$ z scores towards the present in both regions thereafter. The SW-SAM records (Fig. 2.4i) have their most positive $\delta^{18}O_{spel}$ z scores in the early Holocene with a gradual trend to more negative scores towards the present. By contrast, the IAM z scores (Fig. 2.4g) are most positive at 12 ka, gradually decrease until ca. 5 ka and are relatively flat thereafter.

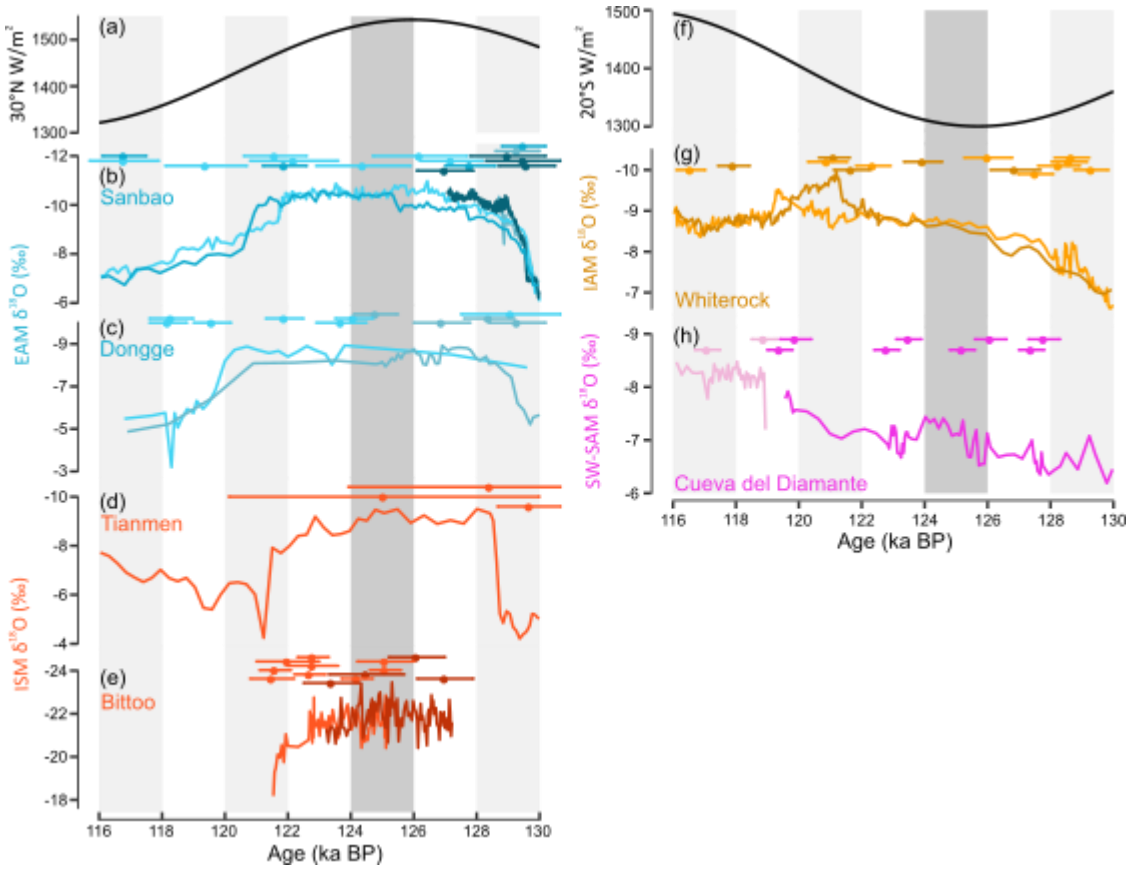

Figure 2.5 Comparison of changes in summer insolation and $\delta^{18}O_{spel}$ through the peak of the Last Interglacial (Marine Isotope Stage 5e) from the (b, c) East Asian monsoon (EAM), (d, e) Indian summer monsoon (ISM), (g) southwestern South American monsoon (SW-SAM) and (h) Indonesian–Australian monsoon (IAM) regions. The U–Th dates and uncertainties are shown for each record. The summer insolation curves (Berger, 1978) are for May through September at 30°N in the Northern Hemisphere (a) and for November through March for 20°S in the Southern Hemisphere (f). Note that the isotope axes are reversed, so that the most negative anomalies are at the top of the plot, to be consistent with the assumed relationship with the changes in insolation. The LIG (Marine Isotope Stage 5e) time slice used in the analysis in Sect. 2.4 is shown by the dark-grey bar.

There are insufficient data to create composite curves for the LIG, but individual records from the four regions (Fig. 2.5) show similar features to the Holocene trends. Records from the ISM and EAM (Fig. 2.5

left), for example, are characterised by an initial sharp decrease in $\delta^{18}O_{spel}$ values of about 4 ‰ between 130 and 129 ka, and most of the records (Dykoski et al., 2005; Kathayat et al., 2016; Wang et al., 2008) then show little variability for several thousand years. Despite the fact that the Tianmen record (Cai et al., 2010, 2012) shows considerable variability between 123 and 127 ka, there is nevertheless a similar plateau in the average observed value before the rapid change to less negative values after 127 ka. Similar to the Holocene, the SW-SAM record (Cheng et al., 2013) shows increasingly negative $\delta^{18}O_{spel}$ values through the LIG. The trend shown for Whiterock Cave (Carolin et al., 2016) also displays similar features to the IAM Holocene composite, with a gradual trend towards more negative values initially and a relatively complacent curve towards the end of the interglacial (Fig. 2.5 right).

2.5.4 Multiple regression analysis of Holocene $\delta^{18}O_{precip}$

The MLR analyses of simulated $\delta^{18}O_{precip}$ trends identify the impact of an individual climate variable on $\delta^{18}O_{precip}$ in the absence of changes in other variables. The global MLR model includes the Holocene (1–9 ka) $\delta^{18}O_{precip}$ trends combined across all monsoon regions (CAM, ISM, EAM, SWSAM, NE-SAM, SAfM, IAM). This global monsoon MLR model has a pseudo-R^2 of 0.80 and shows statistically significant relationships between the anomalies in $\delta^{18}O_{precip}$ and anomalies in regional precipitation, temperature and surface wind direction (Table 2.3). The partial residual plots (Fig. 2.6) show there is a strong negative relationship with regional precipitation (t value of −8.75) and a strong positive relationship (t value of 8.03) with surface wind direction over the moisture source region, an index of changes in either source area or moisture pathway. This indicates that increases in regional precipitation alone will lead to a decrease in $\delta^{18}O$, whereas changes in source area and/or moisture pathway, in the absence of changes in other variables, will lead to a significant change in $\delta^{18}O$. The relationship with temperature over the moisture source region is weaker, but positive (t value of 2.05), i.e. an increase in temperature over the moisture source region will lead to an increase in $\delta^{18}O$ if there are no changes in other climate variables. Precipitation recycling is not significant in this global analysis. The exact choice of source region has a negligible impact

on the model – for example, expanding the ISM source region to include the Bay of Bengal does not change the outcome of this analysis (Fig. S9, Table S1).

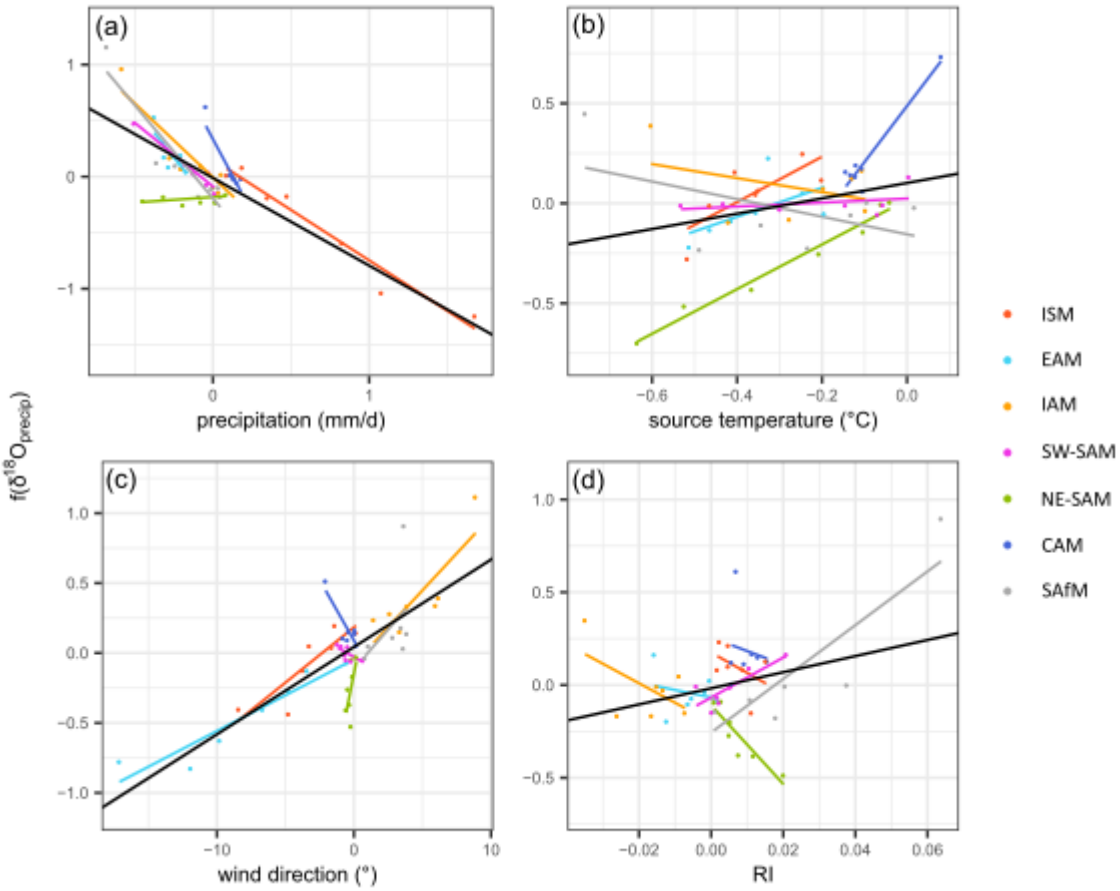

Figure 2.6 Partial residual plots from the multiple linear regression analysis, showing the relationship between anomalies in simulated $\delta^{18}O_{precip}$ and the four predictor variables, after considering the fitted partial effects of all the other predictors. The simulated $\delta^{18}O_{precip}$ values are anomalies relative to the pre-industrial control simulation and are annual values weighted by precipitation amount. The predictor variables are precipitation in the delineated monsoon region (mm d^{-1}), temperature in the source region (°C), surface wind direction over the source region (°) as an index of potential changes in source region and the ratio of precipitation recycling to total precipitation over the monsoon region (RI, unitless). The predictor variables are summer mean values, representing the summer monsoon, where summer is defined as May to September for the Northern Hemisphere monsoons and November to March for the Southern Hemisphere monsoons.

	Regression coefficient	*t* value
Regional precipitation	**-0.78**	-8.75
Source area temperature	**0.39**	2.05
Wind direction	**0.06**	8.03
Precipitation recycling	4.34	1.92

Table 2.3 Results of the multiple linear regression analysis. Significant relationships (P <0.01) are shown in bold.

There are too few data points to make regressions for individual monsoon regions, but the distribution of data points for each region in the partial residual plots (Fig. 2.6) is indicative of the degree of conformity to the global MLR model (representing the combined response across all monsoon regions). Data points from the ISM, SW-SAM, IAM and SAfM are well aligned with the overall relationship with regional precipitation (Fig. 2.6a), indicating that precipitation is an important control on changes in $\delta^{18}O_{precip}$ in these regions. The NE-SAM, EAM and CAM values deviate somewhat from the overall relationship and, although there are relatively few points, this suggests that changes in precipitation are a less important influence on $\delta^{18}O_{precip}$ changes in these regions. The impact of temperature changes (Fig. 2.6b) in the ISM, EAM and SW-SAM is broadly consistent with the overall relationship. The slope of the relationship with temperature is negative for the IAM and NE-SAM, and as this is physically implausible, it suggests that some factor not currently included in the MLR is influencing these records. However, the inconsistencies between the regional signals helps to explain why the global relationship between anomalies in temperature and $\delta^{18}O_{precip}$ is weak (Fig. 2.6b) and probably reflects the fact that tropical temperature changes during the Holocene are small. Data points from the EAM, ISM and IAM are well aligned with the overall relationship between changes in $\delta^{18}O_{precip}$ and changes in wind direction (Fig. 2.6c), indicating that changes in source area or moisture pathway are an important control on changes in $\delta^{18}O_{precip}$ in these regions. However, values for CAM, SW-SAM, NESAM and SAfM deviate strongly from the overall relationship. Recycling does not appear to be an important contributor to changes in $\delta^{18}O_{precip}$ except in SW-SAM and SAfM (Fig. 2.6d).

2.6 Discussion

We have shown that it is possible to derive an objective regionalisation of speleothem records based on the PCoA of the oxygen-isotope trends through the Holocene (Fig. 2.2). This approach separates out regions with a distinctive Northern Hemisphere signal (e.g., ISM, EAM, NE-SAM) from regions with a distinctive Southern Hemisphere signal (e.g. SW-SAM, SAfM), reflecting the fact that the evolution of regional monsoons in each hemisphere follows, to some extent, insolation forcing. It also identifies regions that have an intermediate pattern (e.g. IAM). The robustness of the regionalisation is borne out

by the fact that Holocene composite trends from each region have tight confidence intervals (Fig. 2.4), showing that the signals of individual records across a region show broad similarities. The monsoon regions identified by PCoA are consistent with previous studies (Wang et al., 2014). The tracking of Northern Hemisphere insolation is a recognised feature of monsoon systems in India and China (see reviews by Kaushal et al., 2018; Zhang et al., 2019). The separation of speleothem records from NE-SAM from those in SW-SAM is consistent with the precipitation dipole that exists between north-eastern Brazil (Nordeste) and the continental interior (Berbery and Barros, 2002; Boers et al., 2014). The anti-phasing of speleothem records from the two regions during the Holocene has been recognised in previous studies (Cruz et al., 2009; Deininger et al., 2019). The intermediate nature of the records from the maritime continent is consistent with the fact that the Indonesian– Australian (IAM) summer monsoon is influenced by cross equatorial air flow and, hence, can be influenced by Northern Hemisphere conditions (Trenberth et al., 2000). Palaeoenvironmental records from this region show mixed signals for the Holocene: some have been interpreted as showing enhanced (Beaufort et al., 2010; Mohtadi et al., 2011; Quigley et al., 2010; Wyrwoll and Miller, 2001) and others reduced precipitation (Kuhnt et al., 2015; Steinke et al., 2014) during the early and mid-Holocene. Modelling studies have shown that this region is highly sensitive to SST changes in the Indian Ocean and South China Sea, which in turn reflect changes in the Northern Hemisphere winter monsoons. Although most climate models produce a reduction in precipitation across the IAM during the mid-Holocene in response to orbital forcing, this is less than might be expected in the absence of ocean feedbacks associated with changes in the Indian Ocean (Zhao and Harrison, 2012).

The separation of northern and southern monsoon regions is consistent with the idea that changes in monsoon rainfall are primarily driven by changes in insolation (Ding and Chan, 2005; Kutzbach et al., 2008). Indeed, regional $\delta^{18}O_{spel}$ composites from the EAM, ISM and SW-SAM show a clear relationship with the long-term trends in local summer insolation (Fig. 2.4). Similar patterns are seen in individual speleothem records from each region confirming that the composite trends are representative. However, the composite trends are not an exact mirror of the insolation signal over the Holocene. For example, the ISM and EAM composites show a more rapid rise during the early Holocene than implied by the insolation forcing. The maximum wet phase in these two regions lasts for ca. 3000 years, again contrasting with the

gradual decline in insolation forcing after its peak at ca. 11 ka. Both the rapid increase and the persistence of wet conditions for several thousand years is also observed in other palaeohydrological records across southern and central China, including pollen (Zhao et al., 2009; Li et al., 2018) and peat records (Hong et al., 2003; Zhou et al., 2004). These features are also characteristic of lake records from India (Misra et al., 2019). The lagged response to increasing insolation is thought to be due to the presence of Northern Hemisphere ice sheets in the early Holocene (Zhang et al., 2018). The persistence of wetter conditions through the early and mid-Holocene is thought to reflect the importance of land surface and ocean feedbacks in sustaining regional monsoons (Dallmeyer et al., 2010; Kutzbach et al., 1996; Marzin and Braconnot, 2009; Rachmayani et al., 2015; Zhao and Harrison, 2012). The evolution of regional monsoons during the LIG shows patterns similar to those observed during the Holocene, including the lagged response to insolation and the persistence of wet conditions after peak insolation. This is again consistent with the idea that internal feedbacks play a role in modulating the monsoon response to insolation forcing. We have also shown that there is little difference in the isotopic values between the MH and the LIG in the ISM and EAM regions, which is also observed in individual speleothem records (Kathayat et al., 2016; Wang et al., 2008). The LIG (125 ka) period was characterised by higher summer insolation, higher CO_2 concentrations (Otto-Bliesner et al., 2017) and lower ice volumes (Dutton and Lambeck, 2012) than the MH, suggesting that the LIG ISM and EAM monsoons should be stronger than the MH monsoons. The lack of a clear differentiation in the isotope signals between the LIG and MH suggests that other factors play a role in modulating the monsoon response to these forcings and may reflect the importance of global constraints on the externally forced expansion of the tropical circulation (Biasutti et al., 2018).

Global relationships between $\delta^{18}O_{precip}$ and climate variables (precipitation amount, temperature and surface wind direction; Fig. 2.6) are consistent with existing studies: a strong relationship with precipitation and a weaker temperature effect have been widely observed at tropical and subtropical latitudes in modern observations (Dansgaard, 1964; Rozanski et al., 1993). The significant global relationship between $\delta^{18}O_{precip}$ and surface winds supports the idea that changes in moisture source and pathway are also important for explaining $\delta^{18}O$ variability over the Holocene. The multiple regression analysis also provides insights into the relative importance of different influences at a regional scale. In

the ISM, the results support existing speleothem studies which suggest that changes in precipitation amount (Cai et al., 2015; Fleitmann et al., 2004) and to a lesser extent moisture pathway (Breitenbach et al., 2010) drive $\delta^{18}O_{spel}$ variability. The $\delta^{18}O$ variability in the IAM region through the Holocene also appears to be strongly driven by changes in precipitation and moisture pathway, consistent with the interpretation of Wurtzel et al. (2018). Changes in regional precipitation (where the cave sites are located) do not seem to explain the observed changes in $\delta^{18}O_{spel}$ in the EAM during the Holocene, where Holocene $\delta^{18}O_{precip}$ evolution is largely driven by changes in atmospheric circulation (indexed by changes in surface winds). This is consistent with existing studies that emphasise changes in moisture source and/or pathway rather than local precipitation changes (Maher, 2016; Maher and Thompson, 2012; Tan, 2014; Yang et al., 2014). Speleothem $\delta^{18}O$ records in the SW-SAM clearly reflect regional-scale changes in precipitation, consistent with interpretations of individual records (Cruz et al., 2009; Kanner et al., 2013). However, this is a region where changes in precipitation recycling also appear to be important. Based on regional water budget estimates, recycling presently contributes ca. 25 %–35 % of the precipitation over the Amazon (Brubaker et al., 1993; Eltahir and Bras, 1994); these figures increase up to ca. 40 %–60 % based on moisture tagging studies (Risi et al., 2013; Yoshimura et al., 2004).

The LGM is characterised by lower Northern Hemisphere summer insolation, globally cooler temperatures, expanded global ice volumes and lower GHG concentrations than either the MH or the LIG. The MH and LIG (Marine Isotope Stage 5e) periods represent peaks in the present and last interglacial periods, whereas the LGM represents maximum ice extent during the Last Glacial Period. Hence, comparison of these time periods provides a snapshot view of glacial– interglacial variability. The $\delta^{18}O_{spel}$ anomalies are more positive during the LGM than during the MH or LIG, suggesting drier conditions in the ISM, EAM and IAM, supported by simulated changes in $\delta^{18}O_{precip}$ and precipitation (Fig. 2.3). Cooler SSTs of approximately 2 ◦C (relative to the MH and LIG) in the ISM and EAM and of approximately 3°C in IAM source areas, along with a ca. 5 % decrease in relative humidity (Yue et al., 2011), would result in a water vapour $\delta^{18}O$ signal at the source that is ca. 1 ‰ more depleted than seawater. This depletion results from the temperature dependence of equilibrium fractionation during evaporation and kinetic isotope effects related to humidity (Clark and Fritz, 1997). This fractionation counteracts any impact from enriched

seawater $\delta^{18}O$ values during the LGM (ca. +1 ‰ relative to the MH or LIG; Waelbroeck et al., 2002). Cooler air temperatures will also result in a depletion of $\delta^{18}O_{spel}$ during the LGM of ca. 0.4 ‰ and 0.6 ‰ for the ISM/EAM and IAM respectively, as a result of water–calcite (or water–aragonite) fractionation (Grossman and Ku, 1986; Tremaine et al., 2011). This has the effect of slightly reducing the regional LGM $\delta^{18}O_{spel}$ signals, although the change is small and within the uncertainty of the regional signals. Enriched $\delta^{18}O_{precip}$ and $\delta^{18}O_{spel}$ values during the LGM must therefore be caused by a significant decrease in atmospheric moisture and precipitation that resulted from the cooler conditions.

We have used version 2 of the SISAL database (Atsawawaranunt et al., 2018; Comas-Bru et al., 2020a) in our analyses. Despite the fact that SISALv2 includes more than 70 % of known speleothem isotope records, there are still too few records from some regions (e.g. Africa, the Caribbean) to make meaningful analyses. The records for older time periods are also sparse. For example, there are only 14 records from monsoon regions covering the LIG in SISALv2. Nevertheless, our analyses show that there are robust and explicable patterns for most monsoon regions during the Holocene and sufficient records to make meaningful analyses of the LGM and LIG. Whilst there is a need for the generation of new speleothem records from key regions such as northern Africa, further expansion of the SISAL database will certainly provide additional opportunities to analyse the evolution of the monsoons through time.

The impact of age uncertainties, included in SISALv2, are not taken into account in our analyses. Age uncertainties during the Holocene are smaller than the interval used for binning records and the width of the time windows used and, thus, should not have a significant effect on our conclusions. The mean age uncertainty at the LGM and LIG is ca. 430 and 1140 years respectively. However, varying the window length for the selection of LGM and LIG samples from ±500 to ±2000 years, thereby encompassing this uncertainty, has a negligible effect (< 0.5 ‰) on the average $\delta^{18}O$ values. Thus, the interglacial–glacial contrast in regional $\delta^{18}O_{spel}$ is also robust to age uncertainties.

Isotope-enabled climate models are used in this study to explore observed regional-scale trends in $\delta^{18}O_{spel}$. There is a limited number of isotope-enabled models, and there are no simulations of the same time period using the same experimental protocol. Although there are simulations of the MH from both

ECHAM5-wiso and GISS, for example, these models have different grid resolutions and used different boundary conditions. This could help to explain why the two models yield different estimates of the change in regional $\delta^{18}O_{precip}$ (of 0.5‰) at the MH. However, both models show trends in $\delta^{18}O_{precip}$ that reproduce the observed changes in regional $\delta^{18}O_{spel}$ (Figs. 2.3, 2.4), and this provides a basis for using these models to explore the causes of these trends on different timescales. The failure to reproduce the LGM $\delta^{18}O_{spel}$ signal in SW-SAM in the ECHAM5-wiso model, which precluded a consideration of interglacial–glacial shifts in this region, is a common feature of other isotope-enabled simulations (Caley et al., 2014; Risi et al., 2010). Identifying the underlying relationships between $\delta^{18}O_{precip}$ and monsoon climate variables using multiple linear regression allows us to identify plausible mechanistic controls on $\delta^{18}O$ variability in the monsoon regions. Correlations between $\delta^{18}O$ and specific climate variables do not explicitly indicate causality. However, the relationships identified in the MLR model are consistent with the theoretical understanding of oxygen isotope systematics, and the findings of this paper are consistent with existing studies, suggesting that these relationships provide a plausible explanation for observed changes.

This study illustrates a novel data–model approach to investigate the relationship between $\delta^{18}O_{spel}$ and monsoon climate under past conditions: we compare composite regional records and then use multiple linear regression of isotope-enabled palaeoclimate simulations to determine the change in individual climate variables associated with these trends. This obviates the need to use modern $\delta^{18}O_{precip}$–climate relationships to explain changes under conditions considerably different from today or to rely on coherency between different palaeohydrological archives which may respond to different climate variables. This model interrogation approach could be employed to address questions about the regional drivers of speleothem records outside the monsoon regions.

2.7 Conclusions

Geographically distributed speleothem $\delta^{18}O$ records and isotope-enabled climate models can be used together to understand the underlying relationships between $\delta^{18}O_{spel}$ and monsoon climate in the past and, therefore, elucidate possible drivers of $\delta^{18}O$ variability. Speleothem records, objectively grouped into

monsoon regions by record correlation and multivariate ordination techniques, show regional trends that are consistent with changes in summer insolation but modulated by land surface and ocean feedbacks. LGM $\delta^{18}O_{spel}$ signals are best explained by a large decrease in precipitation, as a consequence of lower atmospheric moisture content driven by global cooling. The evolution of $\delta^{18}O_{spel}$ through the Holocene across the global monsoon domain is closely correlated with changes in precipitation, atmospheric circulation and temperature. At the regional scale, our analyses support the increasing number of studies suggesting that East Asian monsoon speleothem $\delta^{18}O$ evolution through the Holocene relates to changes in atmospheric circulation (i.e. changes in moisture pathway and/or source). Changes in regional precipitation are the predominant driver of Holocene $\delta^{18}O_{spel}$ evolution in the Indian, southwestern South American and Indonesian–Australian monsoons, although changes in atmospheric circulation also contribute in the Indian and Indonesian–Australian monsoon regions and changes in precipitation recycling appear to be important in southwestern South America.

2.8 Code and data availability

The SISAL (Speleothem Isotopes Synthesis and AnaLysis) database version 2 is available through the University of Reading Research Data Archive at https://doi.org/10.17864/1947.256 (Comas-Bru et al., 2020a). The ECHAM5-wiso MH and LGM simulations are available at https://doi.org/10.1594/PANGAEA.902347 (Werner, 2019). The ECHAM LIG simulation is available at https://doi.org/10.1594/PANGAEA.879229 (Gierz et al., 2017a). The OIPC mean annual $\delta^{18}O_{precip}$ data are available at http://waterisotopes.org (last access: 10 May 2021, Waterisotopes Database, 2017). CRUTS4.01 mean annual temperature data are available at https://doi.org/10.5285/58a8802721c94c66ae45c3baa4d814d0 (Harris and Jones, 2017). The GISS simulations and code used to generate the figures in this paper are available at https://doi.org/10.5281/zenodo.3875496 (Parker, 2020).

2.9 Acknowledgements

Ideas in this paper were developed at a meeting of the SISAL (Speleothem Isotopes Synthesis and AnaLysis) working group of the Past Global Changes (PAGES) programme. We thank PAGES for their support of this meeting and our colleagues in SISAL for the useful discussions. We thank Gabriele Messori for help with the code for calculating precipitation recycling. We also thank Steven Clemens and two anonymous reviewers for their helpful comments on this paper. Sarah E. Parker, Sandy P. Harrison and Laia Comas-Bru acknowledge funding support from the ERC-funded project GC2.0 (Global Change 2.0: Unlocking the past for a clearer future). Sandy P. Harrison also acknowledges support from the JPI-Belmont Forum PaCMEDy (Palaeoclimate Constraints on Monsoon Evolution and Dynamics) project rum PaCMEDy (Palaeoclimate Constraints on Monsoon Evolution and Dynamics) project funded through NERC.

2.10 References

Aggarwal, P. K., Alduchov, O. A., Froehlich, K. O., Araguas-Araguas, L. J., Sturchio, N. C., and Kurita, N.: Stable isotopes in global precipitation: A unified interpretation based on atmospheric moisture residence time, Geophys. Res. Lett., 39, L11705, https://doi.org/10.1029/2012GL051937, 2012.

Atsawawaranunt, K., Comas-Bru, L., Amirnezhad Mozhdehi, S., Deininger, M., Harrison, S. P., Baker, A., Boyd, M., Kaushal, N., Ahmad, S. M., Ait Brahim, Y., Arienzo, M., Bajo, P., Braun, K., Burstyn, Y., Chawchai, S., Duan, W., Hatvani, I. G., Hu, J., Kern, Z., Labuhn, I., Lachniet, M., Lechleitner, F. A., Lorrey, A., Pérez-Mejías, C., Pickering, R., Scroxton, N., and SISAL Working Group Members: The SISAL database: a global resource to document oxygen and carbon isotope records from speleothems, Earth Syst. Sci. Data, 10, 1687–1713, https://doi.org/10.5194/essd-10-1687-2018, 2018.

Ayliffe, L. K., Gagan, M. K., Zhao, J. X., Drysdale, R. N., Hellstrom, J. C., Hantoro, W. S., Griffiths, M. L., Scott-Gagan, H., St Pierre, E., Cowley, J. A., and Suwargadi, B. W.: Rapid interhemispheric climate links via the

Australasian monsoon during the last deglaciation, Nat. Commun., 4, 1–6, https://doi.org/10.1038/ncomms3908, 2013.

Bailey, A., Posmentier, E., and Feng, X.: Patterns of evaporation and precipitation drive global isotopic changes in atmospheric moisture, Geophys. Res. Lett., 45, 7093–7101, https://doi.org/10.1029/2018GL078254, 2018.

Bar-Matthews, M., Ayalon, A., and Kaufman, A.: Late Quaternary paleoclimate in the eastern Mediterranean region from stable isotope analysis of speleothems at Soreq Cave, Israel, Quaternary Res., 47, 155–168, https://doi.org/10.1006/qres.1997.1883, 1997.

Battacharya, S. K., Froehlich, K., Aggarwal, P. K., and Kulkarni, K. M.: Isotopic variation in Indian Monsoon precipitation: Records from Bombay and New Delhi, Geophys. Res. Lett., 30, 2285, https://doi.org/10.1029/2003GL018453, 2003.

Battisti, D. S., Ding, Q., and Roe, G. H.: Coherent pan-Asian climatic and isotopic response to orbital forcing of tropical insolation, J. Geophys. Res.-Atmos., 119, 11997–12020, https://doi.org/10.1002/2014JD021960, 2014.

Beaufort, L., van der Kaars, S., Bassinot, F. C., and Moron, V.: Past dynamics of the Australian monsoon: precession, phase and links to the global monsoon concept, Clim. Past, 6, 695–706, https://doi.org/10.5194/cp-6-695-2010, 2010.

Bennett, K. D.: Determination of the number of zones in a biostratigraphical sequence, New Phytol., 132, 155–170, https://doi.org/10.1111/j.1469-8137.1996.tb04521.x, 1996.

Berbery, E. H. and Barros, V. R.: The hydrologic cycle of the La Plata basin in South America, J. Hydrometeorol., 3, 630–645, https://doi.org/10.1175/1525- 7541(2002)0032.0.CO;2, 2002.

Berger, A. and Loutre, M. F.: Insolation values for the climate of the last 10 million years, Quaternary Sci. Rev., 10, 297–317, https://doi.org/10.1016/0277-3791(91)90033-Q, 1991.

Berger, A. L.: Long-term variations of daily insolation and Quaternary climatic changes, J. Atmos. Sci., 35, 2362–2367, https://doi.org/10.1175/1520- 0469(1978)0352.0.CO;2, 1978.

Berkelhammer, M., Sinha, A., Mudelsee, M., Cheng, H., Edwards, R. L., and Cannariato, K.: Persistent multidecadal power of the Indian Summer Monsoon, Earth Planet. Sc. Lett., 290, 166–172, https://doi.org/10.1016/j.epsl.2009.12.017, 2010.

Biasutti, M., Voigt, A., Boos, W., Braconnot, P., Hargreaves, J. C., Harrison, S. P., Kang, S. M., Mapes, B. E., Scheff, J., Schumaker, C., Sobel, A. H., and Xie, S. P.: Global energetics and local physics as drivers of past, present and future monsoons, Nat. Geosci., 11, 392–400, https://doi.org/10.1038/s41561-018- 0137-1, 2018.

Bin, C., Xiang-De, X., and Tianliang, Z.: Main moisture sources affecting lower Yangtze River Basin in boreal summers during 2004–2009, Int. J. Climatol., 33, 1035–1046, https://doi.org/10.1002/joc.3495, 2013.

Boers, N., Rheinwalt, A., Bookhagen, B., Barbosa, H. M. J., Marwan, N., Marengo, J., and Kurths, J.: The South American rainfall dipole: A complex network analysis of extreme events, Geophys. Res. Lett., 41, 7397–7405, https://doi.org/10.1002/2014GL061829, 2014.

Bowen, G.: Gridded maps of the isotopic composition of meteoric waters, WaterIsotopes.org, The University of Utah, available at: http://waterisotopes.org, last access: 10 May 2021. Bowen, G. J. and Revenaugh, J.: Interpolating the isotopic composition of modern meteoric precipitation, Water Resour. Res., 39, 1299, https://doi.org/10.1029/2003WR002086, 2003.

Breitenbach, S. F. M., Adkins, J. F., Meyer, H., Marwan, N., Kumar, K. K., and Haug, G. H.: Strong influence of water vapor source dynamics on stable isotopes in precipitation observed in Southern Meghalaya, NE India, Earth Planet. Sc. Lett., 292, 212–220, https://doi.org/10.1016/j.epsl.2010.01.038, 2010.

Brook, E. J., Harder, S., Severinghaus, J., Steig, E. J., and Sucher, C. M.: On the origin and timing of rapid changes in atmospheric methane during the Last Glacial Period, Global Biogeochem. Cy., 14, 559–572, https://doi.org/10.1029/1999GB001182, 2000.

Brubaker, K. L., Entekhabi, D., and Eagleson, P. S.: Estimation of continental precipitation recycling, J. Climate, 6, 1077–1089, https://doi.org/10.1175/1520- 0442(1993)0062.0.CO;2, 1993.

Cai, Y., Cheng, H., An, Z., Lawrence Edwards, R., Wang, X., Tan, L., and Wang, J.: Large variations of oxygen isotopes in precipitation over south-central Tibet during Marine Isotope Stage 5, Geology, 38, 243–246, https://doi.org/10.1130/G30306.1, 2010.

Cai, Y., Zhang, H., Cheng, H., An, Z., Lawrence Edwards, R., Wang, X., Tan, L., Liang, F., Wang, J., and Kelly, M.: The Holocene Indian monsoon variability over the southern Tibetan Plateau and its teleconnections, Earth Planet. Sc. Lett., 335, 135– 144, https://doi.org/10.1016/j.epsl.2012.04.035, 2012.

Cai, Y., Fung, I. Y., Edwards, R. L., An, Z., Cheng, H., Lee, J. E., Tan, L., Shen, C. C., Wang, X., Day, J. A., Zhou, W., Kelly, M. J., and Chiang, J. C. H.: Variability of stalagmite-inferred Indian monsoon precipitation over the past 252,000 y, P. Natl. Acad. Sci. USA, 112, 2954–2959, https://doi.org/10.1073/pnas.1424035112, 2015.

Caley, T., Roche, D. M., Waelbroeck, C., and Michel, E.: Oxygen stable isotopes during the Last Glacial Maximum climate: perspectives from data–model (iLOVECLIM) comparison, Clim. Past, 10, 1939–1955, https://doi.org/10.5194/cp-10-1939-2014, 2014.

Carlson, A. E., LeGrande, A. N., Oppo, D. W., Came, R. E., Schmidt, G. A., Anslow, F. S., Licciardi, J. M., and Obbink, E. A.: Rapid early Holocene deglaciation of the Laurentide ice sheet, Nat. Geosci., 1, 620–624, https://doi.org/10.1038/ngeo285, 2008.

Carolin, S. A., Cobb, K. M., Lynch-Stieglitz, J., Moerman, J. W., Partin, J. W., Lejau, S., Malang, J., Clark, B., Tuen, A. A., and Adkins, J. F.: Northern Borneo stalagmite records reveal West Pacific hydroclimate across MIS 5 and 6, Earth Planet. Sc. Lett., 439, 182–193, https://doi.org/10.1016/j.epsl.2016.01.028, 2016.

Cheng, H., Edwards, R. L., Wang, Y., Kong, X., Ming, Y., Kelly, M. J., Wang, X., Gallup, C. D., and Liu, W.: A penultimate glacial monsoon record from Hulu Cave and two-phase glacial terminations, Geology, 34, 217–220, https://doi.org/10.1130/G22289.1, 2006.

Cheng, H., Edwards, R. L., Broecker, W. S., Denton, G. H, Kong, X., Wang, Y., Zhang, R., and Wang, X.: Ice Age Terminations, Science, 326, 248–252, https://doi.org/10.1126/science.1177840, 2009.

Cheng, H., Sinha, A., Cruz, F. W., Wang, X., Edwards, R. L., d'Horta, F. M., Ribas, C. C., Vuille, M., Stott, L. D., and Auler, A. S.: Climate change patterns in Amazonia and biodiversity, Nat. Commun., 4, 1411, https://doi.org/10.1038/ncomms2415, 2013.

Cheng, H., Edwards, R. L., Sinha, A., Spötl, C., Yi, L., Chen, S., Kelly, M., Kathayat, G., Wang. X., Li, X., Kong, Y., Wang, Y., Ning, Y., and Zhang, W.: The Asian monsoon over the past 640,000 years and ice age terminations, Nature, 634, 640–649, https://doi.org/10.1038/nature18591, 2016.

Cheng, H., Zhang, H., Zhao, J., Li, H., Ning, Y., and Kathayat, G.: Chinese stalagmite paleoclimate researches: A review and perspective, Sci. China Earth Sci., 62, 1489–1513, https://doi.org/10.1007/s11430-019-9478-3, 2019.

Clark, I. and Fritz, P.: Environmental Isotopes in Hydrology, Lewis Publishers, New York, ISBN: 1-56670-249-6, 1997. Cleveland, W. S. and Devlin, S. J.: Locally weighted regression: An approach to regression analysis by local fitting, J. Am. Stat. Assoc., 83, 596–610, https://doi.org/10.1080/01621459.1988.10478639, 1988.

Cobb, K. M., Adkins, J. F., Partin, J. W., and Clark, B.: Regional-scale climate influences on temporal variations of rainwater and cave dripwater oxygen isotopes in northern Borneo, Earth Planet. Sc. Lett., 263, 207–220, https://doi.org/10.1016/j.epsl.2007.08.024, 2007.

Cole, J. E., Rind, D., Webb, R. S., Jouzel, J., and Healy, R.: Climatic controls on interannual variability of precipitation δ 18O: Simulated influence of temperature, precipitation amount, and vapor source region, J. Geophys. Res., 104, 14223–14235, https://doi.org/10.1029/1999JD900182, 1999.

Comas-Bru, L., Harrison, S. P., Werner, M., Rehfeld, K., Scroxton, N., Veiga-Pires, C., and SISAL working group members: Evaluating model outputs using integrated global speleothem records of climate change since the last glacial, Clim. Past, 15, 1557– 1579, https://doi.org/10.5194/cp-15-1557-2019, 2019.

Comas-Bru, L., Atsawawaranunt, K., Harrison, S., and SISAL working group members: SISAL (Speleothem Isotopes Synthesis and AnaLysis Working Group) database version 2.0, University of Reading [data set], https://doi.org/10.17864/1947.256, 2020a.

Comas-Bru, L., Rehfeld, K., Roesch, C., Amirnezhad-Mozhdehi, S., Harrison, S. P., Atsawawaranunt, K., Ahmad, S. M., Brahim, Y. A., Baker, A., Bosomworth, M., Breitenbach, S. F. M., Burstyn, Y., Columbu, A., Deininger, M., Demény, A., Dixon, B., Fohlmeister, J., Hatvani, I. G., Hu, J., Kaushal, N., Kern, Z., Labuhn, I., Lechleitner, F. A., Lorrey, A., Martrat, B., Novello, V. F., Oster, J., Pérez-Mejías, C., Scholz, D., Scroxton, N., Sinha, N., Ward, B. M., Warken, S., Zhang, H., and SISAL Working Group members: SISALv2: a comprehensive speleothem isotope database with multiple age–depth models, Earth Syst. Sci. Data, 12, 2579–2606, https://doi.org/10.5194/essd-12-2579- 2020, 2020b.

Coplen, T. B., Kendall, C., and Hopple, J.: Comparison of stable isotope reference samples, Nature, 302, 236–238, https://doi.org/10.1038/302236a0, 1983.

Craig, H. and Gordon, L. I.: Deuterium and oxygen 18 variations in the ocean and the marine atmosphere, in: Stable isotopes in Oceanographic Studies and Paleotemperatures, edited by: Tongiorgi, E., Consiglio Nazionake delle Ricerche Laboratoria di Geologia Nucleare, Pisa, 9–130, 1965. Cruz, F. W., Burns, S. J., Karmann, I., Sharp, W. D., Vuille, M., Cardoso, A. O., Ferrari, J. A., Silva Dias, P. L., and Viana, O.: Insolation-driven changes in atmospheric circulation over the past 116,000 years in subtropical Brazil, Nature, 434, 63–66, https://doi.org/10.1038/nature03365, 2005.

Crucifix, M. (2016) ‘palinsol: Insolation for palaeoclimate studies. R package version 0.93’. Available at: https://cran.r-project.org/package=palinsol.

Cruz, F. W., Burns, S. J., Karmann, I., Sharp, W. D., and Vuille, M.: Reconstruction of regional atmospheric circulation features during the late Pleistocene in subtropical Brazil from oxygen isotope composition of speleothems, Earth Planet. Sc. Lett., 248, 495–507, https://doi.org/10.1016/j.epsl.2006.06.019, 2006.

Cruz, F. W., Vuille, M., Burns, S. J., Wang, X., Cheng, H., Werner, M., Lawrence Edwards, R., Karmann, I., Auler, A. S., and Nguyen, H.: Orbitally driven east-west antiphasing of South American precipitation, Nat. Geosci., 2, 210–214, https://doi.org/10.1038/ngeo444, 2009.

D'Abreton, P. C. and Tyson, P. D.: Three-dimensional kinematic trajectory modelling of water vapour transport over Southern Africa, Water SA, 22, 297–306, 1996. Dallmeyer, A., Claussen, M., and Otto, J.: Contribution of oceanic and vegetation feedbacks to Holocene climate change in monsoonal Asia, Clim. Past, 6, 195–218, https://doi.org/10.5194/cp6-195-2010, 2010.

Dansgaard, W.: Stable isotopes in precipitation, Tellus, 16, 436– 468, https://doi.org/10.3402/tellusa.v16i4.8993, 1964.

Deininger, M., Ward, B. M., Novello, V. F., and Cruz, F. W.: Late Quaternary variations in the South American monsoon system as inferred by speleothems–New perspectives using the SISAL database, Quaternary, 2, 6, https://doi.org/10.3390/quat2010006, 2019.

Ding, Y. and Chan, J. C. L.: The East Asian summer monsoon: an overview, Meteorol. Atmos. Phys., 89, 117–142, https://doi.org/10.1007/s00703-005-0125-z, 2005.

Dong, J., Wang, Y., Cheng, H., Hardt, B., Lawrence Edwards, R., Kong, X., Wu, J., Chen, S., Liu, D., Jiang, X., and Zhao, K.: A high-resolution stalagmite record of the Holocene East Asian monsoon from Mt Shennongjia, central China, Holocene, 20, 257–264, https://doi.org/10.1177/0959683609350393, 2010.

Drumond, A., Nieto, R., Gimeno, L., and Ambrizzi, T.: A Lagrangian identification of major sources of moisture over Central Brazil and la Plata Basin, J. Geophys. Res., 113, D14128, https://doi.org/10.1029/2007JD009547, 2008.

Drumond, A., Nieto, R., Trigo, R., Ambrizzi, T., Souza, E., and Gimeno, L.: A Lagrangian identification of the main sources of moisture affecting northeastern Brazil during its pre-rainy and rainy seasons, PLoS One, 5, e11205, https://doi.org/10.1371/journal.pone.0011205, 2010.

Durán-Quesada, A. M., Gimeno, L., Amador, J. A., and Nieto, R.: Moisture sources for Central America: Identification of moisture sources using a Lagrangian analysis technique, J. Geophys. Res., 115, D05103, https://doi.org/10.1029/2009JD012455, 2010.

Dutton, A. and Lambeck, K.: Ice volume and sea level during the last interglacial, Science, 337, 216–219, https://doi.org/10.1126/science.1205749 2012.

Dykoski, C. A., Edwards, R. L., Cheng, H., Yuan, D., Cai, Y., Zhang, M., Lin, Y., Qing, J., An, Z., and Revenaugh, J.: A high resolution, absolute-dated Holocene and deglacial Asian monsoon record from Dongge Cave, China, Earth Planet. Sc. Lett., 233, 71–86, https://doi.org/10.1016/J.EPSL.2005.01.036, 2005.

Eltahir, E. A. B. and Bras, R. L.: Precipitation recycling in the Amazon basin, Q. J. Roy. Meteor. Soc., 120, 861–880, https://doi.org/10.1002/qj.49712051806, 1994.

Fairchild, I. J. and Baker, A.: Speleothem Science: From Process to Past Environments, 1st edn., Wiley-Blackwell, Chichester, 2012.

Fleitmann, D., Burns, S. J., Mudelsee, M., Neff, U., Kramers, J., Mangini, A., and Matter, A.: Holocene Forcing of the Indian Monsoon Recorded in a Stalagmite from Southern Oman, Science, 300, 1737–1739, https://doi.org/10.1126/science.1083130, 2003.

Fleitmann, D., Burns, S. J., Neff, U., Mudelsee, M., Mangini, A., and Matter, A.: Palaeoclimatic interpretation of high-resolution oxygen isotope profiles derived from annually laminated speleothems from Southern Oman, Quaternary Sci. Rev., 23, 935–945, https://doi.org/10.1016/j.quascirev.2003.06.019, 2004.

Friedman, I., Harris, J. M., Smith, G. I., and Johnson, C. A.: Stable isotope composition of waters in the Great Basin, United States 1. Air-mass trajectories, J. Geophys. Res., 107, 4400, https://doi.org/10.1029/2001JD000565, 2002.

Gat, J. R.: Oxygen and hydrogen isotopes in the hydrological cycle, Annu. Rev. Earth Pl. Sc., 24, 225–262, https://doi.org/10.1146/annurev.earth.24.1.225, 1996.

Gierz, P., Werner, M., and Lohmann, G.: Simulating climate and stable water isotopes during the last interglacial using a coupled climate-isotope model, link to model results, PANGAEA [data set], https://doi.org/10.1594/PANGAEA.879229, 2017a.

Gierz, P., Werner, M., and Lohmann, G.: Simulating climate and stable water isotopes during the Last Interglacial using a coupled climate-isotope model, J. Adv. Model. Earth Sy., 9, 2027–2045, https://doi.org/10.1002/2017MS001056, 2017b.

Goldschneider, N., Chen, Z., Auler, A. S., Bakalowicz, M., Broda, S., Drew, D., Hartmann, J., Jiang, G., Moosdorf, N., Stevanovic, Z., and Veni, G.: Global distribution of carbonate rocks and karst water resources, Hydrogeol. J., 28, 1661–1677, https://doi.org/10.1007/s10040-020-02139-5, 2020.

Gower, J. C.: Some distance properties of latent root and vector methods used in multivariate analysis, Biometrika, 53, 325–338, https://doi.org/10.2307/2333639, 1966.

Griffiths, M. L., Drysdale, R. N., Gagan, M. K., Zhao, J. X., Ayliffe, L. K., Hellstrom, J. C., Hantoro, W. S., Frisia, S., Feng, Y. X., Cartwright, I., Pierre, E. S., Fischer, M. J., and Suwargadi, B. W.: Increasing Australian-Indonesian monsoon rainfall linked to early Holocene sea-level rise, Nat. Geosci., 2, 636–639, https://doi.org/10.1038/ngeo605, 2009.

Grossman, E. L. and Ku, T. L.: Oxygen and carbon isotope fractionation in biogenic aragonite: Temperature effects, Chem. Geol. Isot. Geosci. Sect., 59, 59–74, https://doi.org/10.1016/0168- 9622(86)90057-6, 1986.

Haese, B., Werner, M., and Lohmann, G.: Stable water isotopes in the coupled atmosphere–land surface model ECHAM5-JSBACH, Geosci. Model Dev., 6, 1463–1480, https://doi.org/10.5194/gmd-6-1463-2013, 2012.

Harris, I. C. and Jones, P. D.: CRU TS4.01: Climatic Research Unit (CRU) Time-Series (TS) version 4.01 of high-resolution gridded data of month-by-month variation in climate (Jan. 1901-Dec. 2016), Centre for Environmental Data Analysis [data set], https://doi.org/10.5285/58a8802721c94c66ae45c3baa4d814d0, 2017.

Harris, I., Osborn, T. J., Jones, P. and Lister, D.: Version 4 of the CRU TS monthly high-resolution gridded multivariate climate dataset, Sci. Data, 7, 109, https://doi.org/10.1038/s41597-020- 0453-3, 2020.

Hong, Y. T., Hong, B., Lin, Q. H., Zhu, Y. X., Shibata, Y., Hirota, M., Uchida, M., Leng, X. T., Jiang, H. B., Xu, H., Wang, H., and Yi, L.: Correlation between Indian Ocean summer monsoon and North Atlantic climate during the Holocene, Earth Planet. Sc. Lett., 211, 371–380, https://doi.org/10.1016/S0012-821X(03)00207-3, 2003.

Hu, J., Emile-Geay, J., Tabor, C., Nusbaumer, J., and Partin, J.: Deciphering oxygen isotope records from Chinese speleothems with an isotope-enabed climate model, Paleoceanography and Paleoclimatology, 43, 2098–2112, https://doi.org/10.1029/2019PA003741, 2019.

IAEA/WMO: Global Network of Isotopes in Precipitation, The GNIP Database, available at: https://nucleus.iaea.org/wiser (last access: 20 May 2021), 2018.

Indermühle, A., Stocker, T. F., Joos, F., Fischer, H., Smith, H. J., Wahlen, M., Deck, B., Mastroianni, D., Tschumi, J., Blunier, T., Meyer, R., and Stauffer, B.: Holocene carbon-cycle dynamics based on CO2 trapped in ice at Taylor Dome, Antarctica, Nature, 398, 121–126, https://doi.org/10.1038/18158, 1999.

Kanner, L. C., Burns, S. J., Cheng, H., Edwards, R. L., and Vuille, M.: High-resolution variability of the South American summer monsoon over the last seven millennia: Insights from a speleothem record from the central Peruvian Andes, Quaternary Sci. Rev., 75, 1–10, https://doi.org/10.1016/j.quascirev.2013.05.008, 2013.

Kärkkäinen, T. and Saarela, M.: Robust Principal Component Analysis of Data with Missing Values, in: Machine Learning and Data Mining in Pattern Recognition. MLDM 2015, edited by: Perner, P., Springer, Cham, Lecture Notes in Computer Science, vol. 9166, https://doi.org/10.1007/978-3-319-21024-7_10, 2015.

Kathayat, G., Cheng, H., Sinha, A., Spötl, C., Edwards, R. L., Zhang, H., Li, X., Yi, L., Ning, Y., Cai, Y., Lui, W. L., and Breitenbach, S. F. M.: Indian monsoon variability on millennial-orbital timescales, Sci. Rep., 6, 24374, https://doi.org/10.1038/srep24374, 2016.

Kaushal, N., Breitenbach, S. F. M., Lechleitner, F. A., Sinha, A., Tewari, V. C., Ahmad, S. M., Berkelhammer, M., Band, S., Yadava, M., Ramesh, R., and Henderson, G. M.: The Indian Summer Monsoon from a Speleothem δ 18O Perspective–A Review, Quaternary, 1, 29, https://doi.org/10.3390/quat1030029, 2018.

Kennett, D. J., Breitenbach, S. F. M., Aquino, V. V., Asmerom, Y., Awe, J., Baldini, J. U. L., Bartlein, P., Culleton, B. J., Ebert, C., Jazwa, C., Macri, M. J., Marwan, N., Polyak, V., Prufer, K. M., Ridley, H. E., Sodemann, H., Winterhalder, B., and Haug, G. H.: Development and disintegration of Maya political systems in response to climate change, Science, 338, 788–791, https://doi.org/10.1126/science.1226299, 2012.

Krause, C. E., Gagan, M. K., Dunbar, G. B., Hantoro, W. S., Hellstrom, J. C., Cheng, H., Edwards, R. L., Suwargadi, B. W., Abram, N. J., and Rifai, H.: Spatio-temporal evolution of Australasian monsoon hydroclimate over the last 40,000 years, Earth Planet. Sc. Lett., 513, 103–112, https://doi.org/10.1016/j.epsl.2019.01.045, 2019.

Kuhnt, W., Holbourn, A., Xu, J., Opdyke, B., De Deckker, P., Röhl, U., and Mudelsee, M.: Southern Hemisphere control on Australian monsoon variability during the late deglaciation and Holocene, Nat. Commun., 6, 1–7, https://doi.org/10.1038/ncomms6916, 2015.

Kutzbach, J., Bonan, G., Foley, J., and Harrison, S. P.: Vegetation and soil feedbacks on the response of the African monsoon to orbital forcing in the early to middle Holocene, Nature, 384, 623– 626, https://doi.org/10.1038/384623a0, 1996.

Kutzbach, J. E., Liu, X., Liu, Z., and Chen, G.: Simulation of the evolutionary response of global summer monsoons to orbital forcing over the past 280,000 years, Clim. Dynam., 30, 567–579, https://doi.org/10.1007/s00382-007-0308-z, 2008.

Lachniet, M. S.: Climatic and environmental controls on speleothem oxygen-isotope values, Quaternary Sci. Rev., 28, 412–432, https://doi.org/10.1016/j.quascirev.2008.10.021, 2009.

Lachniet, M. S.: Are aragonite stalagmites reliable paleoclimate proxies? Tests for oxygen isotope time-series replication and equilibrium, Bull. Geol. Soc. Am., 127, 1521–1533, https://doi.org/10.1130/B31161.1, 2015.

Langebroek, P. M., Werner, M., and Lohmann, G.: Climate information imprinted in oxygen-isotopic composition of precipitation in Europe, Earth Planet. Sc. Lett., 311, 144–154, https://doi.org/10.1016/j.epsl.2011.08.049, 2011.

Legendre, P. and Legendre, L.: Numerical Ecology, 2nd edn., Elsevier B.V., Amsterdam, 1998. LeGrande, A. N. and Schmidt, G. A.: Global gridded data set of the oxygen isotopic composition in seawater, Geophys. Res. Lett., 33, L12604, https://doi.org/10.1029/2006GL026011, 2006.

LeGrande, A. N. and Schmidt, G. A.: Sources of Holocene variability of oxygen isotopes in paleoclimate archives, Clim. Past, 5, 441–455, https://doi.org/10.5194/cp-5-441-2009, 2009.

Lewis, S. C., LeGrande, A. N., Kelley, M., and Schmidt, G. A.: Water vapour source impacts on oxygen isotope variability in tropical precipitation during Heinrich events, Clim. Past, 6, 325–343, https://doi.org/10.5194/cp-6-325-2010, 2010.

Lewis, S. C., LeGrande, A. N., Schmidt, G. A., and Kelley, M.: Comparison of forced ENSO-like hydrological expressions in simulations of the preindustrial and midHolocene, J. Geophys, Res.-Atmos., 119, 7064–7082, https://doi.org/10.1002/2013JD020961, 2014.

Li, J., Dodson, J., Yan, H., Wang, W., Innes, J. B., Zong, Y., Zhang, X., Xu, Q., Ni, J., and Lu, F.: Quantitative Holocene climatic reconstructions for the lower Yangtze region of China, Clim. Dynam., 50, 1101–1113, https://doi.org/10.1007/s00382-017-3664- 3, 2018.

Licciardi, J. M., Clark, P. U., Jenson, J. W., and Macayeal, D. R.: Deglaciation of a soft-bedded Laurentide Ice Sheet, Quaternary Sci. Rev., 17, 427–448, https://doi.org/10.1016/S0277- 3791(97)00044-9, 1998.

Liu, Z., Wen, X., Brady, E. C., Otto-Bliesner, B., Yu, G., Lu, H., Cheng, H., Wang, Y., Zheng, W., Ding, Y., Edwards, R. L., Cheng, J., Liu, W., and Yang, H.: Chinese cave records and the East Asia Summer Monsoon, Quaternary Sci. Rev., 83, 115–128, https://doi.org/10.1016/j.quascirev.2013.10.021, 2014.

Maher, B. A.: Holocene variability of the East Asian summer monsoon from Chinese cave records: A re-assessment, Holocene, 18, 861–866, https://doi.org/10.1177/0959683608095569, 2008. Maher, B. A.: Palaeoclimatic records of the loess/palaeosol sequences of the Chinese Loess Plateau, Quaternary Sci. Rev., 154, 23–84, https://doi.org/10.1016/j.quascirev.2016.08.004, 2016.

Maher, B. A. and Thompson, R.: Oxygen isotopes from Chinese caves: Records not of monsoon rainfall but of circulation regime, J. Quat. Sci., 27, 615–624, https://doi.org/10.1002/jqs.2553, 2012.

Marlon, J. R., Bartlein, P. J., Carcaillet, C., Gavin, D. G., Harrison, S. P., Higuera, P. E., Joos, F., Power, M. J., and Prentice, I. C.: Climate and human influences on global biomass burning over the past two millennia, Nat. Geosci., 1, 697–702, https://doi.org/10.1038/ngeo313, 2008.

Marzin, C. and Braconnot, P.: Variations of Indian and African monsoons induced by insolation changes at 6 and 9.5 kyr BP, Clim. Dynam., 33, 215–231, https://doi.org/10.1007/s00382- 009-0538-3, 2009.

McDermott, F.: Palaeo-climate reconstruction from stable isotope variations in speleothems: A review, Quaternary Sci. Rev., 23, 901–918, https://doi.org/10.1016/j.quascirev.2003.06.021, 2004.

Misra, P., Tandon, S. K., and Sinha, R.: Holocene climate records from lake sediments in India: Assessment of coherence across climate zones, Earth-Sci. Rev., 190, 370–397, https://doi.org/10.1016/j.earscirev.2018.12.017, 2019.

Moerman, J. W., Cobb, K. M., Adkins, J. F., Sodemann, H., Clark, B., and Tuen, A. A.: Diurnal to interannual rainfall δ 18O variations in northern Borneo driven by regional hydrology. Earth Planet. Sc. Lett., 369, 108–119, https://doi.org/10.1016/j.epsl.2013.03.014, 2013.

Mohtadi, M., Oppo, D. W., Steinke, S., Stuut, J. B. W., De Pol-Holz, R., Hebbeln, D., and Lückge, A.: Glacial to Holocene swings of the Australian-Indonesian monsoon, Nat. Geosci., 4, 540–544, https://doi.org/10.1038/ngeo1209, 2011.

Nivet, F., Bergonzini, L., Mathé, P. E., Noret, A., Monvoisin, G., Majule, A., and Williamson, D.: Influence of the balance of the intertropical front on seasonal variations of the isotopic composition in rainfall at Kisiba Masoko (Rungwe Volcanic Province, SW, Tanzania), Isotopes Environ. Health Stud., 54, 352–369, https://doi.org/10.1080/10256016.2018.1443923, 2018.

Oksanen, J., Blanchet, F. G., Friendly, M., Kindt, R., Legendre, P., McGlinn, D., Minchin, P. R., O'Hara, R. B., Simpson, G. L., Solymos, P., Stevens, M. H. H., Szoecs, E., and Wagner, H.: vegan: Community Ecology Package, R package version 2.5-2, Cran R, 2019.

Otto-Bliesner, B. L., Braconnot, P., Harrison, S. P., Lunt, D. J., Abe-Ouchi, A., Albani, S., Bartlein, P. J., Capron, E., Carlson, A. E., Dutton, A., Fischer, H., Goelzer, H., Govin, A., Haywood, A., Joos, F., LeGrande, A. N., Lipscomb, W. H., Lohmann, G., Mahowald, N., Nehrbass-Ahles, C., Pausata, F. S. R., Peterschmitt, J.-Y., Phipps, S. J., Renssen, H., and Zhang, Q.: The PMIP4 contribution to CMIP6 – Part 2: Two interglacials, scientific objective and experimental design for Holocene and Last Interglacial simulations, Geosci. Model Dev., 10, 3979–4003, https://doi.org/10.5194/gmd-10-3979-2017, 2017.

Parker, S. E.: Speleothem_orbital_monsoon_var, Zenodo [code], https://doi.org/10.5281/zenodo.3875496, 2020.

Pausata, F. S. R., Battisti, D. S., Nisancioglu, K. H., and Bitz, C. M.: Chinese stalagmite δ 18O controlled by changes in the Indian monsoon during a simulated Heinrich event, Nat. Geosci., 4, 474–480, https://doi.org/10.1038/ngeo1169, 2011.

Quigley, M. C., Horton, T., Hellstrom, J. C., Cupper, M. L., and Sandiford, M.: Holocene climate change in arid Australia from speleothem and alluvial records, Holocene, 20, 1093–1104, https://doi.org/10.1177/0959683610369508, 2010.

R Core Team: R: A Language and Environment for Statistical Computing, available at: https://www.r-project.org/ (last access: 31 January 2021), 2019.

Rachmayani, R., Prange, M., and Schulz, M.: North African vegetation–precipitation feedback in early and mid-Holocene climate simulations with CCSM3-DGVM, Clim. Past, 11, 175–185, https://doi.org/10.5194/cp-11-175-2015, 2015.

Rao, C. R.: The use and interpretation of principal component analysis in applied research, Sankhya Indian J. Stat. Ser. A, 329–358, 1964. Risi, C., Bony, S., and Vimeux, F.: Influence of convective processes on the isotopic composition (δ 18O and δD) of precipitation and water vapor in the tropics: 2. Physical interpretation of the amount effect, J. Geophys. Res., 113, D19306, https://doi.org/10.1029/2008JD009943, 2008.

Risi, C., Bony, S., Vimeux, F., and Jouzel, J.: Water-stable isotopes in the LMDZ4 general circulation model: Model evaluation for present-day and past climates and applications to climatic interpretations of tropical isotopic records, J. Geophys. Res., 115, D12118, https://doi.org/10.1029/2009JD013255, 2010.

Risi, C., Noone, D., Frankenberg, C., and Worden, J.: Role of continental recycling in intraseasonal variations of continental moisture as deduced from model simulations and water vapor isotopic measurements, Water Resour. Res., 49, 4136–4156, https://doi.org/10.1002/wrcr.20312, 2013.

Rohlf, F. J.: An Empirical Comparison of Three Ordination Techniques in Numerical Taxonomy, Syst. Biol., 21, 271–280, https://doi.org/10.1093/sysbio/21.3.271, 1972.

Rozanski, K., Araguás-Araguás, L., and Gonfiantini, R.: Isotopic patterns in modern global precipitation, Geophys Monogr., 78, 1–36, https://doi.org/10.1029/GM078p0001, 1993.

Salati, E., Dall'Olio, A., Matsui, E., and Gat, J. R.: Recycling of water in the Amazon Basin: An isotopic study, Water Resour. Res., 15, 1250–1258, https://doi.org/10.1029/WR015i005p01250, 1979.

Schäfer-Neth, C. and Paul, A.: The Atlantic Ocean at the Last Glacial Maximum: 1. Objective mapping of the GLAMAP seasurface conditions, in: The South Atlantic in the Late Quaternary, edited by: Wefer, G., Mulitza, S., and Ratmeyer, V., Springer, Berlin, Heidelberg, 531–548, 2003.

Sinha, A., Kathayat, G., Cheng, H., Breitenbach, S.F., Berkelhammer, M., Mudelsee, M., Biswas, J., and Edwards, R.L.: Trends and oscillations in the Indian summer monsoon rainfall over the last two millennia, Nat. Commun., 6, 1–8, https://doi.org/10.1038/ncomms7309, 2015.

Sjolte, J. and Hoffmann, G.: Modelling stable water isotopes in monsoon precipitation during the previous interglacial, Quaternary Sci. Rev., 85, 119–135, https://doi.org/10.1016/j.quascirev.2013.12.006, 2014.

Sowers, T.: Ice core records of atmospheric N2O covering the last 106,000 years, Science, 301, 945–948, https://doi.org/10.1126/science.1085293, 2003. Steinke, S., Mohtadi, M., Prange, M., Varma, V., Pittauerova, D., and Fischer, H. W.: Mid- to Late-Holocene Australian-Indonesian summer monsoon variability, Quaternary Sci. Rev., 93, 142–154, https://doi.org/10.1016/j.quascirev.2014.04.006, 2014.

Tabor, C. R., Otto-Bliesner, B. L., Brady, E. C., Nusbaumer, J., Zhu, J., Erb, M. P., Wong, T. E., Liu, Z., and Noone, D.: Interpreting Precession-Driven δ 18O Variability in the South Asian Monsoon Region, J. Geophys. Res.-Atmos., 123, 5927–5946, https://doi.org/10.1029/2018JD028424, 2018.

Tan, M.: Circulation effect: climatic significance of the short term variability of the oxygen isotopes in stalagmites from monsoonal China, Quat. Sci., 29, 851–862, 2009.

Tan, M.: Tread-wind driven inverse coupling between stalagmite δ 18O from monsoon region of China and large scale temperaturecirculation effect on decadal to precessional timescales, Quat. Sci., 31, 1086–1097, 2011.

Tan, M.: Circulation effect: Response of precipitation δ 18O to the ENSO cycle in monsoon regions of China, Clim. Dynam., 42, 1067–1077, https://doi.org/10.1007/s00382-013-1732-x, 2014.

Tan, L. C., Cai, Y., Cheng, H., Edwards, R. L., Shen, C., Gao, Y., and An, Z.: Climate significance of speleothem δ 18O from central China on decadal timescale, J. Asian Earth Sci., 106, 150–155, https://doi.org/10.1016/j.jseaes.2015.03.008, 2015.

Tremaine, D. M., Froelich, P. N., and Wang, Y.: Speleothem calcite farmed in situ: Modern calibration of δ 18O and δ 13C paleoclimate proxies in a continuously-monitored natural cave system, Geochim. Cosmochim. Ac., 75, 4929–4950, https://doi.org/10.1016/j.gca.2011.06.005, 2011.

Trenberth, K. E., Stepaniak, D. P., and Caron, J. M.: The global monsoon as seen through the divergent atmospheric circulation, J. Climate, 13, 3969–3993, https://doi.org/10.1175/1520- 0442(2000)013 2.0.CO;2, 2000.

Varma, V., Prange, M., Merkel, U., Kleinen, T., Lohmann, G., Pfeiffer, M., Renssen, H., Wagner, A., Wagner, S., and Schulz, M.: Holocene evolution of the Southern Hemisphere westerly winds in transient simulations with global climate models, Clim. Past, 8, 391–402, https://doi.org/10.5194/cp-8-391-2012, 2012.

Wackerbarth, A., Langebroek, P. M., Werner, M., Lohmann, G., Riechelmann, S., Borsato, A., and Mangini, A.: Simulated oxygen isotopes in cave drip water and speleothem calcite in European caves, Clim. Past, 8, 1781–1799, https://doi.org/10.5194/cp-8-1781-2012, 2012.

Waelbroeck, C., Labeyrie, L., Michel, E., Duplessy, J. C., McManus, J. F., Lambeck, K., Balbon, E., and Labracherie, M.: Sealevel and deep water temperature changes derived from benthic foraminifera isotopic records, Quaternary Sci. Rev., 21, 295–305, https://doi.org/10.1016/S0277-3791(01)00101-9, 2002.

Wang, B. and Ding, Q.: Global monsoon: Dominant mode of annual variation in the tropics, Dynam. Atmos. Oceans, 44, 165–183, https://doi.org/10.1016/j.dynatmoce.2007.05.002, 2008.

Wang, P. X., Wang, B., Cheng, H., Fasullo, J., Guo, Z. T., Kiefer, T., and Liu, Z. Y.: The global monsoon across timescales: coherent variability of regional monsoons, Clim. Past, 10, 2007–2052, https://doi.org/10.5194/cp-10-2007-2014, 2014.

Wang, X., Auler, A. S., Edwards, R. L., Cheng, H., Ito, E., and Solheid, M.: Interhemispheric anti-phasing of rainfall during the last glacial period, Quaternary Sci. Rev., 25, 3391–3403, https://doi.org/10.1016/j.quascirev.2006.02.009, 2006.

Wang, Y., Cheng, H., Edwards, R. L., Kong, X., Shao, X., Chen, S., Wu, J., Jiang, X., Wang, X., and An, Z.: Millennial- and orbital-scale changes in the East Asian monsoon over the past 224,000 years, Nature, 451, 1090–1093, https://doi.org/10.1038/nature06692, 2008.

Wang, Y. J., Cheng, H., Edwards, R. L., An, Z. S., Wu, J. Y., Shen, C. C., and Dorale, J. A.: A high-resolution absolute-dated late Pleistocene monsoon record from Hulu Cave, China, Science, 294, 2345–2348, https://doi.org/10.1126/science.1064618, 2001.

Waterisotopes Database: OIPC mean annual δ 18Oprecip data, WaterIsotopes.org, University of Utah [data set], available at: http: //waterisotopes.org, last access: 10 May 2021.

Werner, M.: ECHAM5-wiso simulation data – present-day, midHolocene, and Last Glacial Maximum, PANGAEA [data set], https://doi.org/10.1594/PANGAEA.902347, 2019.

Werner, M., Langebroek, P. M., Carlsen, T., Herold, M., and Lohmann, G.: Stable water isotopes in the ECHAM5 general circulation model: Toward high-resolution isotope modeling on a global scale, J. Geophys. Res., 116, D15109, https://doi.org/10.1029/2011JD015681, 2011.

Werner, M., Jouzel, J., Masson-Delmotte, V., and Lohmann, G.: Reconciling glacial Antarctic water stable isotopes with ice sheet topography and the isotopic paleothermometer, Nat. Commun., 9, 1–10, https://doi.org/10.1038/s41467-018-05430-y, 2018.

Wickham, H.: ggplot2: Elegant Graphics for Data Analysis, Springer-Verlag, New York, available at: https://ggplot2. tidyverse.org (last access: 31 January 2021), 2016.

Wurtzel, J. B., Abram, N. J., Lewis, S. C., Bajo, P., Hellstrom, J. C., Troitzsch, U., and Heslop, D.: Tropical IndoPacific hydroclimate response to North Atlantic forcing during the last deglaciation as recorded by a speleothem from Sumatra, Indonesia, Earth Planet. Sci. Lett., 492, 264–278, https://doi.org/10.1016/j.epsl.2018.04.001, 2018.

Wyrwoll, K. H. and Miller, G. H.: Initiation of the Australian summer monsoon 14,000 years ago, Quatern. Int., 83, 119–128, https://doi.org/10.1016/S1040-6182(01)00034-9, 2001.

Xu, X., Werner, M., Butzin, M., and Lohmann, G.: Water isotope variations in the global ocean model MPI-OM, Geosci. Model Dev., 5, 809–818, https://doi.org/10.5194/gmd-5-809- 2012, 2012.

Yang, X., Liu, J., Liang, F., Yuan, D., Yang, Y., Lu, Y., and Chen, F.: Holocene stalagmite δ 18O records in the East Asian monsoon region and their correlation with those in the Indian monsoon region, Holocene, 24, 1657–1664, https://doi.org/10.1177/0959683614551222, 2014.

Yonge, C. J., Ford, D. C., Gray, J., and Schwarcz, H. P.: Stable isotope studies of cave seepage water, Chem. Geol. Isot. Geosci. Sect., 58, 97–105, https://doi.org/10.1016/0168-9622(85)90030- 2, 1985.

Yoshimura, K., Oki, T., Ohte, N., and Kanae, S.: Colored moisture analysis estimates of variations in 1998 Asian Monsoon water sources, J. Meteorol. Soc. Jpn., 82, 1315–1329, https://doi.org/10.2151/jmsj.2004.1315, 2004.

Yuan, D., Cheng, H., Edwards, R. L., Dykoski, C. A., Kelly, M. J., Zhang, M., Qing, J., Lin, Y., Wang, Y., Wu, J., Dorale, J. A., An, Z., and Cai, Y.: Timing, duration, and transitions of the Last Interglacial Asian monsoon, Science, 304, 575–578, https://doi.org/10.1126/science.1091220, 2004.

Yue, X., Wang, H., Liao, H., and Jiang, D.: Simulation of the Direct Radiative Effect of Mineral Dust Aerosol on the Climate at the Last Glacial Maximum, J. Climate, 24, 843–858, https://doi.org/10.1175/2010JCLI3827.1, 2011.

Zhang, H., Ait Brahim, Y., Li, H., Zhao, J., Kathayat, G., Tian, Y., Baker, J., Wang, J., Zhang, F., Ning, Y., Edwards, R. L., and Cheng, H.: The Asian Summer monsoon: Teleconnections and forcing Mechanisms–A

review from Chinese speleothem δ 18O records, Quaternary, 2, 26, https://doi.org/10.3390/quat2030026, 2019.

Zhang, X., Jin, L., Chen, J., Lu, H., and Chen, F.: Lagged response of summer precipitation to insolation forcing on the northeastern Tibetan Plateau during the Holocene, Clim. Dynam., 50, 3117– 3129, https://doi.org/10.1007/s00382-017-3784-9, 2018.

Zhao, Y. and Harrison, S. P.: Mid-Holocene monsoons: A multimodel analysis of the inter-hemispheric differences in the responses to orbital forcing and ocean feedbacks, Clim. Dynam., 39, 1457–1487, https://doi.org/10.1007/s00382-011-1193- z, 2012.

Zhao, Y., Yu, Z., Chen, F., Zhang, J., and Yang, B.: Vegetation response to Holocene climate change in monsooninfluenced region of China, Earth-Sci. Rev., 97, 242–256, https://doi.org/10.1016/j.earscirev.2009.10.007, 2009.

Zhou, W., Yu, X., Jull, A. J. T., Burr, G., Xiao, J. Y., Lu, X., and Xian, F.: High-resolution evidence from southern China of an early Holocene optimum and a mid-Holocene dry event during the past 18,000 years, Quaternary Res., 62, 39–48, https://doi.org/10.1016/j.yqres.2004.05.004, 2004.

2.11 Supplement

Figure S1: ECHAM5-wiso annual precipitation-weighted mean $\delta^{18}O_{precip}$ anomalies for the mid-Holocene period (MH, 6,000 years BP, SMOW, ‰) and SISAL $\delta^{18}O_{spel}$ MH anomalies (6,000 years BP ± 500 years, PDB, ‰), plotted as positive or negative signals with respect to 1850-1990 CE. 54 sites have isotope samples in the base period and the MH, 72% of sites show changes in the same direction as ECHAM MH $\delta^{18}O_{precip}$ anomalies, allowing for an uncertainty of ±0.5 ‰.

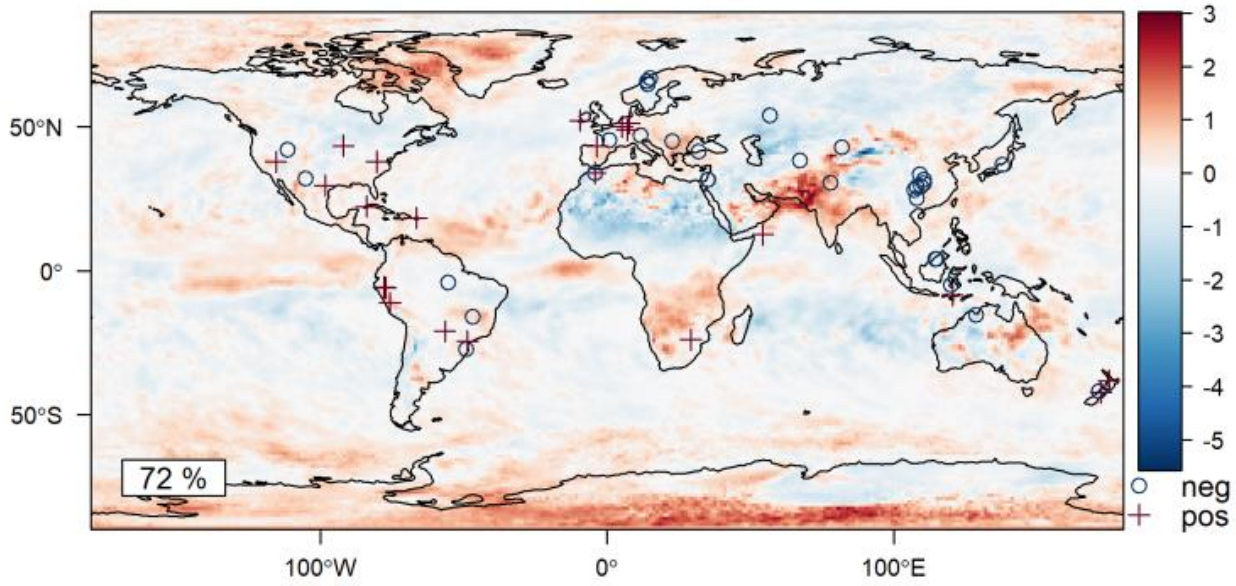

Figure S2: ECHAM5-wiso annual precipitation-weighted mean $\delta^{18}O_{precip}$ anomalies for the LGM (21,000 years BP, SMOW, ‰) and SISAL $\delta^{18}O_{spel}$ LGM anomalies (21,000 years BP ± 1,000 years, PDB, ‰), plotted as positive or negative signals with respect to 1850-1990 CE. 17 sites have isotope samples in the base period and the LGM. 76% of sites show changes in the same direction as ECHAM LGM $\delta^{18}O_{precip}$ anomalies, allowing for an uncertainty of ±0.5 ‰.

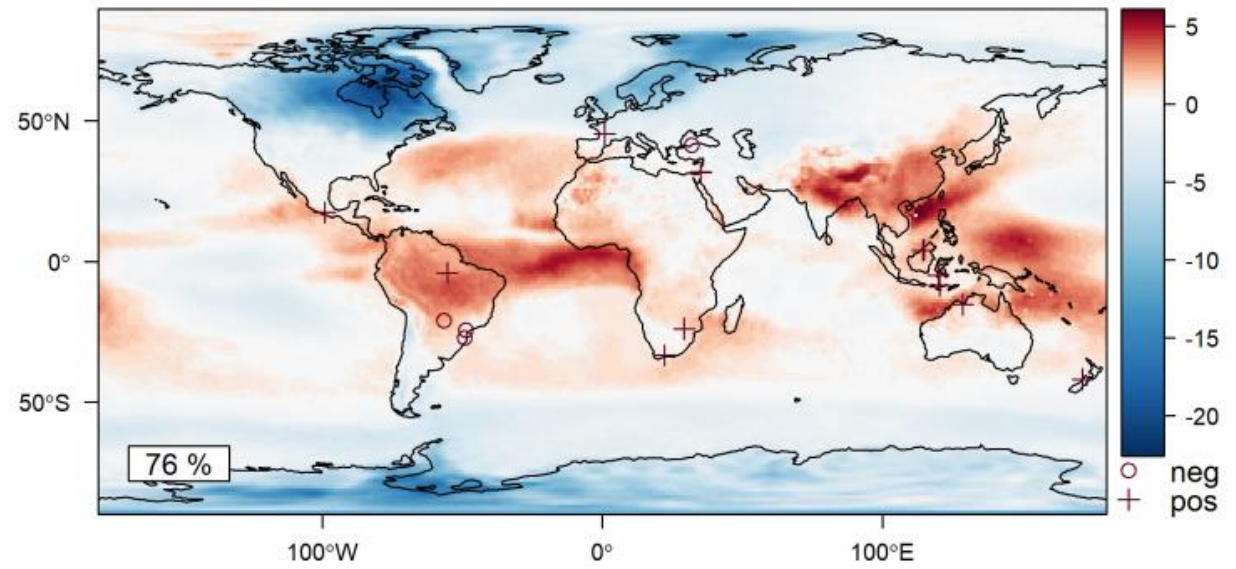

Figure S3: ECHAM5-wiso annual precipitation-weighted mean $\delta^{18}O_{precip}$ anomalies (SMOW, ‰) for the LIG (125,000 years BP) and SISAL $\delta^{18}O_{spel}$ LIG anomalies (125,000 years BP ± 1,000 years, PDB, ‰), plotted as positive and negative signals with respect to 1850-1990 CE. 12 sites have isotope samples in the base period and the LIG. All sites show changes in the same direction as ECHAM LIG $\delta^{18}O_{precip}$ anomalies, allowing for an uncertainty of ±0.5 ‰.

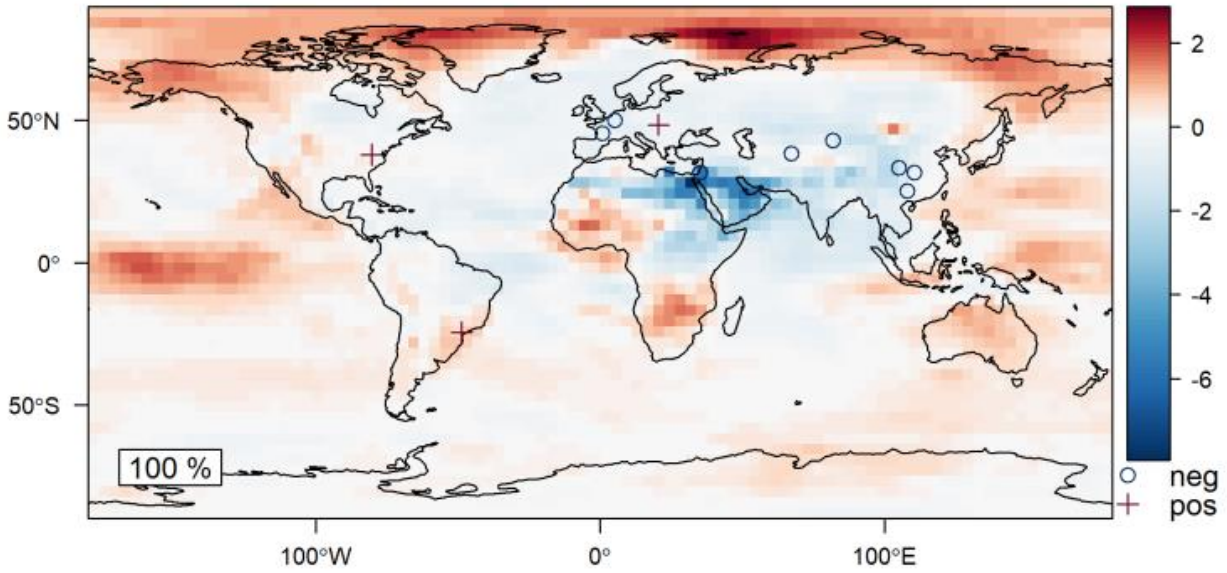

Figure S4: GISS annual precipitation-weighted mean $\delta^{18}O_{precip}$ anomalies for 3,000 years BP (3ka, SMOW, ‰) and SISAL $\delta^{18}O_{spel}$ 3ka anomalies (3,000 years BP ± 500 years, PDB, ‰), plotted as positive and negative signals with respect to 1850 to 1990 CE. 63 sites have isotope values in the base period and 3ka. 87% show changes in the same direction as GISS $\delta^{18}O_{precip}$ 3ka anomalies, allowing for an uncertainty of ±0.5 ‰.

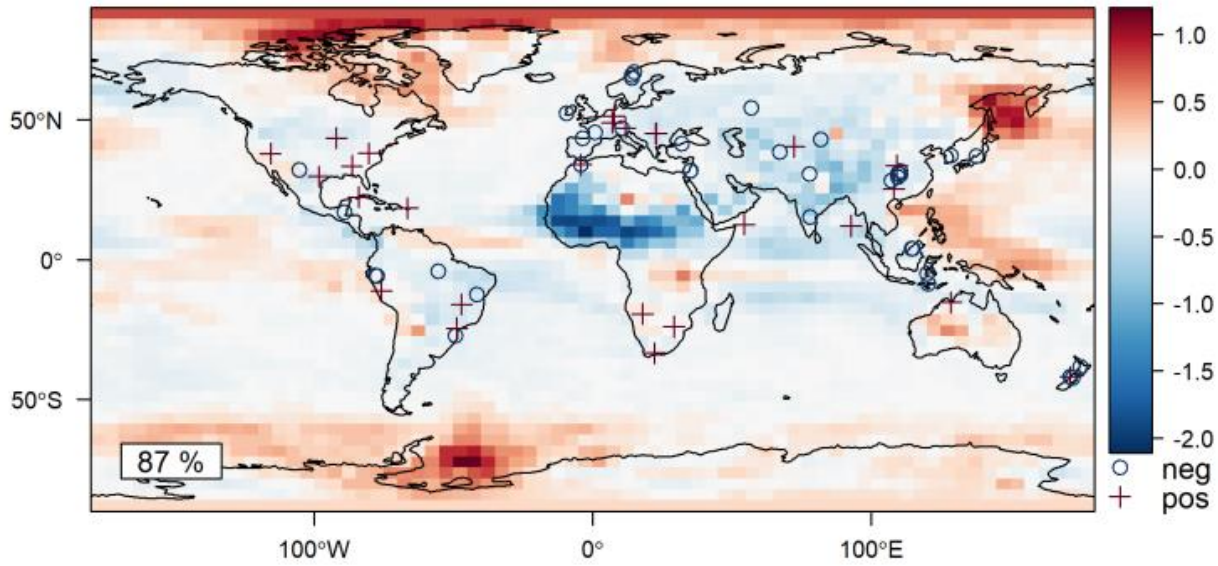

Figure S5: GISS annual precipitation-weighted mean $\delta^{18}O_{precip}$ anomalies for 6,000 years BP (6ka, SMOW, ‰) and SISAL $\delta^{18}O_{spel}$ 6ka anomalies (6,000 years BP ± 500 years, PDB, ‰), plotted as positive and negative signals with respect to 1850 to 1990 CE. 54 sites have isotope values in the base period and 6ka. 87% show changes in the same direction as GISS $\delta^{18}O_{precip}$ 3ka anomalies, allowing for an uncertainty of ±0.5 ‰.

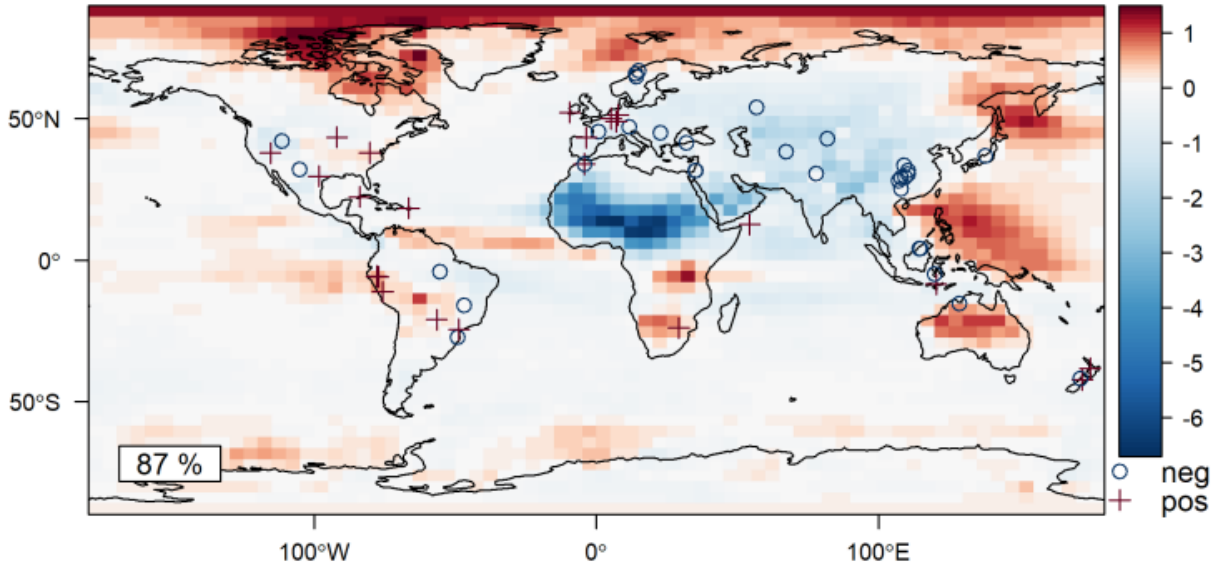

Figure S6: GISS annual precipitation-weighted mean $\delta^{18}O_{precip}$ anomalies for 9,000 years BP (9ka, SMOW, ‰) and SISAL $\delta^{18}O_{spel}$ 9ka anomalies (9,000 years BP ± 500 years, PDB, ‰), plotted as positive and negative signals with respect to 1850 to 1990 CE. 48 sites have isotope values in the base period and 9ka. 81% show changes in the same direction as GISS $\delta^{18}O_{precip}$ 9ka anomalies, allowing for an uncertainty of ±0.5 ‰.

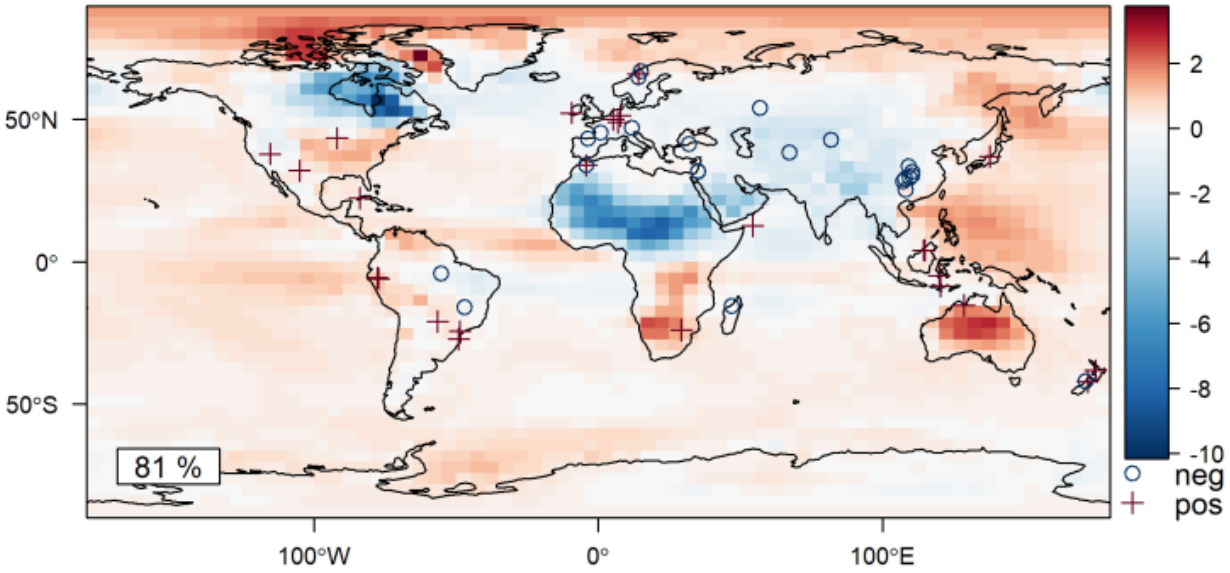

Figure S7: Spatial distribution of speleothem sites used in this study, shown with monsoon regions, defined by the precipitation-based criteria (Wang and Ding, 2008): the annual precipitation range (summer minus winter) exceeds 300 mm and 50 % of the annual mean. Summer is defined as May to September for the northern hemisphere and November to March for the southern hemisphere, vice versa for winter. Precipitation data is from the WFDEI dataset (Weedon et al., 2014).

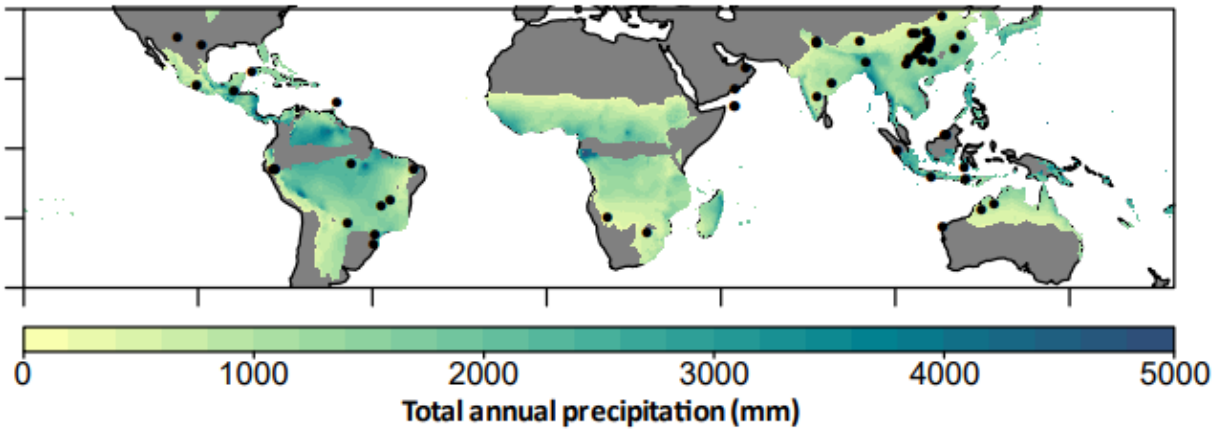

Figure S8: Speleothem $\delta^{18}O$ anomalies, converted to their drip water equivalent, compared to anomalies of $\delta^{18}O_{precip}$ from the ECHAM simulations for the (a) East Asian (EAM), (b) Indian (ISM) and (c) Indonesian-

Australian (IAM) monsoons. $\delta^{18}O_{spel}$ (PBD) is converted to $\delta^{18}O_{drip\ water}$ (SMOW) following the methodology in Comas-Bru et al. (2019), using simulated temperature. The boxes show the median value (line) and the interquartile range, and the whiskers shown the minimum and maximum values, with outliers represented by grey dots. Note that the isotope axes are reversed, so that the most negative anomalies are at the top of the plot, to be consistent with the assumed relationship with the direction of change in precipitation and temperature. The difference in amplitude of $\delta^{18}O$ signals is small (<0.5 ‰) between simulated and observed values for the ISM and IAM. In the EAM, simulated $\delta^{18}O$ values have a ~1.4 ‰ higher amplitude than $\delta^{18}O_{drip\ water}$ observations.

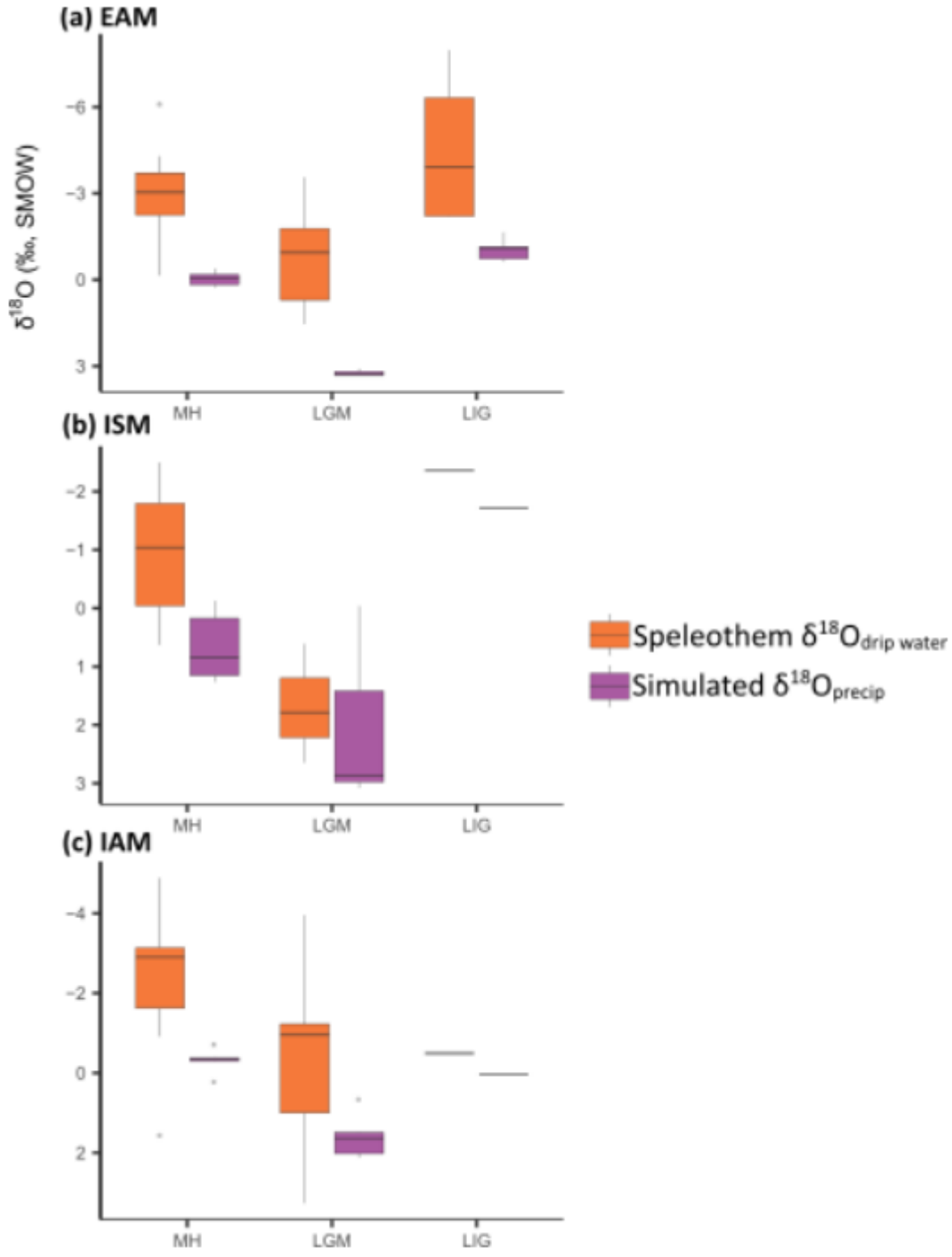

Figure S9: Same as figure 6, except Indian Summer Monsoon (ISM) source region has been expanded to include the Bay of Bengal.

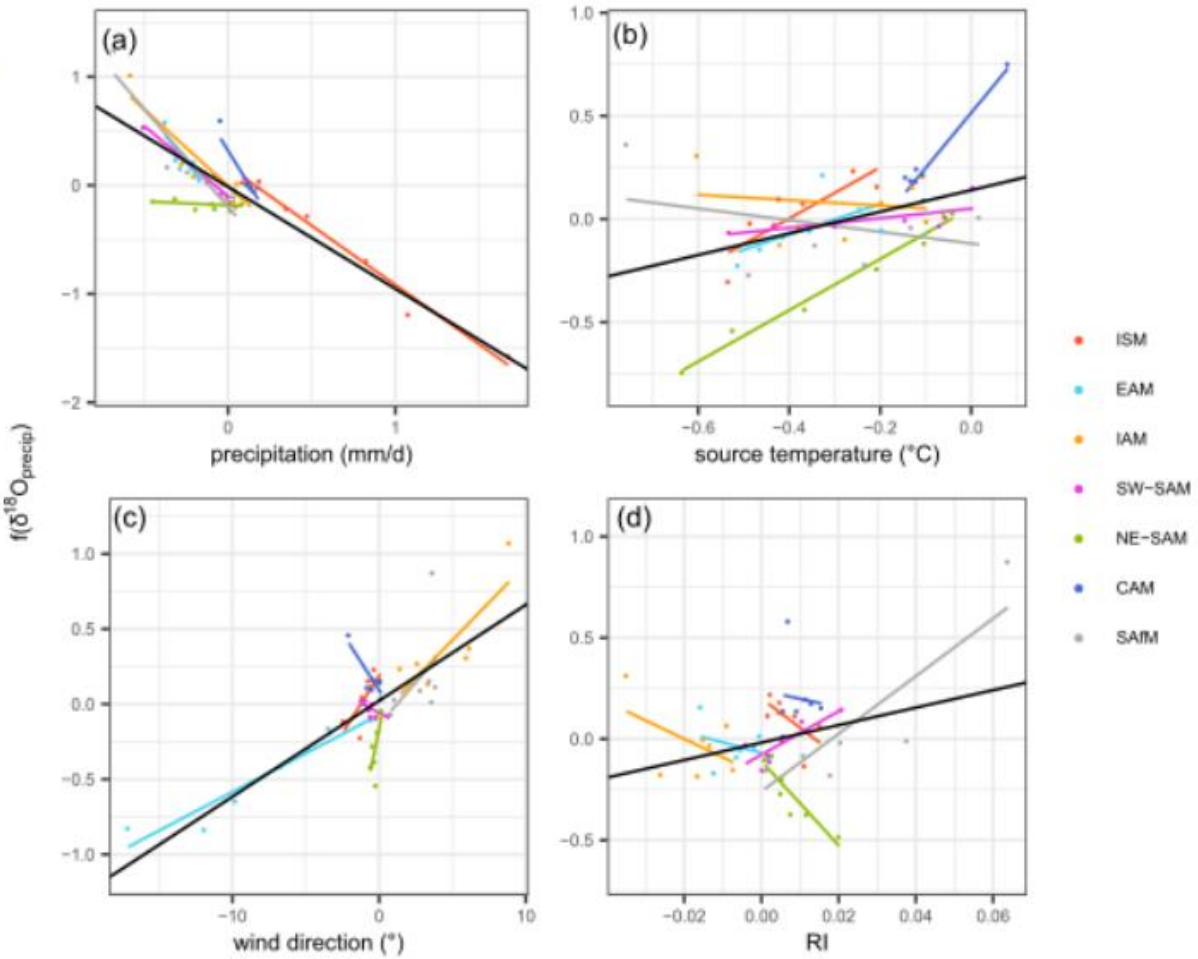

Table S1: Results of the multiple linear regression analysis when the Indian monsoon source region is expanded to include the Bay of Bengal. Significant relationships (P > 0.01) are shown in bold.

	Regression coefficient	t value
Regional precipitation	**-0.94**	-11.22
Source area temperature	**0.52**	2.95
Wind direction	**0.06**	8.30
Precipitation recycling	4.32	1.95

References:

Comas-Bru, L., Harrison, S. P., Werner, M., Rehfield, K., Scroxton, N., Veiga-Pires, C. and SISAL working group members: Evaluating model outputs using integrated global speleothem records of climate change since the last glacial, Clim. Past, 15(4), 1557–1579, https://doi.org/10.5194/cp-15- 1557-2019, 2019.

Wang, B. and Ding, Q.: Global monsoon: Dominant mode of annual variation in the tropics, Dyn. Atmos. Ocean., 44(3–4), 165–183, https://doi.org/10.1016/j.dynatmoce.2007.05.002, 2008.

Weedon, G. P., Balsamo, G., Bellouin, N., Gomes, S., Best, M. J. and Viterbo, P.: The WFDEI meteorological forcing data set: WATCH Forcing Data methodology applied to ERA-Interim reanalysis data, Water Resour. Res., 50(9), 7505–7514, https://doi.org/10.1002/2014WR01

3 Speleothem records of monsoon interannual-interdecadal variability through the Holocene

3.1 Preface

The following chapter is a paper published in Environmental Research Communications and is available to read online at https://doi.org/10.1088/2515-7620/ac3eaa. It has been written and referenced in the style guidelines of this journal. The authors are Sarah E. Parker, Sandy P. Harrison and Pascale Braconnot. The study was designed by SEP and SPH. PB provided climate model outputs. SEP ran the analyses. The first draft of the paper was written by SEP and SPH, and all authors contributed to the final article. Estimated contributions are SEP: 75 %; SPH: 15 % and PB 10 %:

This chapter reconstructs regional monsoon interannual-interdecadal variability (IADV) amplitude through the Holocene epoch and compares these reconstructions with transient climate models. The study investigates the influence of orbital forcing on monsoon IADV and demonstrates a complex relationship. Regional IADV evolutions are unique, likely reflecting an indirect relationship with orbital changes, via a complex interplay between insolation changes, climate modes and regional monsoon precipitation.

3.2 Abstract

Modern observations show considerable interannual to interdecadal variability in monsoon precipitation. However, there are few reconstructions of variability at this timescale through the Holocene, and there is therefore less understanding of how changes in external forcing might have affected monsoon variability in the past. Here, we reconstruct the evolution of the amplitude of interannual to interdecadal variability (IADV) in the East Asian, Indian and South American monsoon regions through the Holocene using a global network of high-resolution speleothem oxygen isotope ($\delta^{18}O$) records. We reconstruct changes in IADV for individual speleothem records using the standard deviation of $\delta^{18}O$ values in sliding time windows after correcting for the influence of confounding factors such as variable sampling resolution, growth

rates and mean climate. We then create composites of IADV changes for each monsoon region. We show that there is an overall increase in δ^{18}O IADV in the Indian monsoon region through the Holocene, with an abrupt change to present-day variability at ~2 ka. In the East Asian monsoon, there is an overall decrease in δ^{18}O IADV through the Holocene, with an abrupt shift also seen at ~2 ka. The South American monsoon is characterised by large multi-centennial shifts in δ^{18}O IADV through the early and mid-Holocene, although there is no overall change in variability across the Holocene. Our regional IADV reconstructions are broadly reproduced by transient climate-model simulations of the last 6 000 years. These analyses indicate that there is no straightforward link between IADV and changes in mean precipitation, or between IADV and orbital forcing, at a regional scale.

3.3 Introduction

More than two thirds of the global population live in regions which are dependent on monsoon rainfall; interannual variability in precipitation has a significant impact on the livelihoods of these people (Wang *et al* 2021). The variability of precipitation in the tropics on interannual to interdecadal timescales (interannual to interdecadal variability: IADV) is influenced by sea surface temperature (SST) changes: the El Niño Southern Oscillation (ENSO) has a major influence on monsoon precipitation IADV (McPhaden *et al* 2006, Messié and Chavez 2011, Wang *et al* 2012). SST variability in the extratropical Pacific (Pacific Decadal Oscillation, PDO, Krishnan and Sugi 2003, Yoon and Yeh 2010), Indian Ocean (Indian Ocean Dipole, IOD, Ashok *et al* 2001, Saji and Yamagata 2003, Ummenhofer *et al* 2011;) and Atlantic Ocean (Atlantic Multidecadal Oscillation, AMO, Grimm and Zilli 2009) also influence the IADV of monsoon precipitation. These modes interact with one another to drive complex and considerable interannual fluctuations in precipitation. They are often associated with extreme events over monsoon regions (Kane 1999, Kirono *et al* 1999) with major impacts on water resources, crop production (Phillips *et al* 2012, Iizumi *et al* 2014, Ray *et al* 2015) and long-term impacts on health (Bouma and Kaay, 1996, Gagnon *et al* 2001, Hashizume *et al* 2012).

Although there has been considerable focus on changes in monsoon IADV in the recent period (Wang *et al* 2012, Yim *et al* 2014), observational records are too short to sample IADV sufficiently and it is therefore difficult to examine how this variability responds to external forcing. Future changes in monsoon precipitation IADV in response to increasing CO_2 concentrations are difficult to predict because of the large uncertainties related to internal variability (Wang *et al* 2021). Climate models disagree, for example, on the how the variability of both ENSO (Stevenson 2012, Chen *et al* 2017, Brown *et al* 2020) and the IOD (Hui and Zheng 2018, Zheng *et al* 2013, Ng *et al* 2018) will change in the future. The palaeorecord provides an alternative way of examining how changes in external forcing have influenced IADV in monsoon regions. Specifically, the Holocene (11.7 thousand years ago, ka, to present) provides an opportunity to examine how monsoon IADV responds to changes in the seasonal and latitudinal distribution of insolation resulting from changes in the Earth's orbit. In the early Holocene, northern hemisphere summer insolation was greater than today whilst southern hemisphere summer insolation was reduced compared to present. Through the Holocene, summer insolation gradually declined (increased) to present-day levels in the northern (southern) hemisphere. These insolation changes altered the mean climate (Wang *et al* 2014, Zhang *et al* 2021) and likely had a marked impact on IADV.

There are only a few reconstructions of Holocene changes in precipitation IADV from tropical continents. Lake records of hydrological variability from the circum-Pacific region show changing precipitation variability through the Holocene, interpreted as ENSO variability. Records show lower precipitation variability in the mid-Holocene than today, with higher variability during the late Holocene (Riedinger *et al* 2002, Conroy *et al* 2008, Zhang *et al* 2014, Thompson *et al* 2017). The time when IADV increases from the MH minimum varies between records. For example, in the Galapagos Islands, Bainbridge Crater Lake shows increasing ENSO variance from 2 ka onwards (Riedinger *et al* 2002) and El Junco Lake shows an increase at∼4 ka (Conroy *et al* 2008, Zhang *et al* 2014). The red-light reflectivity record (Moy *et al* 2002) from lake Pallcacocha, Ecuador, indicates the increase in variability begins at ∼7 ka, whilst a grey-scale record from the same site (Rodbell 1999) shows this change beginning at ∼5 ka. Reconstructions of early Holocene IADV also vary: an algal lipid concentration and hydrogen isotope record from El Junco Lake shows fluctuations between high and low variability (Zhang *et al* 2014), whilst sediment records from El

Junco and Pallcacocha lakes show low variability through the early Holocene (Rodbell 1999, Moy *et al* 2002, Conroy *et al* 2008).

The differences between existing reconstructions highlights the limitations of lake sediment records. For example, the interpretation of the Pallcacocha records has been questioned because the highly non-linear response of sediment accumulation to precipitation could bias the reconstructions (Emile-Geay and Tingley 2016). The lack of a clear wet-dry pattern to ENSO events in the area (Schneider *et al* 2018, Kiefer and Karamperidou 2019) and the influence of catchment differences on lake sediment records (Schneider *et al* 2018) also reduces the reliability of these records as indicators of IADV and ENSO. Furthermore, the spatial complexity of IADV necessitates regional-scale reconstructions to understand differences in IADV changes.

The Gallapagos and Pallcacocha records were a focus for reconstructions of IADV because, compared to most other terrestrial records, they have quasi-annual resolution. Speleothems provide an alternative source of high-resolution data in monsoon regions and can therefore be used to investigate precipitation IADV over land. Speleothems record changes in the strength of the monsoon, via a combination of changes in regional precipitation and circulation changes that cause changes in moisture source and transport pathway (Sinha *et al* 2015, Cheng *et al* 2019, Parker *et al* 2021). However, there are several factors that influence the oxygen isotopic composition of speleothems and might complicate the interpretation of short-term climate variability, including changing growth rates and the mixing of meteoric water in the epikarst (Lachniet 2009) although compositing of speleothem records can be used to minimise the impact of such local factors when deriving regional climate signals (Comas-Bru *et al* 2019, Parker *et al* 2021).

In this paper, we use speleothem oxygen isotope ($\delta^{18}O$) records from the second version of the Speleothem Isotopes Synthesis and AnaLysis (SISAL) database (Atsawawaranunt *et al* 2018, Comas-Bru *et al* 2020a, 2020b) to reconstruct changes in IADV in monsoon regions through the Holocene. We first investigate the potential influence of confounding factors on $\delta^{18}O$ variability using multiple regression. We then reconstruct changes in the amplitude of IADV through the Holocene using the standard deviation

(s.d.) of $\delta^{18}O$ values. We construct regional-scale composite changes in IADV through time for individual monsoon regions and compare these to trends in IADV shown by four transient climate model simulations. Previous data-model comparisons of Holocene IADV have focused on ENSO variability (e.g. Carré *et al* 2021) but have not examined the wider implications for monsoon precipitation IADV. Although we do not associate the changes in IADV with specific climate modes, we compare regional monsoon IADV changes to changes in summer insolation and long-term trends in monsoon precipitation to investigate the relationship with external climate forcing.

3.4 Methods

3.4.1 Speleothem oxygen isotope data

We use speleothem $\delta^{18}O$ data from the SISAL database (Atsawawaranunt *et al* 2018, Comas-Bru *et al* 2020a, 2020b), selected using the following criteria:

- The record is located in a monsoon region, between 40 °N and 35 °S;
- The mineralogy is known and does not vary because oxygen isotope fractionation depends on speleothem mineralogy, introducing a non-climatic influence on δ 18O s.d.;
- The record covers at least 3 000 years of the Holocene;
- The record has a mean sampling resolution of at least 20 years;

This resulted in the selection of 144 records from 79 sites (figure 3.1).

We interpret speleothem $\delta^{18}O$ records ($\delta^{18}O_{spel}$) as changes in the strength of the summer monsoon, via regional precipitation and moisture source pathway and source changes (including oceanic versus land-derived moisture), which likely reinforce one another to give more negative $\delta^{18}O$ when the summer monsoon is stronger (Vuille *et al* 2003, Yang *et al* 2016, Cai *et al* 2017, Kathayat *et al* 2021).

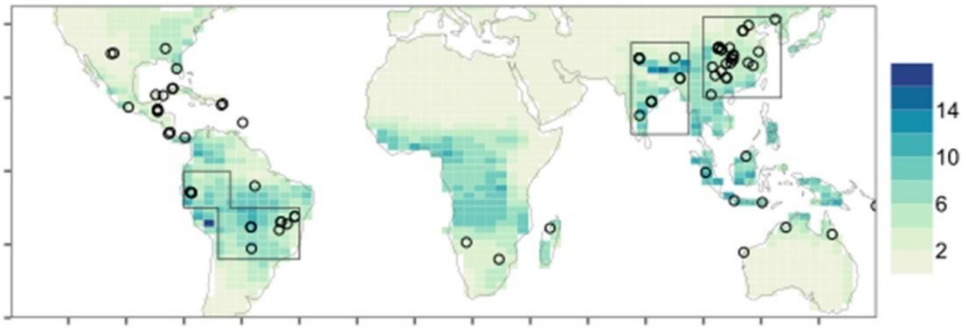

Figure 3.1 Spatial distribution of speleothem records used in this study, shown with the ensemble mean summer precipitation (mm/d) across the IPSLCM5A-LR, IPSL-Sr, AWI-ESM2 and MPI-ESM1.2 simulations, for 1800–1850. Summer is defined as May to September in the northern hemisphere and November to March in the southern hemisphere. Boxes show the limits used to extract regional precipitation from the Earth System models: SAM = South American Monsoon (latitude: −10° to 0°; longitude: −80° to −64° and latitude: −24° to −10°; longitude: −68° to −40°), ISM = Indian Summer Monsoon (latitude: 10° to 35°; longitude: 75° to 95°) and EAM = East Asian Monsoon (latitude: 20° to 43°; longitude: 100° to 127°).

3.4.2 Investigating the impact of potential confounding factors

The use of $\delta^{18}O_{spel}$ variability as an indicator of IADV in regional precipitation relies on showing that other factors have a minimal impact on this variability. Smoothing of the $\delta^{18}O$ signals occurs when groundwater of different ages mixes in the epikarst above the cave (Lachniet 2009). Differences in precipitation amount through time could influence the time taken for water to reach the cave, with epikarst transmission times being faster in wetter climates. Apparent $\delta^{18}O_{spel}$ variability could also be affected by changes in sampling frequency across the record and changes in speleothem growth rate. We used multiple linear regression (MLR) to investigate if confounding factors such as mean climate, speleothem growth rate or sampling frequency show a significant relationship with $\delta^{18}O_{spel}$ variability. The s.d. of $\delta^{18}O_{spel}$ values, calculated for a sliding 100-year window (with 50% overlap) across individual records, was used to represent $\delta^{18}O$ interannual to interdecadal variability ($IADV_{spel}$). We used mean growth rate, number of samples(n-samples) and mean $\delta^{18}O_{spel}$ (as an index of mean climate) for each window as predictors. Mean growth rate was calculated as the gradient of the relationship between distance along a speleothem and age. Initial analyses showed that growth rate and n-samples are correlated ($R^2 = 0.33$), whereas mean $\delta^{18}O$ is not strongly correlated with either growth rate ($R^2 = -0.04$) or n-samples ($R^2 = 0.07$). We therefore constructed two separate MLR models, one using growth rate and mean $\delta^{18}O$ and the other using n-

samples and mean $\delta^{18}O$ as predictors. Northern and southern hemisphere (NH, SH) records were analysed separately since the trajectory of the mean climate differs between the NH and SH as a result of differences in insolation forcing. The use of multiple geographically separated records in the MLR model captures the influence of confounding factors on composite regional IADV reconstructions. We examined whether variables were normally distributed using the Shapiro-Wilk test and log transformed nonnormal variables. Examination of the residuals from the fitted values showed no pattern and confirms that an MLR is appropriate. We used P-values to assess the significance of each predictor and R^2 to determine the influence on $\delta^{18}O_{spel}$ variability. Partial residual plots were used to show the relationship between each predictor variable and $IADV_{spel}$ when other variables were held constant.

3.4.3 Regional-scale IADV amplitude evolution

We reconstructed IADV amplitude through the Holocene for individual monsoon regions by calculating $IADV_{spel}$ for a 100-year sliding window with 50% overlap (as described in section 3.4.2). We corrected for the influence of confounding factors by subtracting the MLR slope and intercept values from the $IADV_{spel}$ values. Regional composites were constructed by fitting a running median and interquartile range through the $IADV_{spel}$ values. These composites represent the evolution of the overall amplitude of IADV represented by numerous sites in each region.

We analysed $IADV_{spel}$ changes through the Holocene using breakpoint analysis to distinguish intervals with coherent behaviour (Bai and Perron 2003). Breakpoint analysis was carried out using the strucchange package in R (Zeileis *et al* 2002, Zeileis *et al* 2003). We identified breakpoints in mean and slope to identify periods with significantly higher or lower IADV (changes in mean) and whether IADV was stable or showed a trend (changes in slope) during these intervals. We determined whether the $IADV_{spel}$ of each segment was significantly different using t-tests.

3.4.4 Relationship between IADV and monsoon long-term evolution

The relationship between IADV and mean climate was investigated by comparing the long-term changes in $\delta^{18}O_{spel}$ with the $IADV_{spel}$ for each region through the Holocene. Long-term changes were calculated by converting $\delta^{18}O_{spel}$ to z-scores, with mean and variance standardised relative to a base period of 3 to 5 ka, then calculating the mean $\delta^{18}O_{spel}$ z-score for each 100-year bin (across each site) to standardise sampling resolution. Mean z-scores were calculated for 100-year windows for each region and a 500-year half-window locally weighted regression (Cleveland and Devlin 1988) was constructed to emphasise multi-millennial scale variability.

3.4.5 Simulated monsoon IADV evolution

We use transient simulations from four climate models: version 2 of the AWI (Alfred Wegener Institute) Earth System model (Sidorenko *et al* 2019), version 1.2 of the MPI (Max Planck Institute) Earth System model (Dallmeyer *et al* 2020) and two versions of the IPSL (Institut Pierre Simon Laplace) Earth system model. The first IPSL simulation uses the IPSLCM5A-LR version, with prescribed vegetation, whilst the second simulation (here termed IPSL-Sr) uses a modified version of IPSLCM5A with a dynamical vegetation module (Dufresne *et al* 2013, Braconnot *et al* 2019b). Simulated IADV from IPSLCM5A-LR and IPSL-Sr have been discussed in Braconnot *et al* (2019a) and Crétat *et al* (2020). The IPSL and AWI simulations were run from 6 ka to 1950 CE; the MPI simulation from 7.95 ka to 1850 CE. All simulations were spun up using boundary conditions appropriate for the start year. Appropriate orbital parameters (Berger 1978) and greenhouse gases were prescribed annually through the transient runs (See Supplementary Information). The use of an ensemble of four different model simulations provides a way of identifying signals that are consistent across the models (Carré *et al* 2021). Model performance has been evaluated for these simulations previously, considering climate mean state and variability (Dufresne *et al* 2013, Duvel *et al* 2013, Hourdin *et al* 2013, Mauritsen *et al* 2019, Sidorenko *et al* 2019, Braconnot *et al* 2019b). Despite common model biases (e.g. Tian and Dong, 2020, Good *et al*, 2021), these comparisons indicate that they capture the tropical climate variability.

We calculated area-averaged summer precipitation over the regional monsoons for each simulation using the region limits in figure 3.1, where summer was defined as May to September for the NH and November to March for the SH (Wang and Ding 2008). We calculated the s.d. of area-averaged precipitation for 100-year sliding windows with 50% overlap to determine the changes in IADV (termed $IADV_{precip}$). We analysed the overall evolution of $IADV_{precip}$ from the mid-Holocene onwards using linear regression. We compared changes in $IADV_{precip}$ to $IADV_{spel}$ by imposing the breakpoints detected from the speleothem records for each region and comparing whether coeval changes in slope and mean were similar. We calculated the relationship between $IADV_{precip}$ and long-term changes by correlating IADV against mean summer regional precipitation for 100- year windows.

3.5 Results

3.5.1 Influence of confounding factors on $\delta^{18}O_{spel}$ variability

The MLR model using growth rate and mean $\delta^{18}O$ and the alternative model, using n-samples and mean $\delta^{18}O$, produced similar results. The models show a significant ($P < 0.001$) relationship between $IADV_{spel}$ and both growth rate (or n-samples) and mean $\delta^{18}O_{spel}$ (table 3.1, table S1 available online at stacks.iop.org/ERC/3/ 121002/mmedia). Growth rate has a significant positive relationship with $IADV_{spel}$ (figures 3.2, S1). There is a significant negative relationship in the NH and a significant positive relationship in the SH between $IADV_{spel}$ and mean $\delta^{18}O_{spel}$ (figure 3.2). The models have low R^2 (NH: 0.06; SH: 0.27) suggesting that confounding factors only have a limited influence on $IADV_{spel}$.

	NH	SH
Growth rate	0.08	0.23
Mean $\delta^{18}O$	-0.03	0.08

Table 3.1 Results of the multiple linear regression analysis, separated into northern hemisphere (NH) and southern hemisphere (SH) sites. Significant relationships (P <0.01) are shown in bold.

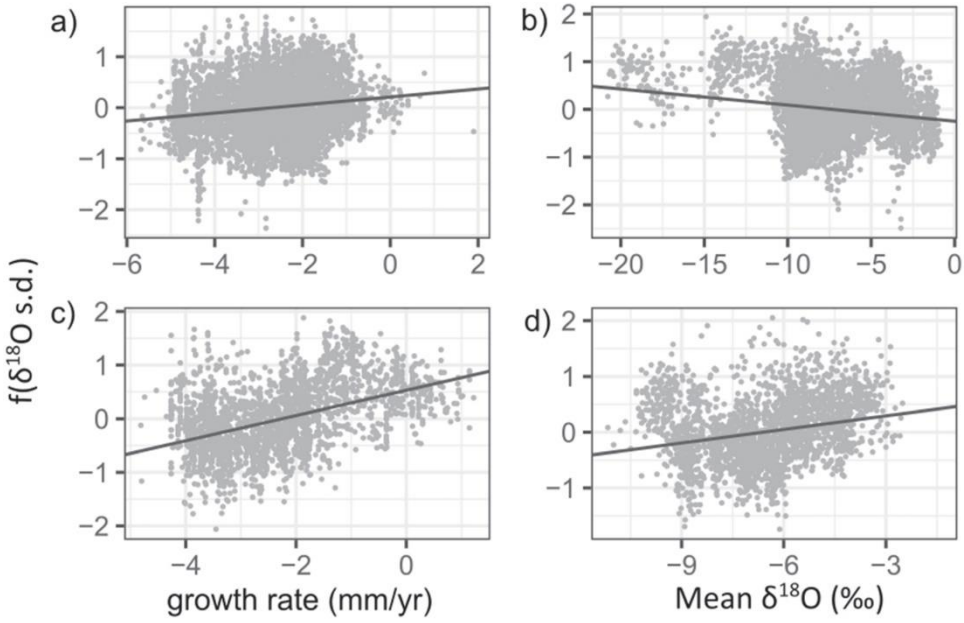

Figure 3.2 Partial residual plots from multiple linear regression analysis, showing the relationship between the standard deviation of speleothem $\delta^{18}O$ ($\delta^{18}O_{spel}$ s.d.) and two predictor variables: growth rate and mean $\delta^{18}O$ (as an indicator of mean climate). Speleothem data is separated into northern hemisphere (top panel) and southern hemisphere (bottom panel) sites. All relationships are significant with P values < 0.001.

3.5.2 Regional $\delta^{18}O_{spel}$ variability evolution

Three regions have sufficient data to reconstruct composites of $IADV_{spel}$: the Indian Monsoon (ISM), East Asian Monsoon (EAM) and South American Monsoon (SAM) (figure 3.1). The Central American and Indonesian-Australian monsoon regions are excluded because they contain too few records of a sufficient length. The regional evolution of corrected and uncorrected $IADV_{spel}$ is very similar (figure 3.3), confirming that changes in growth rate (or n-samples) and mean $\delta^{18}O_{spel}$ are not the main cause of the reconstructed changes in $\delta^{18}O_{spel}$ variability during the Holocene. Any uncertainty arising from combining records of different lengths is small, based on bootstrap resampling (figure S2). Regional composites show a significant amount of centennial-scale variability, nevertheless broad trends can be seen, with differing $IADV_{spel}$ evolution between the three regions.

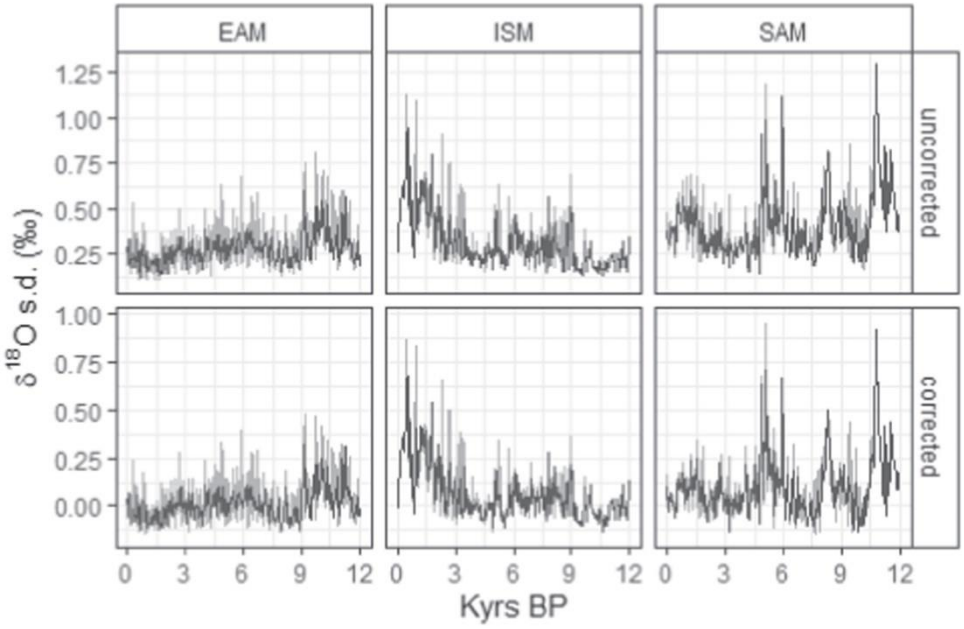

Figure 3.3 Evolution of regional speleothem $\delta^{18}O$ standard deviation ($\delta^{18}O_{spel}$ s.d.) values through the Holocene. Trends are shown with uncorrected values and values with a correction applied, using the relationships constrained in the multiple linear regression model. Regional monsoons are EAM = East Asian Monsoon, ISM = Indian Summer Monsoon, SAM = South American Monsoon. $\delta^{18}O_{spel}$ s.d. values are extracted using a 100-year windows with 50% overlap. Regional composites are expressed as a running median with confidence intervals represented by 5% and 95% quantiles.

The EAM $IADV_{spel}$ record is decomposed into four segments (figure 3.4(a), table S2): The early Holocene interval (12 to 8.9 ka) has significantly higher $IADV_{spel}$ than any subsequent period. The following interval between 8.9 and 7.1 ka has significantly lower $IADV_{spel}$ than the early Holocene interval. The mid-Holocene interval (7.1 to 2 ka) shows a significant increase in $IADV_{spel}$. The last 2 000 years has significantly lower $IADV_{spel}$ than any preceding interval. The ISM $IADV_{spel}$ record is decomposed into three segments (figure 3.4(b), table S2): the early Holocene (12 to 9 ka) has significantly lower $IADV_{spel}$ values than the other two periods. The mid-Holocene period (9 to 1.7 ka) has significantly lower $IADV_{spel}$ than the period after 1.7 ka. Breakpoint analysis of the slopes (figure S3, table S3) show stable $IADV_{spel}$ values, except between 2.05 and 0 ka when they show a significant increase over time. The SAM $IADV_{spel}$ record is decomposed into four segments (figure 3.4(c), table 3.3). The highest values of $IADV_{spel}$ occur in the mid-Holocene (6 to 4.2 ka) and the early Holocene (12 to 10.15 ka). The interval between these two peaks is characterised by $IADV_{spel}$ values that are statistically indistinguishable from the past 4 000 years. Although the recent

interval shows stable variability (figure S3, table S3), the earlier part of the SAM record shows increases in variability with rapid transitions to lower variability at 10.15, 7.9 and 4.75 ka.

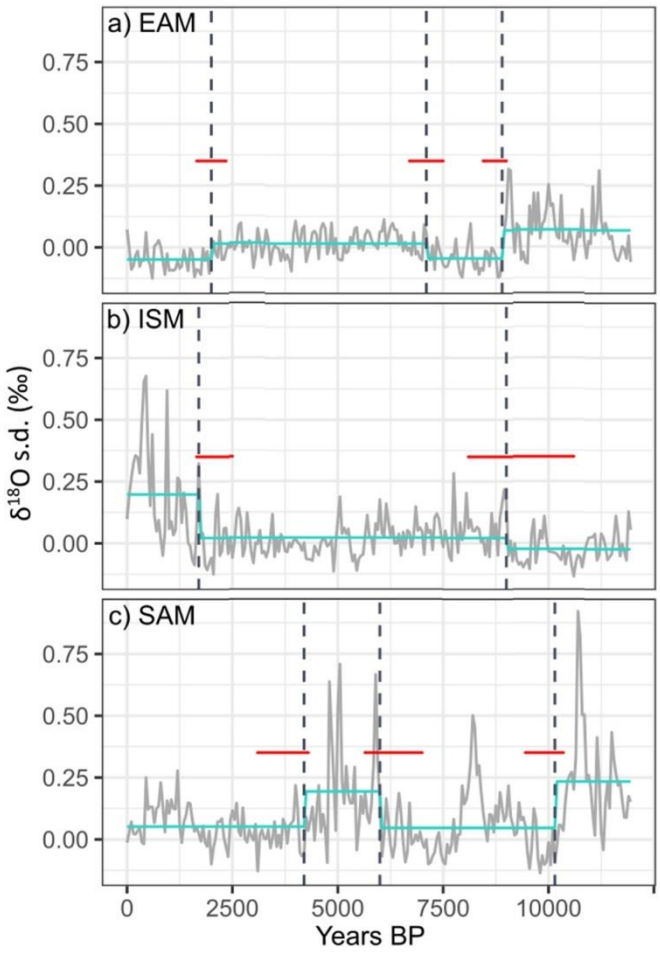

Figure 3.4 Breakpoint models ($IADV_{spel} \sim 1$) of regional $IADV_{spel}$ evolution. Breakpoints are shown with their 2.5 and 97.5% confidence intervals. Step changes in $IADV_{spel}$ are shown. Regional monsoons are EAM = East Asian Monsoon, ISM = Indian Summer Monsoon, SAM = South American Monsoon.

3.5.3 Comparison with simulated monsoon variability

There is no overall change in $IADV_{spel}$ over the last 6 000 years in the EAM (table 3.2), reproduced by the AWI and MPI simulations (table 3.2). The IPSL simulations show a small but significant increase in $IADV_{precip}$ through time. The significant increase in $IADV_{spel}$ from 6 onwards in the ISM is reproduced by all four simulations (figure 3.5, table 3.2). There is no significant change in $IADV_{precip}$ through time in the SAM in any simulation (figure 3.5, table 3.2), whereas $IADV_{spel}$ increases significantly through time. However, this is driven by the peak at 4.2 to 6 ka; a linear regression from 5 ka onwards shows no significant change.

Segments (years BP)	Mean s.d	P-values			
EAM		0-2000	2000-7100	7100-8900	8900-12000
0-2000	-0.049	/			
2000-7100	0.015	**7.88E-07**	/		
7100-8900	-0.045	7.78E-01	**6.13E-06**	/	
8900-12000	0.069	**5.20E-16**	**2.28E-06**	**3.44E-14**	/
ISM		0-1700	1700-9000	9000-12000	
0-1700	0.198	/			
1700-9000	0.022	**1.10E-17**	/		
9000-12000	-0.024	**2.21E-20**	**4.62E-03**	/	
SAM		0-4200	4200-7900	7900-10150	10150-12000
0-4200	0.051	/			
4200-6000	0.1942	**1.40E-06**	/		
6000-10150	0.046	8.20E-01	**8.83E-07**	/	
10150-12000	0.234	**1.04E-09**	1.49E-01	**8.65E-11**	/

Table 3.2 P-values for pairwise t-test, with the null hypothesis that the mean difference between two segments is zero. Segments are separated for each regional monsoon by breakpoint analysis, where the timings of abrupt changes ($IADV_{spel} \sim 1$) were determined. Regional monsoons are: EAM, East Asian monsoon, ISM, Indian summer monsoon, SAM, South American monsoon. Bold values indicate P-values <= 0.001, where the null hypothesis can be rejected.

	spel 6-0ka	IPSLCM5A-LR	IPSL-Sr	AWI-ESM2	MPI-ESM1.2
EAM	0.015	**-1.17E-05**	**-1.01E-05**	9.96E-07	-2.34E-07
ISM	**-0.061**	**-1.22E-05**	**-2.51E-05**	**-1.96E-05**	**-1.26E-05**
SAM	0.02	1.49E-07	-4.85E-06	**-6.40E-06**	-1.89E-06

Table 3.3 Linear regression relationships of regional $\delta^{18}O_{spel}$ s.d. versus time and simulated precipitation s.d. trends versus time (mm/month yr^{-1}) from the mid-Holocene (6 000 years BP) to 0 years BP. Negative relationships represent lower variability (s.d.) at the mid-Holocene than at present. Significant relationships (P <0.0001) are shown in bold. EAM = East Asian monsoon, ISM = Indian Summer monsoon, SAM = South American monsoon.

There are significant changes in simulated $IADV_{precip}$ between the segments identified from the speleothems (table 3.4). In the ISM, all four simulations show significantly higher $IADV_{precip}$ in the 1.7 to 0 ka period than the preceding period (table 3.4), consistent with the $IADV_{spel}$ record. All simulations show a significant increase in $IADV_{precip}$ values from 1.7 ka onwards, but no significant trend prior to this (Table S4). This is consistent with the marked increase in $IADV_{spel}$ during the most recent 1 700 years. In the EAM, the AWI and MPI simulations show no significant difference in either slope or magnitude between the two intervals (tables 3.4, S4), whilst the IPSL simulations show higher $IADV_{precip}$ values for the most recent 2 000 years compared to the prior period. There is no significant difference between the intervals before

and after 4.2 ka in SAM $IADV_{precip}$ and neither interval shows significant changes in IADV through time (tables 3.4, S4). This is not consistent with the speleothem record, which shows higher variability before 4.2 ka than after.

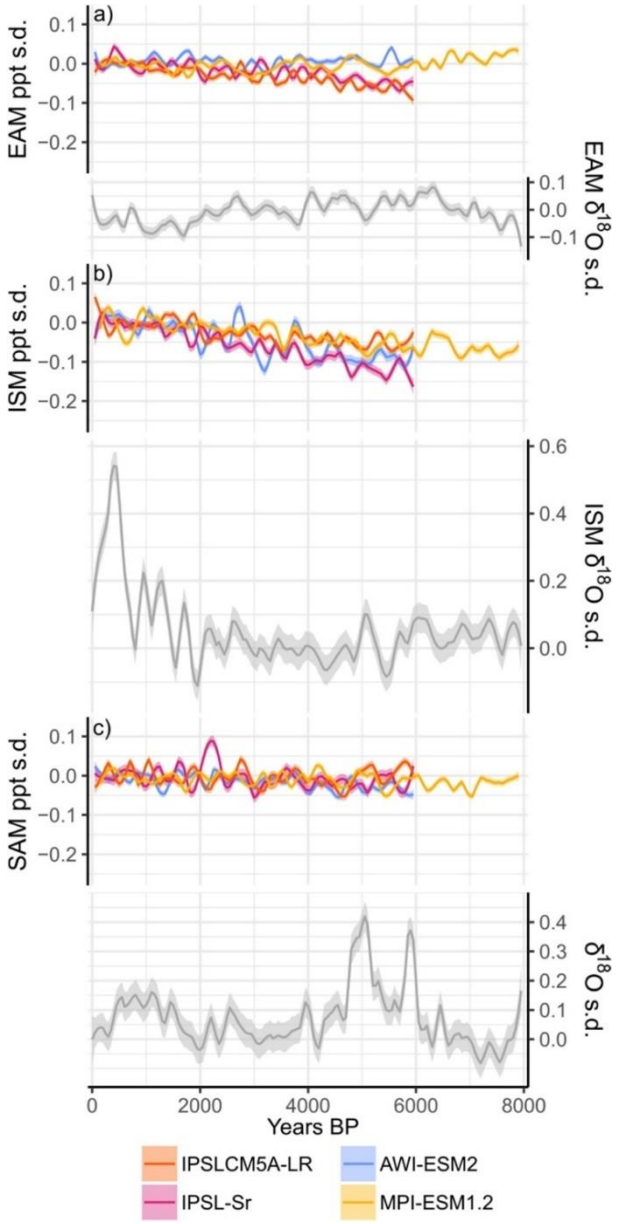

Figure 3.5 Evolution of regional speleothem $\delta^{18}O$ standard deviation ($\delta^{18}O_{spel}$ s.d.) values through the Holocene, compared to regional precipitation standard deviation simulated by four transient Earth System Models. Regional monsoons are: (a) EAM, East Asian Monsoon, (b) ISM, Indian Summer Monsoon, (c) SAM, South American Monsoon. Precipitation and $\delta^{18}O_{spel}$ s.d. values are extracted for 100-year windows with 50% overlap. Precipitation s.d. values are calculated as anomalies to the last 1 000 years. Trends are fitted with a smoothed loess fit (500-year window)

Region	Segments	IPSLCM5A-LR	IPSL-Sr	AWI-ESM2	MPI-ESM1.2
EAM	0-2000	**0.310**	**0.357**	0.274	0.271
	2000-6000	**0.274**	**0.327**	0.271	0.277
ISM	0-1700	**0.355**	**0.465**	**0.479**	**0.413**
	1700-6000	**0.313**	**0.389**	**0.418**	**0.370**
SAM	0-4200	0.442	0.448	0.277	0.305
	4200-6000	0.441	0.434	0.255	0.293

Table 3.4 Mean regional precipitation s.d. values for Holocene segments, identified in the breakpoint analysis of the speleothem trends. Bold values show segments (within an individual region and model) that are significantly different from the other (P <0.0001), determined using pairwise t-test. Regional monsoons are: EAM, East Asian monsoon, ISM, Indian summer monsoon and SAM, South American monsoon.

3.5.4 Relationship between monsoon variability and long-term evolution

Speleothems and simulations show no consistent relationship between IADV and long-term changes in monsoon precipitation. There is declining summer monsoon strength and regional precipitation from the mid-Holocene onwards in the EAM and ISM, with a slower decline from ~ 2 ka, following NH summer insolation (figure 3.6). However, IADV evolution differs between these two regions. In the EAM, the decreasing monsoon strength is mirrored by a decrease in $IADV_{spel}$ (figure 3.7(a), table 3.5). This relationship is reproduced by the AWI and MPI simulations, although only MPI shows a significant relationship between mean precipitation and IADV. In contrast, the declining summer monsoon strength from the mid-Holocene onwards is accompanied by increasing IADV amplitude in the ISM. This relationship is reproduced by all four simulations. SAM observations and simulations show a strengthening monsoon from the mid-Holocene onwards (figure 3.6(e)), mirroring SH summer insolation (figure 3.6(d)). There is no significant relationship between the long-term changes and $IADV_{spel}$ in the SAM. The lack of a relationship is reproduced by three of the four simulations (table 3.5).

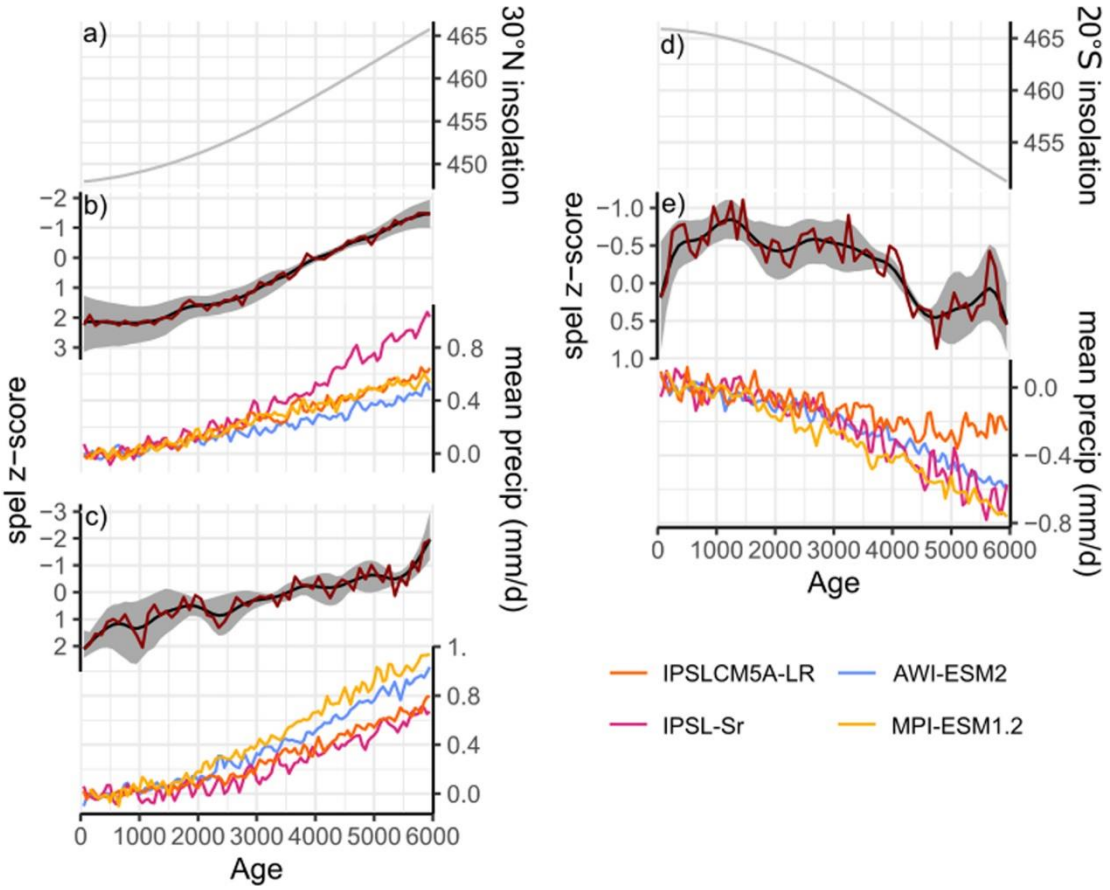

Figure 3.6 Comparison of summer insolation with long-term evolution of monsoon mean state through the Holocene. Regional speleothem $\delta^{18}O$ trends are represented by smoothed (500-year half-window loess fit) z-scores with respect to a base period of 3 000 to 5 000 years and 100 year mean z-score values (dark red line). Simulated monsoon evolution is represented by region-averaged summer precipitation (May to September for Northern Hemisphere monsoons, November to March for Southern hemisphere monsoons), as anomalies to 0–1 000 years BP. Insolation values are calculated as summer means (May to September for Northern hemisphere monsoons, November to March for Southern hemisphere monsoons). Regional monsoons are b) East Asian monsoon (EAM), c) Indian summer monsoon (ISM) and e) Southern American monsoon (SAM). Note that the y-axes for $\delta^{18}O_{spel}$ z-scores have been reversed to match the negative relationship of $\delta^{18}O_{spel}$ with monsoon strength and summer insolation.

3.6 Discussion and conclusions

We have shown that variable growth rate, sampling frequency and mean climate have a minimal impact on $\delta^{18}O_{spel}$ variability overall. Although cave monitoring studies have emphasised the influence of site-specific factors on $\delta^{18}O_{spel}$ (Luo *et al* 2014, Wu *et al* 2014, Pu *et al* 2016), these factors are unimportant when records from different speleothems and cave sites are combined. This is expected because, unlike climate signals, site-specific factors that might affect growth rate are unlikely to be consistent across sites. It might be useful to take account of the residence time of water in the epikarst directly in reconstructing $\delta^{18}O_{spel}$ variability, but this is hard to quantify under the changing climate conditions of the geological past

and may be unnecessary given that climate conditions that influence residence time may be indirectly incorporated via mean $\delta^{18}O_{spel}$. Despite the simplicity of our MLR model, the relationships between $IADV_{spel}$ and the predictor variables are physically plausible and corrected $IADV_{spel}$ evolution is similar between speleothems and sites.

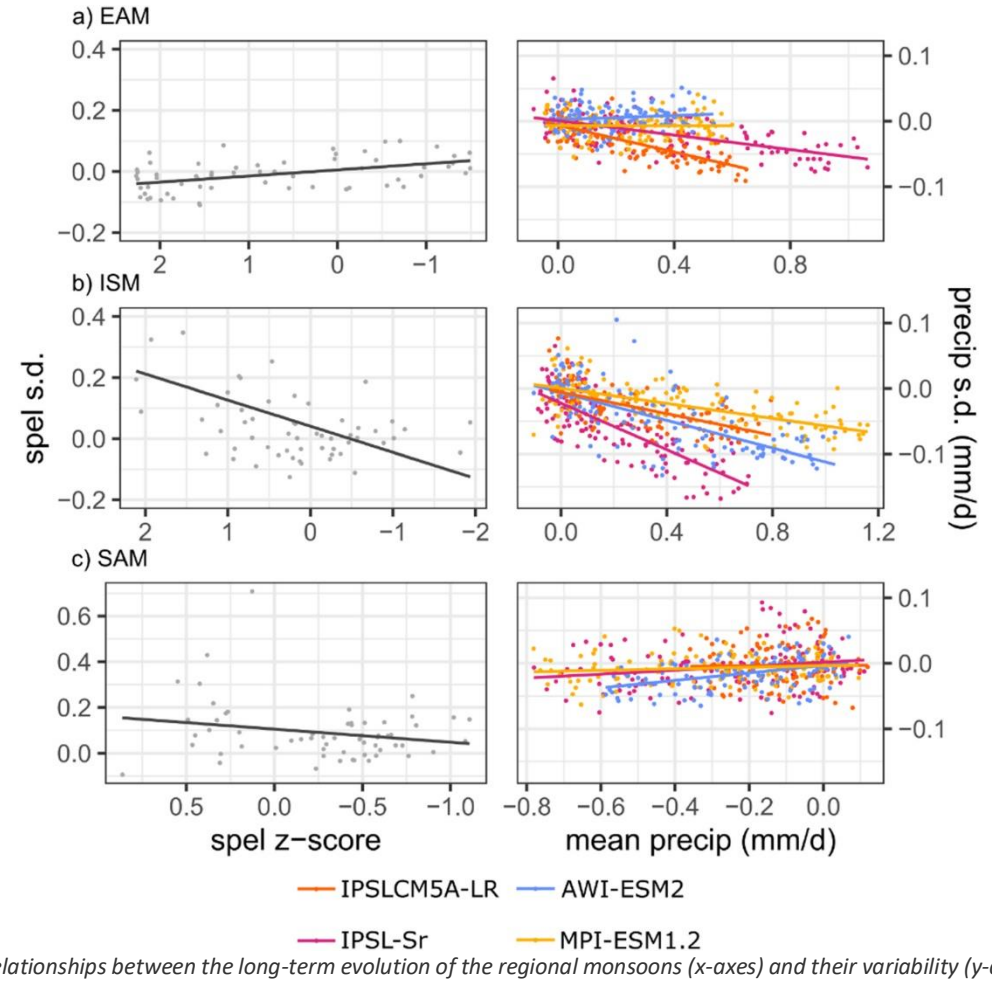

Figure 3.7 Relationships between the long-term evolution of the regional monsoons (x-axes) and their variability (y-axes). We use regional speleothem $\delta^{18}O$ z-score data and mean precipitation for 100 year sliding windows to represent long-term changes in monsoons for speleothem data and modelled precipitation respectively. Variability is represented by the standard deviation of $\delta^{18}O_{spel}$ and precipitation for 100 year sliding windows. Regions are a) EAM, East Asian monsoon, b) ISM, Indian Summer monsoon and c) SAM, South American monsoon. For each region, we show the results from four climate model simulations. Note that the axes for $\delta^{18}O_{spel}$ z-scores have been reversed to match the negative relationship between $\delta^{18}O_{spel}$ and monsoon strength.

Region	Spel	IPSLCM5A-LR	IPSL-Sr	AWI-ESM2	MPI-ESM1.2
EAM	**-0.0245**	**-0.102**	**-0.55**	0.016	**0.027**
ISM	**0.0556**	**-0.083**	**-0.178**	**-0.105**	**-0.051**
SAM	0.105	0.004	0.03	**0.059**	0.017

Table 3.5 Linear regression relationships of s.d. values ($\delta^{18}O_{spel}$ s.d., regional precipitation s.d.) versus long-term evolution ($\delta^{18}O_{spel}$ z-score, mean 100-year regional precipitation). Significant relationships (P <0.0001) are shown in bold. Regions are EAM = East Asian monsoon, ISM = Indian Summer monsoon, SAM = South American monsoon. Note that more negative $\delta^{18}O$ z-scores and higher regional precipitation values represent a stronger monsoon, therefore agreement between speleothem data and models will be opposite direction trends.

Regional $IADV_{spel}$ changes cannot be compared with the Galapagos Islands and Ecuador lake records which are interpreted as ENSO frequency rather than IADV amplitude. However, the hydrogen isotope record from El Junco (Zhang *et al* 2014), which is interpreted as a record of El Niño amplitude, shows large multi-centennial scale fluctuations in the early to mid-Holocene like those in SAM $IADV_{spel}$. Indeed, numerous records show fluctuations of a similar nature, including tropical Pacific reconstructions (Carré *et al* 2021) and the Lake Pallcacocha records (Moy *et al* 2002). The low amplitude variability recorded at El Junco during the mid-Holocene and the abrupt shift to present-day variability at ~3.5 ka is also similar to the ISM $IADV_{spel}$ record. ISM and SAM $IADV_{spel}$ shows similarities with regional reconstructions of IADV amplitude from the tropical Pacific (Carré *et al* 2021). The western Pacific shows lower IADV through the early to mid-Holocene, then an abrupt shift to modern levels at~2 ka, similar to ISM $IADV_{spel}$, whilst central Pacific records show a peak in IADV at~6 ka, similar to the peak in SAM $IADV_{spel}$ at this time. Thus, the speleothem composites provide a coherent picture of regional changes in IADV that are broadly consistent with other Holocene IADV reconstructions.

Some features of the $IADV_{spel}$ records are reproduced by the models. Simulated IADV evolution reproduces the higher IADV of the last 1 700 years compared to the mid-Holocene seen in ISM $IADV_{spel}$ and the lack of an overall long-term Holocene changes in $IADV_{spel}$ in SAM. The AWI and MPI simulations show differing trends between the ISM and EAM, as seen in the $IADV_{spel}$ records. There are, however, differences between speleothem and simulated IADV changes. The IPSL simulations show increasing IADV from the mid-Holocene to present for the EAM, whereas $IADV_{spel}$ decreases. However, these simulations

show smaller changes in IADV in the EAM than the ISM and thus there is a difference in ISM and EAM simulated IADV even though this differentiation is less marked than the opposite changes seen in regional $IADV_{spel}$. The models do not show the large multi-centennial scale fluctuations seen in SAM $IADV_{spel}$. Comparisons of simulated and reconstructed SST IADV in the tropical Pacific also show that these models exhibit less multi-centennial variability than coral and bivalve records (Carré *et al* 2021). These discrepancies between simulated and reconstructed IADV, and indeed between different models, strongly suggests that the controls on monsoon precipitation are only indirectly tied to changes in external forcing.

The long-term evolution of regional precipitation follows summer insolation (figure 3.6), but changes in regional monsoon IADV do not show a direct relationship with insolation. Long-term precipitation changes in the EAM and ISM are similar, but IADV evolution differs and even the abrupt change in IADV at $\sim$ 2 ka has a different sign in the two regions. Analyses of marine records from the Pacific (Carré *et al* 2021) suggests that there is a link between orbital forcing and ENSO variability, but ENSO is not the only cause of changes in rainfall IADV in monsoon regions.

Differences in the relationship between simulated long-term evolution and precipitation IADV between the Indian and west African monsoons have been explained as reflecting the important role of ENSO over India and Atlantic modes over west Africa for precipitation variability (Braconnot *et al* 2019a). Differences in regional $IADV_{spel}$ evolution presumably also reflects the importance of different modes for IADV in each region. In the present-day, IADV over the EAM is influenced by ENSO signals that may also be modulated by the Pacific Decadal Oscillation (Feng *et al* 2014, Zhang *et al* 2018), whilst the ISM may also be influenced by changes in the Indian ocean (Ashok *et al* 2004, Krishnaswamy *et al* 2015). SAM IADV is influenced by changes in the tropical Atlantic and Indian Ocean, as well as ENSO (Grimm and Zilli 2009, Yoon and Zeng 2010, Jimenez *et al* 2021). Furthermore, each monsoon region has a distinct relationship with ENSO, with the nature and strength of the precipitation responses depending strongly on the location of SST anomalies in the tropical Pacific (Kumar *et al* 2006, Tedeschi *et al* 2015, Zhang *et al* 2016). All these regions show a changing relationship with ENSO in recent decades (Samanta *et al* 2020, Seetha *et al* 2019, Zhang *et al* 2018, Wang *et al* 2020) and this was likely the case during the Holocene. In the ISM region, for

example, a weakening of the monsoon precipitation-ENSO relationship in recent decades has been attributed to a warming Eurasian continent (Kumar *et al* 1999), changes in tropical Atlantic SSTs (Kucharski *et al* 2007) and influence from the IOD (Ashok *et al* 2001). Analysis of ISM IADV evolution in the IPSL simulations (Crétat *et al* 2020) emphasised the interaction between ENSO, IOD and ISM precipitation variability. In the East Asian monsoon, the observed changing relationship between monsoon precipitation and ENSO over the last millennium is attributed to interaction with the PDO (Zhang *et al* 2018). Reconstructions and model simulations show changing PDO-like variability through the Holocene, including a positive phase during the early Holocene (Chen *et al* 2021). It is therefore likely that the relationship between EAM precipitation variability and Pacific SSTs was significantly different during this period. Since regional monsoon precipitation variability is influenced by numerous modes that can interact with one another, it is likely that the lack of a direct and linear relationship between monsoon IADV and insolation through the Holocene reflects the complexity of these influences on regional precipitation and the potential for changes in the importance of different climate modes through time. More emphasis should therefore be placed on modes of variability other than ENSO to improve our understanding of the evolution of monsoon climate during the Holocene, using high resolution terrestrial records and model simulations.

3.7 Acknowledgments

SP and SPH acknowledge support from the ERC-funded project GC2.0 (Global Change 2.0: Unlocking the past for a clearer future, grant number 694481). SPH and PB acknowledge support from JPI-Belmont Forum project. Palaeo-climate Constraints on Monsoon Evolution and Dynamics (PACMEDY). We acknowledge the modelling groups of Institut Pierre Simon Laplace, Alfred Wegener Institute and Max Planck Institute for producing and sharing the climate simulations. We thank Laia Comas-Bru for helpful discussion on the speleothem analysis.

3.8 Data and code availability

The code used to generate the results and figures in this study are available at http://doi.org/10.5281/zenodo.5084426 (Parker 2021). SISAL version 2 is available at http://doi.org/10.17864/1947.256. We use R for analyses (R Core Team 2019). The main packages used are tidyverse (Wickham *et al* 2021), ggplot2 (Wickham 2016), RMySQL (Ooms *et al* 2020) and ncdf4 (Pierce 2019).

3.9 Reference

Ashok K, Guan Z, Saji N H and Yamagata T 2004 Individual and combined influences of ENSO and the Indian Ocean dipole on the Indian summer monsoon *J. Clim.* **17** 3141–55

Ashok K, Guan Z and Yamagata T 2001 Impact of the Indian Ocean dipole on the relationship between the Indian monsoon rainfall and ENSO *Geophys. Res. Lett.* **28** 4499–502

Atsawawaranunt Ket al 2018 The SISAL database: A global resource to document oxygen and carbon isotope records from speleothems *Earth System Science Data*, **10** 1687–713

Bai J and Perron P 2003 Computation and analysis of multiple structural change models *Journal of Applied Econometrics* **18** 1–22

Berger A 1978 Long-Term Variations of Daily Insolation and Quaternary Climatic Changes *Journal of the Atmospheric Sciences* **35** 2362–7

Bouma M J and Kaay H J 1996 The EI Niño Southern Oscillation and the historic malaria epidemics on the Indian subcontinent and Sri Lanka: an early warning system for future epidemics? *Tropical Medicine & International Health* **1** 86–96

Braconnot P, Crétat J, Marti O, Balkanski Y, Caubel A and Cozic A 2019a Impact of multiscale variability on last 6000 years Indian and West African monsoon rain *Geophys. Res. Lett.* **46** 14021–9

Braconnot P, Zhu D, Marti O and Servonnat J 2019b Strengths and challenges for transient Mid- to Late Holocene simulations with dynamical vegetation *Climate of the Past* **15** 997–1024

Brown J R et al 2020 Comparison of past and future simulations of ENSO in CMIP5/PMIP3 and CMIP6/PMIP4 models *Climate of the Past*, **16** 1777–805

Cai Z, Tian L and Bowen G J 2017 ENSO variability reflected in precipitation oxygen isotopes across the Asian Summer Monsoon region *Earth Planet. Sci. Lett.* **475** 25–33

Carré M et al 2021 High-resolution marine data and transient simulations support orbital forcing of ENSO amplitude since the mid-Holocene *Quat. Sci. Rev.* **268** 107125

Chen C, Zhao W and Zhang X 2021 Pacific decadal oscillation-like variability at a millennial timescale during the Holocene *Global Planet. Change* **199** 103448

Chen L, Li T, Yu Y and Behera S K 2017 A possible explanation for the divergent projection of ENSO amplitude change under global warming *Clim. Dyn.* **49** 3799–811

Cheng H, Zhang H, Zhao J, Li H, Ning Y and Kathayat G 2019 Chinese stalagmite paleoclimate researches: A review and perspective *Science China Earth Sciences* **62** 1489–513

Cleveland W S and Devlin S J 1988 Locally weighted regression: An approach to regression analysis by local fitting *J. Am. Stat. Assoc.* **83** 596–610

Comas-Bru L, Atsawawaranunt K, Harrison S P and SISAL working group members 2020a SISAL (Speleothem Isotopes Synthesis and AnaLysis Working group) Database Version 2.0. University of Reading (https://doi.org/10.17864/1947.256)

Comas-Bru L, Harrison S P, Werner M, Rehfeld K, Scroxton N and Veiga-Pires C 2019 Evaluating model outputs using integrated global speleothem *Climate of the Past Discussions.* **15** 1557–79

Comas-Bru L et al 2020b SISALv2: a comprehensive speleothem isotope database with multiple age–depth models *Earth System Science Data* **12** 2579–606

Conroy J L, Overpeck J T, Cole J E, Shanahan T M and Steinitz-Kannan M 2008 Holocene changes in eastern tropical Pacific climate inferred from a Galápagos lake sediment record *Quat. Sci. Rev.* **27** 1166–80

Crétat J, Braconnot P, Terray P, Marti O and Falasca F 2020 Mid-Holocene to present-day evolution of the Indian monsoon in transient global simulations *Clim. Dyn.* **55** 2761–84

Dallmeyer A, Claussen M, Lorenz S J and Shanahan T 2020 The end of the African humid period as seen by a transient comprehensive Earth system model simulation of the last 8000 years *Climate of the Past* **16** 117–40

Dufresne J-L et al 2013 Climate change projections using the IPSL-CM5 Earth System Model: from CMIP3 to CMIP5 *Clim. Dyn,* **40** 2123–65

Duvel J P, Bellenger H, Bellon G and Remaud M 2013 An event-by-event assessment of tropical intraseasonal perturbations for general circulation models *Clim. Dyn.* **40** 857–73

Emile-Geay J and Tingley M 2016 Inferring climate variability from nonlinear proxies: Application to palaeo-ENSO studies *Climate of the Past* **12** 31–50

Feng J, Wang L and Chen W 2014 How does the East Asian summer monsoon behave in the decaying phase of El Niño during different PDO phases? *J. Clim.* **27** 2682–98

Gagnon A, Bush A and Smoyer-Tomic K 2001 Dengue epidemics and the El Niño Southern Oscillation *Climate Research* **19** 35–43

Good P, Chadwick R, Holloway C E, Kennedy J, Lowe J A, Roehrig R and Rushley S S 2021 High sensitivity of tropical precipitation to local sea surface temperature *Nature* **589** 408–14

Grimm A M and Zilli M T 2009 Interannual variability and seasonal evolution of summer monsoon rainfall in South America *J. Clim.* **22** 2257–75

Hashizume M, Chaves L F and Minakawa N 2012 Indian Ocean dipole drives malaria resurgence in East African highlands *Sci. Rep.* **2** 1–6

Hourdin F et al 2013 Impact of the LMDZ atmospheric grid configuration on the climate and sensitivity of the IPSL-CM5A coupled model. *Climate Dynamics* **40** 2167–92

Hui C and Zheng X 2018 Uncertainty in Indian Ocean Dipole response to global warming: the role of internal variability *Climate Dynamics* **51** 3597–611

Iizumi T, Luo J-J, Challinor A J, Sakurai G, Yokozawa M, Sakuma H, Brown M E and Yamagata T 2014 Impacts of El Niño Southern Oscillation on the global yields of major crops *Nat. Commun.* **5** 3712

Jimenez J C, Marengo J A, Alves L M, Sulca J C, Takahashi K, Ferrett S and Collins M 2021 The role of ENSO flavours and TNA on recent droughts over Amazon forests and the Northeast Brazil region Int. *J. Climatol.* **41** 3761–80

Kane R P 1999 Some characteristics and precipitation effects of the El Niño of 1997–1998 *J. Atmos. Sol. Terr. Phys.* **61** 1325–46

Kathayat G, Sinha A, Tanoue M, Yoshimura K, Li H, Zhang H and Cheng H 2021 Interannual oxygen isotope variability in Indian summer monsoon precipitation reflects changes in moisture sources *Communications Earth & Environment* **2** 96

Kiefer J and Karamperidou C 2019 High-resolution modeling of ENSO-induced precipitation in the tropical Andes: Implications for proxy interpretation *Paleoceanography and Paleoclimatology* **34** 217–36

Kirono D G C, Tapper N J and McBride J L 1999 Documenting Indonesian rainfall in the 1997/1998 El Niño event *Physical Geography* **20** 422–35

Krishnan R and Sugi M 2003 Pacific decadal oscillation and variability of the Indian summer monsoon rainfall *Clim. Dyn.* **21** 233–42

Krishnaswamy J, Vaidyanathan S, Rajagopalan B, Bonell M, Sankaran M, Bhalla R S and Badiger S 2015 Non-stationary and non-linear influence of ENSO and Indian Ocean Dipole on the variability of Indian monsoon rainfall and extreme rain events *Clim. Dyn.* **45** 175–84

Kucharski F, Bracco A, Yoo J H and Molteni F 2007 Low-frequency variability of the Indian monsoon–ENSO relationship and the tropical Atlantic: The 'weakening' of the 1980s and 1990s *J. Clim.* **20** 4255–66

Kumar K K, Rajagopalan B, Hoerling M, Bates G and Cane M 2006 Unraveling the mystery of Indian monsoon failure during El Niño *Science* **314** 115–9

Kumar K K, Rajagopalan B and Cane M A 1999 On the weakening relationship between the Indian monsoon and ENSO *Science* **284** 2156–9

Lachniet M S 2009 Climatic and environmental controls on speleothem oxygen-isotope values *Quat. Sci. Rev.* **28** 412–32

Luo W, Wang S, Zeng G, Zhu X and Liu W 2014 Daily response of drip water isotopes to precipitation in Liangfeng Cave, Guizhou Province, SW China *Quat. Int*. **349** 153–8

Mauritsen T et al 2019 Developments in the MPI-M Earth System Model version 1.2 (MPI-ESM1.2) and Its Response to Increasing CO2 *Journal of Advances in Modeling Earth Systems* **11** 998–1038

McPhaden M J, Zebiak S E and Glantz M H 2006 ENSO as an integrating concept in earth science *Science* **314** 1740–5

Messié M and Chavez F 2011 Global modes of sea surface temperature variability in relation to regional climate indices *J. Clim.* **24** 4314–31

Moy C M, Seltzer G O, Rodbell D T and Anderson D M 2002 Variability of El Niño/Southern Oscillation activity at millennial timescales during the Holocene epoch *Nature* **420** 162–5

Ng B, Cai W, Cowan T and Bi D 2018 Influence of internal climate variability on Indian Ocean Dipole properties *Sci. Rep.* **8** 1–8

Ooms J, James D, DebRoy S, Wickham H and Horner J 2020 RMySQL: Database Interface and 'MySQL' Driver for R. R package version 0.10.22.https://CRAN.R-project.org/package=RMySQL

Parker S E 2021 Zenodo Code for'Speleothem records of monsoon interannual-interdecadal variability through the Holocene [Accessed 28 November 2021] (https://doi.org/10.5281/zenodo.5084426)

Parker S E, Harrison S P, Comas-Bru L, Kaushal N, LeGrande A N and Werner M 2021 A data–model approach to interpreting speleothem oxygen isotope records from monsoon regions *Climate of the Past* **17** 1119–38

Phillips T, Nerem R S, Fox-Kemper B, Famiglietti J S and Rajagopalan B 2012 The influence of ENSO on global terrestrial water storage using GRACE *Geophys. Res. Lett.* **39**

Pierce D 2019 ncdf4: Interface to Unidata netCDF (Version 4 or Earlier) Format Data Files. R package version 1.18.https://CRAN.R-project. org/package=ncdf4

Pu J, Wang A, Shen L, Yin J, Yuan D and Zhao H 2016 Factors controlling the growth rate, carbon and oxygen isotope variation in modern calcite precipitation in a subtropical cave, Southwest China *J. Asian Earth Sci.* **119** 167–78

Ray D K, Gerber J S, MacDonald G K and West P C 2015 Climate variation explains a third of global crop yield variability *Nat. Commun*. **6** 5989

Riedinger M A, Steinitz-Kannan M, Last W M and Brenner M 2002 A∼6100 14C yr record of El Niño activity from the Galápagos Islands *J. Paleolimnol.* **27** 1–7

Rodbell D T 1999 An 15,000-Year record of El Niño-driven alluviation in southwestern Ecuador Science 283 516–20 Saji N and Yamagata T 2003 Possible impacts of Indian Ocean dipole mode events on global climate *Climate Research* **25** 151–69

Samanta D, Rajagopalan B, Karnauskas K B, Zhang L and Goodkin N F 2020 La Niña's Diminishing Fingerprint on the Central Indian Summer Monsoon *Geophysical Research Letters* **47** e2019GL086237

Schneider T, Hampel H, Mosquera P V, Tylmann W and Grosjean M 2018 Paleo-ENSO revisited: Ecuadorian Lake Pallcacocha does not reveal a conclusive El Niño signal *Global Planet. Change* **168** 54–66

Seetha C J, Varikoden H, Babu C A and Kuttippurath J 2019 Significant changes in the ENSO-monsoon relationship and associated circulation features on multidecadal timescale *Climate Dynamics* **54** 1491–506

Sidorenko D et al 2019 Evaluation of FESOM2.0 Coupled to ECHAM6.3: Preindustrial and HighResMIP Simulations *Journal of Advances in Modeling Earth Systems* **11** 3794–815

Sinha A, Kathayat G, Cheng H, Breitenbach S F M, Berkelhammer M, Mudelsee M, Biswas J and Edwards R L 2015 Trends and oscillations in the Indian summer monsoon rainfall over the last two millennia *Nat. Commun.* **6** 6309

Stevenson S L 2012 Significant changes to ENSO strength and impacts in the twenty-first century: Results from CMIP5 *Geophys. Res. Lett.* **39** 17

R Core Team 2019 R: A Language and Environment for Statistical Computing. (Vienna, Austria) Tian B and Dong X 2020 The double-ITCZ Bias in CMIP3, CMIP5, and CMIP6 models based on annual mean precipitation *Geophys. Res. Lett.* **47** e2020GL087232

Tedeschi R G, Grimm A M and Cavalcanti I F 2015 Influence of Central and East ENSO on extreme events of precipitation in South America during austral spring and summer *Int. J. Climatol*. **35** 2045–64

Thompson D M et al 2017 Tropical Pacific climate variability over the last 6000 years as recorded in Bainbridge Crater Lake, Galápagos *Paleoceanography* **32** 903–22 Ummenhofer C C, Gupta A S, Li Y, Taschetto A S and England M H 2011 Multi-decadal modulation of the El Nino–Indian monsoon relationship by Indian Ocean variability *Environ. Res. Lett.* **6** 034006

Vuille M, Bradley R S, Werner M, Healy R and Keimig F 2003 Modeling δ 18O in precipitation over the tropical Americas: 1. Interannual variability and climatic controls *J. Geophys. Res. D: Atmos.* **108** D6

Wang B and Ding Q 2008 Global monsoon: Dominant mode of annual variation in the tropics *Dyn. Atmos. Oceans* **44** 165–83

Wang B, Liu J, Kim H J, Webster P J and Yim S Y 2012 Recent change of the global monsoon precipitation (1979-2008) *Clim. Dyn.* **39** 1123–35

Wang B, Luo X and Liu J 2020 How robust is the Asian Precipitation-ENSO relationship during the industrial warming period (1901-2017)? *J. Clim.* **33** 2779–92

Wang B et al 2021 Monsoons climate change assessment Bull. Am. *Meteorol. Soc.* **102** E1–19

Wang P X, Wang B, Cheng H, Fasullo J, Guo Z T, Kiefer T and Liu Z Y 2014 The global monsoon across timescales: coherent variability of regional monsoons *Climate of the Past* **10** 2007–52

Wickham H 2016 ggplot2: Elegant Graphics for Data Analysis(New York, NY: Springer) 978-3-319-24277-4

Wickham H, François R, Henry L and Müller K 2021 dplyr: A Grammar of Data Manipulation. R package version 1.0.5https://CRAN.Rproject.org/package=dplyr

Wu X, Zhu X, Pan M and Zhang M 2014 Seasonal variability of oxygen and hydrogen stable isotopes in precipitation and cave drip water at Guilin, southwest China *Environmental Earth Sciences* **72** 3183–91

Yang H, Johnson K R, Griffiths M L and Yoshimura K 2016 Interannual controls on oxygen isotope variability in Asian monsoon precipitation and implications for paleoclimate reconstructions *J. Geophys. Res.* **14** 8410-8428

Yim S Y, Wang B, Liu J andWu Z 2014 A comparison of regional monsoon variability using monsoon indices Clim. Dyn. 43 1423–37 Yoon J-H and Zeng N 2010 An Atlantic influence on Amazon rainfall *Clim. Dyn.* **34** 249–64

Yoon J and Yeh S-W 2010 Influence of the Pacific decadal oscillation on the relationship between El Niño and the northeast Asian summer monsoon *J. Clim.* **23** 4525–37

Zeileis A, Kleiber C, Kraemer W and Hornik K 2003 Testing and dating of structural changes in Ppractice Comput. *Stat. Data Anal.* **44** 109–23

Zeileis A, Leisch F, Hornik K and Christian K 2002 strucchange: An R package for testing for structural change in linear regression models *Journal of Statistical Software* **7** 1–38

Zhang H et al 2021 A data-model comparison pinpoints Holocene spatiotemporal pattern of East Asian summer monsoon *Quat. Sci. Rev.* **261** 106911

Zhang X, Wu M, Liu Y, Hao Z and Zheng J 2018 The relationship between the East Asian Summer Monsoon and El Niño-Southern Oscillation revealed by reconstructions and a control simulation for millennium *Quat. Int.* **493** 106–13

Zhang Q, Wang Y, Singh V P, Gu X, Kong D and Xiao M 2016 Impacts of ENSO and ENSO Modoki + A regimes on seasonal precipitation variations and possible underlying causes in the Huai River basin, China *J. Hydrol.* **533** 308–19

Zhang Z, Leduc G and Sachs J P 2014 El Niño evolution during the Holocene revealed by a biomarker rain gauge in the Galápagos Islands *Earth Planet. Sci. Lett.* **404** 420–34

Zheng X-T, Xie S-P, Du Y, Liu L, Huang G and Liu Q 2013 Indian Ocean dipole response to global warming in the CMIP5 multimodel ensemble *J. Clim.* **26** 606

3.10 Supplement

Description of climate model simulations

IPSL simulations

The first IPSL simulation was run using the IPSLCM5A-LR version (Dufresne et al., 2013). The simulation starts from the final year of a MH time-slice experiment and runs from 6000 to 0 years BP. The atmospheric component has a resolution of 3.75° longitude and 1.875° latitude. The carbon cycle is fully interactive over the land and ocean, but vegetation is prescribed and does not change through time. Greenhouse gases (GHGs) are prescribed annually using ice-core data (Otto-Bliesner et al., 2017). The second IPSL simulation was run using a modified version of IPSLCM5A-MR (Dufresne et al., 2013; Braconnot et al., 2019), which includes a dynamic vegetation module, 11-layer soil hydrology and a prognostic snow model. The model has a grid resolution of 2.5° longitude and 1.125° latitude. The simulation was run from 6,000 to 0 years BP. GHGs were prescribed annually as in the first IPSL simulation.

AWI simulation

The AWI simulation was run using the AWI Earth System model version 2 (AWI-ESM2), with a horizontal resolution of 1.875° longitude and ~1.86° latitude at the equator (Sidorenko et al., 2019). The simulation was run from 6,000 to 0 years BP, starting from a 1,000-year MH spin-up where GHGs and orbital parameters were specified following the PMIP4 protocol for MH time slice experiments (Otto-Bleisner et al., 2017). GHGs during the transient simulation were prescribed using ice core record values from Köhler et al. (2017).

MPI simulation

The MPI simulation was run using the MPI Earth System model version 1.2 (MPI-ESM1.2: Mauritsen et al., 2019), which includes an atmospheric model (ECHAM6), ocean module (MPI-OM), sea-ice and biogeochemistry model (HAMOCC) and land-surface model (JSBACH) . The model has a spectral resolution of T63, equivalent to approximately 200 km on a Gaussian grid. Vegetation is fully interactive and GHGs are prescribed using updated ice core data (Dallmeyer et al., 2020). The simulation was run from 7950 to 100 years BP, starting from a 3000-year spin-up using boundary conditions fixed at 7950 years BP.

Fig. S1: Multiple linear regression of $\delta^{18}O$ standard deviation (s.d.) versus n-samples (number of $\delta^{18}O$ samples) and mean $\delta^{18}O$. All variables are extracted for 100-year windows with 50% overlap. $\delta^{18}O$ s.d. and n-samples were log transformed to ensure normal distribution. Speleothem data is separated into northern hemisphere (top panel) and southern hemisphere (bottom panel) sites. The northern hemisphere model has an R^2 value of 0.04 and the southern hemisphere model has an R^2 value of 0.18

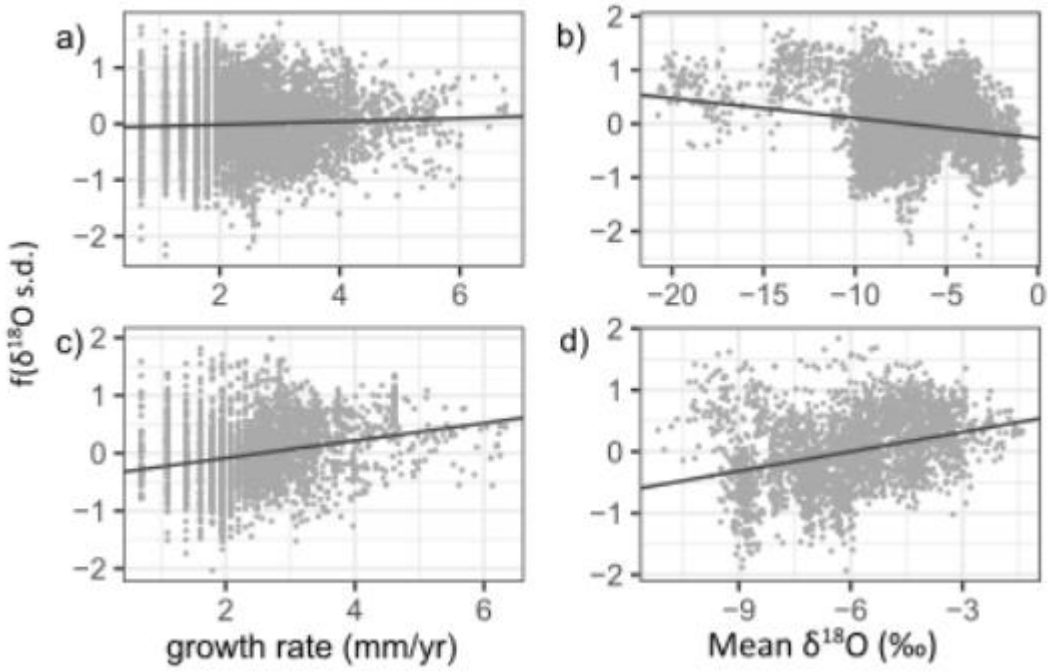

Fig. S2: Evolution of regional speleothem $\delta^{18}O$ standard deviation ($\delta^{18}O_{spel}$ s.d.) values through the Holocene. Trends are shown with uncorrected values and values with a correction applied, using the relationships constrained in the multiple linear regression model. Regional monsoons are EAM = East Asian Monsoon, ISM = Indian Summer Monsoon, SAM = South American Monsoon. $\delta^{18}O_{spel}$ s.d. values are extracted using a 100-year windows with 50% overlap. Confidence intervals (10%, 90%) are obtained by bootstrapping by record..

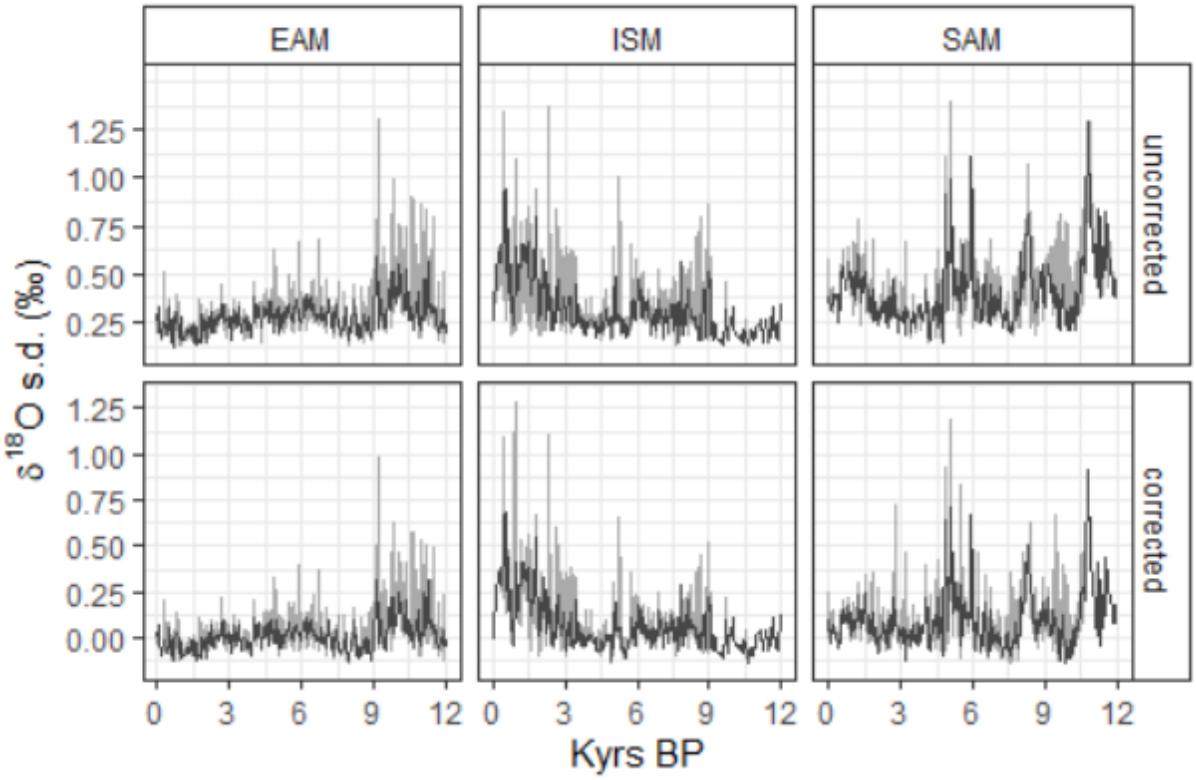

Fig. S3: Breakpoint models (IAV_{spel} ~ Age) of regional IAV_{spel} evolution. Breakpoints are shown with their 2.5 and 97.5% confidence intervals. Step changes in IAV_{spel} are shown. Regional monsoons are EAM = East Asian Monsoon, ISM = Indian Summer Monsoon, SAM = South American Monsoon.

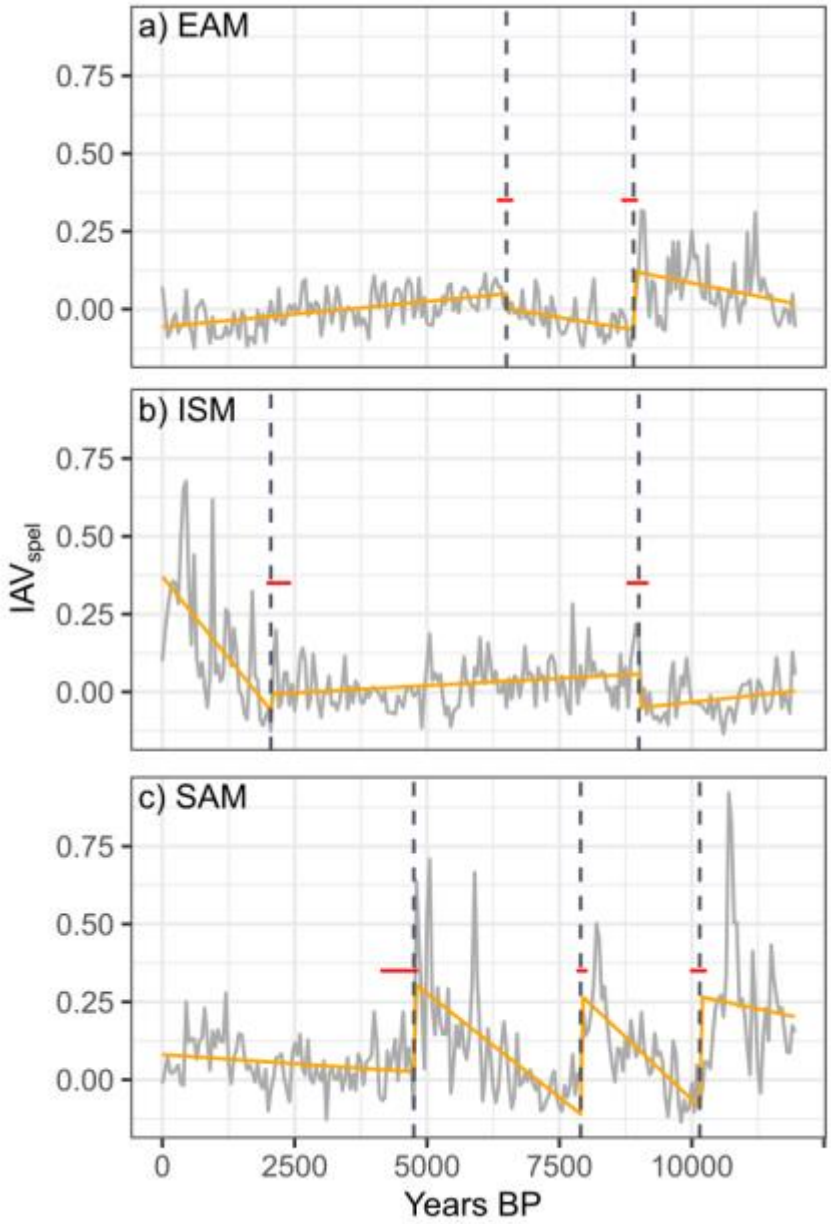

Fig. S4: Simulated mean summer precipitation (mm/d) for 1800-1850 (pre-industrial) for each individual model simulation. Summer is defined as May to September for the northern hemisphere and November to March for the southern hemisphere.

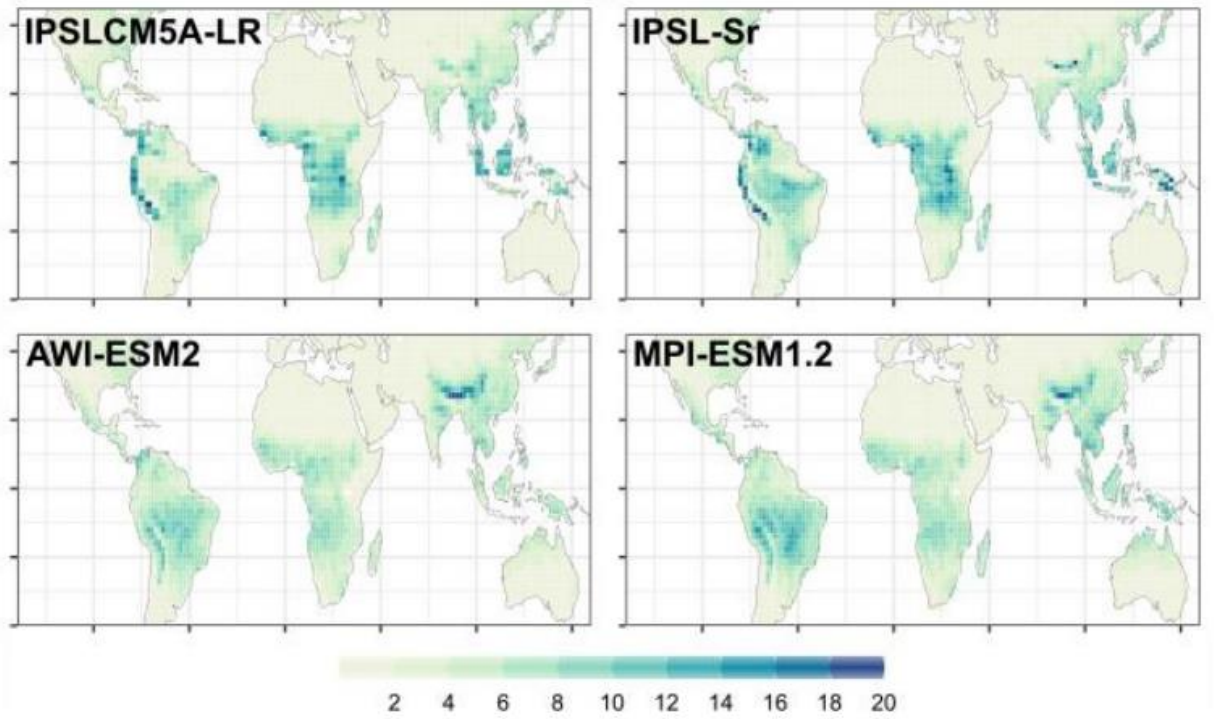

Fig. S5: Summer precipitation variability through time ($IADV_{precip}$ kyr^{-1}) for each grid in the four model simulations. Positive values represent decreasing $IADV_{precip}$ (calculated as the standard deviation of summer precipitation for 100-year bins) from the mid-Holocene to present, whilst negative values represent decreasing $IADV_{precip}$. Summer is defined as May to September for the Northern Hemisphere and November to March for the Southern Hemisphere.

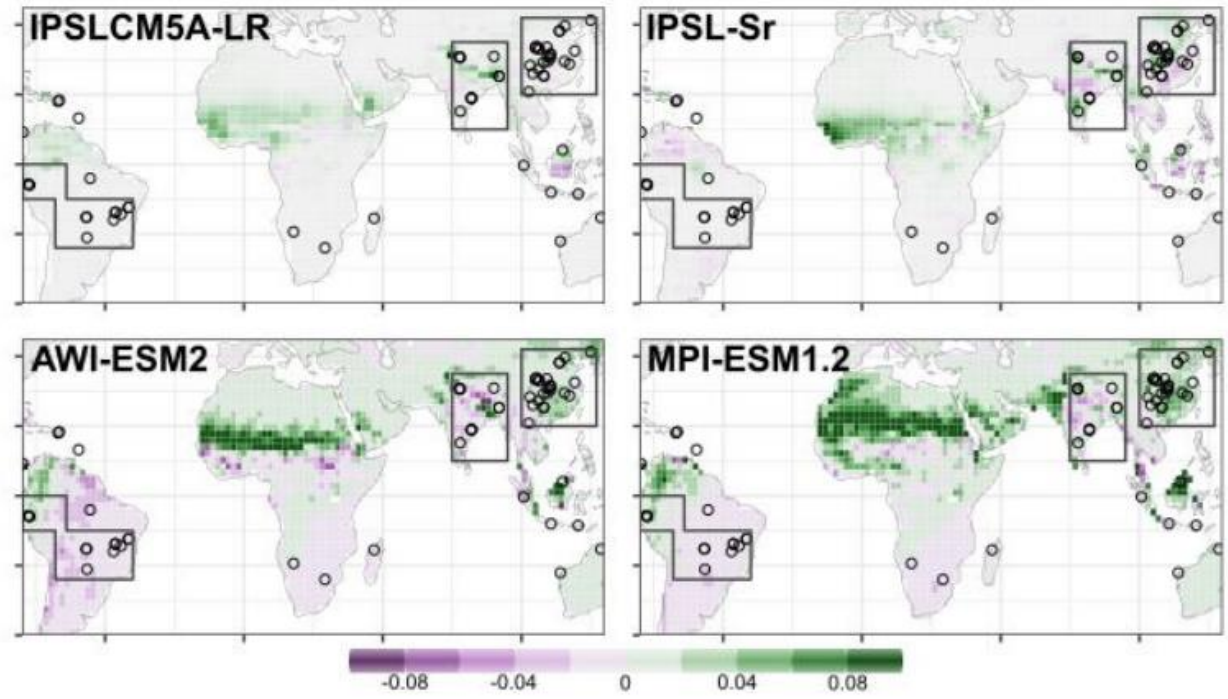

Table S1: Results of the multiple linear regression analysis of $\delta^{18}O$ standard deviation versus n-samples and mean $\delta^{18}O$. Significant relationships (P <0.001) are shown in bold.

	NH	SH
N-samples	**0.03**	**0.15**
Mean $\delta^{18}O$	**-0.04**	**0.11**

Table S2: Age of breakpoints at which $\delta^{18}O_{spel}$ s.d. values ($\delta^{18}O_{spel}$ s.d. ~ 1, i.e. changes in intercept) and trend through time ($\delta^{18}O_{spel}$ s.d. ~ age) change significantly, detected using breakpoint analysis. Confidence intervals (CI) are also shown. Regional monsoons are: EAM, East Asian monsoon, ISM, Indian summer monsoon and SAM, South American monsoon.

Region	Model	Breakpoint (years BP)	2.5% CI	97.5% CI
EAM	s.d. ~ 1	2000	1650	2350
		7100	6700	7500
		8900	8450	9000
	s.d ~ age	6500	6350	6600
		8900	8700	8950
ISM	s.d. ~ 1	1700	1650	2500
		9000	8100	10600
	sd ~ age	2050	2000	2400
		9000	8800	9150
SAM	s.d. ~ 1	4200	3100	4300
		6000	5650	7000
		10150	9450	10350
	sd ~ age	4750	4150	4800
		7900	7850	8000
		10150	10000	10250

Table S3: Relationships between $\delta^{18}O$ s.d. and time for segments. Segments are separated for each regional monsoon by breakpoint analysis (s.d. ~ age). Regional monsoons are: EAM, East Asian monsoon, ISM, Indian summer monsoon, SAM, South American monsoon. Bold values indicate significant relationships (P-values <= 0.001).

Region	Segment	IAVspel ~ age
EAM	0-6500	**1.63E-05**
	6500-8900	-2.81E-05
	8900-12000	-3.38E-05
ISM	0-2050	**-2.09E-04**
	2050-9000	9.37E-06
	9000-12000	1.83E-05
SAM	0-4750	-1.17E-05
	4750-7900	**-1.34E-04**
	7900-10150	**-1.60E-04**
	10150-12000	-3.62E-05

Table S4: Relationships between regional precipitation s.d. and time for segments, where segments are defined using breakpoints identified in the IAV_{spel} trends. Regional monsoons are: EAM, East Asian monsoon, ISM, Indian summer monsoon, SAM, South American monsoon. Bold values indicate significant relationships (P-values <= 0.001).

Region	Segments	IPSLCM5A-LR	IPSL-Sr	AWI-ESM2	MPI-ESM1.2
EAM	0-1700	**-1.16E-05**	**-1.02E-05**	3.75E-06	5.62E-06
	1700-6000	-1.10E-05	-7.11E-06	1.09E-05	-1.13E-05
ISM	0-2000	**-9.47E-06**	**-2.49E-05**	**-1.87E-05**	**-1.13E-05**
	2000-6000	-4.25E-06	-1.50E-05	-1.01E-05	-6.65E-06
SAM	0-4200	3.43E-05	-1.58E-06	-2.35E-06	-4.25E-06
	4200-6000	-1.83E-06	-5.28E-06	-1.12E-07	-4.65E-06

References:

Braconnot, P. *et al.* (2019) 'Strengths and challenges for transient Mid- to Late Holocene simulations with dynamical vegetation', *Climate of the Past*, 15(3), pp. 997–1024. doi: 10.5194/cp-15-997-2019.

Dallmeyer, A. *et al.* (2020) 'The end of the African humid period as seen by a transient comprehensive Earth system model simulation of the last 8000 years', *Climate of the Past*, 16(1), pp. 117–140. doi: 10.5194/cp-16-117-2020.

Dufresne, J.-L. *et al.* (2013) 'Climate change projections using the IPSL-CM5 Earth System Model: from CMIP3 to CMIP5', *Climate Dynamics*, 40(9–10), pp. 2123–2165. doi: 10.1007/s00382-012-1636-1.

Köhler, P. *et al.* (2017) 'A 156 kyr smoothed history of the atmospheric greenhouse gases CO_2, CH_4, and N_2O and their radiative forcing', *Earth System Science Data*, 9(1), pp. 363–387. doi: 10.5194/essd-9-363-2017.

Mauritsen, T. *et al.* (2019) 'Developments in the MPI-M Earth System Model version 1.2 (MPI-ESM1.2) and Its Response to Increasing CO 2', *Journal of Advances in Modeling Earth Systems*, 11(4), pp. 998–1038. doi: 10.1029/2018MS001400.

Otto-Bliesner, B. L. *et al.* (2017) 'The PMIP4 contribution to CMIP6 – Part 2: Two interglacials, scientific objective and experimental design for Holocene and Last Interglacial simulations', *Geoscientific Model Development*, 10(11), pp. 3979–4003. doi: 10.5194/gmd-10-3979-2017.

Sidorenko, D. *et al.* (2019) 'Evaluation of FESOM2.0 Coupled to ECHAM6.3: Preindustrial and HighResMIP Simulations', *Journal of Advances in Modeling Earth Systems*, 11(11), pp. 3794–3815. doi: 10.1029/2019MS001696.

4 The timing, duration and magnitude of the 8.2 ka event in global speleothem records

4.1 Preface

The following chapter is a paper published in Scientific Reports. It has been written and referenced in the style guidelines of this journal. The authors are Sarah E. Parker and Sandy P. Harrison. The study was designed by SEP and SPH. SEP ran the analyses. The paper was written by SEP and SPH. Estimated contributions are SEP: 80 % and SPH: 20 %.

This study objectively identifies globally significant abrupt events in global speleothem records through the Holocene epoch. It demonstrates that the 8.2 ka event is the largest and most significant abrupt event of the Holocene. The speleothem 8.2 ka anomalies show a global monsoon response (antiphase interhemispheric signals in the tropics). The timing and duration of the event registered in global speleothem records are very similar, demonstrating a rapid transmission of climate signals from the North Atlantic across the tropics.

4.2 Abstract

Abrupt events are a feature of many palaeoclimate records during the Holocene. The best example is the 8.2 ka event, which was triggered by a release of meltwater into the Labrador Sea and resulted in a weakening of poleward heat transport in the North Atlantic. We use an objective method to identify rapid climate events in globally distributed speleothem oxygen isotope records during the Holocene. We show that the 8.2 ka event can be identified in >70% of the speleothem records and is the most coherent signal of abrupt climate change during the last 12,000 years. The isotopic changes during the event are regionally homogenous: positive oxygen isotope anomalies are observed across Asia and negative anomalies are seen across Europe, the Mediterranean, South America and southern Africa. The magnitude of the isotopic excursions in Europe and Asia are statistically indistinguishable. There is no significant difference in the duration and timing of the 8.2

ka event between regions, or between the speleothem records and Greenland ice core records. Our study supports a rapid and global climate response to the 8.2 ka freshwater pulse into the North Atlantic, likely transmitted globally via atmospheric teleconnections.

4.3 Introduction

The Holocene epoch (11,700 years BP to present) has been punctuated by several large-scale and rapid changes in the climate system [1–3], termed abrupt events. Numerous abrupt events have been identified, although many have not been studied extensively or have only been identified in a limited number of regions, and the causes of the events are not always clear. Two events that have been studied and examined more extensively are the 4.2 and 8.2 ka (ka; thousand years ago) events. The 4.2 ka event is a 300-year megadrought identified predominantly in Eurasian and Middle Eastern palaeoclimate records [4–6], although the exact mechanism is still debated [7,8].

The largest and most-significant abrupt event of the last 12,000 years is the 8.2 ka event [9,10]. During this event, an influx of freshwater into the Labrador Sea from a retreating Laurentide ice slowed down the Atlantic Meridional Overturning Circulation (AMOC), reducing northwards meridional heat transport [11,12]. This triggered a large drop in temperature across the North Atlantic region; Greenland ice cores show >2°C cooling over an interval of 165 years [13]. The 8.2 ka event has been identified in a large number of palaeoclimate records. A global compilation of reconstructions using marine, lake, ice and peat cores and speleothem records by Morrill et al. (2013) [14] showed widespread cooling over Europe of ~1 to 1.5°C. Drier conditions were shown in the northern hemisphere tropics, with wetter conditions in the southern hemisphere tropics. While this compilation has been used to evaluate climate model simulations of the 8.2 ka event [15–17], only 13% of the records provide quantitative estimates of temperature and precipitation and most of the information consists of qualitative indications of the direction of the change in climate. Furthermore, most of the records included in this compilation were of insufficient temporal resolution to estimate the duration of the event, and the exact timing of the event was also not examined. Questions therefore remain about the global signature and nature of this event.

Speleothem oxygen isotope ($\delta^{18}O$) records are ideal for reconstructing global-scale patterns of abrupt climate events, such as the 8.2 ka event, because they often have sub-annual to decadal temporal resolution and well-constrained chronologies. Speleothem $\delta^{18}O$ can be influenced by multiple climate factors, including regional precipitation, atmospheric circulation and temperature [18–20], which can make their climate interpretation challenging. Nevertheless, the 8.2 ka event has been identified in numerous individual speleothem records around the world [21–24] and there are now sufficient numbers of published speleothem records, especially compared to the status at the time of the Morrill et al. (2013) 8.2 ka synthesis [14], to facilitate a global-scale analysis [25].

Here, we used the Speleothem Isotope Synthesis and AnaLysis (SISAL) database [26,27] to identify potential abrupt climate events in the Holocene, by using breakpoint analysis to detect shifts in $\delta^{18}O$ values objectively and determining whether these excursions were above the inherent variability of climate and spatially coherent. We then focus on the nature of the 8.2 ka event, and specifically the timing, duration and magnitude of the anomalies registered in each speleothem record at this time. We compare our speleothem synthesis to other lines of evidence, including Greenland ice core data, speleothem trace element records and the global synthesis by Morrill et al. [14]. Our new global synthesis allows us to address the following questions: 1) Is the 8.2 ka event a significant and prominent feature of the Holocene epoch? 2) How rapidly was the event transmitted to regions distant from the North Atlantic? 3) What is the speleothem $\delta^{18}O$ spatial fingerprint of this event, and what does it tell us about the climate response?

4.4 Results

We examined the presence and timing of significant abrupt climate events through the Holocene using 275 globally distributed speleothem records (Fig. 4.1). There are several intervals where the proportion of records showing an abrupt isotope excursion exceeds the randomly generated noise (Fig. 4.2), including at 0.6–0.9, 1.5–1.8, 3.6–3.9, 6.6–6.9, 8.1–8.4, 10.2–10.5 and 11.1–11.4 ka. The early Holocene peaks coincide with Bond event 7 (10.3 ka) and 8 (11.1 ka, or the pre-Boreal

oscillation)[27,28]. However, the isotope excursions associated with each of these two peaks show little coherency in their spatial pattern, timing and duration (Fig. S1). The excursions identified between 8 ka and present do not coincide with any previously identified abrupt climate events. Although the interval around 4.2 ka is often identified as a period of rapid climate change[4,5,6], it is not detected by the speleothem records. The most prominent period of abrupt climate change in the Holocene is at ~ 8.2 ka, where 72% of the records show an abrupt isotope excursion.

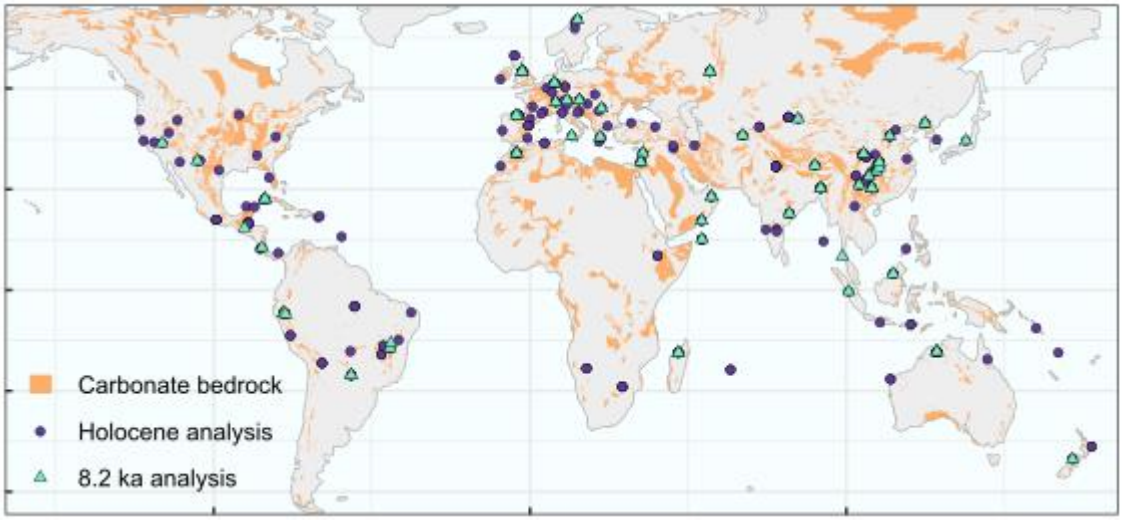

Figure 4.1 Spatial distribution of speleothem $\delta^{18}O$ records used in this study. Purple dots show sites that were only used to detect globally significant abrupt events through the Holocene, and blue dots show those used both in the Holocene analysis and to examine the 8.2 ka event. Carbonate bedrock distribution is from the WOKAM (WOrld Karst Aquifer Mapping) project (Goldschneider et al., 2020).

We examined the isotope excursion at 8.2 ka using 73 speleothem $\delta^{18}O$ records (Fig. 4.1) of sufficiently high temporal resolution and length (see "Methods" section). Most records show a remarkably consistent timing (Fig. 4.3) of the event, allowing for age uncertainties. The global speleothem records show the event starting at 8.22 ± 0.012 ka and ending at 8.06 ± 0.014 ka (Table 4.1). Furthermore, the timing of the global $\delta^{18}O$ excursion coincides with the 8.2 ka event excursion identified in Greenland ice core records, within age uncertainties[12]. The median duration registered globally in speleothem $\delta^{18}O$ records (Table. 4.1) is ~ 159 years, which is the same (within error) as the duration of the event calculated by layer counting in Greenland ice cores (of 160.5 years[12]). Both the timing and the duration of the event are statistically indistinguishable between Europe and Asia,

the two regions with sufficient records to perform a t-test, and between these two regions and Greenland. The median magnitude of the 8.2 ka $\delta^{18}O$ excursion is also indistinguishable between Europe and Asia (Table 4.1).

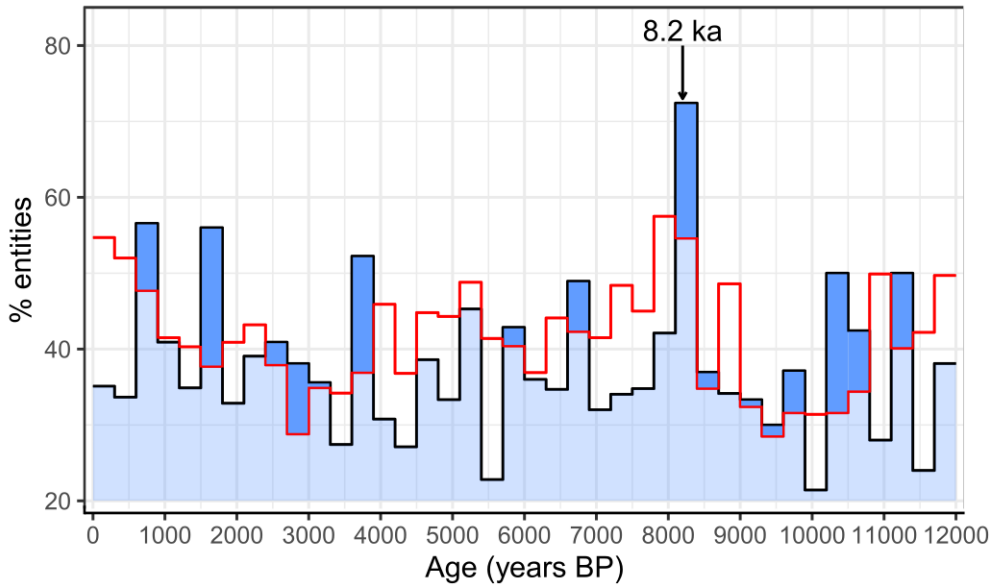

Figure 4.2 Percentage of high-resolution speleothem records that show at least two abrupt shifts in oxygen isotope values, for a given 300-year bin, across the Holocene epoch. The 8.2 ka event is annotated. The red line represents the percentage of randomly generated records (with red noise) that show >= 2 breakpoints in a 300-year bin. The bins that are higher than the randomly generated noise (and therefore significant) are shown in dark blue.

Speleothem $\delta^{18}O$ anomalies of the 8.2 ka event show homogeneous signals over broad regions (Fig. 4a). Over Europe and the Mediterranean region, 15 out of 20 sites exhibit an 8.2 ka excursion. These excursions show negative 8.2 ka $\delta^{18}O$ anomalies, i.e. $\delta^{18}O$ values across the event are lower (more negative) than before or after. Over Asia, anomalies are registered in 13 out of 16 sites, with consistently higher (positive) $\delta^{18}O$ anomalies, where $\delta^{18}O$ across the event are less negative than before and after the event. Speleothem $\delta^{18}O$ anomalies are negative across the South American continent and southern Africa, registered in 4 out of 6 sites. All the central American sites show an 8.2 ka isotope excursion, although more southerly sites show positive excursions and more northern sites show negative $\delta^{18}O$ anomalies. However, these sites show larger age uncertainties (Fig. 4.3) than other regions and there is therefore some uncertainty associated with the identification of the 8.2 ka isotope excursion. There is no significant 8.2 ka isotope excursion recorded in any of the four sites located in the Oceania region or in the two sites from North America.

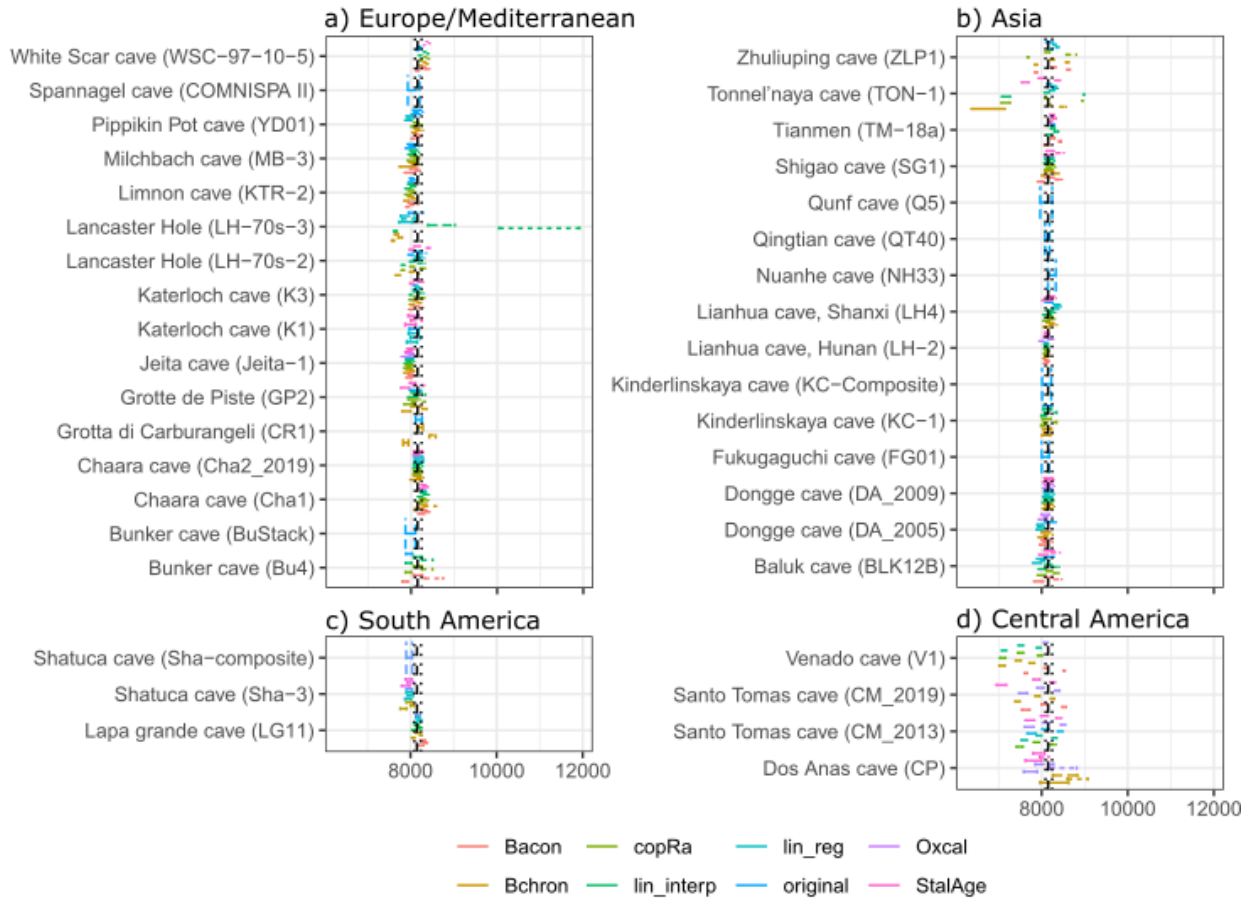

Figure 4.3 Start and end of the 8.2 ka event, constrained by breakpoint analysis, for each record and each age-depth model approach. Timings are given with their age uncertainties (dashed lines).

The patterns in the speleothem $\delta^{18}O$ anomalies (Fig. 4.4a) can be compared with evidence from speleothem growth rate, trace element and calcium isotope data (Fig. 4.4b, Table S3) and the Morrill et al.[13] 8.2 ka reconstructions. The homogenous negative speleothem isotope signals across Europe are mirrored by widespread cooling signals (Fig. 4.4d). However, the precipitation anomalies (Fig. 4.4c) inferred by Morrill et al.[13] and indicated by other speleothem evidence (Fig. 4.4b) are heterogeneous over the region, and indeed differ from one another. This heterogeneity could reflect the fact that different climate archives record different aspects of the hydrological cycle. For example, wet anomalies in west Europe from the Morrill et al. synthesis were explained as reflecting increased runoff from spring snowmelt, whilst dry signals in the east were inferred from pollen-based reconstructions of annual precipitation. Site-specific influences may also be obscuring regional climate signals in some records. Nevertheless, precipitation patterns in Fig. 4b, c do not

show the homogeneity characteristic of the $\delta^{18}O$ anomalies. The widespread positive speleothem isotope anomalies over Asia are mirrored by dry anomalies over the region (Fig. 4.4c), inferred from speleothem trace elements, growth rate and calcium isotopes, and peat $\delta^{13}C$ and a South China Sea salinity record[13].

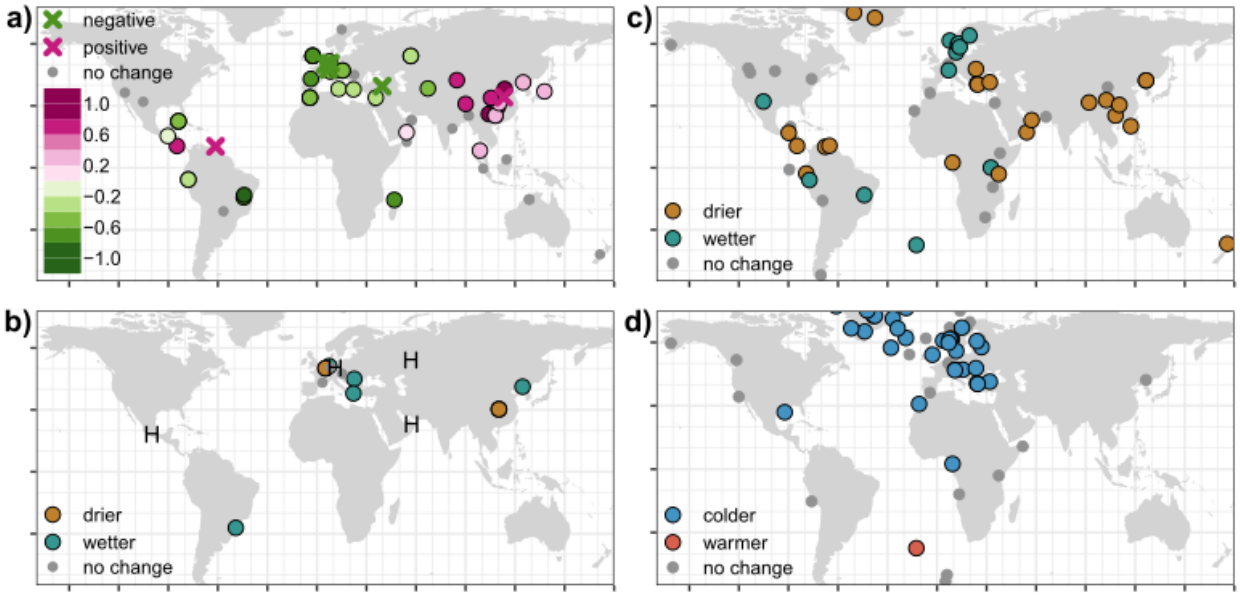

Figure 4.4 ***a)*** *Oxygen isotope anomalies for the 8.2 ka event, registered by speleothem records. The 8.2 ka anomaly is calculated as the mean $\delta^{18}O$ value between the start and end of the event, calculated by breakpoint analysis. Anomalies are given relative to a base period mean $\delta^{18}O$, defined as 7.8 ka to the event end and the start to 8.4 ka. Where studies have identified a speleothem $\delta^{18}O$ excursion, but data is unavailable, anomalies are simply given as positive or negative (table S2).* ***b)*** *Speleothem evidence of wetter/drier 8.2 ka event conditions, inferred from non-oxygen isotope evidence. H indicates records with a hiatus spanning the 8.2 ka event and therefore assumed to record drier conditions. Metadata for these records are given in table S3.* ***c, d)*** *Inferred precipitation and temperature anomalies during the 8.2 ka event from the Morrill et al. (2013) synthesis* (Morrill *et al.*, 2013).

	Magnitude (permil)	**Start (years BP)**	**End (years BP)**	**Duration (years)**
Global	0.5 (0.04)	8223 (12)	8062 (14)	159 (11)
Europe	0.4 (0.05)	8192 (27)	7968 (33)	166 (22)
Asia	0.49 (0.07)	8257 (14)	8081 (16)	163 (15)
Greenland		8247 (47)	8086 (47)	160.5 (5.5)

Table 4.1 Median start, end and duration of the 8.2 ka event registered in speleothem records, globally and for the Europe/Mediterranean and Asia regions. Standard error associated with each value is given in brackets. For all variables, regional values are insignificant from one another, according to a t test (at P <0.01). Timing and duration of the 8.2 ka event in Greenland ice core are also shown, with their uncertainty (Vinther *et al.*, 2006; Thomas *et al.*, 2007).

There are very few high-resolution 8.2 ka records in South America beyond speleothem $\delta^{18}O$ evidence, however a trace element record from Botuverá Cave (Brazil)[29] suggests wetter conditions during the event (Fig. 4.3b;[29]), consistent with the negative $\delta^{18}O$ anomalies in the region. Drier

conditions are inferred over central America by Morrill et al.[13], whereas the speleothem isotope signals show a more mixed signal.

4.5 Discussion

The prominence of the 8.2 ka event in Greenland records is perhaps unsurprising, given that it was forced by a large change in freshwater flux to the North Atlantic[11,30,31]. Its prominence in the speleothem records shows that this change was sufficient to trigger a global reorganisation of the climate system. We have shown that the 8.2 ka event shows remarkable global coherency with respect to timing, duration, magnitude and spatial pattern. The coeval timing of the event in regions both close and far from the north Atlantic (Europe and the Mediterranean versus Asia) supports the indirect evidence of global synchronicity from Greenland ice core methane records[32], which reflect hydrological changes over methane producing regions, mainly tropical wetlands. The 8.2 ka methane excursion is coeval (within 4 years) with changes in $\delta^{14}N$ (which reflects changes in local temperature) in Greenland, indicating that the North Atlantic and global climate response to the 8.2 ka freshwater influx is indeed synchronous. The Greenland ice core $\delta^{18}O$ record and a sub-annual resolution speleothem record from Heshang Cave, China were found to be statistically indistinguishable, supporting a rapid (annual) teleconnection between these regions[33]. Furthermore, a comparison of eight speleothem records from China, Oman and Brazil[34] showed the event occurred at the same time in all the records, within the dating uncertainties. Oceanic teleconnections operate on decadal to centennial timescales[35]. Since lags on these timescales are not observed (even within uncertainties) between near (Europe) and far (Asia) regions, our study supports the idea that the transmission of the 8.2 ka event occurred through suitably rapid atmospheric processes.

One atmospheric mechanism for the transmission of the North Atlantic signal globally is a southward shift in the mean position of the intertropical convergence zone (ITCZ)[36], in response to cooler sea-surface temperatures (SSTs) in the North Atlantic. Such a shift in the mean position of the ITCZ is supported by the spatial patterning of the speleothem isotope signals (Fig. 4.4a). The antiphase

pattern of positive signals in the northern hemisphere tropics of Asia and negative signals in the southern hemisphere tropics of South America and southern Africa is consistent with the weakening of northern hemisphere monsoons and strengthening of southern hemisphere monsoons in response to a shift in the ITCZ. Negative (positive) speleothem isotope signals in the monsoon regions have been interpreted as reflecting a stronger (weaker) monsoon, via a combination of processes, including regional precipitation and atmospheric circulation changes driving moisture transport changes[37,38]. The antiphase pattern in the tropics is also evident in precipitation anomalies13 and other lines of speleothem evidence (Fig. 4.4b). Quantitative precipitation reconstructions from Chinese speleothem records also support a significant drying over Asia during the 8.2 ka event. A calcium isotope record from Heshang cave (China) show a ~ 1/3rd decrease in precipitation at the onset of the event[39], whilst a rainfall reconstruction using the difference in speleothem $\delta^{18}O$ between two Chinese cave sites along a moisture pathway indicate a maximum 24% decrease of rainfall at the onset (350 mm year−1)[40]. Drier conditions in the northern hemisphere tropics and wetter conditions in the southern hemisphere tropics are also simulated by numerous climate model simulations of the 8.2 ka event and attributed to a shift in the ITCZ[14,15]. Thus, both palaeoclimate observations and climate model simulations support the idea that the 8.2 ka event was transmitted to the low latitudes via a shift in the mean position of the ITCZ.

The lack of 8.2 ka signal in the Indonesia/Australia region is inconsistent with this antiphase pattern in the tropics. There is no evident signal in other hydrological palaeoclimate records in the region[41] and climate models typically show a mixed and non-significant rainfall response there[16,42]. This likely reflects the complexity of climate variability in the region, with ocean feedbacks playing a significant role[43,44]. Over central America, the mixed speleothem isotope signal contrasts with the drying signal inferred from lake records[13] and simulated by climate models[15,16,42]. It is possible that the negative $\delta^{18}O$ anomalies observed in the northern sites reflect lower $\delta^{18}O$ of seawater in the north of the Gulf of Mexico, observed in a marine $\delta^{18}O$ record[45]. However, the age uncertainties of these speleothem records are larger than most records (Fig. 4.3) and there are other $\delta^{18}O$ excursions at around this time. In the study documenting the Dos Anas and Santo Tomas records, an earlier positive $\delta^{18}O$

anomaly is tentatively suggested as reflecting the 8.2 ka event[46]. More high-resolution speleothem records of the 8.2 ka event are needed in this region to understand the climate response in the central America region better.

The negative speleothem isotope anomalies over Europe are consistent with the widespread cooling observed in numerous palaeoclimate records[13]. Quantitative temperature estimates suggest a cooling of between 1 and 1.5 °C[13,47]. Based on the observed and modelled temperature/δ^{18}Oprecipitation gradients of 0.17‰ to 0.9‰ °C^{-1}, and an equilibrium isotope fractionation between drip water and calcite of − 0.18 to − 0.23 ‰ °C^{-1} [18], the regional δ^{18}O speleothem anomaly of 0.4 ‰ could be fully explained by the regional temperature decrease. The oxygen isotopic composition of moisture delivered to Europe was also likely lower during the 8.2 ka event, further contributing to negative isotope anomalies in the region. Lower δ^{18}O of seawater (of ~ 0.4 ‰[48]) in the North Atlantic region and cooler SSTs (of ~ 1 °C[49,50]), would deliver moisture that is ~ 0.5 ‰ more depleted. Other studies have emphasised other possible causes of the depleted δ^{18}O values in the region, including changing rainfall seasonality[51] and precipitation amount[51,52]. Future studies comparing the oxygen isotope synthesis presented here with isotope-enabled climate model simulations could elucidate the drivers of δ^{18}O excursions during the 8.2 ka event.

Other events during the Holocene epoch are clearly less globally prominent than the 8.2 ka event. A significant number of abrupt events were identified at ~ 11.2 ka, associated with the Preboreal Oscillation, supporting the idea that freshwater pulses induced large changes in the climate system. However, the global fingerprint of this event is less coherent than that of the 8.2 ka event. Although there appear to be some statistically significant speleothem isotope excursions in the second part of the Holocene, none of these correspond to abrupt climate events that have been identified in other studies, such as the 4.2 ka event[4,5]. There is still little consensus about the spatial extent and cause of these later Holocene events, which have been interpreted as a response to changes in solar irradiance[53,54] or volcanicity (or both)[32,55] and which have also been considered as a manifestation of internal (unforced) climate variability56. The lack of a significant 4.2 ka event in our speleothem

analysis could reflect the complexity of the event; records of the event do not always show a well-constrained timing[4,57,58] or a signal with an amplitude larger than the noise of the record[59] Furthermore, the signal of this event sometimes consists of several oscillations rather than one straightforward excursion[4,60]. However, it seems more likely that this event was not of global extent. There is no regional 4.2 ka event in the north Atlantic region[61] and even in the Mediterranean region, where evidence of the event is clearest[4], there are numerous palaeoclimate records that do not show the event[57].

4.6 Conclusion

We have shown that the 8.2 ka event is the most prominent abrupt climate event in the Holocene. The event shows a globally extensive, coherent and synchronous climate response. The coherency of the regional $\delta^{18}O$ anomalies indicates that the freshwater pulse at 8.2 ka triggered a widespread reorganisation of climate systems. The synchronicity of isotope signals globally suggests that the North Atlantic freshening was transmitted via rapid atmospheric teleconnections. We have provided the first global speleothem isotope synthesis of the 8.2 ka event, that can be used to test the ability of climate models to simulate the impacts of ice sheet melting and ocean circulation changes.

4.7 Methods

4.7.1 Holocene abrupt event detection analysis

We determine the presence and timing of abrupt events during the Holocene using a global dataset of speleothem $\delta^{18}O$ records from the SISAL (Speleothem Isotopes Synthesis and Analysis) version 2 database[25,26,62]. We identify abrupt events during a moving 1000-year window (with 50% overlap). For each window, we select speleothem records using the following criteria:

- They have a mean sampling resolution of < = 30 years within the window;
- They have a minimum length within the window of 500 years;

- This resulted in the selection of 275 speleothem records from 170 sites for this analysis (Fig. 4.1). The choice of a minimum resolution of < = 30 years gives a minimum of five data points for abrupt events of ~ 150 years duration and ensures that there are sufficient records included in the analysis to identify a global signal.

To detect abrupt events within a window objectively, we carried out breakpoint analysis using the Strucchange package in R[63,64]. The method detects significant shifts in speleothem $\delta^{18}O$ data using a dynamical programming approach. The optimal number of breakpoints (and location) is determined using a Bayesian Information Criterion. Where two breakpoints occur within < 300 years, it suggests an abrupt event, whereby there is a rapid shift in $\delta^{18}O$ values, which are maintained for at least a few years, then a shift back. To prevent the breakpoint analysis from detecting changes in $\delta^{18}O$ values that relate to long-term changes, the speleothem records are first individually detrended and normalised by fitting a linear regression through each record across the 1000-year window, then subtracting the predicted $\delta^{18}O$ values from the linear model from the observed $\delta^{18}O$ values.

We calculate the number of records within 300-year bins across the Holocene that show > = 2 breakpoints (Fig. 4.2), given as a percentage of the total records in that bin (thereby ensuring plotted values do not reflect the changing number of records through the Holocene). 300-year bins are chosen to examine the presence of abrupt events because they are sufficiently short to exclude multi-centennial scale variability but long enough to capture the full length of an abrupt event. As a further step, we determined which bins were statistically significant above randomly generated noise. This was important because speleothem $\delta^{18}O$ records often have a high degree of autocorrelation, which can cause statistically spurious breakpoints to be detected[65]. We therefore carried out the same breakpoint analysis on randomly generated records with the same sampling resolution and autocorrelation as the speleothem records, using the arima.sim function in R. We carried out these steps 1000 times and calculated the mean percentage of randomly generated records with > = 2 breakpoints within a bin. Bins where the actual speleothem records have a higher percentage than the randomly generated noise are considered statistically significant.

4.7.2 8.2 ka anomalies

To identify the presence of the 8.2 ka event, and characterise the timing, duration and magnitude of speleothem oxygen isotope anomalies at the event, we selected speleothem records from SISAL version 2 covering the interval 7.8 to 8.4 ka. Records were selected using the following criteria:

- They have a mean temporal resolution of < = 30 years within the period;
- They are at least 300 years long within the period;

This resulted in the selection of 67 speleothem records from 48 sites for this analysis (Fig. 4.1). We added a further 6 records (from 6 sites), that are not available in SISALv2 (Table S1). Although we used a mean temporal resolution of < = 30 years to select the records for this analysis, 95% of records have a mean resolution of < 20 years and 67% have a mean resolution of < 10 years (Table S1).

We detected abrupt shifts in $\delta^{18}O$ values by carrying out breakpoint analysis over each individual, detrended record. Where a speleothem record shows < = 1 breakpoint, there is no significant $\delta^{18}O$ excursion (Fig. 4.5a). Where a speleothem record shows 2 breakpoints, the record shows one simple $\delta^{18}O$ excursion (Fig. 4.5b). If a record shows > 2 breakpoints (i.e. an excursion can be separated into segments, or there are several significant fluctuations), we determine which segments are significantly different from the base period (before and after the event). If all significant segments have the same sign anomaly (relative to the base period), this suggests they represent an event with a more complex evolution (Fig. 4.5c). If significant segments show a changing sign of anomaly, this suggests that the record shows numerous fluctuations and therefore the record does not show one clear 8.2 ka excursion (Fig. 4.5d).

The oldest breakpoint is defined as the start of the excursion and the youngest breakpoint defined as the end (Fig. 4.5b). We calculate the event duration in each individual record as the difference between the start and the end of the event. Anomalies are calculated as the mean $\delta^{18}O$ between the start and the end of the event, minus the mean $\delta^{18}O$ of before and after the event (Fig. 4.5).

To ensure no spurious results related to the record noise are included in our synthesis, we remove any records where the ~8.2 ka $\delta^{18}O$ anomaly is smaller than the standard deviation of the base period (before and after the event).

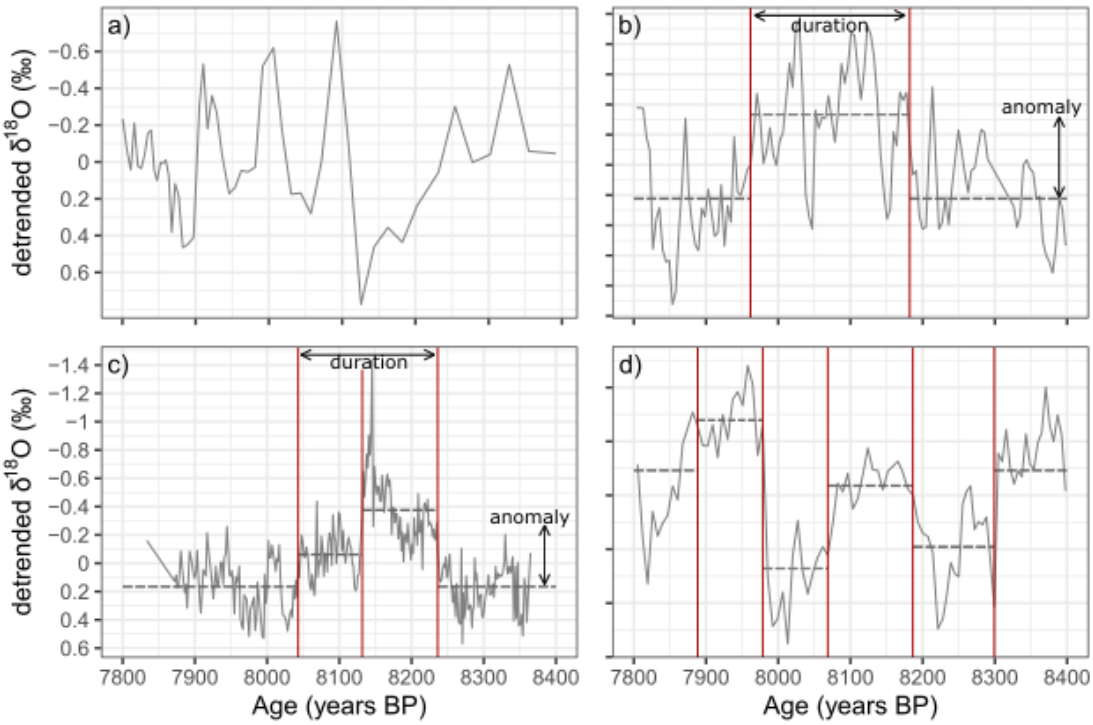

Figure 4.5 Detection of 8.2 ka isotope excursions. a) shows a record (entity id = 590 in the SISAL database) with no breakpoints and therefore no excursion, b) shows a record (entity id = 199) with an excursion constrained by 2 breakpoints, c) shows a record (entity id = 129) with an excursion constrained by >2 breakpoints, d) shows a record (entity id = 305) with >2 breakpoints, but isotope excursions of varying direction and therefore no clear 8.2 ka event.

We also examined the age uncertainties associated with the 8.2 ka $\delta^{18}O$ excursions using age uncertainty data available in the SISAL v2 database. The database contains chronologies from seven different age-depth modelling approaches [27]. Age uncertainties were calculated from the spread of individual ensembles in six modelling approaches (linear interpolation, linear regression, Bchron, Bacon, OxCal, COPRA). For the StalAge approach, age uncertainties are obtained in the model through a Monte Carlo approach, but individual ensembles are not outputted. We calculated the timing of the excursion using all available age-depth modelling approaches for each record, thereby assessing uncertainty associated with the choice of model. We also calculated the timing for the upper and lower age uncertainties of each record and age-model approach. Where age uncertainties

are too large and therefore the timing of the 8.2 ka isotope excursion too poorly constrained, we excluded the entity from our analysis.

4.8 Data availability

The Speleothem Isotopes Synthesis and AnaLysis (SISAL) database version 2 is available through the University of Reading Data Archive, at https://doi.org/10.17864/1947.256. 62. The dataset generated in this study is available in a GitHub repository, available at https://doi.org/10.5281/zenodo.5871176. We use R for analyses66. The code used to run the analyses and generate the figures in this study are also available at https://doi.org/10.5281/zenodo.5871176.

4.9 References

1. Dykoski, C. A. *et al.* A high-resolution, absolute-dated Holocene and deglacial Asian monsoon record from Dongge Cave, China. Earth Planet. Sci. Lett. **233**, 71–86 (2005).
2. Morrill, C., Overpeck, Jonathon, T. & Cole, J. E. A synthesis of abrupt changes in the Asian summer monsoon since the last deglaciation. The Holocene **13**, 465–476 (2003).
3. Stríkis, N. M. *et al.* Abrupt variations in South American monsoon rainfall during the Holocene based on a speleothem record from central-eastern Brazil. Geology **39**, 1075–1078 (2011).
4. Bini, M. *et al.* The 4.2 ka BP Event in the Mediterranean region: an overview. Clim. Past **15**, 555–577 (2019).
5. Kaniewski, D., Marriner, N., Cheddadi, R., Guiot, J. & Van Campo, E. The 4.2 ka BP event in the Levant. Clim. Past **14**, 1529–1542 (2018).
6. Scuderi, L. A., Yang, X., Ascoli, S. E. & Li, H. The 4.2 ka BP Event in northeastern China: a geospatial perspective. Clim. Past **15**, 367–375 (2019).
7. Toth, L. T. & Aronson, R. B. The 4.2 ka event, ENSO, and coral reef development. Clim. Past **15**, 105–119 (2019).
8. Yan, M. & Liu, J. Physical processes of cooling and mega-drought during the 4.2 ka BP event: results from TraCE-21ka simulations. Clim. Past **15**, 265–277 (2019).
9. Vinther, B. M. *et al.* A synchronized dating of three Greenland ice cores throughout the Holocene. J. Geophys. Res. Atmos. **111**, (2006).

10. Tan, L. *et al.* Holocene monsoon change and abrupt events on the western Chinese Loess Plateau as revealed by accurately dated stalagmites. Geophys. Res. Lett. **47**, e2020GL090273 (2020).

11. Alley, R. B. *et al.* Holocene climatic instability: A prominent, widespread event 8200 yr ago. Geology **25**, 483–486 (1997).

12. Barber, D. C. *et al.* Forcing of the cold event of 8,200 years ago by catastrophic drainage of Laurentide lakes. Nature **400**, 344–348 (1999).

13. Thomas, E. R. *et al.* The 8.2ka event from Greenland ice cores. Quat. Sci. Rev. **26**, 70–81 (2007).

14. Morrill, C. *et al.* Proxy benchmarks for intercomparison of 8.2 ka simulations. Clim. Past **9**, 423–432 (2013).

15. Morrill, C., LeGrande, A. N., Renssen, H., Bakker, P. & Otto-Bliesner, B. L. Model sensitivity to North Atlantic freshwater forcing at 8.2 ka. Clim. Past **9**, 955–968 (2013).

16. Matero, I. S. O., Gregoire, L. J., Ivanovic, R. F., Tindall, J. C. & Haywood, A. M. The 8.2 ka cooling event caused by Laurentide ice saddle collapse. Earth Planet. Sci. Lett. **473**, 205–214 (2017).

17. Morrill, C., Ward, E. M., Wagner, A. J., Otto-Bliesner, B. L. & Rosenbloom, N. Large sensitivity to freshwater forcing location in 8.2 ka simulations. Paleoceanography **29**, 930–945 (2014).

18. Parker, S. E. *et al.* A data–model approach to interpreting speleothem oxygen isotope records from monsoon regions. Clim. Past **17**, 1119–1138 (2021).

19. Lachniet, M. S. Climatic and environmental controls on speleothem oxygen-isotope values. Quat. Sci. Rev. **28**, 412–432 (2009).

20. Sinha, A. *et al.* Trends and oscillations in the Indian summer monsoon rainfall over the last two millennia. Nat. Commun. **6**, 6309 (2015).

21. Cheng, H. *et al.* Timing and structure of the 8.2 kyr BP event inferred from $\delta^{18}O$ records of stalagmites from China, Oman, and Brazil. Geology **37**, 1007–1010 (2009).

22. Duan, P. *et al.* The timing and structure of the 8.2 ka event revealed through high-resolution speleothem records from northwestern Madagascar. Quat. Sci. Rev. **268**, 107104 (2021).

23. Peckover, E. N. *et al.* Coupled stalagmite–Alluvial fan response to the 8.2 ka event and early Holocene palaeoclimate change in Greece. Palaeogeogr. Palaeoclimatol. Palaeoecol. **532**, 109252 (2019).

24. Waltgenbach, S. *et al.* Climate and structure of the 8.2 ka event reconstructed from three speleothems from Germany. Glob. Planet. Change **193**, 103266 (2020).

25. Comas-Bru, L. & Harrison, S. P. SISAL: Bringing Added Value to Speleothem Research. Quaternary (2019) doi:10.3390/quat2010007.

26. Atsawawaranunt, K. *et al.* The SISAL database: A global resource to document oxygen and carbon isotope records from speleothems. Earth Syst. Sci. Data **10**, 1687–1713 (2018).

27. Comas-Bru, L. *et al.* SISALv2: a comprehensive speleothem isotope database with multiple age–depth models. Earth Syst. Sci. Data **12**, 2579–2606 (2020).

28. Bond, G. *et al.* A pervasive millennial-scale cycle in North Atlantic Holocene and glacial climates. Science (80-.). **278**, 1257–1266 (1997).

29. Fisher, T. G., Smith, D. G. & Andrews, J. T. Preboreal oscillation caused by a glacial Lake Agassiz flood. Quat. Sci. Rev. **21**, 873–878 (2002).

30. Bernal, J. P. *et al.* High-resolution Holocene South American monsoon history recorded by a speleothem from Botuverá Cave, Brazil. Earth Planet. Sci. Lett. **450**, 186–196 (2016).

31. Gregoire, L. J., Payne, A. J. & Valdes, P. J. Deglacial rapid sea level rises caused by ice-sheet saddle collapses. Nature **487**, 219–222 (2012).

32. Ullman, D. J. *et al.* Final Laurentide ice-sheet deglaciation and Holocene climate-sea level change. Quat. Sci. Rev. **152**, 49–59 (2016).

33. Fleitmann, D. *et al.* Holocene forcing of the Indian Monsoon recorded in a stalagmite from southern Oman. Science (80-.). **300**, 1737–1739 (2003).

34. Wang, Y. *et al.* The Holocene Asian monsoon: Links to solar changes and North Atlantic climate. Science (80-.). **308**, 854–857 (2005).

35. Kobashi, T. *et al.* Volcanic influence on centennial to millennial Holocene Greenland temperature change. Sci. Rep. **7**, 1–10 (2017).

36. Wanner, H., Solomina, O., Grosjean, M., Ritz, S. P. & Jetel, M. Structure and origin of Holocene cold events. Quat. Sci. Rev. **30**, 3109–3123 (2011).

37. Wanner, H. & Buetikofer, J. Holocene Bond Cycles: real or imaginary. Geografie **113**, 338–349 (2008).

38. Finné, M., Holmgren, K., Sundqvist, H. S., Weiberg, E. & Lindblom, M. Climate in the eastern Mediterranean, and adjacent regions, during the past 6000 years–A review. J. Archaeol. Sci. **38**, 3153–3173 (2011).

39. Burstyn, Y. *et al.* Speleothems from the Middle East: an example of water limited environments in the SISAL database. Quaternary **2**, 16 (2019).

40. Ön, Z. B., Greaves, A. M., Akçer-Ön, S. & Özeren, M. S. A Bayesian test for the 4.2 ka BP abrupt climatic change event in southeast Europe and southwest Asia using structural time series analysis of paleoclimate data. Clim. Change **165**, (2021).

41. Railsback, L. B. *et al.* The timing, two-pulsed nature, and variable climatic expression of the 4.2 ka event: A review and new high-resolution stalagmite data from Namibia. Quat. Sci. Rev. **186**, 78–90 (2018).

42. Bradley, R. S. & Bakke, J. Is there evidence for a 4.2 ka BP event in the northern North Atlantic region? Clim. Past **15**, 1665–1676 (2019).

43. Liu, Y. H. *et al.* Links between the East Asian monsoon and North Atlantic climate during the 8,200 year event. Nat. Geosci. **6**, 117–120 (2013).

44. Cheng, H. *et al.* Timing and structure of the 8.2 kyr B.P. event inferred from $\delta^{18}O$ records of stalagmites from China, Oman, and Brazil. Geology **37**, 1007–1010 (2009).

45. Liu, Z. & Alexander, M. Atmospheric bridge, oceanic tunnel, and global climatic teleconnections. Rev. Geophys. **45**, (2007).

46. Chiang, J. C., Cheng, W. & Bitz, C. M. Fast teleconnections to the tropical Atlantic sector from Atlantic thermohaline adjustment. Geophys. Res. Lett. **35**, (2008).

47. Wang, Y. J. *et al.* A high-resolution absolute-dated late Pleistocene monsoon record from Hulu Cave, China. Science (80-.). **294**, 2345–2348 (2001).

48. Cheng, H. *et al.* Chinese stalagmite paleoclimate researches: A review and perspective. Sci. China Earth Sci. **62**, 1489–1513 (2019).

49. Owen, R. A. *et al.* Calcium isotopes in caves as a proxy for aridity: Modern calibration and application to the 8.2 kyr event. Earth Planet. Sci. Lett. **443**, 129–138 (2016).

50. Liu, Y. & Hu, C. Quantification of southwest China rainfall during te 8.2 ka BP event with response to North Atlantic cooling. Clim. Past **12**, 1583–1590 (2016).

51. Gingele, F., De Deckker, P. & Norman, M. Late Pleistocene and Holocene climate of SE Australia reconstructed from dust and river loads deposited offshore the River Murray Mouth. Earth Planet. Sci. Lett. **255**, 257–272 (2007).

52. Wagner, A. J., Morrill, C., Otto-Bliesner, B. L., Rosenbloom, N. & Watkins, K. R. Model support for forcing of the 8.2 ka event by meltwater from the Hudson Bay ice dome. Clim. Dyn. **41**, 2855–2873 (2013).

53. Zhao, Y. & Harrison, S. P. Mid-Holocene monsoons: A multi-model analysis of the inter-hemispheric differences in the responses to orbital forcing and ocean feedbacks. Clim. Dyn. **39**, 1457–1487 (2012).

54. D'Agostino, R. *et al.* Contrasting southern hemisphere monsoon response: MidHolocene orbital forcing versus future greenhouse gas-induced global warming. J. Clim. **33**, 9595–9613 (2020).

55. LoDico, J. M., Flower, B. P. & Quinn, T. M. Subcentennial-scale climatic and hydrologic variability in the Gulf of Mexico during the early Holocene. Paleoceanography **21**, (2006).

56. Fensterer, C. *et al.* Millennial-scale climate variability during the last 12.5 ka recorded in a Caribbean speleothem. Earth Planet. Sci. Lett. **361**, 143–151 (2013).

57. Affolter, S. *et al.* Central Europe temperature constrained by speleothem fluid inclusion water isotopes over the past 14,000 years. Sci. Adv. **5**, eaav3809 (2019).

58. Ellison, C. R. W., Chapman, M. R. & Hall, I. R. Surface and deep ocean interactions during the cold climate event 8200 years ago. Science (80-.). **312**, 1929–1932 (2006).

59. Farmer, E. J., Chapman, M. R. & Andrews, J. E. Centennial-scale Holocene North Atlantic surface temperatures from Mg/Ca ratios in Globigerina bulloides. Geochemistry, Geophys. Geosystems **9**, (2008).

60. Thornalley, D. J. R., Elderfield, H. & McCave, I. N. Holocene oscillations in temperature and salinity of the surface subpolar North Atlantic. Nature **457**, 711–714 (2009).

61. Surić, M. *et al.* Holocene hydroclimate changes in continental Croatia recorded in speleothem δ13C and $\delta^{18}O$ from Nova Grgosova Cave. The Holocene **31**, 1401–1416 (2021).

62. Fohlmeister, J. *et al.* Bunker Cave stalagmites: an archive for central European Holocene climate variability. Clim. Past **8**, 1751–1764 (2012).

63. Comas-Bru, L., Atsawawaranunt, K., Harrison, S. P. & SISAL working group members. SISAL (Speleothem Isotopes Synthesis and AnaLysis Working group) database version 2.0. (2020) doi:http://dx.doi.org/10.17864/1947.242.

64. Zeileis, A., Leisch, F., Hornik, K. & Christian, K. strucchange: An R package for testing for structural change in linear regression models. J. Stat. Softw. **7**, 1–38 (2002).

65. Zeileis, A., Kleiber, C., Kraemer, W. & Hornik, K. Testing and Dating of Structural Changes in Practice. Comput. Stat. Data Anal. **44**, 109–123 (2003).

66. Topál, D., Matyasovszky, I., Kern, Z. & Hatvani, I. G. Detecting breakpoints in artificially modified- and real-life time series using three state-of-the-art methods. Open Geosci. **8**, 78–98 (2016).

67. R Core Team. R: A Language and Environment for Statistical Computing. (2019).

4.10 Supplement

Fig S1: Spatial distribution and timing of $\delta^{18}O$ anomalies for periods in the Holocene when a significant number of abrupt excursions are identified.

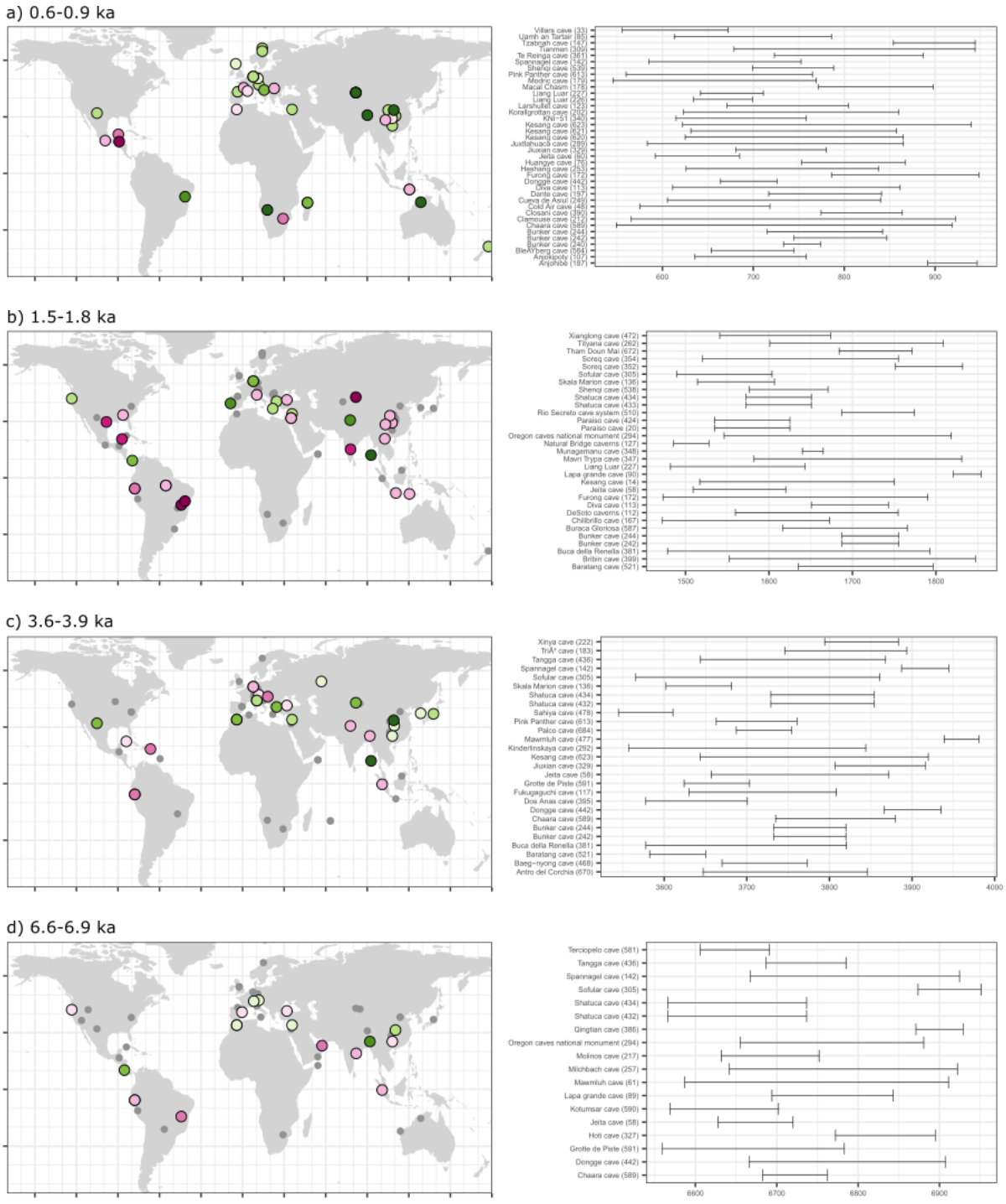

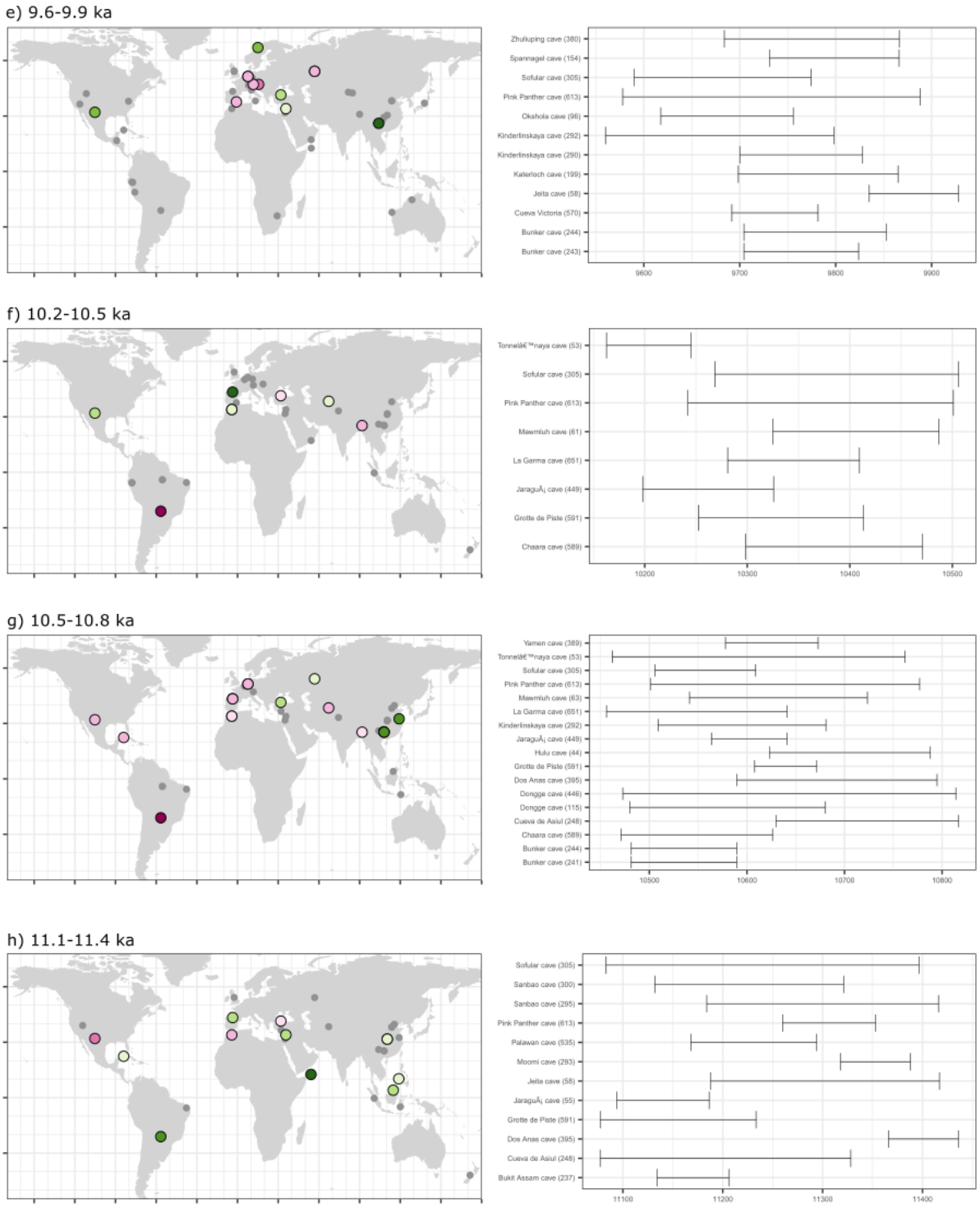

Table S1: 8.2 ka anomalies, timing and duration, obtained by breakpoint analysis. All oxygen isotope anomalies are larger than speleothem record measurement uncertainties.

entity id	site name	longitude	latitude	Start (years BP)	End (years BP)	Duration (years)	Anomaly (‰)	Notes
	Anjohibe cave	46.89	-15.54	8217	8069	148	-0.80	Not in SISALv2, data from (Duan *et al.*, 2021)
520	Baluk cave	84.73	42.43	8285	8062	222	0.70	
242	Bunker cave	7.66	51.37	8030	7877	153	-0.38	
244	Bunker cave	7.66	51.37	8101	7869	233	-0.29	
588	Chaara cave	-4.25	33.96	8270	8065	205	-0.18	
589	Chaara cave	-4.25	33.96	8343	8232	111	-0.56	
442	Dongge cave	108.08	25.28	8325	8080	245	0.19	
475	Dongge cave	108.08	25.28	8257	8065	192	0.35	
395	Dos Anas cave	-83.97	22.38	8275	7851	424	-0.36	
117	Fukugaguchi cave	137.80	36.99	8170	8000	170	0.28	
277	Grotta di Carburangeli	13.16	38.17	8253	8105	148	-0.38	
591	Grotte de Piste	-4.25	33.95	8229	7968	261	0.25	
58	Jeita cave	35.65	33.95	8047	7881	166	-0.24	
	Kaite cave	-3.66	43.04	8211	8147	63	-0.73	Not in SISALv2, data from (Domínguez-Villar *et al.*, 2017)
199	Katerloch cave	15.55	47.08	8182	7962	221	-0.56	
200	Katerloch cave	15.55	47.08	8135	8049	86	-0.46	
290	Kinderlinskaya cave	56.85	54.15	8238	8041	197	-0.37	
292	Kinderlinskaya cave	56.85	54.15	8223	8011	212	-0.35	
	Klang cave	98.73	8.33	8281	8183	98	0.29	Not in SISALv2, data from (Chawchai *et al.*, 2021)
51	Lancaster Hole	-2.52	54.22	8199	8050	149	0.53	Removed from synthesis, age uncertainties too large
52	Lancaster Hole	-2.52	54.22	8272	7942	330	-0.62	
89	Lapa grande cave	-44.28	-14.37	8215	8124	91	-0.72	
496	Lianhua cave, Hunan	109.53	29.48	8147	8064	83	0.63	
529	Lianhua cave, Shanxi	113.72	38.17	8252	8088	164	0.90	
671	Limnon cave	22.14	37.96	8060	7965	95	-0.37	
256	Milchbach cave	8.08	46.62	8141	7918	223	-0.50	
466	Nuanhe cave	124.92	41.33	8328	8147	181	0.39	
	Padre cave	-44.05	-13.22	8213	8144	69	-1.34	Not in SISALv2, data from (Cheng, Fleitmann, Edwards, Wang,

								Cruz, Auler, Mangini, Wang, Kong and Burns, 2009)
129	Pippikin Pot cave	-2.51	54.21	8236	8043	193	-0.41	
385	Qingtian cave	110.37	31.33	8183	8081	102	0.39	
351	Qunf cave	54.30	17.17	8245	7967	278	0.14	
	Rey Marcos cave	-90.30	15.40	8314	8155	159	-0.17	Not in SISALv2, data from (Winter *et al.*, 2020)
388	Santo Tomas cave	-83.84	22.55	8202	8027	175	-0.46	
608	Santo Tomas cave	-83.84	22.55	8048	7896	152	-0.42	
433	Shatuca cave	-77.90	-5.70	8037	7900	137	-0.27	
434	Shatuca cave	-77.90	-5.70	8037	7900	137	-0.27	
540	Shigao cave	107.17	28.18	8272	8081	191	0.15	
142	Spannagel cave	11.67	47.08	8197	7924	274	-0.19	
308	Tianmen	90.07	30.92	8298	8217	81	0.79	
53	Tonnel'naya cave	67.23	38.40	8225	8117	108	-0.49	
640	Venado cave	-84.77	10.55	8144	8050	95	0.78	
150	White Scar cave	-2.44	54.17	8216	8143	73	-1.07	
	Wuya cave	105.43	33.82	8226	8065	161	0.73	Not in SISALv2, data from (Tan *et al.*, 2020)
379	Zhuliuping cave	104.10	26.02	8260	8104	156	0.94	

Table S2: Speleothem records with evidence for an 8.2 ka oxygen isotope excursion (used in Fig. 4.4a) but where no data is available to carry out breakpoint analysis.

Site name	Latitude	Longitude	Isotope signal	Reference
Galeria Das Lâminas	39.51	39.51	negative	(Benson *et al.*, 2021)
Magou cave	34.19	113.23	positive	(Cai *et al.*, 2021)
Gasparee cave	10.39	-61.39	positive	(Boyd, 2015)
Herbstlabyrinth	50.69	8.21	negative	(Waltgenbach *et al.*, 2020)
Milandre cave	47.49	7.02	negative	(Affolter *et al.*, 2019)
Père Noël cave	50.13	5.16	negative	(Allan *et al.*, 2018)

Table S3: Speleothem records where the 8.2 ka event has been identified from trace element, growth rate/lamina thickness or calcium isotope measurements (used in Fig. 4.4b). Interpretations of measurements are those made by the authors of the study.

Site name	Latitude	Longitude	Measurement	Anomaly	Interpretation	Reference

Ascunsă cave	45	22.6	Growth rate	positive	wetter	(Drăguşin *et al.*, 2014)
Botuverá cave	-27.13	-49.09	Sr/Ca	negative	wetter	(Bernal *et al.*, 2016)
Bunker cave	51.22	7.39	Mg/Ca	negative	wetter	(Waltgenbach *et al.*, 2020)
Herbstlabyrinth	50.6878	8.2066	Mg/Ca		no change	(Waltgenbach *et al.*, 2020)
Heshang cave	30.27	110.25	Mg/Ca	positive	drier	(Liu *et al.*, 2013)
Heshang cave	30.27	110.25	Growth rate	negative	drier	(Liu *et al.*, 2013)
Heshang cave	30.27	110.25	δ44/42Ca	higher	drier	(Owen *et al.*, 2016)
Kaite cave	43.2	3.39	Growth rate		no change	(Dominguez-Villar *et al.*, 2009)
Katerloch cave	47.5	15.33	Growth rate		no change	(Boch, Spötl and Kramers, 2009)
Limnon cave	37.9605	22.1403	Mg/Ca	negative	wetter	(Peckover *et al.*, 2019)
Nuanhe cave	41.2	124.55	Ba/Ca	negative	wetter	(Wu *et al.*, 2012)
Père Noël	50.13	5.16	Sr, Ba, Mg	negative	drier	(Allan *et al.*, 2018)
Père Noël	50.13	5.16	Growth rate	negative	drier	(Allan *et al.*, 2018)

References:

1. Duan, P. et al. The timing and structure of the 8.2 ka event revealed through high-resolution speleothem records from northwestern Madagascar. Quat. Sci. Rev. 268, 107104 (2021).
2. Domínguez-Villar, D., Wang, X., Krklec, K., Cheng, H. & Edwards, R. L. The control of the tropical North Atlantic on Holocene millennial climate oscillations. Geology 45, 303–306 (2017).
2. Chawchai, S. et al. Hydroclimate variability of central Indo-Pacific region during the Holocene. Quat. Sci. Rev. 253, (2021).
3. Cheng, H. et al. Timing and structure of the 8.2 kyr BP event inferred from $\delta^{18}O$ records of stalagmites from China, Oman, and Brazil. Geology 37, 1007–1010 (2009).
4. Winter, A. et al. Initiation of a stable convective hydroclimatic regime in Central America circa 9000 years BP. Nat. Commun. 2020 111 11, 1–8 (2020).

5. Tan, L. et al. Holocene Monsoon Change and Abrupt Events on the Western Chinese Loess Plateau as Revealed by Accurately Dated Stalagmites. Geophys. Res. Lett. 47, e2020GL090273 (2020).
6. Benson, A. et al. A speleothem record from Portugal reveals phases of increased winter precipitation in western Iberia during the Holocene. Holocene 31, 1339–1350 (2021).
7. Cai, Y. et al. Holocene variability of East Asian summer monsoon as viewed from the speleothem $\delta^{18}O$ records in central China. Earth Planet. Sci. Lett. 558, (2021).
8. Boyd, M. Speleothems from warm climates: holocene records from the Caribbean and Mediterranean regions. (Stockholm University, 2015).
9. Waltgenbach, S. et al. Climate and structure of the 8.2 ka event reconstructed from three speleothems from Germany. Glob. Planet. Change 193, 103266 (2020).
10. Affolter, S. et al. Central Europe temperature constrained by speleothem fluid inclusion water isotopes over the past 14,000 years. Sci. Adv. 5, eaav3809 (2019).
11. Allan, M. et al. High-resolution reconstruction of 8.2-ka BP event documented in Père Noël cave, southern Belgium. J. Quat. Sci. 33, 840–852 (2018).
12. Drăguşin, V. et al. Constraining Holocene hydrological changes in the Carpathian-Balkan region using speleothem $\delta^{18}O$ and pollen-based temperature reconstructions. Clim. Past 10, 1363–1380 (2014).
13. Bernal, J. P. et al. High-resolution Holocene South American monsoon history recorded by a speleothem from Botuverá Cave, Brazil. Earth Planet. Sci. Lett. 450, 186–196 (2016).
14. Liu, Y. H. et al. Links between the East Asian monsoon and North Atlantic climate during the 8,200 year event. Nat. Geosci. 6, 117–120 (2013).
15. Owen, R. A. et al. Calcium isotopes in caves as a proxy for aridity: Modern calibration and application to the 8.2 kyr event. Earth Planet. Sci. Lett. 443, 129–138 (2016).
16. Dominguez-Villar, D. et al. Oxygen isotope precipitation anomaly in the North Atlantic region during the 8.2 ka event. Geology 37, 1095–1098 (2009).

17. Boch, R., Spötl, C. & Kramers, J. High-resolution isotope records of early Holocene rapid climate change from two coeval stalagmites of Katerloch Cave, Austria. Quat. Sci. Rev. 28, 2527–2538 (2009).
18. Peckover, E. N. et al. Coupled stalagmite–Alluvial fan response to the 8.2 ka event and early Holocene palaeoclimate change in Greece. Palaeogeogr. Palaeoclimatol. Palaeoecol. 532, 109252 (2019).
19. Wu, J. Y., Wang, Y. J., Cheng, H., Kong, X. G. & Liu, D. B. Stable isotope and trace element investigation of two contemporaneous annually-laminated stalagmites from northeastern China surrounding the 8.2 ka event. Clim. Past 8, 1497–1507 (2012).
20. Comas-Bru, L. et al. SISALv2: a comprehensive speleothem isotope database with multiple age–depth models. Earth Syst. Sci. Data 12, 2579–2606 (2020).

5 Discussion

The overall aim of this thesis was to reconstruct past monsoon variability at the regional and global-scale, using the SISAL database and data-model comparisons.

The research in this thesis has been presented as three individual papers, each with their own separate discussions. In this chapter, the overall implications of the research are discussed under three integrative themes: (1) the role of large-scale speleothem syntheses for climate reconstructions, (2) what can be learned from data-model comparisons, and (3) the palaeo-history of the global and regional monsoons. These discussions summarise common findings across all three papers and their implications for current knowledge of the palaeomonsoons.

5.1 The use of speleothems for spatio-temporal reconstructions

Speleothems have long been recognised as a rich archive of information about terrestrial palaeoclimates. Existing speleothem studies have often (qualitatively) compared a handful of records to infer past regional climate change (Cheng *et al.*, 2009, 2012, 2013; Li *et al.*, 2014). Speleothem records have also been incorporated into some global scale analyses (Morrill *et al.*, 2013; Scussolini *et al.*, 2019), together with other palaeoclimate archives. However, it was not until the creation of the SISAL database in 2018 (Atsawawaranunt *et al.*, 2018) that it became possible to undertake large-scale or global analyses of speleothem records. The current version of the database (Comas-Bru *et al.*, 2020) includes more than 690 individual records, together with standardised metadata and age models, allowing records to be processed and analysed in a consistent manner. This allows a fuller picture of past spatio-temporal monsoon variability to be gained. The papers in this thesis are amongst the first research to utilise the SISAL database to investigate past monsoon climates, with more than 120 speleothem records processed and analysed in every paper presented here.

Much of the research in this thesis required records with high temporal resolution and precise age control that cover multiple millennia. This precludes the use of other sources of data, such as lower resolution

sediment core records, or high-resolution but short-lived tree-ring, coral and mollusc records. The reconstructions of monsoon interannual-interdecadal variability (IADV) in chapter 3 was only possible because speleothems can provide continuous and high-resolution records of terrestrial climate. Changes in IADV using other terrestrial palaeoclimate archives had to be inferred from changes in the mean state (e.g. Conroy *et al.*, 2008). High resolution coral and mollusc records have provided past reconstructions of ENSO (El Niño Southern Oscillation) variability (Emile-Geay *et al.*, 2016; Carré *et al.*, 2021), however these records only provide very short samples of the long-term trends, and this adds considerable uncertainty to their interpretation. Furthermore, these analyses only provided a record of IADV as registered over the ocean; it is unclear how/if these signals translated into terrestrial climate. The speleothem-based regional monsoon IADV reconstructions presented in Chapter 3 therefore provide a unique insight into IADV over the land.

The research in chapter 4 on the registration of abrupt events during the Holocene further demonstrates the power of the SISAL database. Capturing short-lived abrupt climate events is a challenge in palaeoclimate research; records need to have high temporal resolution to capture short-lived events (Lechleitner *et al.*, 2018), whilst the correlation of abrupt excursions across numerous records requires low age uncertainties (Daley *et al.*, 2011; Bini *et al.*, 2019) to be confident that they are the same event. Many palaeoclimate records do not meet both these criteria. The most recent global-scale synthesis of the 8.2 ka event (Morrill *et al.*, 2013) selected records with a sampling resolution of 50 years or better and age uncertainties that were “better than several hundred years”. These criteria are less than ideal, because a 50-year sampling resolution would only give ~3 data points spanning the 8.2 ka event and the age uncertainties could be substantially larger than the duration of the 8.2 ka event. However, stricter criteria would have severely limited the number of records in the synthesis. This shows the difficulty in investigating past abrupt events; compromises on data quality are often required, which could lead to spurious results and obscure the big-picture climate signals. The 4.2 ka event is another example of this problem. The signals identified as the event are often smaller than the noise of the palaeo-records (Ön *et al.*, 2021) and the possible incorrect identification of the event because of poor chronology or low resolution would therefore obscure the reconstructed regional and global signals. Analyses drawing on

the SISAL database circumvent many of these problems: strict criteria were used to detect abrupt events in chapter 4, but this had minimal impact on the number of records used in the analyses. The availability of seven different SISAL age chronologies, each with multiple realisations providing confidence intervals on age assignments, allowed both inherent dating uncertainties and the uncertainties that arise from the choice of age model to be examined in detail, to explore which excursions could plausibly be the same abrupt event. Speleothem data in the SISAL database were the basis for the first global synthesis of the 8.2 ka event that included timing and duration for all records.

The SISAL database has provided the opportunity to process and analyse records using numerous statistical techniques. The use of these techniques to identify features in the palaeo-record objectively is a major feature of the research in this thesis but is comparatively new in speleothem research. For example, compositing numerous records (whereby records are processed in a consistent manner, then combined to determine a coherent regional signal) has been frequently used with charcoal records (Power *et al.*, 2008; Daniau *et al.*, 2012). However, this approach has not been widely used in speleothem research. Compositing is advantageous because it allows common features and trends across numerous records in a region to be identified and highlighted. The importance of features that are only observed in one or two individual records, and therefore do not reflect regional climate, is minimised through compositing. These composites help to minimise the impact of variation in $\delta^{18}O_{spel}$ signals that relate to soil, karst and cave processes, which cannot be expected to have the same effect on speleothems from different sites (or even individual records from the same site) due to the diversity of cave, karst and soil conditions. Furthermore, uncertainty within a regional trend can be quantified by bootstrap resampling of the records (Daniau *et al.*, 2012), whereby a high degree of agreement amongst records gives narrow confidence intervals and less agreement gives wider intervals. Speleothem composites were used in chapters 2 and 3 to identify regional signals in Holocene monsoon climate evolution. These regional composites also provide a better comparison with climate models (see section 5.2).

Compositing requires separation of speleothems records into distinct regions. In chapter 2, regionalisation was confirmed using ordination techniques: Principal Coordinate Analysis (PCoA) was used to investigate

the (dis)similarity between speleothem records, then Redundancy Analysis (RDA) was used to investigate how this (dis)similarity related to the records' geographic location (longitude and latitude). This novel approach allowed investigation of regional versus global patterns exhibited by the SISAL speleothem records.

The breakpoint analysis employed in chapter 4 is a way of identifying abrupt events objectively by an iterative statistical approach. Many previous studies have identified abrupt events by eye (e.g. Dykoski *et al.*, 2005; Shao *et al.*, 2006; Stríkis *et al.*, 2011), but this approach can introduce biases that influence the results and identified excursions may not necessarily be statistically significant above the noise of the records. Ön et al. (2021) used a Bayesian structural time series approach to determine the significance of the 4.2 ka event in numerous records that have been cited as evidence for the event. They found that over 40 % (8/19) of the records show no statistically significant excursion or change at 4.2 ka. This emphasises why it is important to use techniques such as break-point analysis to identify statistically significant abrupt excursions in the records. The objective approach used to identify abrupt events was made possible by the SISAL database; the large number of records allowed many globally distributed records to be analysed, and the consistent structure of the database allowed records to be easily selected (based on suitable sampling resolution, length, age uncertainties) then iteratively analysed.

The SISAL database provides a unique resource to examine past climate variability. Nevertheless, the research in this thesis was sometimes limited by the spatial and temporal distribution of the data. One example of this is the lack of records in the core region of the WAfM (West African Monsoon). Analysis of monsoon variability in this region from a speleothem perspective could have provided insights into the early to mid-Holocene expansion of the WAfM. This is not a shortcoming of the SISAL database, which includes approximately three quarters of all identified speleothem records (Comas-Bru et al., 2020), but reflects a comparative lack of speleothem research in this region and insufficient high-quality records to construct regional composites. Another region that could have benefitted from more data is CAM (Central American Monsoon). Only one SISAL record from this region covers most of the Holocene. Discontinuous records are harder to combine into regional composites because the necessary standardisation (either via

calculating z-scores, or anomalies) requires a base period that is common across all records. The lack of a robust basis for creating composites for the CAM precludes investigating whether the significant spatial variability identified in lake records for the late Holocene, with a gradient observed in the present between the wetter, tropical south and drier sub-tropical north (Metcalfe, Barron and Davies, 2015), is realistic. The SAM (South American Monsoon) domain also shows spatial heterogeneity in monsoon precipitation between the northeast and southwest of the region at the present-day. This dipole pattern was identified in its Holocene evolution (chapter 2), but lack of data meant that it was not possible to determine whether this pattern was present at other timescales.

Most of the analyses presented in this thesis focused on the Holocene because the number of available records in SISAL is much reduced further back in time. Although individual Last Interglacial records were used to compare with the Holocene records in chapter 2 to determine whether there are similar trajectories during the two intervals, there were insufficient records to construct composite curves for each region. Although chapter 2 includes an analysis of regional signals during the Last Glacial Maximum, the thesis has not focused on glacial climates although this could have provided a fuller picture of monsoon climate variability under considerably different conditions to today. Further expansion of the SISAL database would make it worthwhile to revisit this. Similarly, it would be interesting for comparison with the analyses of the 8.2 ka event to examine regional-scale monsoon evolution during glacial Dansgaard-Oeschger warming events and during Heinrich events. This would provide insights into the differences in monsoon climate sensitivity to large freshwater fluxes into the North Atlantic during interglacial and glacial periods.

Regardless of the gaps in data coverage, the research in this thesis has demonstrated the insights that a large-scale speleothem synthesis can provide into past monsoon variability. Speleothem research is a rapidly growing discipline: ~270 more speleothem $\delta^{18}O$ records have been published and identified by the SISAL working group since the creation of the first version of the SISAL database. The availability of these data will make it possible to conduct statistical analyses of the sort employed in this thesis to address other palaeoclimate questions.

Future speleothem research should focus on the gaps identified by the SISAL database to advance the field. Speleothem records from the West African monsoon region would allow every region to be represented in global reconstructions. More records from the southern hemisphere will provide a more balanced picture of northern versus southern hemisphere monsoon climate change, whilst more glacial climate records will allow for a more detailed comparison of monsoon climate change under different boundary conditions.

5.2 Lessons from data-model comparisons

Data-model comparisons can be used to provide a detailed understanding of past monsoon climate variability, by both identifying the large-scale patterns of change (through the observations) and investigating the underlying causes and mechanisms (through the models). This approach was employed by the COHMAP (Cooperative Holocene Mapping Project) group, where global climate was reconstructed at 3,000-year intervals from the Last Glacial Maximum to present, using lake, pollen and marine records. These syntheses were compared to climate model simulations of the same intervals and established, for the first time, the close relationship between the northern hemisphere monsoon climates and orbital forcing (Kutzbach and Street-Perrott, 1985; COHMAP Members, 1988). Since then, similar data-model approaches have been applied using a growing range and number of paleoclimate records, including charcoal (Daniau *et al.*, 2012; Brücher *et al.*, 2014; Martin Calvo, Prentice and Harrison, 2014), pollen (Texier *et al.*, 1997; Harrison and Prentice, 2003; Wohlfahrt, Harrison and Braconnot, 2004) and lake records (Jolly *et al.*, 1998; Harrison *et al.*, 2003; Yu *et al.*, 2003; Bartlein, Harrison and Izumi, 2017). However, speleothem records have not been frequently used for this kind of data-model comparison.

The development of isotope-enabled models has enabled more direct comparisons between speleothem data and models (Sturm, Zhang and Noone, 2010). Speleothems have been used to evaluate the ability of climate models is several studies (Wackerbarth *et al.*, 2012; Gierz, Werner and Lohmann, 2017; Comas-Bru *et al.*, 2019). Some studies have used climate model simulations to explain past $\delta^{18}O_{spel}$ observations (Lewis *et al.*, 2010; Pausata *et al.*, 2011; Tabor *et al.*, 2018; J. Hu *et al.*, 2019; Tabor, Otto-Bliesner and Liu, 2020), however these studies generally use a small handful of speleothem records and focus on one

region. The speleothem-based data-model comparisons carried out in chapters 2 and 3 of this thesis were employed to carry this type of approach a stage further, using larger numbers of records to look at monsoon climates. An isotope-based data-model comparison was used in chapter 2 of this thesis to investigate which climate processes were responsible for the observed Holocene and mid-Holocene-Last Glacial Maximum-Last Interglacial $\delta^{18}O_{spel}$ evolution. Comparisons were carried out for all the monsoon regions with sufficient data. The findings from this data-model study confirmed the ability of $\delta^{18}O_{spel}$ records to record past monsoon intensity, mainly via the processes of regional precipitation changes and changes in atmospheric circulation (driving changes in moisture source location and transport pathway). The results from this study also demonstrated regional differences in the importance of different drivers of $\delta^{18}O_{spel}$. These techniques could profitably be applied to different time periods (such as the last glacial period), timescales of variability (e.g. interdecadal to centennial) and regions (such as the mid to high latitudes) in the future.

In chapter 2, it was necessary to infer processes associated with atmospheric circulation (source location, moisture pathways) and precipitation recycling, but these could be directly included in analyses if climate models incorporated moisture tagging so that the initial source of water vapour can be traced (Hu *et al.*, 2019; Kathayat *et al.*, 2021). Unfortunately, relatively few isotope-enabled palaeoclimate simulations have included moisture tagging and there are none for Holocene evolution, because it introduces further components into already complex and computationally expensive models. The multiple regression analyses used to disentangle the climate influences on $\delta^{18}O$ in chapter 2 relied on seven equilibrium experiments spanning the Holocene epoch (LeGrande and Schmidt, 2009) and the linear regressions were therefore made using only a small number of data points. Transient isotope-enabled simulations of the Holocene epoch could provide a far greater number of data points for the analysis and thus provide a test of the robustness of chapter 2's conclusions. However, there are no isotope-enabled transient Holocene simulations. An isotope-enabled version of the transient Trace-21ka simulations is currently being run (iTRACE-21) (He *et al.*, 2021a; He *et al.*, 2021b), which will provide an exciting opportunity for isotope-enabled data-model comparisons in the near future.

Previous speleothem data-model comparisons have made direct comparisons of individual speleothem records with simulated $\delta^{18}O_{precip}$ in co-located model grids (e.g. Wackerbarth *et al.*, 2012). However, such comparisons require a conversion of either the observed $\delta^{18}O_{spel}$ values or the simulated $\delta^{18}O_{precip}$ values, and a calculation of values as anomalies (where signals are given relative to either the pre-industrial or present day). This requires speleothems to record both the present-day or pre-industrial period and the period of interest, which often severely limits the number of records that can be included (Comas-Bru *et al.*, 2019). The methodology for data-model comparison from Comas-Bru *et al.* (2019) involved converting $\delta^{18}O_{spel}$ values to their drip water equivalent, using an empirical speleothem-based calcite-water fractionation factor and mean annual surface air temperatures simulated by the climate models. This approach assumes that drip water $\delta^{18}O$ values correspond closely to the annual precipitation-weighted mean $\delta^{18}O_{precip}$ values above the cave, and that cave temperatures are accurately estimated by simulated mean annual temperature at the model-grid scale.

Another approach for comparisons between speleothem records and models involves the transformation of modelled $\delta^{18}O_{precip}$ values into their equivalent $\delta^{18}O_{spel}$ values using speleothem system models. These models use simplified representations of the soil-epikarst-cave system to approximate $\delta^{18}O_{spel}$ values (Bradley *et al.*, 2010; Truebe, Ault and Cole, 2010; Dee *et al.*, 2015). However, they require estimates of mean epikarst transit time, with the exact choice of value having a significant (first order) effect on modelled $\delta^{18}O_{spel}$ values (Dee *et al.*, 2015). Karst and cave parameters are hard to estimate for a global network of speleothems, as many of these sites have not been monitored. Furthermore, epikarst and caves are dynamic environments and so these parameters are likely to change through time.

These direct data-model comparisons therefore require several assumptions and estimates, adding uncertainty to the analyses. The data-model comparisons carried out in chapter 2 and 3 circumvent several of these issues by taking a more simplistic but effective approach. Regional-scale observations (using composites) were compared with regional-scale simulated $\delta^{18}O_{precip}$ and monsoon climate variable trends. This approach circumvented the issue of directly comparing an individual record with the model grid (that can encompass hundreds of kilometres). It also allows the regional climate trends to be

examined (in both simulations and observations), minimising the importance of anomalous records or model grids and instead emphasising the large-scale picture. Conversions of observed $\delta^{18}O_{spel}$ or simulated $\delta^{18}O_{precip}$ are not required in this approach.

The comparisons carried out in chapters 2 and 3 showed a good agreement between the regional evolution of speleothems and models, showing that the models are simulating physically plausible causes and processes. In chapter 2, the similarity between the regional evolution of $\delta^{18}O_{spel}$ and $\delta^{18}O_{precip}$ (simulated by a fully coupled ocean-atmosphere climate model) demonstrated that monsoon climate changes through the Holocene can be explained by the imposed boundary conditions, including a significant influence from orbital forcing, with modulation by oceanic feedbacks and the remnant Laurentide ice sheet (at 9 ka). In chapter 3, the similarity between simulated and observed regional IADV evolution suggests that monsoon IADV changes can be explained by orbital forcing and internal feedbacks. These are amongst the most significant findings in this project; speleothem oxygen isotope records may be a mixed signal of numerous climate and non-climate variables and climate models continue to have systematic biases and inaccuracies, but the consistency between speleothem data and models indicates that the climate change reconstructed in these chapters is real and robust.

The use of climate models to explain the speleothem observations relies on the models simulating accurate (and therefore plausible) $\delta^{18}O_{precip}$ changes. The simulations in chapters 2 and 3 were accurate, enabling data-model comparisons. In chapter 4, we showed that the 8.2 ka $\delta^{18}O_{spel}$ anomalies were globally distributed, with significant magnitudes and short (~150 to 200 year) durations. The isotope-enabled climate model simulations of the 8.2 ka event fail to reproduce these $\delta^{18}O_{spel}$ observations. For example, isotope-enabled 8.2 ka simulations using the GISS (LeGrande and Schmidt, 2008) and the HadCM3 (Tindall and Valdes, 2011) models only produce very small and/or short-lived (<40 years) $\delta^{18}O_{precip}$ signals. A simulation run using the University of Victoria's climate model (Aguiar *et al.*, 2021) underestimates 8.2 ka $\delta^{18}O_{precip}$ signals in the tropics. The findings in chapter 4 therefore emphasise the need for improved isotope-enabled 8.2 ka simulations. A non-isotope-enabled simulation from the HadCM3 model using a scenario of ice saddle collapse has produced temperature anomalies in the North

Atlantic that have the same duration and magnitude as observations (Matero *et al.*, 2017). This suggests that isotope-enabled simulations of the 8.2 ka event which are based on a similar ice saddle collapse scenario could be more realistic and potentially show a better agreement with the 8.2 ka $\delta^{18}O_{spel}$ synthesis from chapter 4, providing insight into the most likely scenario of the meltwater pulse that triggered the global event and allowing for investigations of the teleconnections responsible for the global climate response.

Future data-model comparison research will require more isotope-enabled simulations. These simulations provide a more direct comparison with numerous palaeoclimate archives, from speleothems to lake, marine and peat cores. Furthermore, more frequent use of moisture tagging and tracing in these simulations will provide researchers with the data needed to disentangle the processes and mechanisms behind past $\delta^{18}O$ and climate changes.

Further progression of the data-model comparison field is the transformation of speleothem or modelled $\delta^{18}O$ values (using speleothem system models) to convert $\delta^{18}O_{precip}$ to $\delta^{18}O_{spel}$ values, or vice versa. This would allow more detailed and direct comparisons between models and speleothem data. However, this will not be feasible until speleothem studies consistently and systematically include data on cave temperature, pCO_2, humidity, karst water transit times and an estimation of which months are contributing to drip water $\delta^{18}O$. Future speleothem research should therefore be collecting these measurements, to aid the climatic interpretation, and transformation, of speleothem $\delta^{18}O$ values.

5.3 Global versus regional monsoons

Tropical speleothem records in the SISAL database show a global-scale organisation at multi-millennial timescales (chapter 2) and during centennial abrupt events (chapter 4). This is consistent with the "global monsoon" framework (Trenberth, Stepaniak and Caron, 2000). The global monsoon is a key component of the tropical overturning circulation and is closely connected to Hadley (meridional) cells. Therefore, a global monsoon response is expected when there are changes in meridional energy gradients.

Through the Holocene epoch, orbitally induced insolation changes resulted in enhanced (reduced) seasonality in the northern (southern) hemisphere during the early and mid-Holocene (relative to today), driving a change in interhemispheric energy gradients. Summer insolation and seasonal amplitude gradually diminished to present-day values in the northern hemisphere through the mid and late Holocene, and vice versa for the southern hemisphere. Under these conditions, it is expected that the northern hemisphere monsoons were stronger in the early and mid-Holocene and weakened in the late-Holocene. The opposite is expected for the southern hemisphere monsoons, with weaker summer monsoons in the early and mid-Holocene, strengthening in the late Holocene. Numerous palaeoclimate studies over the last few decades have confirmed these trends; lake and pollen records across the northern hemisphere monsoons have shown wetter conditions in the early and mid-Holocene (COHMAP Members, 1988; Street-Perrott and Perrott, 1993; Lézine *et al.*, 2011; Metcalfe, Barron and Davies, 2015; Goldsmith *et al.*, 2017b; Misra, Tandon and Sinha, 2019), when northern hemisphere summer insolation was higher. Individual speleothem records also show more depleted $\delta^{18}O_{spel}$ values from the early to mid-Holocene (Fleitmann *et al.*, 2003; Cai *et al.*, 2010; Tan *et al.*, 2020), interpreted as a stronger monsoon, although most studies have only used a small number of records to investigate this hemispheric picture. In the southern hemisphere, drier conditions at the early and mid-Holocene have been inferred for South America from pollen and lake records (Prado *et al.*, 2013; Smith and Mayle, 2018), and from less depleted $\delta^{18}O_{spel}$ values (Cruz *et al.*, 2009; Cheng *et al.*, 2012). This global pattern is also a robust feature of the latest ensemble of mid-Holocene climate model simulations from phase 4 of the Palaeoclimate Modelling Intercomparison Project, PMIP4 (Brierley *et al.*, 2020). The findings in chapter 2 therefore further support the consensus that there was a global monsoon climate response to orbital forcing through the Holocene epoch. The research in chapter 2 was the first to investigate the Holocene global monsoon response using the SISAL database. The inclusion of 125 speleothem records in the analysis of regional and global patterns ensured that the identified global monsoon pattern was robust. Furthermore, by using ordination techniques to relate speleothem (dis)similarity to geographic location, we were able to show separation of northern and southern hemisphere trends in an objective way, rather than relying on visual inspection.

The globally coherent picture seen in monsoon Holocene trends breaks down when examining changes in IADV (chapter 3) since the amplitude of IADV through the Holocene differs between monsoon regions. The ISM (Indian Monsoon) and EAM (East Asian Monsoon) show opposite trends in IADV amplitude, despite experiencing the same summer insolation changes and long-term evolution in mean climate. This difference in response between the two regions is also seen in an ensemble of transient climate model simulations. This indicates that the observed IADV trends are not simply a result of unforced internal variability, which would be unlikely to produce agreement between the observations and the models. Although these trends in IADV are probably related to changes in orbital forcing, the difference between the EAM and ISM trends indicates that the relationship between monsoon precipitation IADV and orbital forcing is neither linear nor direct. These results suggest that orbital forcing influences the internal modes of variability (including ENSO, PDO, IOD and AMO), which then produces a complex, spatially and temporally variable, effect on the regional monsoons.

The identification and examination of abrupt events in chapter 4 has shown that the 8.2 ka event is the most significant and globally extensive abrupt event in the Holocene epoch. Examination of the spatial fingerprint of this event shows a global monsoon pattern (i.e. an antiphase interhemispheric trend) with largely positive $\delta^{18}O_{spel}$ anomalies across the northern hemisphere tropics and negative anomalies in the southern hemisphere tropics. This spatial pattern is consistent with a freshwater influx induced temperature gradient in the Atlantic Ocean. At 8.2 ka, a meltwater influx from the Laurentide Ice Sheet into the North Atlantic (via the Labrador Sea) (Barber *et al.*, 1999; Gregoire, Payne and Valdes, 2012) dramatically cooled regional SSTs (sea surface temperatures) by up to ~3°C (Hoffman *et al.*, 2012) and reduced bottom water formation in the North Atlantic (Kleiven *et al.*, 2008) slowing down the AMOC. Both factors introduced a strong thermal interhemispheric contrast in the Atlantic region and would therefore be capable of inducing a change in global monsoon climates, assuming the freshwater influx was large enough. Early research suggested the 8.2 ka event was confined to the north Atlantic region (Alley *et al.*, 1997; Rohling and Pälike, 2005), however later work based (mainly) on speleothem $\delta^{18}O$ records suggested this was not true. A global synthesis by Morrill et al. (2013), using speleothems with several other palaeoclimate archives, showed an overall wetting response in the northern hemisphere

tropics and drying in the southern hemisphere tropics. The synthesis in chapter 4 used a far greater number of speleothem records with more precise chronologies and higher temporal resolution and corroborated the finding that the short-lived (~160 year) 8.2 ka event was registered across the tropics. This demonstrates the sensitivity of global monsoon climates to changes in the North Atlantic. Furthermore, by also constraining the timing and duration of the 8.2 ka excursions, we were able to show that the global monsoon responded rapidly via atmospheric teleconnections. However, the analyses in chapter 4 have shown no evidence of a significant global monsoon response to the mid and late Holocene abrupt events that have been identified in the literature. The periods with significant abrupt excursions identified do not coincide with any commonly cited mid to late Holocene abrupt events, notably including the 4.2 ka event. This indicates that the later Holocene events are either small in magnitude (and therefore hard to distinguish) or they are not a significant feature in the tropics. Several drivers of these abrupt events have been suggested that would likely not have a globally extensive and/or coherent response, including solar variability (Bond *et al.*, 2001; Fleitmann *et al.*, 2003; Gupta, Das and Anderson, 2005) and volcanicity (Kobashi *et al.*, 2017). It could also be that these abrupt events are not forced, but instead result from internal variability which would produce a more spatially heterogeneous climate response with more complex evolution through time. The ~4.2 ka signals that have been identified in previous studies often show different timings, even in nearby records (Bini *et al.*, 2019). Furthermore, the evolution of the identified 4.2 ka events can differ substantially between palaeoclimate records (Kaniewski *et al.*, 2018; Bini *et al.*, 2019). Both of these features support the idea that the event was an unforced oscillation.

A consistent feature across the research in this thesis is the complexity of $\delta^{18}O_{spel}$ signals in the IAM (Indonesian-Australian Monsoon) and CAM regions. As shown in both chapter 2 and 4, the IAM and CAM regions do not fit into the global monsoon picture. IAM Holocene evolution does not follow southern hemisphere tropical summer insolation (Fig. 5.1 right) and there is no 8.2 ka event recorded there, despite being observed in the other southern hemisphere monsoon regions. CAM showed no consistent regional changes in $\delta^{18}O_{spel}$ through the Holocene (Fig. 5.1 left), and mixed signals during the 8.2 ka event. These two regions have a large oceanic component (relative to land) and interactions between land and sea may play a strong role in determining their response.

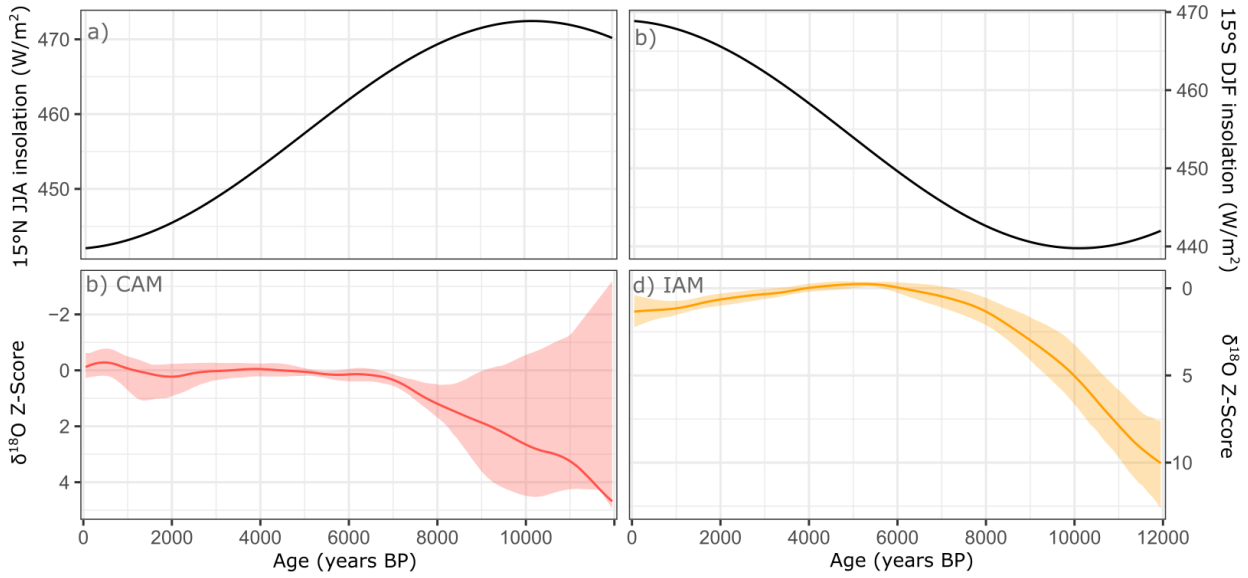

Figure 5.1 Central American Monsoon (CAM) and Indonesian-Australian Monsoon (IAM) speleothem $\delta^{18}O$ evolution through the Holocene epoch. Speleothem $\delta^{18}O$ records have been standardised to z-scores, using a base period of 5,000 to 3,000 years BP. Composites have been constructed using a loess fit with a half window of 1,500 years, and 5% and 95% confidence intervals (obtained by bootstrap resampling by site). CAM evolution does not follow northern hemisphere summer insolation and there is no agreement amongst speleothem records in the early Holocene. IAM evolution does not follow southern hemisphere summer insolation.

Climate model simulations certainly indicate that ocean feedbacks influence the MH IAM. Zhao and Harrison (2012) compared an ensemble of atmosphere-only models to coupled ocean-atmosphere climate models (AOGCMs). The ensembles show a reduced mid-Holocene IAM in response to the orbitally induced reduction is southern hemisphere summer insolation. However, this reduction is weaker in the AOCGM simulations. Nevertheless, climate models do simulate reduced rainfall at the mid-Holocene in the IAM region. The most recent mid-Holocene simulations from PMIP4 show an overall reduction in mid-Holocene precipitation in the IAM, compared to present (Brierley *et al.*, 2020). This reduction is inconsistent with speleothem $\delta^{18}O$ records, which show $\delta^{18}O_{spel}$ signals that are indistinguishable from the present. This may reflect the fact that some feedback mechanisms are not fully or accurately incorporated in the models. There are fewer simulations of the 8.2 ka event and the analyses of these simulations have tended to focus on the North Atlantic climate response (Matero *et al.*, 2017; Aguiar *et al.*, 2021) and so provide little insight into the lack of an IAM 8.2 ka response. It is possible that the lack of response is because of distance from the North Atlantic region, but more likely that the oceanic processes that climate models indicate are influential at the MH also dampen the response during the 8.2 ka event. More 8.2 ka

simulations are needed, and there needs to be more focus on the response in the southern hemisphere tropics, to resolve this question.

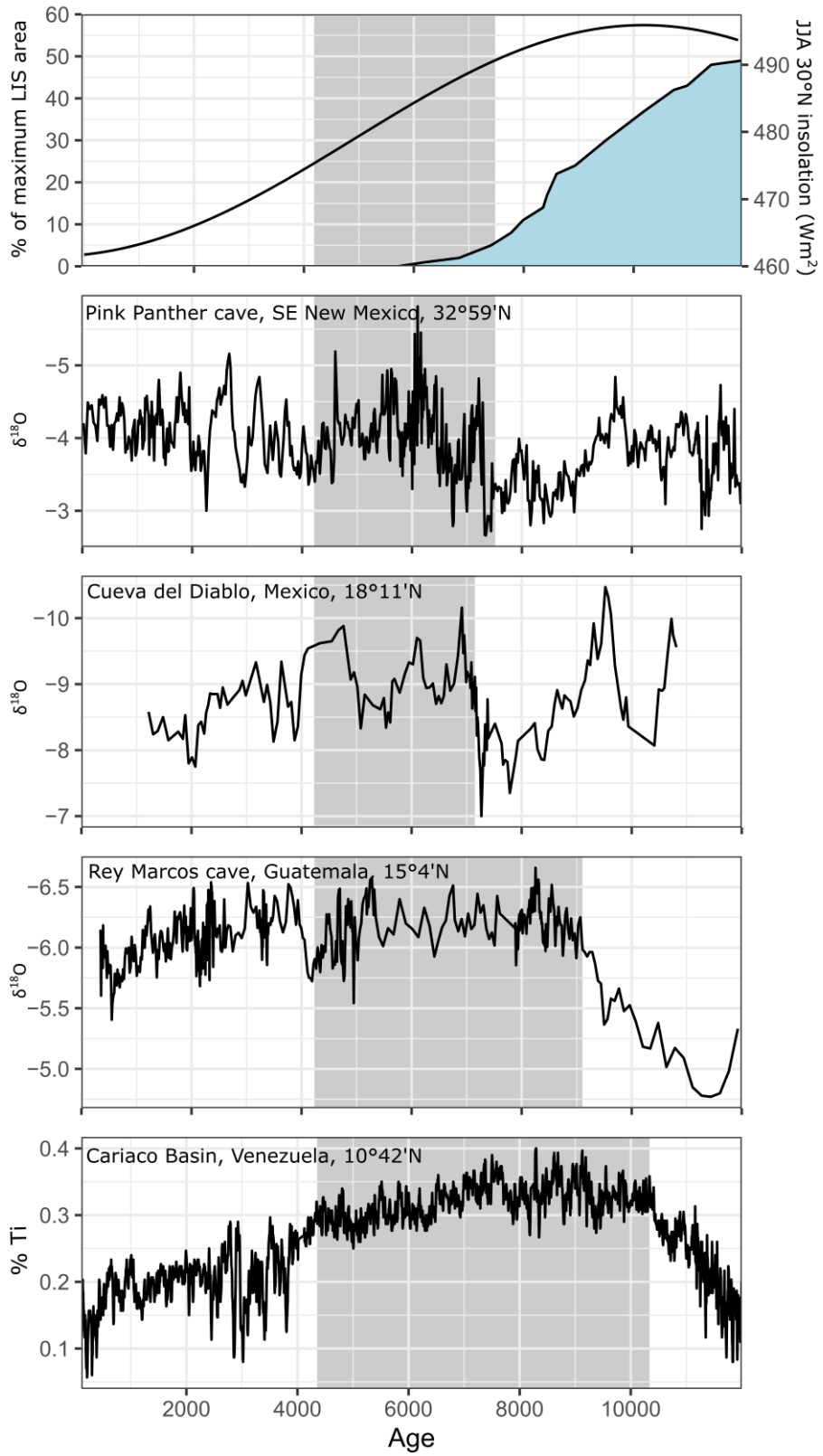

Figure 5.2 Comparison of Holocene CAM records, adapted from Metcalfe et al. (2015), including the Cariaco Basin % Ti record from Haug et al. (2001), and speleothem $\delta^{18}O$ records from Rey Marcos cave (Winter et al., 2020), Cueva del Diablo (Bernal et al., 2011) and Pink Panther cave (Asmerom et al., 2007). These are shown with local summer insolation and Dyke's (2004) estimate of the size of the Laurentide Ice Sheet. Records are ordered by latitude, to show the possible effect of the Laurentide Ice on CAM records.

The evolution of $\delta^{18}O_{spel}$ through the Holocene in the CAM region differs from the other northern hemisphere regional monsoons (Fig. 5.1 left). Holocene climate reconstructions from lake records also show a different evolution from the rest of the northern hemisphere tropics (Metcalfe, Barron and Davies, 2015). CAM climate is influenced by conditions in the Gulf of Mexico. Interaction between the terrestrial monsoon climate and the Gulf of Mexico could explain the complex climate response in this region to orbital forcing and meltwater fluxes through the Holocene. Metcalfe et al. (2015) theorised that early Holocene climate evolution in CAM reflected the influence of the remnant Laurentide ice sheet over North America, such that the presence and retreat of the Laurentide ice sheet influenced the magnitude and rate of change of warming over the North American land mass, Gulf of Mexico SSTs and the northward progression of the ITCZ. This may have suppressed EH rainfall in much of the CAM region, counteracting the enhanced rainfall that is expected with higher summer insolation (Fig. 5.2). Climate models support a relationship between the presence of the Laurentide ice sheet and CAM climate (Feng, Hu and Oglesby, 2011).

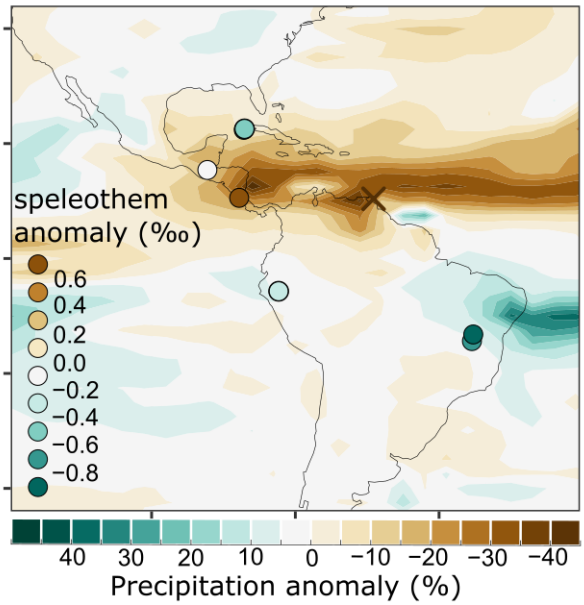

Figure 5.3 Speleothem 8.2 ka event $\delta^{18}O$ anomalies (from chapter 4) from the Americas, shown with simulated 8.2 ka event precipitation anomalies from Matero et al. (2017). Positive $\delta^{18}O$ anomalies from the Central American Monsoon (CAM) occur in a band of very dry anomalies, interpreted as a southwards displacement of the intertropical convergence zone (ITCZ).

There is little correlation or agreement amongst CAM palaeohydrological records from ~5 ka onwards, consistent with the lack of consistency amongst $\delta^{18}O_{spel}$ records. Lake records also show a complex and spatially heterogeneous pattern through this period (Metcalfe, Barron and Davies, 2015). This spatial

complexity is hard to reconcile with a change in the mean position of the ITCZ. Several studies have suggested that ENSO played a key role in CAM climate evolution through the late Holocene. ENSO variability was suppressed in the mid-Holocene but shifted toward modern values at ~5 ka (Carré *et al.*, 2021) and modern-day ENSO has a spatially heterogeneous influence on the region (Giannini, Kushnir and Cane, 2000). More studies are needed to investigate the possible link between CAM late Holocene evolution and ENSO.

The spatial heterogeneity of 8.2 ka signals in the CAM region may reflect the complex influence of the Gulf of Mexico moisture source. Records from the northern Gulf of Mexico (~27°N) show a significant negative excursion in sea water $\delta^{18}O$ values of ~0.8 ‰ at 8.2 ka (LoDico, Flower and Quinn, 2006) but there is no excursion in $\delta^{18}O$ values further south (at ~24°N) (Schmidt *et al.*, 2012). This spatial gradient in surface water $\delta^{18}O$ values during the 8.2 ka event likely reflects the tropical Atlantic source for the southern part of the Gulf of Mexico and the North American continent source of northernmost Gulf of Mexico waters. The negative $\delta^{18}O$ values of the moisture source are likely reflected in the northernmost CAM $\delta^{18}O$ signals. The positive $\delta^{18}O_{spel}$ anomalies observed south of ~15°N likely reflect drier 8.2 ka conditions, as inferred from lake records (Morrill *et al.*, 2013) and simulated precipitation patterns (Wagner *et al.*, 2013; Morrill *et al.*, 2014; Matero *et al.*, 2017). The spatial separation of sites with negative versus positive $\delta^{18}O_{spel}$ anomalies coincides with the separation of weak precipitation anomalies and strong dry anomalies simulated by Matero et al. (2017) (Fig. 5.3). Although the 8.2 ka anomalies identified in the CAM region have a lower confidence than other regions, due to larger age uncertainties and small $\delta^{18}O$ excursions, the consistency of these anomalies with simulated precipitation anomalies suggests the latitudinal dipole is real. The results from chapter 4 again emphasise the complex climate variability in CAM, and the need for a) isotope-enabled simulations of the 8.2 ka event and b) more high-quality speleothem records from CAM.

5.4 Concluding remarks

The research in this thesis has demonstrated the ability of large-scale speleothem syntheses and data-model comparisons in improving our understanding of past monsoon climate.

This thesis has shown how comparisons between SISAL records and isotope-enabled climate models can be used to improve understanding of the climatic interpretation of the speleothem $\delta^{18}O$ records, including how multiple linear regression of isotope-enabled climate model variables can be used to disentangle the various climate processes that influence $\delta^{18}O_{spel}$. The results support the use of $\delta^{18}O_{spel}$ records as archives of monsoon climate, mainly via the processes of regional precipitation and atmospheric circulation changes.

Analysis of spatially distributed $\delta^{18}O_{spel}$ records has emphasised the globally coherent monsoon response to orbital forcing through the Holocene epoch, and during the abrupt 8.2 ka event, with both showing an interhemispheric, antiphase pattern. Global-scale analyses of speleothem records have also shown that the Indonesian-Australian and central American monsoon regions exhibit a more complex response to insolation changes and the 8.2 ka freshwater influx, which probably reflects complex land-ocean interactions in these two regions.

This thesis has provided the first regional reconstructions of monsoon precipitation interannual-interdecadal variability (IADV). Comparison of these reconstructions with simulated precipitation IADV from transient simulations has shown the complex interplay between orbital forcing and internal modes of variability in driving regionally distinct monsoon precipitation IADV evolution through the Holocene.

This thesis shows that the most significant abrupt event of (almost) global extent during the Holocene is the 8.2 ka event. The speleothem records indicate a timing and duration of this event similar to that observed in Greenland, indicating that the North Atlantic signal is rapidly transmitted via atmospheric teleconnections. There are no other significant abrupt events registered in global speleothem records during the mid- to late-Holocene.

5.5 References

Abram, N. J. *et al.* (2007) 'Seasonal characteristics of the Indian Ocean Dipole during the Holocene epoch', *Nature*, 445(7125), pp. 299–302. doi: 10.1038/nature05477.

Abram, N. J. *et al.* (2015) 'Optimized coral reconstructions of the Indian Ocean Dipole: An assessment of location and length considerations', *Paleoceanography*, 30(10), pp. 1391–1405. doi: 10.1002/2015PA002810.

Adams, D. K. and Comrie, A. C. (1997) 'The North American Monsoon', *Bulletin of the American Meteorological Society*, 78(10), pp. 2197–2213. doi: 10.1175/1520-0477(1997)078<2197:TNAM>2.0.CO;2.

Affolter, S. *et al.* (2019) 'Central Europe temperature constrained by speleothem fluid inclusion water isotopes over the past 14,000 years', *Science advances*, 5(6), p. eaav3809.

Aggarwal, P. K. *et al.* (2004) 'Stable isotope evidence for moisture sources in the asian summer monsoon under present and past climate regimes', *Geophysical Research Letters*, 31(8), pp. 2–5. doi: 10.1029/2004GL019911.

Aggarwal, P. K. *et al.* (2012) 'Stable isotopes in global precipitation: A unified interpretation based on atmospheric moisture residence time', *Geophysical Research Letters*, 39(11). doi: 10.1029/2012GL051937.

Aguiar, W. *et al.* (2021) 'Magnitude of the 8.2 ka event freshwater forcing based on stable isotope modelling and comparison to future Greenland melting', *Scientific Reports*, 11(1), p. 5473. doi: 10.1038/s41598-021-84709-5.

Allan, M. *et al.* (2018) 'High-resolution reconstruction of 8.2-ka BP event documented in Père Noël cave, southern Belgium', *Journal of Quaternary Science*, 33(7), pp. 840–852. doi: 10.1002/jqs.3064.

Alley, R. B. *et al.* (1997) 'Holocene climatic instability: A prominent, widespread event 8200 yr ago', *Geology*, 25(6), pp. 483–486. doi: 10.1130/0091-7613(1997)025<0483:HCIAPW>2.3.CO;2.

Amador, J. A. (2008) 'The Intra-Americas Sea low-level jet: Overview and future research', *Annals of the New York Academy of Sciences*, 1146, pp. 153–188. doi: 10.1196/annals.1446.012.

Andreoli, R. V. and Kayano, M. T. (2005) 'ENSO-related rainfall anomalies in South America and

associated circulation features during warm and cold Pacific decadal oscillation regimes', *International Journal of Climatology*, 25(15), pp. 2017–2030. doi: 10.1002/joc.1222.

Aragão, L. E. O. C. *et al.* (2018) '21st Century drought-related fires counteract the decline of Amazon deforestation carbon emissions', *Nature Communications*, 9(1), p. 536. doi: 10.1038/s41467-017-02771-y.

Araguás-Araguás, L., Froehlich, K. and Rozanski, K. (1998) 'Stable isotope composition of precipitation over southeast Asia', *Journal of Geophysical Research Atmospheres*, 103(D22), pp. 28721–28742. doi: 10.1029/98JD02582.

Ashok, K., Guan, Z. and Yamagata, T. (2001) 'Impact of the Indian Ocean dipole on the relationship between the Indian monsoon rainfall and ENSO', *Geophysical Research Letters*, 28(23), pp. 4499–4502. doi: 10.1029/2001GL013294.

Asmerom, Y. *et al.* (2007) 'Solar forcing of Holocene climate: New insights from a speleothem record, southwestern United States', *Geology*, 35(1), p. 1. doi: 10.1130/G22865A.1.

Atsawawaranunt, K. *et al.* (2018) 'The SISAL database: A global resource to document oxygen and carbon isotope records from speleothems', *Earth System Science Data*, 10, pp. 1687–1713. doi: 10.5194/essd-10-1687-2018.

Ayliffe, L. K. *et al.* (2013) 'Rapid interhemispheric climate links via the Australasian monsoon during the last deglaciation', *Nature Communications*, 4(1), pp. 1–6. doi: 10.1038/ncomms3908.

Bader, J. *et al.* (2020) 'Global temperature modes shed light on the Holocene temperature conundrum', *Nature Communications*, 11(1), p. 4726. doi: 10.1038/s41467-020-18478-6.

Bagniewski, W., Meissner, K. J. and Menviel, L. (2017) 'Exploring the oxygen isotope fingerprint of Dansgaard-Oeschger variability and Heinrich events', *Quaternary Science Reviews*, 159, pp. 1–14. doi: 10.1016/j.quascirev.2017.01.007.

Bailey, A., Posmentier, E. and Feng, X. (2018) 'Patterns of evaporation and precipitation drive global

isotopic changes in atmospheric moisture', *Geophysical Research Letters*, 45(14). doi: 10.1029/2018GL078254.

Baker, A. *et al.* (2008) 'Annually laminated speleothems: a review', *International Journal of Speleology*, 37(3), pp. 193–206. doi: 10.5038/1827-806X.37.3.4.

Baker, A. *et al.* (2019) 'Global analysis reveals climatic controls on the oxygen isotope composition of cave drip water', *Nature Communications*, 10(2984). doi: 10.1038/s41467-019-11027-w.

Baker, P. A. *et al.* (2005) 'Holocene hydrologic variation at Lake Titicaca, Bolivia/Peru, and its relationship to North Atlantic climate variation', *Journal of Quaternary Science*, 20(7–8), pp. 655–662. doi: 10.1002/jqs.987.

Baldini, J. U. L. *et al.* (2008) 'Very high-frequency and seasonal cave atmosphere P_{CO2} variability: Implications for stalagmite growth and oxygen isotope-based paleoclimate records', *Earth and Planetary Science Letters*, 272(1–2), pp. 118–129. doi: 10.1016/j.epsl.2008.04.031.

Bar-Matthews, M. *et al.* (2003) 'Sea–land oxygen isotopic relationships from planktonic foraminifera and speleothems in the Eastern Mediterranean region and their implication for paleorainfall during interglacial intervals', *Geochimica et Cosmochimica Acta*, 67(17), pp. 3181–3199. doi: 10.1016/S0016-7037(02)01031-1.

Bar-Matthews, M., Ayalon, A. and Kaufman, A. (1997) 'Late Quaternary paleoclimate in the eastern Mediterranean region from stable isotope analysis of speleothems at Soreq Cave, Israel', *Quaternary Research*, 47(2), pp. 155–168. doi: 10.1006/qres.1997.1883.

Barber, D. C. *et al.* (1999) 'Forcing of the cold event of 8,200 years ago by catastrophic drainage of Laurentide lakes', *Nature*, 400(6742), pp. 344–348. doi: 10.1038/22504.

Barichivich, J. *et al.* (2018) 'Recent intensification of Amazon flooding extremes driven by strengthened Walker circulation', *Science Advances*, 4(9). doi: 10.1126/sciadv.aat8785.

Barlow, M., Nigam, S. and Berbery, E. H. (1998) 'Evolution of the North American monsoon system',

Journal of Climate, 11(9), pp. 2238–2257. doi: 10.1175/1520-0442(1998)011<2238:EOTNAM>2.0.CO;2.

Bartlein, P. J., Harrison, S. P. and Izumi, K. (2017) 'Underlying causes of Eurasian midcontinental aridity in simulations of mid-Holocene climate', *Geophysical Research Letters*, 44(17), pp. 9020–9028. doi: 10.1002/2017GL074476.

Battisti, D. S., Ding, Q. and Roe, G. H. (2014) 'Coherent pan-Asian climatic and isotopic response to orbital forcing of tropical insolation', *Journal of Geophysical Research: Atmospheres*, 119(21), pp. 11,997-12,020. doi: 10.1002/2014JD021960.

Benson, A. *et al.* (2021) 'A speleothem record from Portugal reveals phases of increased winter precipitation in western Iberia during the Holocene', *Holocene*, 31(8), pp. 1339–1350. doi: 10.1177/09596836211011666.

Berbery, E. H. and Barros, V. R. (2002) 'The hydrologic cycle of the La Plata basin in South America', *Journal of Hydrometeorology*, 3(6), pp. 630–645. doi: 10.1175/1525-7541(2002)003<0630:THCOTL>2.0.CO;2.

Berkelhammer, M. *et al.* (2010) 'Persistent multidecadal power of the Indian Summer Monsoon', *Earth and Planetary Science Letters*, 290(1–2), pp. 166–172. doi: 10.1016/j.epsl.2009.12.017.

Bernal, J. P. *et al.* (2011) 'A speleothem record of Holocene climate variability from southwestern Mexico', *Quaternary Research*, 75(1), pp. 104–113. doi: 10.1016/j.yqres.2010.09.002.

Bernal, J. P. *et al.* (2016) 'High-resolution Holocene South American monsoon history recorded by a speleothem from Botuverá Cave, Brazil', *Earth and Planetary Science Letters*, 450, pp. 186–196.

Biasutti, M. *et al.* (2018) 'Global energetics and local physics as drivers of past, present and future monsoons', *Nature Geoscience*, 11(6), pp. 392–400. doi: 10.1038/s41561-018-0137-1.

Bini, M. *et al.* (2019) 'The 4.2 ka BP Event in the Mediterranean region: an overview', *Climate of the Past*, 15(2), pp. 555–577. doi: 10.5194/cp-15-555-2019.

Boch, R., Spötl, C. and Kramers, J. (2009) 'High-resolution isotope records of early Holocene rapid

climate change from two coeval stalagmites of Katerloch Cave, Austria', *Quaternary Science Reviews*, 28(23–24), pp. 2527–2538. doi: 10.1016/j.quascirev.2009.05.015.

Bond, G. *et al.* (1997) 'A pervasive millennial-scale cycle in North Atlantic Holocene and glacial climates', *Science*, 278(5341), pp. 1257–1266. doi: 10.1126/science.278.5341.1257.

Bond, G. *et al.* (2001) 'Persistent Solar Influence on North Atlantic Climate During the Holocene', *Science*, 294(5549), pp. 2130–2136. doi: 10.1126/science.1065680.

Bowen, G. J. and Revenaugh, J. (2003) 'Interpolating the isotopic composition of modern meteoric precipitation', *Water Resources Research*, 39(10). doi: 10.1029/2003WR002086.

Boyd, M. (2015) *Speleothems from warm climates: holocene records from the Caribbean and Mediterranean regions*. Stockholm University.

Braconnot, P. *et al.* (2004) 'Evaluation of PMIP coupled ocean-atmosphere simulations of the Mid-Holocene', in Battarbee, R. W., Gasse, F., and Stickley, C. E. (eds) *Past Climate Variability through Europe and Africa. Developments in Paleoenvironmental Research*. Dordrecht: Springer, pp. 515–533. doi: 10.1007/978-1-4020-2121-3_24.

Braconnot, P., Crétat, J., *et al.* (2019) 'Impact of multiscale variability on last 6000 years Indian and West African monsoon rain', *Geophysical Research Letters*, 46(23), pp. 14021–14029. doi: 10.1029/2019GL084797.

Braconnot, P., Zhu, D., *et al.* (2019) 'Strengths and challenges for transient Mid- to Late Holocene simulations with dynamical vegetation', *Climate of the Past*, 15(3), pp. 997–1024. doi: 10.5194/cp-15-997-2019.

Bradley, C. *et al.* (2010) 'Hydrological uncertainties in the modelling of cave drip-water $\delta^{18}O$ and the implications for stalagmite palaeoclimate reconstructions', *Quaternary Science Reviews*, 29(17–18), pp. 2201–2214. doi: 10.1016/j.quascirev.2010.05.017.

Braun, K. *et al.* (2019) 'Late Pleistocene records of speleothem stable isotopic compositions from

Pinnacle Point on the South African south coast', *Quaternary Research (United States)*, 91(1), pp. 265–288. doi: 10.1017/qua.2018.61.

Breitenbach, S. F. M. *et al.* (2010) 'Strong influence of water vapor source dynamics on stable isotopes in precipitation observed in Southern Meghalaya, NE India', *Earth and Planetary Science Letters*, 292(1–2), pp. 212–220. doi: 10.1016/j.epsl.2010.01.038.

Brierley, C. M. *et al.* (2020) 'Large-scale features and evaluation of the PMIP4-CMIP6 *midHolocene* simulations', *Climate of the Past*, 16(5), pp. 1847–1872. doi: 10.5194/cp-16-1847-2020.

Brücher, T. *et al.* (2014) 'Comparing modelled fire dynamics with charcoal records for the Holocene', *Climate of the Past*, 10(2), pp. 811–824. doi: 10.5194/cp-10-811-2014.

Bühler, J. C. *et al.* (2021) 'Comparison of the oxygen isotope signatures in speleothem records and iHadCM3 model simulations for the last millennium', *Climate of the Past*, 17(3), pp. 985–1004. doi: 10.5194/cp-17-985-2021.

Burns, S. J. *et al.* (1998) 'Speleothem-based paleoclimate record from northern Oman', *Geology*, 26(6), p. 499. doi: 10.1130/0091-7613(1998)026<0499:SBPRFN>2.3.CO;2.

Bustamante, M. G. *et al.* (2016) 'Holocene changes in monsoon precipitation in the Andes of NE Peru based on $\delta^{18}O$ speleothem records', *Quaternary Science Reviews*, 146, pp. 274–287. doi: 10.1016/J.QUASCIREV.2016.05.023.

Cai, W. *et al.* (2020) 'Climate impacts of the El Niño–Southern Oscillation on South America', *Nature Reviews Earth & Environment*, 1(4), pp. 215–231. doi: 10.1038/s43017-020-0040-3.

Cai, Y. *et al.* (2010) 'The variation of summer monsoon precipitation in central China since the last deglaciation', *Earth and Planetary Science Letters*, 291(1–4), pp. 21–31. doi: 10.1016/j.epsl.2009.12.039.

Cai, Y. *et al.* (2015) 'Variability of stalagmite-inferred Indian monsoon precipitation over the past 252,000 y', *Proceedings of the National Academy of Sciences of the United States of America*, 112(10), pp. 2954–2959. doi: 10.1073/pnas.1424035112.

Cai, Y. *et al.* (2021) 'Holocene variability of East Asian summer monsoon as viewed from the speleothem $\delta^{18}O$ records in central China', *Earth and Planetary Science Letters*, 558. doi: 10.1016/j.epsl.2021.116758.

Caley, T. and Roche, D. M. (2013) 'δ18O water isotope in the LOVECLIM model (version 1.0)-Part 3: A palaeo-perspective based on present-day data-model comparison for oxygen stable isotopes in carbonates', *Geoscientific Model Development*, 6, pp. 1505–1516. doi: 10.5194/gmd-6-1505-2013.

Carolin, S. A. *et al.* (2016) 'Northern Borneo stalagmite records reveal West Pacific hydroclimate across MIS 5 and 6', *Earth and Planetary Science Letters*, 439, pp. 182–193. doi: 10.1016/j.epsl.2016.01.028.

Carré, M. *et al.* (2021) 'High-resolution marine data and transient simulations support orbital forcing of ENSO amplitude since the mid-Holocene', *Quaternary Science Reviews*, 268, p. 107125. doi: 10.1016/j.quascirev.2021.107125.

Cauquoin, A., Werner, M. and Lohmann, G. (2019) 'Water isotopes-climate relationships for the mid-Holocene and preindustrial period simulated with an isotope-enabled version of MPI-ESM', *Climate of the Past*, 15(6), pp. 1913–1937. doi: 10.5194/cp-2019-72.

Chandan, D. and Peltier, W. R. (2020) 'African Humid Period Precipitation Sustained by Robust Vegetation, Soil, and Lake Feedbacks', *Geophysical Research Letters*, 47(21). doi: 10.1029/2020GL088728.

Chawchai, S. *et al.* (2021) 'Hydroclimate variability of central Indo-Pacific region during the Holocene', *Quaternary Science Reviews*, 253. doi: 10.1016/j.quascirev.2020.106779.

Chen, C., Zhao, W. and Zhang, X. (2021) 'Pacific Decadal Oscillation-like variability at a millennial timescale during the Holocene', *Global and Planetary Change*, 103448. doi: 10.1016/j.gloplacha.2021.103448.

Chen, S. *et al.* (2016) 'A high-resolution speleothem record of western equatorial Pacific rainfall: Implications for Holocene ENSO evolution', *Earth and Planetary Science Letters*, 442, pp. 61–71. doi: 10.1016/j.epsl.2016.02.050.

Chen, W. *et al.* (2020) 'Feedbacks of soil properties on vegetation during the Green Sahara period', *Quaternary Science Reviews*, 240, p. 106389. doi: 10.1016/j.quascirev.2020.106389.

Cheng, H. *et al.* (2006) 'A penultimate glacial monsoon record from Hulu Cave and two-phase glacial terminations', *Geology*, 34(3), pp. 217–220. doi: 10.1130/G22289.1.

Cheng, H., Edwards, R. L., *et al.* (2009) 'Ice age terminations', *Science*, 326(5950), pp. 248–252. doi: 10.1126/science.1177840.

Cheng, H., Fleitmann, D., Edwards, R. L., Wang, X., Cruz, F. W., Auler, A. S., Mangini, A., Wang, Y., Kong, X., Burns, S. J., *et al.* (2009) 'Timing and structure of the 8.2 kyr B.P. event inferred from $\delta^{18}O$ records of stalagmites from China, Oman, and Brazil', *Geology*, 37(11), pp. 1007–1010. doi: 10.1130/G30126A.1.

Cheng, H., Fleitmann, D., Edwards, R. L., Wang, X., Cruz, F. W., Auler, A. S., Mangini, A., Wang, Y., Kong, X. and Burns, S. J. (2009) 'Timing and structure of the 8.2 kyr BP event inferred from δ18O records of stalagmites from China, Oman, and Brazil', *Geology*, 37(11), pp. 1007–1010.

Cheng, H. *et al.* (2012) 'The Global Paleomonsoon as seen through speleothem records from Asia and the Americas', *Climate Dynamics*, 39(5), pp. 1045–1062. doi: 10.1007/s00382-012-1363-7.

Cheng, H., Sinha, A., *et al.* (2013) 'Climate change patterns in Amazonia and biodiversity', *Nature Communications*, 4(1), pp. 1–6. doi: 10.1038/ncomms2415.

Cheng, H., Lawrence Edwards, R., *et al.* (2013) 'Improvements in 230Th dating, ^{230}Th and ^{234}U half-life values, and U–Th isotopic measurements by multi-collector inductively coupled plasma mass spectrometry', *Earth and Planetary Science Letters*, 371–372, pp. 82–91. doi: 10.1016/j.epsl.2013.04.006.

Cheng, H. *et al.* (2016) 'The Asian monsoon over the past 640,000 years and ice age terminations', *Nature*. doi: 10.1038/nature18591.

Cheng, H. *et al.* (2019) 'Chinese stalagmite paleoclimate researches: A review and perspective', *Science China Earth Sciences*, 62(10), pp. 1489–1513. doi: 10.1007/s11430-019-9478-3.

Chevalier, M., Brewer, S. and Chase, B. M. (2017) 'Qualitative assessment of PMIP3 rainfall simulations across the eastern African monsoon domains during the mid-Holocene and the Last Glacial Maximum', *Quaternary Science Reviews*, 156, pp. 107–120. doi: 10.1016/j.quascirev.2016.11.028.

Chiang, J. C. H. *et al.* (2015) 'Role of seasonal transitions and westerly jets in East Asian paleoclimate', *Quaternary Science Reviews*. doi: 10.1016/j.quascirev.2014.11.009.

Chung, C. T. Y. and Power, S. B. (2017) 'The non-linear impact of El Niño, La Niña and the Southern Oscillation on seasonal and regional Australian precipitation', *Journal of Southern Hemisphere Earth Systems Science*, 67(1), p. 25. doi: 10.1071/ES17004.

Clark, I. and Fritz, P. (1997) *Environmental Isotopes in Hydrology*. New York: Lewis Publishers.

Claussen, M. and Gayler, V. (1997) 'The Greening of the Sahara during the Mid-Holocene: Results of an Interactive Atmosphere-Biome Model', *Global Ecology and Biogeography Letters*, 6(5), pp. 369–377. doi: 2997337.

Cobb, K. M. *et al.* (2007) 'Regional-scale climate influences on temporal variations of rainwater and cave dripwater oxygen isotopes in northern Borneo', *Earth and Planetary Science Letters*, 263(3–4), pp. 207–220. doi: 10.1016/j.epsl.2007.08.024.

COHMAP Members (1988) 'Climatic Changes of the Last 18,000 Years: Observations and Model Simulations', *Science*, 241(4869), pp. 1043–1052. doi: 10.1126/science.241.4869.1043.

Cole, J. E. *et al.* (1999) 'Climatic controls on interannual variability of precipitation $\delta^{18}O$: Simulated influence of temperature, precipitation amount, and vapor source region', *Journal of Geophysical Research Atmospheres*, 104(D12), pp. 14223–14235. doi: 10.1029/1999JD900182.

Comas-Bru, L., Harrison, Sandy P;, *et al.* (2019) 'Evaluating model outputs using integrated global speleothem records of climate change since the last glacial', *Climate of the Past*, 15(4), pp. 1557–1579. doi: 10.5194/cp-15-1557-2019.

Comas-Bru, L., Harrison, Sandy P., *et al.* (2019) 'Evaluating model outputs using integrated global

speleothem records of climate change since the last glacial', *Climate of the Past Discussions*. doi: 10.5194/cp-2019-25.

Comas-Bru, L. *et al.* (2020) 'SISALv2: a comprehensive speleothem isotope database with multiple age–depth models', *Earth System Science Data*, 12(4), pp. 2579–2606. doi: 10.5194/essd-12-2579-2020.

Comas-Bru, L. and Harrison, S. P. (2019) 'SISAL: Bringing Added Value to Speleothem Research', *Quaternary*, 2(1), p. 7. doi: 10.3390/quat2010007.

Comas-Bru, L. and McDermott, F. (2015) 'Data-model comparison of soil–water $\delta^{18}O$ at a temperate site in N. Spain with implications for interpreting speleothem $\delta^{18}O$', *Journal of Hydrology*, 530, pp. 216–224. doi: 10.1016/j.jhydrol.2015.09.053.

Conroy, J. L. *et al.* (2008) 'Holocene changes in eastern tropical Pacific climate inferred from a Galápagos lake sediment record', *Quaternary Science Reviews*, 27(11–12), pp. 1166–1180. doi: 10.1016/j.quascirev.2008.02.015.

Cook, K. H. and Vizy, E. K. (2019) 'Contemporary Climate Change of the African Monsoon Systems', *Current Climate Change Reports*, 5(3), pp. 145–159. doi: 10.1007/s40641-019-00130-1.

Cosford, J. *et al.* (2008) 'Millennial-scale variability in the Asian monsoon: Evidence from oxygen isotope records from stalagmites in southeastern China', *Palaeogeography, Palaeoclimatology, Palaeoecology*, 266(1–2), pp. 3–12. doi: 10.1016/J.PALAEO.2008.03.029.

Craig, H. and Gordon, L. I. (1965) 'Deuterium and oxygen 18 variations in the ocean and the marine atmosphere', in Tongiorgi, E. (ed.) *Stable isotopes in Oceanographic Studies and Paleotemperatures*. Pisa: Consiglio Nazionake delle Ricerche Laboratoria di Geologia Nucleare, pp. 9–130.

Crétat, J. *et al.* (2020) 'Mid-Holocene to present-day evolution of the Indian monsoon in transient global simulations', *Climate Dynamics*, 55(9–10), pp. 2761–2784. doi: 10.1007/s00382-020-05418-9.

Cruz, F. W., Burns, S. J., *et al.* (2005) 'Insolation-driven changes in atmospheric circulation over the past 116,000 years in subtropical Brazil', *Nature*, 434(7029), pp. 63–66. doi: 10.1038/nature03365.

Cruz, F. W., Karmann, I., *et al.* (2005) 'Stable isotope study of cave percolation waters in subtropical Brazil: Implications for paleoclimate inferences from speleothems', *Chemical Geology*, 220(3–4), pp. 245–262. doi: 10.1016/j.chemgeo.2005.04.001.

Cruz, Francisco W. *et al.* (2006) 'A stalagmite record of changes in atmospheric circulation and soil processes in the Brazilian subtropics during the Late Pleistocene', *Quaternary Science Reviews*, 25(21–22), pp. 2749–2761. doi: 10.1016/j.quascirev.2006.02.019.

Cruz, F.W. *et al.* (2006) 'Reconstruction of regional atmospheric circulation features during the late Pleistocene in subtropical Brazil from oxygen isotope composition of speleothems', *Earth and Planetary Science Letters*, 248(1–2), pp. 495–507. doi: 10.1016/j.epsl.2006.06.019.

Cruz, F. W. *et al.* (2009) 'Orbitally driven east-west antiphasing of South American precipitation', *Nature Geoscience*, 2(3), pp. 210–214. doi: 10.1038/ngeo444.

Daley, T. J. *et al.* (2011) 'The 8200yr BP cold event in stable isotope records from the North Atlantic region', *Global and Planetary Change*, 79(3–4), pp. 288–302. doi: 10.1016/j.gloplacha.2011.03.006.

Dallmeyer, A. *et al.* (2015) 'The evolution of sub-monsoon systems in the Afro-Asian monsoon region during the Holocene - Comparison of different transient climate model simulations', *Climate of the Past*, 11(2), pp. 305–326. doi: 10.5194/cp-11-305-2015.

Daniau, A. -L. *et al.* (2012) 'Predictability of biomass burning in response to climate changes', *Global Biogeochemical Cycles*, 26(4), p. 2011GB004249. doi: 10.1029/2011GB004249.

Dansgaard, W. (1964) 'Stable isotopes in precipitation', *Tellus*, 16(4), pp. 436–468. doi: 10.3402/tellusa.v16i4.8993.

Dee, S. *et al.* (2015) 'PRYSM: An open-source framework for PRoxY System Modeling, with applications to oxygen-isotope systems', *Journal of Advances in Modeling Earth Systems*, 7(3), pp. 1220–1247. doi: 10.1002/2015MS000447.

Deininger, M. *et al.* (2019) 'Late Quaternary variations in the South American monsoon system as

inferred by speleothems—New perspectives using the SISAL database', *Quaternary*, 2(1), p. 6. doi: 10.3390/quat2010006.

Delaygue, G., Jouzel, J. and Dutay, J. C. (2000) 'Oxygen 18-salinity relationship simulated by an oceanic general circulation model', *Earth and Planetary Science Letters*, 178(1–2), pp. 113–123. doi: 10.1016/S0012-821X(00)00073-X.

Deplazes, G. *et al.* (2014) 'Weakening and strengthening of the Indian monsoon during Heinrich events and Dansgaard-Oeschger oscillations', *Paleoceanography*, 29(2), pp. 99–114. doi: 10.1002/2013PA002509.

Ding, Y. and Chan, J. C. L. (2005) 'The East Asian summer monsoon: an overview', *Meteorology and Atmospheric Physics*, 89(1–4), pp. 117–142. doi: 10.1007/s00703-005-0125-z.

Dominguez-Villar, D. *et al.* (2009) 'Oxygen isotope precipitation anomaly in the North Atlantic region during the 8.2 ka event', *Geology*, 37(12), pp. 1095–1098. doi: 10.1130/G30393A.1.

Domínguez-Villar, D. *et al.* (2017) 'The control of the tropical North Atlantic on Holocene millennial climate oscillations', *Geology*, 45(4), pp. 303–306. doi: 10.1130/G38573.1.

Dong, J. *et al.* (2010) 'A high-resolution stalagmite record of the Holocene East Asian monsoon from Mt Shennongjia, central China', *Holocene*, 20(2), pp. 257–264. doi: 10.1177/0959683609350393.

Dorale, J. A. and Liu, Z. (2009) 'Limitations of hendy test criteria in judging the paleoclimatic suitability of speleothems and the need for replication', *Journal of Cave and Karst Studies*, 71(1), pp. 73–80.

Drăguşin, V. *et al.* (2014) 'Constraining Holocene hydrological changes in the Carpathian-Balkan region using speleothem δ18O and pollen-based temperature reconstructions', *Climate of the Past*, 10(4), pp. 1363–1380. doi: 10.5194/cp-10-1363-2014.

Dreybrodt, W. and Deininger, M. (2014) 'The impact of evaporation to the isotope composition of DIC in calcite precipitating water films in equilibrium and kinetic fractionation models', *Geochimica et Cosmochimica Acta*, 125, pp. 433–439. doi: 10.1016/j.gca.2013.10.004.

Duan, P. *et al.* (2021) 'The timing and structure of the 8.2 ka event revealed through high-resolution speleothem records from northwestern Madagascar', *Quaternary Science Reviews*, 268, p. 107104.

Dykoski, C. A. *et al.* (2005) 'A high-resolution, absolute-dated Holocene and deglacial Asian monsoon record from Dongge Cave, China', *Earth and Planetary Science Letters*, 233(1–2), pp. 71–86. doi: 10.1016/J.EPSL.2005.01.036.

Emile-Geay, J. *et al.* (2016) 'Links between tropical Pacific seasonal, interannual and orbital variability during the Holocene', *Nature Geoscience*, 9, pp. 168–173. doi: 10.1038/ngeo2608.

Even, H. *et al.* (1986) 'Timing the transport of water through the upper vadose zone in a Karstic system above a cave in Israel', *Earth Surface Processes and Landforms*, 11(2), pp. 181–191. doi: 10.1002/esp.3290110208.

Fairchild, I. J. and Baker, A. (2012) *Speleothem Science: From Process to Past Environments*. 1st edn. Chichester: Wiley-Blackwell.

Feng, S., Hu, Q. and Oglesby, R. J. (2011) 'Influence of Atlantic sea surface temperatures on persistent drought in North America', *Climate Dynamics*, 37(3–4), pp. 569–586. doi: 10.1007/s00382-010-0835-x.

Fisher, T. G., Smith, D. G. and Andrews, J. T. (2002) 'Preboreal oscillation caused by a glacial Lake Agassiz flood', *Quaternary Science Reviews*, 21(8–9), pp. 873–878.

Fleitmann, D. *et al.* (2003) 'Holocene forcing of the Indian Monsoon recorded in a stalagmite from southern Oman', *Science*, 300(5626), pp. 1737–1739. doi: 10.1126/science.1083130.

Fleitmann, D. *et al.* (2004) 'Palaeoclimatic interpretation of high-resolution oxygen isotope profiles derived from annually laminated speleothems from Southern Oman', *Quaternary Science Reviews*, 23(7–8), pp. 935–945. doi: 10.1016/j.quascirev.2003.06.019.

Fleitmann, D. *et al.* (2007) 'Holocene ITCZ and Indian monsoon dynamics recorded in stalagmites from Oman and Yemen (Socotra)', *Quaternary Science Reviews*, 26(1–2), pp. 170–188. doi: 10.1016/j.quascirev.2006.04.012.

Flohr, P. *et al.* (2017) 'Late Holocene droughts in the Fertile Crescent recorded in a speleothem from northern Iraq', *Geophysical Research Letters*, 44(3), pp. 1528–1536. doi: 10.1002/2016GL071786.

Frappier, A. B. *et al.* (2007) 'Stalagmite stable isotope record of recent tropic cyclone events', *Geology*, 35(2), pp. 111–114. doi: 10.1130/G23145A.1.

Friedman, I. *et al.* (2002) 'Stable isotope composition of waters in the Great Basin, United States 1. Air-mass trajectories', *Journal of Geophysical Research Atmospheres*. doi: 10.1029/2001JD000565.

Ganopolski, A. *et al.* (1998) 'The Influence of Vegetation-Atmosphere-Ocean Interaction on Climate During the Mid-Holocene', *Science*, 280(5371), pp. 1916–1919. doi: 10.1126/science.280.5371.1916.

Gat, J. R. (1996) 'Oxygen and hydrogen isotopes in the hydrological cycle', *Annual Review of Earth and Planetary Sciences*, 24(1), pp. 225–262. doi: 10.1146/annurev.earth.24.1.225.

Geen, R. *et al.* (2020) 'Monsoons, ITCZs, and the Concept of the Global Monsoon', *Reviews of Geophysics*, 58(4), pp. 1–45. doi: 10.1029/2020RG000700.

Gershunov, A. and Barnett, T. P. (1998) 'Interdecadal Modulation of ENSO Teleconnections', *Bulletin of the American Meteorological Society*, 79(12), pp. 2715–2725. doi: 10.1175/1520-0477(1998)079<2715:IMOET>2.0.CO;2.

Giannini, A., Kushnir, Y. and Cane, M. A. (2000) 'Interannual Variability of Caribbean Rainfall, ENSO, and the Atlantic Ocean', *Journal of Climate*, 13(2), pp. 297–311. doi: 10.1175/1520-0442(2000)013<0297:IVOCRE>2.0.CO;2.

Gierz, P., Werner, M. and Lohmann, G. (2017) 'Simulating climate and stable water isotopes during the Last Interglacial using a coupled climate-isotope model', *Journal of Advances in Modeling Earth Systems*, 9(5), pp. 2027–2045. doi: 10.1002/2017MS001056.

Goldsmith, Y. *et al.* (2017a) 'Northward extent of East Asian monsoon covaries with intensity on orbital and millennial timescales', *Proceedings of the National Academy of Sciences*, 114(8), pp. 1817–1821. doi: 10.1073/pnas.1616708114.

Goldsmith, Y. *et al.* (2017b) 'Northward extent of East Asian monsoon covaries with intensity on orbital and millennial timescales', *Proceedings of the National Academy of Sciences*, 114(8), pp. 1817–1821. doi: 10.1073/pnas.1616708114.

Goswami, B. N. *et al.* (2006) 'A physical mechanism for North Atlantic SST influence on the Indian summer monsoon', *Geophysical Research Letters*, 33(2), p. L02706. doi: 10.1029/2005GL024803.

Gregoire, L. J., Payne, A. J. and Valdes, P. J. (2012) 'Deglacial rapid sea level rises caused by ice-sheet saddle collapses', *Nature*, 487(7406), pp. 219–222. doi: 10.1038/nature11257.

Griffiths, M. L. *et al.* (2009a) 'Increasing Australian-Indonesian monsoon rainfall linked to early Holocene sea-level rise', *Nature Geoscience*, 2(9), pp. 636–639. doi: 10.1038/ngeo605.

Griffiths, M. L. *et al.* (2009b) 'Increasing Australian-Indonesian monsoon rainfall linked to early Holocene sea-level rise', *Nature Geoscience*, 2(9), pp. 636–639. doi: 10.1038/ngeo605.

Gupta, A. K., Anderson, D. M. and Overpeck, J. T. (2003) 'Abrupt changes in the Asian southwest monsoon during the holocene and their links to the North Alantic Ocean', *Nature*, 421(6921), pp. 354–357. doi: 10.1038/nature01340.

Gupta, A. K., Das, M. and Anderson, D. M. (2005) 'Solar influence on the Indian summer monsoon during the Holocene', *Geophysical Research Letters*, 32(17). doi: 10.1029/2005GL022685.

Hagos, S. M. and Cook, K. H. (2007) 'Dynamics of the West African monsoon jump', *Journal of Climate*, 20(21), pp. 5264–5284. doi: 10.1175/2007JCLI1533.1.

Han, Z. *et al.* (2015) 'Extreme monsoon aridity episodes recorded in South China during Heinrich Events', *Palaeogeography, Palaeoclimatology, Palaeoecology*, 440, pp. 467–474. doi: 10.1016/j.palaeo.2015.09.037.

Harrison, S. P. *et al.* (2003) 'Mid-Holocene climates of the Americas: a dynamical response to changed seasonality', *Climate Dynamics*, 20(7–8), pp. 663–688. doi: 10.1007/s00382-002-0300-6.

Harrison, S. P. and Prentice, C. I. (2003) 'Climate and CO_2 controls on global vegetation distribution at

the last glacial maximum: analysis based on palaeovegetation data, biome modelling and palaeoclimate simulations', *Global Change Biology*, 9(7), pp. 983–1004. doi: 10.1046/j.1365-2486.2003.00640.x.

Hart, N. C. G., Reason, C. J. C. and Fauchereau, N. (2010) 'Tropical-extratropical interactions over southern Africa: Three cases of heavy summer season rainfall', *Monthly Weather Review*, 138(7), pp. 2608–2623. doi: 10.1175/2010MWR3070.1.

Haug, G. H. *et al.* (2001) 'Southward migration of the intertropical convergence zone through the holocene', *Science*, 293(5533), pp. 1304–1308. doi: 10.1126/science.1059725.

Haywood, A. M. *et al.* (2011) 'Pliocene Model Intercomparison Project (PlioMIP): experimental design and boundary conditions (Experiment 2)', *Geoscientific Model Development*, 4(3), pp. 571–577. doi: 10.5194/gmd-4-571-2011.

He, Chengfei *et al.* (2021) 'Abrupt Heinrich Stadial 1 cooling missing in Greenland oxygen isotopes', *Science Advances*, 7(25). doi: 10.1126/sciadv.abh1007.

He, C. *et al.* (2021) 'Hydroclimate footprint of pan-Asian monsoon water isotope during the last deglaciation', *Science Advances*, 7(4). doi: 10.1126/sciadv.abe2611.

Hellstrom, J., McCulloch, M. and Stone, J. (1998) 'A detailed 31,000-year record of climate and vegetation change, from the isotope geochemistry of two New Zealand speleothems', *Quaternary Research*, 50(2), pp. 167–178. doi: 10.1006/qres.1998.1991.

Hendon, H. H. (2003) 'Indonesian Rainfall Variability: Impacts of ENSO and Local Air–Sea Interaction', *Journal of Climate*, 16(11), pp. 1775–1790. doi: 10.1175/1520-0442(2003)016<1775:IRVIOE>2.0.CO;2.

Hendy, C. H. (1971) 'The isotopic geochemistry of speleothems-I. The calculation of the effects of different modes of formation on the isotopic composition of speleothems and their applicability as palaeoclimatic indicators', *Geochimica et Cosmochimica Acta*, 35(8), pp. 801–824. doi: 10.1016/0016-7037(71)90127-X.

Higgins, R. W., Chen, Y. and Douglas, A. V. (1999) 'Interannual Variability of the North American Warm

Season Precipitation Regime', *Journal of Climate*, 12(3), pp. 653–680. doi: 10.1175/1520-0442(1999)012<0653:IVOTNA>2.0.CO;2.

Hill, C. A. and Forti, P. (1995) 'The classification of cave minerals and speleothems', *International Journal of Speleology*, 24(1), pp. 77–82. doi: 10.5038/1827-806X.24.1.5.

Hoffman, J. S. *et al.* (2012) 'Linking the 8.2 ka event and its freshwater forcing in the Labrador Sea', *Geophysical Research Letters*, 39(18). doi: 10.1029/2012GL053047.

Holloway, M. D. *et al.* (2016) 'Reconstructing paleosalinity from δ18O: Coupled model simulations of the Last Glacial Maximum, Last Interglacial and Late Holocene', *Quaternary Science Reviews*, 131(Part B), pp. 350–364. doi: 10.1016/j.quascirev.2015.07.007.

Hu, C. *et al.* (2008) 'Quantification of Holocene Asian monsoon rainfall from spatially separated cave records', *Earth and Planetary Science Letters*, 266(3–4), pp. 221–232. doi: 10.1016/j.epsl.2007.10.015.

Hu, Jun *et al.* (2019) 'Deciphering oxygen isotope records from Chinese speleothems with an isotope-enabled climate model', *Paleoceanography and Paleoclimatology*, 34(12), pp. 2098–2112. doi: 10.1029/2019PA003741.

Hu, J. *et al.* (2019) 'Deciphering Oxygen Isotope Records From Chinese Speleothems With an Isotope-Enabled Climate Model', *Palaeogeography, Palaeoclimatology, Palaeoecology*, 43, pp. 2098–2112.

Ivanochko, T. S. *et al.* (2008) 'Geochemical reconstruction of Pacific decadal variability from the eastern North Pacific during the Holocene', *Canadian Journal of Earth Sciences*, 45(11), pp. 1317–1329. doi: 10.1139/E08-037.

Ivanovic, R. F. *et al.* (2016) 'Transient climate simulations of the deglaciation 21–9 thousand years before present (version 1) – PMIP4 Core experiment design and boundary conditions', *Geoscientific Model Development*, 9(7), pp. 2563–2587. doi: 10.5194/gmd-9-2563-2016.

Johnson, B. J. *et al.* (1999) '65,000 Years of Vegetation Change in Central Australia and the Australian Summer Monsoon', *Science*, 284(5417), pp. 1150–1152. doi: 10.1126/science.284.5417.1150.

Jolly, D. *et al.* (1998) 'Simulated climate and biomes of Africa during the late quaternary', *Quaternary Science Reviews*, 17(6–7), pp. 629–657. doi: 10.1016/S0277-3791(98)00015-8.

Jones, I. C. and Banner, J. L. (2003) 'Estimating recharge thresholds in tropical karst island aquifers: Barbados, Puerto Rico and Guam', *Journal of Hydrology*, 278(1–4), pp. 131–143. doi: 10.1016/S0022-1694(03)00138-0.

Jungclaus, J. H. *et al.* (2017) 'The PMIP4 contribution to CMIP6 – Part 3: The last millennium, scientific objective, and experimental design for the PMIP4 *past1000* simulations', *Geoscientific Model Development*, 10(11), pp. 4005–4033. doi: 10.5194/gmd-10-4005-2017.

Kageyama, M. *et al.* (2021) 'The PMIP4 Last Glacial Maximum experiments: preliminary results and comparison with the PMIP3 simulations', *Climate of the Past*, 17(3), pp. 1065–1089. doi: 10.5194/cp-17-1065-2021.

Kaniewski, D. *et al.* (2018) 'The 4.2 ka BP event in the Levant', *Climate of the Past*, 14(10), pp. 1529–1542. doi: 10.5194/cp-14-1529-2018.

Kanner, L. C. *et al.* (2013) 'High-resolution variability of the South American summer monsoon over the last seven millennia: Insights from a speleothem record from the central Peruvian Andes', *Quaternary Science Reviews*, 75, pp. 1–10. doi: 10.1016/j.quascirev.2013.05.008.

Kathayat, G. *et al.* (2016) 'Indian monsoon variability on millennial-orbital timescales', *Scientific Reports*, 6, p. 24374. doi: 10.1038/srep24374.

Kathayat, G. *et al.* (2021) 'Interannual oxygen isotope variability in Indian summer monsoon precipitation reflects changes in moisture sources', *Communications Earth & Environment*, 2(1), p. 96. doi: 10.1038/s43247-021-00165-z.

Kaufmann, G. (2003) 'Stalagmite growth and palaeo-climate: The numerical perspective', *Earth and Planetary Science Letters*, 214(1–2), pp. 251–266. doi: 10.1016/S0012-821X(03)00369-8.

Kaushal, N. *et al.* (2018) 'The Indian Summer Monsoon from a Speleothem $\delta^{18}O$ Perspective—A Review',

Quaternary, 1(3), p. 29. doi: 10.3390/quat1030029.

Kim, S.-T. and O'Neil, J. R. (1997) 'Equilibrium and nonequilibrium oxygen isotope effects in synthetic carbonates', *Geochimica et Cosmochimica Acta*, 61(16), pp. 3461–3475. doi: 10.1016/S0016-7037(97)00169-5.

Kirby, M. E. *et al.* (2010) 'A Holocene record of Pacific Decadal Oscillation (PDO)-related hydrologic variability in Southern California (Lake Elsinore, CA)', *Journal of Paleolimnology*, 44(3), pp. 819–839. doi: 10.1007/s10933-010-9454-0.

Kleiven, H. (Kikki) F. *et al.* (2008) 'Reduced North Atlantic Deep Water Coeval with the Glacial Lake Agassiz Freshwater Outburst', *Science*, 319(5859), pp. 60–64. doi: 10.1126/science.1148924.

Knudsen, M. F. *et al.* (2011) 'Tracking the Atlantic Multidecadal Oscillation through the last 8,000 years', *Nature Communications*, 2(1), p. 178. doi: 10.1038/ncomms1186.

Kobashi, T. *et al.* (2017) 'Volcanic influence on centennial to millennial Holocene Greenland temperature change', *Scientific reports*, 7(1), pp. 1–10.

Kodama, Y. (1992) 'Large-scale common features of subtropical precipitation zones (the Baiu frontal zone, the SPCZ, and the SACZ) part I: Characteristics of subtropical frontal zones', *Journal of the Meteorological Society of Japan*, 70(4), pp. 813–836. doi: 10.2151/jmsj1965.70.4_813.

Koster, R. D., de Valpine, D. P. and Jouzel, J. (1993) 'Continental water recycling and $H_2{}^{18}O$ concentrations', *Geophysical Research Letters*, 20(20), pp. 2215–2218. doi: 10.1029/93GL01781.

Krause, C. E. *et al.* (2019) 'Spatio-temporal evolution of Australasian monsoon hydroclimate over the last 40,000 years', *Earth and Planetary Science Letters*, 513, pp. 103–112. doi: 10.1016/j.epsl.2019.01.045.

Krishnamurthy, V. and Goswami, B. N. (2000) 'Indian Monsoon–ENSO Relationship on Interdecadal Timescale', *Journal of Climate*, 13(3), pp. 579–595. doi: 10.1175/1520-0442(2000)013<0579:IMEROI>2.0.CO;2.

Kumar, K. K., Rajagopalan, B. and Cane, M. A. (1999) 'On the Weakening Relationship Between the

Indian Monsoon and ENSO', *Science*, 284(5423), pp. 2156–2159. doi: 10.1126/science.284.5423.2156.

Kutzbach, J. *et al.* (1996) 'Vegetation and soil feedbacks on the response of the African monsoon to orbital forcing in the early to middle Holocene', *Nature*, 384(6610), pp. 623–626. doi: 10.1038/384623a0.

Kutzbach, J. E. and Guetter, P. J. (1986) 'The Influence of Changing Orbital Parameters and Surface Boundary Conditions on Climate Simulations for the Past 18 000 Years', *Journal of the Atmospheric Sciences*, 43(16), pp. 1726–1759. doi: 10.1175/1520-0469(1986)043<1726:TIOCOP>2.0.CO;2.

Kutzbach, J. E. and Street-Perrott, F. A. (1985) 'Milankovitch forcing of fluctuations in the level of tropical lakes from 18 to 0 kyr BP', *Nature*, 317(6033), pp. 130–134. doi: 10.1038/317130a0.

Lachniet, M. S. *et al.* (2004) 'Tropical response to the 8200 yr B.P. cold event? Speleothem isotopes indicate a weakened early Holocene monsoon in Costa Rica', *Geology*, 32(11), p. 957. doi: 10.1130/G20797.1.

Lachniet, M. S. (2009) 'Climatic and environmental controls on speleothem oxygen-isotope values', *Quaternary Science Reviews*, 28(5–6), pp. 412–432. doi: 10.1016/j.quascirev.2008.10.021.

Lebel, T., Diedhiou, A. and Laurent, H. (2003) 'Seasonal cycle and interannual variability of the Sahelian rainfall at hydrological scales', *Journal of Geophysical Research: Atmospheres*, 108(8), pp. 1–11. doi: 10.1029/2001jd001580.

Lechleitner, F. A. *et al.* (2018) 'The Potential of Speleothems from Western Europe as Recorders of Regional Climate: A Critical Assessment of the SISAL Database', *Quaternary*, 1(3), p. 30. doi: 10.3390/quat1030030.

Lee, J. E. *et al.* (2007) 'Analysis of the global distribution of water isotopes using the NCAR atmospheric general circulation model', *Journal of Geophysical Research Atmospheres*, 112(D16). doi: 10.1029/2006JD007657.

Lee, J. E. and Fung, I. (2008) '"Amount effect" of water isotopes and quantitative analysis of post-

condensation processes', *Hydrological Processes*, 22(1), pp. 1–8. doi: 10.1002/hyp.6637.

LeGrande, A. N. and Schmidt, G. A. (2006) 'Global gridded data set of the oxygen isotopic composition in seawater', *Geophysical Research Letters*, 33(12). doi: 10.1029/2006GL026011.

LeGrande, A. N. and Schmidt, G. A. (2008) 'Ensemble, water isotope-enabled, coupled general circulation modeling insights into the 8.2 ka event', *Paleoceanography*, 23(PA3207). doi: 10.1029/2008PA001610.

LeGrande, A. N. and Schmidt, G. A. (2009) 'Sources of Holocene variability of oxygen isotopes in paleoclimate archives', *Climate of the Past*, 5(3), pp. 441–455. doi: 10.5194/cp-5-441-2009.

Lewis, S. C. *et al.* (2010) 'Water vapour source impacts on oxygen isotope variability in tropical precipitation during Heinrich events', *Climate of the Past*, 6(3), pp. 325–343. doi: 10.5194/cp-6-325-2010.

Lézine, A.-M. *et al.* (2011) 'Sahara and Sahel vulnerability to climate changes, lessons from Holocene hydrological data', *Quaternary Science Reviews*, 30(21–22), pp. 3001–3012. doi: 10.1016/j.quascirev.2011.07.006.

Li, Y. *et al.* (2014) 'Synchronous or asynchronous Holocene Indian and East Asian summer monsoon evolution: A synthesis on Holocene Asian summer monsoon simulations, records and modern monsoon indices', *Global and Planetary Change*, 116, pp. 30–40. doi: 10.1016/j.gloplacha.2014.02.005.

Liu, W., Cook, K. H. and Vizy, E. K. (2020) 'Role of the West African westerly jet in the seasonal and diurnal cycles of precipitation over West Africa', *Climate Dynamics*, 54(1–2), pp. 843–861. doi: 10.1007/s00382-019-05035-1.

Liu, Y. H. *et al.* (2013) 'Links between the East Asian monsoon and North Atlantic climate during the 8,200 year event', *Nature Geoscience*, 6(2), pp. 117–120.

Liu, Y. and Hu, C. (2016) 'Quantification of southwest China rainfall during the 8.2 ka BP event with response to North Atlantic cooling', *Climate of the Past*, 12(7), pp. 1583–1590. doi: 10.5194/cp-12-1583-

2016.

Liu, Z. *et al.* (2009) 'Transient Simulation of Last Deglaciation with a New Mechanism for Bølling-Allerød Warming', *Science*, 325(5938), pp. 310–314. doi: 10.1126/science.1171041.

Liu, Z. *et al.* (2014) 'Chinese cave records and the East Asia Summer Monsoon', *Quaternary Science Reviews*, 83, pp. 115–128. doi: 10.1016/j.quascirev.2013.10.021.

LoDico, J. M., Flower, B. P. and Quinn, T. M. (2006) 'Subcentennial-scale climatic and hydrologic variability in the Gulf of Mexico during the early Holocene', *Paleoceanography*, 21(3). doi: 10.1029/2005PA001243.

Lu, R., Dong, B. and Ding, H. (2006) 'Impact of the Atlantic Multidecadal Oscillation on the Asian summer monsoon', *Geophysical Research Letters*, 33(24), p. L24701. doi: 10.1029/2006GL027655.

Magee, J. W. *et al.* (2004) 'Continuous 150 k.y. monsoon record from Lake Eyre, Australia: Insolation-forcing implications and unexpected Holocene failure', *Geology*, 32(10), pp. 885–888. doi: 10.1130/G20672.1.

Maher, B. A. (2008) 'Holocene variability of the East Asian summer monsoon from Chinese cave records: A re-assessment', *Holocene*, 18(6), pp. 861–866. doi: 10.1177/0959683608095569.

Maher, B. A. and Thompson, R. (2012) 'Oxygen isotopes from Chinese caves: records not of monsoon rainfall but of circulation regime', *Journal of Quaternary Science*, 27(6), pp. 615–624. doi: 10.1002/jqs.2553.

Mantua, N. J. *et al.* (1997) 'A Pacific Interdecadal Climate Oscillation with Impacts on Salmon Production', *Bulletin of the American Meteorological Society*, 78(6), pp. 1069–1079. doi: 10.1175/1520-0477(1997)078<1069:APICOW>2.0.CO;2.

Mantua, N. J. and Hare, S. R. (2002) 'The Pacific Decadal Oscillation', *Journal of Oceanology*, 58, pp. 35–44. doi: 10.1023/A:1015820616384.

Mao, J. and Wu, G. (2007) 'Interannual variability in the onset of the summer monsoon over the Eastern

Bay of Bengal', *Theoretical and Applied Climatology*, 89(3–4), pp. 155–170. doi: 10.1007/s00704-006-0265-1.

Marchant, R. *et al.* (2007) 'The Indian Ocean dipole – the unsung driver of climatic variability in East Africa', *African Journal of Ecology*, 45(1), pp. 4–16. doi: 10.1111/j.1365-2028.2006.00707.x.

Marengo, J. A. *et al.* (2012) 'Recent developments on the South American monsoon system', *International Journal of Climatology*, 32(1), pp. 1–21. doi: 10.1002/joc.2254.

Martin Calvo, M., Prentice, I. C. and Harrison, S. P. (2014) 'Climate versus carbon dioxide controls on biomass burning: a model analysis of the glacial–interglacial contrast', *Biogeosciences*, 11(21), pp. 6017–6027. doi: 10.5194/bg-11-6017-2014.

Martin, E. R. and Thorncroft, C. D. (2014) 'The impact of the AMO on the West African monsoon annual cycle', *Quarterly Journal of the Royal Meteorological Society*, 140(678), pp. 31–46. doi: 10.1002/qj.2107.

Marzin, C. and Braconnot, P. (2009) 'Variations of Indian and African monsoons induced by insolation changes at 6 and 9.5 kyr BP', *Climate Dynamics*, 33(2–3), pp. 215–231. doi: 10.1007/s00382-009-0538-3.

Matero, I. S. O. *et al.* (2017) 'The 8.2 ka cooling event caused by Laurentide ice saddle collapse', *Earth and Planetary Science Letters*, 473, pp. 205–214. doi: 10.1016/j.epsl.2017.06.011.

McDermott, F. (2004) 'Palaeo-climate reconstruction from stable isotope variations in speleothems: A review', *Quaternary Science Reviews*, 23(7–8), pp. 901–918. doi: 10.1016/j.quascirev.2003.06.021.

McPhaden, M. J., Zebiak, S. E. and Glantz, M. H. (2006) 'ENSO as an integrating concept in earth science', *Science*, 314(5806), pp. 1740–1745. doi: 10.1126/science.1132588.

Menviel, L. *et al.* (2014) 'Hindcasting the continuum of Dansgaard–Oeschger variability: mechanisms, patterns and timing', *Climate of the Past*, 10(1), pp. 63–77. doi: 10.5194/cp-10-63-2014.

Menviel, L. *et al.* (2019) 'The penultimate deglaciation: protocol for Paleoclimate Modelling Intercomparison Project (PMIP) phase 4 transient numerical simulations between 140 and 127 ka, version 1.0', *Geoscientific Model Development*, 12(8), pp. 3649–3685. doi: 10.5194/gmd-12-3649-2019.

Menviel, L., Spence, P. and England, M. H. (2015) 'Contribution of enhanced Antarctic Bottom Water formation to Antarctic warm events and millennial-scale atmospheric CO2 increase', *Earth and Planetary Science Letters*, 413, pp. 37–50. doi: 10.1016/j.epsl.2014.12.050.

Mestas-Nuñez, A. M., Enfield, D. B. and Zhang, C. (2007) 'Water vapor fluxes over the Intra-Americas Sea: Seasonal and interannual variability and associations with rainfall', *Journal of Climate*, 20(9), pp. 1910–1922. doi: 10.1175/JCLI4096.1.

Metcalfe, S. E., Barron, J. A. and Davies, S. J. (2015) 'The Holocene history of the North American Monsoon: "known knowns" and "known unknowns" in understanding its spatial and temporal complexity', *Quaternary Science Reviews*, pp. 1–27. doi: 10.1016/j.quascirev.2015.04.004.

Mickler, P. J., Stern, L. A. and Banner, J. L. (2006) 'Large kinetic isotope effects in modern speleothems', *Geological Society of America Bulletin*, 118(1–2), pp. 65–81. doi: 10.1130/B25698.1.

Misra, P., Tandon, S. K. and Sinha, R. (2019) 'Holocene climate records from lake sediments in India: Assessment of coherence across climate zones', *Earth-Science Reviews*, 190, pp. 370–397. doi: 10.1016/j.earscirev.2018.12.017.

Moerman, J. W. *et al.* (2013) 'Diurnal to interannual rainfall δ18O variations in northern Borneo driven by regional hydrology', *Earth and Planetary Science Letters*. doi: 10.1016/j.epsl.2013.03.014.

Moore, G. W. (1952) 'Speleothem - A new cave term', *National Speleological Society News*, 10(6), p. 2.

Morrill, C. *et al.* (2013) 'Proxy benchmarks for intercomparison of 8.2 ka simulations', *Climate of the Past*, 9(1), pp. 423–432. doi: 10.5194/cp-9-423-2013.

Morrill, C. *et al.* (2014) 'Large sensitivity to freshwater forcing location in 8.2 ka simulations', *Paleoceanography*, 29(10), pp. 930–945. doi: 10.1002/2014PA002669.

Munksgaard, N. C. *et al.* (2012) 'First continuous shipboard $\delta^{18}O$ and δD measurements in sea water by diffusion sampling—cavity ring-down spectrometry', *Environmental Chemistry Letters*, 10(3), pp. 301–307. doi: 10.1007/s10311-012-0371-5.

Myers, C. G. *et al.* (2015) 'Northeast Indian stalagmite records Pacific decadal climate change: Implications for moisture transport and drought in India', *Geophysical Research Letters*, 42(10), pp. 4124–4132. doi: 10.1002/2015GL063826.

Niedermeyer, E. M. *et al.* (2014) 'Hydroclimate of the western Indo-Pacific Warm Pool during the past 24,000 years', *Proceedings of the National Academy of Sciences of the United States of America*, 111(26), pp. 9402–9406. doi: 10.1073/pnas.1323585111.

Novello, V. F. *et al.* (2017) 'A high-resolution history of the South American Monsoon from Last Glacial Maximum to the Holocene', *Scientific Reports*, 7(1), p. 44267. doi: 10.1038/srep44267.

Ön, Z. B. *et al.* (2021) 'A Bayesian test for the 4.2 ka BP abrupt climatic change event in southeast Europe and southwest Asia using structural time series analysis of paleoclimate data', *Climatic Change*, 165(1–2). doi: 10.1007/s10584-021-03010-6.

Otto-Bliesner, B. L. *et al.* (2021) 'Large-scale features of Last Interglacial climate: results from evaluating the *lig127k* simulations for the Coupled Model Intercomparison Project (CMIP6)–Paleoclimate Modeling Intercomparison Project (PMIP4)', *Climate of the Past*, 17(1), pp. 63–94. doi: 10.5194/cp-17-63-2021.

Owen, R. A. *et al.* (2016) 'Calcium isotopes in caves as a proxy for aridity: Modern calibration and application to the 8.2 kyr event', *Earth and Planetary Science Letters*, 443, pp. 129–138.

Pape, J. R. *et al.* (2010) 'Controls on oxygen isotope variability in precipitation and cave drip waters, central Texas, USA', *Journal of Hydrology*, 385(1–4), pp. 203–215. doi: 10.1016/j.jhydrol.2010.02.021.

Parthasarathy, B., Munot, A. A. and Kothawale, D. R. (1994) 'All-India monthly and seasonal rainfall series: 1871-1993', *Theoretical and Applied Climatology*, 49(4), pp. 217–224. doi: 10.1007/BF00867461.

Partin, J. W. *et al.* (2007) 'Millennial-scale trends in west Pacific warm pool hydrology since the Last Glacial Maximum', *Nature*, 449(7161), pp. 452–455. doi: 10.1038/nature06164.

Pausata, F. S. R. *et al.* (2011) 'Chinese stalagmite $\delta^{18}O$ controlled by changes in the Indian monsoon during a simulated Heinrich event', *Nature Geoscience*, 4(7), pp. 474–480. doi: 10.1038/ngeo1169.

Peckover, E. N. *et al.* (2019) 'Coupled stalagmite–Alluvial fan response to the 8.2 ka event and early Holocene palaeoclimate change in Greece', *Palaeogeography, Palaeoclimatology, Palaeoecology*, 532, p. 109252.

Perrin, J., Jeannin, P.-Y. and Zwahlen, F. (2003) 'Epikarst storage in a karst aquifer: a conceptual model based on isotopic data, Milandre test site, Switzerland', *Journal of Hydrology*, 279(1–4), pp. 106–124. doi: 10.1016/S0022-1694(03)00171-9.

Peyron, O. *et al.* (2006) 'Quantitative reconstructions of annual rainfall in Africa 6000 years ago: Model-data comparison', *Journal of Geophysical Research*, 111(D24), p. D24110. doi: 10.1029/2006JD007396.

Pomposi, C. *et al.* (2016) 'Understanding Pacific Ocean influence on interannual precipitation variability in the Sahel', *Geophysical Research Letters*, 43(17), pp. 9234–9242. doi: 10.1002/2016GL069980.

Power, M. J. *et al.* (2008) 'Changes in fire regimes since the Last Glacial Maximum: An assessment based on a global synthesis and analysis of charcoal data', *Climate Dynamics*, 30, pp. 887–907. doi: 10.1007/s00382-007-0334-x.

Power, S. *et al.* (1999) 'Inter-decadal modulation of the impact of ENSO on Australia', *Climate Dynamics*, 15(5), pp. 319–324. doi: 10.1007/s003820050284.

Prado, L. F. *et al.* (2013) 'A mid-Holocene climate reconstruction for eastern South America', *Climate of the Past*, 9(5), pp. 2117–2133. doi: 10.5194/cp-9-2117-2013.

Pu, B. and Cook, K. H. (2012) 'Role of the west African westerly jet in sahel rainfall variations', *Journal of Climate*, 25(8), pp. 2880–2896. doi: 10.1175/JCLI-D-11-00394.1.

Rachmayani, R., Prange, M. and Schulz, M. (2015) 'North African vegetation-precipitation feedback in early and mid-Holocene climate simulations with CCSM3-DGVM', *Climate of the Past*, 11(2). doi: 10.5194/cp-11-175-2015.

Railsback, L. B. *et al.* (2018) 'The timing, two-pulsed nature, and variable climatic expression of the 4.2 ka event: A review and new high-resolution stalagmite data from Namibia', *Quaternary Science Reviews*,

186, pp. 78–90. doi: 10.1016/j.quascirev.2018.02.015.

Ran, M. and Chen, L. (2019) 'The 4.2 ka BP climatic event and its cultural responses', *Quaternary International*, 521, pp. 158–167. doi: 10.1016/j.quaint.2019.05.030.

Ratnam, J. V. *et al.* (2014) 'Remote Effects of El Niño and Modoki Events on the Austral Summer Precipitation of Southern Africa', *Journal of Climate*, 27(10), pp. 3802–3815. doi: 10.1175/JCLI-D-13-00431.1.

Richards, D. A. *et al.* (1998) 'U-Pb dating of a speleothem of Quaternary age', *Geochimica et Cosmochimica Acta*, 62(23–24), pp. 3683–3688. doi: 10.1016/S0016-7037(98)00256-7.

Richards, D. A. (2003) 'Uranium-series Chronology and Environmental Applications of Speleothems', *Reviews in Mineralogy and Geochemistry*, 52(1), pp. 407–460. doi: 10.2113/0520407.

Risi, C. *et al.* (2010) 'Water-stable isotopes in the LMDZ4 general circulation model: Model evaluation for present-day and past climates and applications to climatic interpretations of tropical isotopic records', *Journal of Geophysical Research Atmospheres*, 115(D12). doi: 10.1029/2009JD013255.

Risi, C., Bony, S. and Vimeux, F. (2008) 'Influence of convective processes on the isotopic composition ($\delta^{18}O$ and δD) of precipitation and water vapor in the tropics: 2. Physical interpretation of the amount effect', *Journal of Geophysical Research Atmospheres*, 113(D19). doi: 10.1029/2008JD009943.

Rodríguez-Fonseca, B. *et al.* (2011) 'Interannual and decadal SST-forced responses of the West African monsoon', *Atmospheric Science Letters*, 12(1), pp. 67–74. doi: 10.1002/asl.308.

Rohling, E. J. and Pälike, H. (2005) 'Centennial-scale climate cooling with a sudden cold event around 8,200 years ago', *Nature*, 434(7036), pp. 975–979. doi: 10.1038/nature03421.

Rowe, C. (2007) 'A palynological investigation of Holocene vegetation change in Torres Strait, seasonal tropics of northern Australia', *Palaeogeography, Palaeoclimatology, Palaeoecology*, 251(1), pp. 83–103. doi: 10.1016/j.palaeo.2007.02.019.

Rozanski, K., Araguás-Araguás, L. and Gonfiantini, R. (1993) 'Isotopic patterns in modern global

precipitation', *Geophysical Monograph*, 75, pp. 1–36. doi: 10.1029/GM078p0001.

Salati, E. *et al.* (1979) 'Recycling of water in the Amazon Basin: An isotopic study', *Water Resources Research*, 15(5), pp. 1250–1258. doi: 10.1029/WR015i005p01250.

Schmidt, M. W. *et al.* (2012) 'Solar forcing of Florida Straits surface salinity during the early Holocene', *Paleoceanography*, 27(3). doi: 10.1029/2012PA002284.

Scholz, D. and Hoffmann, D. (2008) '^{230}Th/U-dating of fossil corals and speleothems', *E&G Quaternary Science Journal*, 57(1/2), pp. 52–76. doi: 10.3285/eg.57.1-2.3.

Scuderi, L. A. *et al.* (2019) 'The 4.2 ka BP Event in northeastern China: a geospatial perspective', *Climate of the Past*, 15(1), pp. 367–375. doi: 10.5194/cp-15-367-2019.

Scussolini, P. *et al.* (2019) 'Agreement between reconstructed and modeled boreal precipitation of the last interglacial', *Science Advances*, 5(11), pp. 1–12. doi: 10.1126/sciadv.aax7047.

Seetha, C. J. *et al.* (2020) 'Significant changes in the ENSO-monsoon relationship and associated circulation features on multidecadal timescale', *Climate Dynamics*, 54(3–4), pp. 1491–1506. doi: 10.1007/s00382-019-05071-x.

Sengupta, S. and Sarkar, A. (2006) 'Stable isotope evidence of dual (Arabian Sea and Bay of Bengal) vapour sources in monsoonal precipitation over north India', *Earth and Planetary Science Letters*, 250(3–4), pp. 511–521. doi: 10.1016/j.epsl.2006.08.011.

Shao, X. *et al.* (2006) 'Long-term trend and abrupt events of the Holocene Asian monsoon inferred from a stalagmite δ^{18}O record from Shennongjia in Central China', *Chinese Science Bulletin*, 51(2), pp. 221–228. doi: 10.1007/s11434-005-0882-6.

Sharp, Z. (2017) *Principles of Stable Isotope Geochemistry*. 2nd Editio. Pearson. doi: https://doi.org/10.25844/h9q1-0p82.

Shi, X. *et al.* (2021) 'Calendar effects on surface air temperature and precipitation based on model-ensemble equilibrium and transient simulations from PMIP4 and PACMEDY', *Climate of the Past*

Discussions. doi: 10.5194/cp-2021-163.

Singarayer, J. S. and Burrough, S. L. (2015) 'Interhemispheric dynamics of the African rainbelt during the late Quaternary', *Quaternary Science Reviews*, pp. 48–67. doi: 10.1016/j.quascirev.2015.06.021.

Sinha, A. *et al.* (2005) 'Variability of Southwest Indian summer monsoon precipitation during the Bølling-Ållerød', *Geology*, 33(10), p. 813. doi: 10.1130/G21498.1.

Sinha, A. *et al.* (2011) 'The leading mode of Indian Summer Monsoon precipitation variability during the last millennium', *Geophysical Research Letters*, 38(15). doi: 10.1029/2011GL047713.

Sinha, A. *et al.* (2015) 'Trends and oscillations in the Indian summer monsoon rainfall over the last two millennia', *Nature Communications*, 6(1), p. 6309. doi: 10.1038/ncomms7309.

Sjolte, J. and Hoffmann, G. (2014) 'Modelling stable water isotopes in monsoon precipitation during the previous interglacial', *Quaternary Science Reviews*, 85, pp. 119–135. doi: 10.1016/j.quascirev.2013.12.006.

Smith, R. J. and Mayle, F. E. (2018) 'Impact of mid- to late Holocene precipitation changes on vegetation across lowland tropical South America: a paleo-data synthesis', *Quaternary Research*, 89(1), pp. 134–155. doi: 10.1017/qua.2017.89.

Street-Perrott, F. A. and Perrott, R. A. (1993) 'Holocene vegetation, lake levels and climate of Africa', in Wright, H. E. et al. (eds) *Global climates since the last glacial maximum*. Minneapolis: University of Minnesota Press, pp. 318–356.

Street, F. A. and Grove, A. T. (1979) 'Global maps of lake-level fluctuations since 30,000 yr B.P.', *Quaternary Research*. doi: 10.1016/0033-5894(79)90092-9.

Stríkis, N. M. *et al.* (2011) 'Abrupt variations in South American monsoon rainfall during the Holocene based on a speleothem record from central-eastern Brazil', *Geology*, 39(11), pp. 1075–1078. doi: 10.1130/G32098.1.

Sturm, C., Zhang, Q. and Noone, D. (2010) 'An introduction to stable water isotopes in climate models:

Benefits of forward proxy modelling for paleoclimatology', *Climate of the Past*, 6(1), pp. 115–129. doi: 10.5194/cp-6-115-2010.

Sultan, B. and Janicot, S. (2003) 'The West African monsoon dynamics. Part II: The "preonset" and "onset" of the summer monsoon', *Journal of Climate*, 16(21), pp. 3407–3427. doi: 10.1175/1520-0442(2003)016<3407:TWAMDP>2.0.CO;2.

Sutton, R. T. and Hodson, D. L. R. (2005) 'Atlantic Ocean Forcing of North American and European Summer Climate', *Science*, 309(5731), pp. 115–118. doi: 10.1126/science.1109496.

Tabor, C., Otto-Bliesner, B. and Liu, Z. (2020) 'Speleothems of South American and Asian Monsoons Influenced by a Green Sahara', *Geophysical Research Letters*, 47(22), pp. 1–11. doi: 10.1029/2020GL089695.

Tabor, C. R. *et al.* (2018) 'Interpreting Precession-Driven $\delta^{18}O$ Variability in the South Asian Monsoon Region', *Journal of Geophysical Research: Atmospheres*, 123(11), pp. 5927–5946. doi: 10.1029/2018JD028424.

Tan, L. *et al.* (2020) 'Holocene Monsoon Change and Abrupt Events on the Western Chinese Loess Plateau as Revealed by Accurately Dated Stalagmites', *Geophysical Research Letters*, 47(21), p. e2020GL090273. doi: 10.1029/2020GL090273.

Tan, M. (2014) 'Circulation effect: Response of precipitation $\delta^{18}O$ to the ENSO cycle in monsoon regions of China', *Climate Dynamics*, 42(3–4), pp. 1067–1077. doi: 10.1007/s00382-013-1732-x.

Tang, K. and Feng, X. (2001) 'The effect of soil hydrology on the oxygen and hydrogen isotopic compositions of plants' source water', *Earth and Planetary Science Letters*, 185(3–4), pp. 355–367. doi: 10.1016/S0012-821X(00)00385-X.

Texier, D. *et al.* (1997) 'Quantifying the role of biosphere-atmosphere feedbacks in climate change: coupled model simulations for 6000 years BP and comparison with palaeodata for northern Eurasia and northern Africa', *Climate Dynamics*, 13(12), pp. 865–881. doi: 10.1007/s003820050202.

Thomas, E. R. *et al.* (2007) 'The 8.2ka event from Greenland ice cores', *Quaternary Science Reviews*, 26(1–2), pp. 70–81. doi: 10.1016/j.quascirev.2006.07.017.

Thompson, L. G., Mosley-Thompson, E. and Henderson, K. A. (2000) 'Ice-core palaeoclimate records in tropical South America since the Last Glacial Maximum', *Journal of Quaternary Science*, 15(4), pp. 377–394. doi: 10.1002/1099-1417(200005)15:4<377::AID-JQS542>3.0.CO;2-L.

Tindall, J. C. and Valdes, P. J. (2011) 'Modeling the 8.2ka event using a coupled atmosphere-ocean GCM', *Global and Planetary Change*, 79(3–4), pp. 312–321. doi: 10.1016/j.gloplacha.2011.02.004.

Trenberth, K. E., Stepaniak, D. P. and Caron, J. M. (2000) 'The global monsoon as seen through the divergent atmospheric circulation', *Journal of Climate*, 13(22), pp. 3969–3993. doi: 10.1175/1520-0442(2000)013<3969:TGMAST>2.0.CO;2.

Truebe, S. A., Ault, T. R. and Cole, J. E. (2010) 'A forward model of cave dripwater $\delta^{18}O$ and application to speleothem records', *IOP Conference Series: Earth and Environmental Science*, 9, p. 012022. doi: 10.1088/1755-1315/9/1/012022.

Vera, C. *et al.* (2006) 'Toward a unified view of the American monsoon systems', *Journal of Climate*, 19(20), pp. 4977–5000. doi: 10.1175/JCLI3896.1.

Vinther, B. M. *et al.* (2006) 'A synchronized dating of three Greenland ice cores throughout the Holocene', *Journal of Geophysical Research: Atmospheres*, 111(D13). doi: 10.1029/2005JD006921.

Voarintsoa, N. R. G. *et al.* (2019) 'Investigating the 8.2 ka event in northwestern Madagascar: Insight from data–model comparisons', *Quaternary Science Reviews*, 204, pp. 172–186. doi: 10.1016/j.quascirev.2018.11.030.

Wackerbarth, A. *et al.* (2012) 'Simulated oxygen isotopes in cave drip water and speleothem calcite in European caves', *Climate of the Past*, 8(6), pp. 1781–1799. doi: 10.5194/cp-8-1781-2012.

Waelbroeck, C. *et al.* (2002) 'Sea-level and deep water temperature changes derived from benthic foraminifera isotopic records', *Quaternary Science Reviews*, 21(1–3), pp. 295–305. doi: 10.1016/S0277-

3791(01)00101-9.

Wagner, A. J. *et al.* (2013) 'Model support for forcing of the 8.2 ka event by meltwater from the Hudson Bay ice dome', *Climate Dynamics*, 41(11–12), pp. 2855–2873. doi: 10.1007/s00382-013-1706-z.

Walker, J. M. and Bordoni, S. (2016) 'Onset and withdrawal of the large-scale South Asian monsoon: A dynamical definition using change point detection', *Geophysical Research Letters*, 43(22), pp. 11,815-11,822. doi: 10.1002/2016GL071026.

Walker, M. *et al.* (2018) 'Formal ratification of the subdivision of the Holocene Series/Epoch (Quaternary System/Period): two new Global Boundary Stratotype Sections and Points (GSSPs) and three new stages/subseries', *Episodes*, 41(4), pp. 213–223. doi: 10.18814/epiiugs/2018/018016.

Waltgenbach, S. *et al.* (2020) 'Climate and structure of the 8.2 ka event reconstructed from three speleothems from Germany', *Global and Planetary Change*, 193, p. 103266.

Wang, B. *et al.* (2012) 'Recent change of the global monsoon precipitation (1979-2008)', *Climate Dynamics*, 39(5), pp. 1123–1135. doi: 10.1007/s00382-011-1266-z.

Wang, B. *et al.* (2021) 'Monsoons climate change assessment', *Bulletin of the American Meteorological Society*, 102(1), pp. E1–E19. doi: 10.1175/BAMS-D-19-0335.1.

Wang, B. and Ding, Q. (2008) 'Global monsoon: Dominant mode of annual variation in the tropics', *Dynamics of Atmospheres and Oceans*, 44(3–4), pp. 165–183. doi: 10.1016/j.dynatmoce.2007.05.002.

Wang, B., Ding, Q. and Joseph, P. V. (2009) 'Objective definition of the Indian summer monsoon onset', *Journal of Climate*, 22(12), pp. 3303–3316. doi: 10.1175/2008JCLI2675.1.

Wang, B. and LinHo (2002) 'Rainy season of the Asian-Pacific summer monsoon', *Journal of Climate*, 15(4), pp. 386–398. doi: 10.1175/1520-0442(2002)015<0386:RSOTAP>2.0.CO;2.

Wang, P. X. *et al.* (2014) 'The global monsoon across timescales: Coherent variability of regional monsoons', *Climate of the Past*, pp. 2007–2052. doi: 10.5194/cp-10-2007-2014.

Wang, X. *et al.* (2006) 'Interhemispheric anti-phasing of rainfall during the last glacial period',

Quaternary Science Reviews, 25(23–24), pp. 3391–3403. doi: 10.1016/j.quascirev.2006.02.009.

Wang, X. *et al.* (2007) 'Millennial-scale precipitation changes in southern Brazil over the past 90,000 years', *Geophysical Research Letters*, 34(23). doi: 10.1029/2007GL031149.

Wang, Y. *et al.* (2005) 'The Holocene Asian monsoon: Links to solar changes and North Atlantic climate', *Science*, 308(5723), pp. 854–857. doi: 10.1126/science.1106296.

Wang, Y. *et al.* (2008) 'Millennial- and orbital-scale changes in the East Asian monsoon over the past 224,000 years', *Nature*, 451(7182), pp. 1090–1093. doi: 10.1038/nature06692.

Wang, Y. J. *et al.* (2001) 'A high-resolution absolute-dated late Pleistocene monsoon record from Hulu Cave, China', *Science*, 294(5550), pp. 2345–2348. doi: 10.1126/science.1064618.

Werner, M. *et al.* (2016) 'Glacial-interglacial changes in $H_2{}^{18}O$, HDO and deuterium excess-results from the fully coupled ECHAM5/MPI-OM Earth system model', *Geoscientific Model Development*, 9(2), pp. 647–670. doi: 10.5194/gmd-9-647-2016.

Werner, M. *et al.* (2018) 'Reconciling glacial Antarctic water stable isotopes with ice sheet topography and the isotopic paleothermometer', *Nature Communications*, 9(1), pp. 1–10. doi: 10.1038/s41467-018-05430-y.

Wheeler, M. C. and McBride, J. L. (2012) 'Australasian monsoon', in Lau, W. K. (ed.) *Intraseasonal Variability in the Atmosphere-Ocean Climate System*. Berlin, Heidelberg: Springer Berlin Heidelberg, pp. 147–197. doi: 10.1007/978-3-642-13914-7_5.

Winter, A. *et al.* (2020) 'Initiation of a stable convective hydroclimatic regime in Central America circa 9000 years BP', *Nature Communications 2020 11:1*, 11(1), pp. 1–8. doi: 10.1038/s41467-020-14490-y.

Wohlfahrt, J., Harrison, S. P. and Braconnot, P. (2004) 'Synergistic feedbacks between ocean and vegetation on mid- and high-latitude climates during the mid-Holocene', *Climate Dynamics*, 22(2–3), pp. 223–238. doi: 10.1007/s00382-003-0379-4.

Woodhead, J. *et al.* (2006) 'U-Pb geochronology of speleothems by MC-ICPMS', *Quaternary*

Geochronology. doi: 10.1016/j.quageo.2006.08.002.

Wu, J. Y. *et al.* (2012) 'Stable isotope and trace element investigation of two contemporaneous annually-laminated stalagmites from northeastern China surrounding the 8.2 ka event', *Climate of the Past*, 8(5), pp. 1497–1507. doi: 10.5194/cp-8-1497-2012.

Wurtzel, J. B. *et al.* (2018) 'Tropical Indo-Pacific hydroclimate response to North Atlantic forcing during the last deglaciation as recorded by a speleothem from Sumatra, Indonesia', *Earth and Planetary Science Letters*, 492, pp. 264–278. doi: 10.1016/J.EPSL.2018.04.001.

Xiao, J. *et al.* (2018) 'The 4.2 ka BP event: multi-proxy records from a closed lake in the northern margin of the East Asian summer monsoon', *Climate of the Past*, 14(10), pp. 1417–1425. doi: 10.5194/cp-14-1417-2018.

Yadava, M. G., Ramesh, R. and Pant, G. B. (2004) 'Past monsoon rainfall variations in peninsular India recorded in a 331-year-old speleothem', *Holocene*, 14(4), pp. 517–524. doi: 10.1191/0959683604hl728rp.

Yim, S. Y. *et al.* (2014) 'A comparison of regional monsoon variability using monsoon indices', *Climate Dynamics*, 43(5–6), pp. 1423–1437. doi: 10.1007/s00382-013-1956-9.

Yonge, C. J. *et al.* (1985) 'Stable isotope studies of cave seepage water', *Chemical Geology: Isotope Geoscience Section*, 58(1–2), pp. 97–105. doi: 10.1016/0168-9622(85)90030-2.

Yoon, J. and Yeh, S.-W. (2010) 'Influence of the Pacific Decadal Oscillation on the Relationship between El Niño and the Northeast Asian Summer Monsoon', *Journal of Climate*, 23(17), pp. 4525–4537. doi: 10.1175/2010JCLI3352.1.

Yu, G. *et al.* (2003) 'LGM lake records from China and an analysis of climate dynamics using a modelling approach', *Global and Planetary Change*, 38(3–4), pp. 223–256. doi: 10.1016/S0921-8181(02)00257-6.

Yu, S.-Y. *et al.* (2010) 'Freshwater Outburst from Lake Superior as a Trigger for the Cold Event 9300 Years Ago', *Science*, 328(5983), pp. 1262–1266. doi: 10.1126/science.1187860.

Yuan, D. *et al.* (2004) 'Timing, duration, and transitions of the Last Interglacial Asian monsoon', *Science*, 304(5670), pp. 575–578. doi: 10.1126/science.1091220.

Yuan, Y. *et al.* (2008) 'Influences of the Indian Ocean dipole on the Asian summer monsoon in the following year', *International Journal of Climatology*, 28(14), pp. 1849–1859. doi: 10.1002/joc.1678.

Zhang *et al.* (2019) 'The Asian Summer monsoon: Teleconnections and forcing Mechanisms—A review from Chinese speleothem $\delta^{18}O$ records', *Quaternary*, 2(3), p. 26. doi: 10.3390/quat2030026.

Zhang, H. *et al.* (2021) 'A data-model comparison pinpoints Holocene spatiotemporal pattern of East Asian summer monsoon', *Quaternary Science Reviews*, 261, p. 106911. doi: 10.1016/j.quascirev.2021.106911.

Zhang, R. and Delworth, T. L. (2006) 'Impact of Atlantic multidecadal oscillations on India/Sahel rainfall and Atlantic hurricanes', *Geophysical Research Letters*, 33(17), p. L17712. doi: 10.1029/2006GL026267.

Zhang, S. and Wang, B. (2008) 'Global summer monsoon rainy seasons', *International Journal of Climatology*, 28, pp. 1563–1578. doi: 10.1002/joc.

Zhang, W. *et al.* (2016) 'Unraveling El Niño's impact on the East Asian Monsoon and Yangtze River summer flooding', *Geophysical Research Letters*, 43(21). doi: 10.1002/2016GL071190.

Zhao, J. *et al.* (2019) 'Reconstructing the western boundary variability of the Western Pacific Subtropical High over the past 200 years via Chinese cave oxygen isotope records', *Climate Dynamics*, 52(5–6), pp. 3741–3757. doi: 10.1007/s00382-018-4456-0.

Zhao, Y. *et al.* (2009) 'Vegetation response to Holocene climate change in monsoon-influenced region of China', *Earth-Science Reviews*, 97(1–4), pp. 242–256. doi: 10.1016/j.earscirev.2009.10.007.

Zhao, Y. and Harrison, S. P. (2012) 'Mid-Holocene monsoons: A multi-model analysis of the inter-hemispheric differences in the responses to orbital forcing and ocean feedbacks', *Climate Dynamics*, 39(6), pp. 1457–1487. doi: 10.1007/s00382-011-1193-z.

Zimmerman, U., Ehhalt, D. and Münnich, K. O. (1969) 'Soil water movement and evapotranspiration:

changes in the isotopic composition of the water', in *Isotopes in Hydrology*. Vienna: International Atomic Energy Agency, pp. 567–584.